Vibrational spectroscopy of zeolite complexes

Jaqueline Mary Nicol

VIBRATIONAL SPECTROSCOPY OF ZEOLITE COMPLEXES

by

JACQUELINE MARY NICOL

(B.Sc. Dunelm)

A thesis submitted for the degree of

Doctor of Philosophy

Department of Chemistry,
University of Durham

October 1985

Dedicated to

My Parents

With thanks for their support and

encouragement during my years in Durham

Science is always wrong:
it never solves a problem
without creating ten more.

BERNARD SHAW.

ABSTRACT

VIBRATIONAL SPECTROSCOPY OF ZEOLITE COMPLEXES

Using infrared spectroscopy, studies of the interaction of small molecules (*e.g.* CO, C_2H_2, CH_3CHO) with zeolites have been carried out. The work has resulted in the observation of both stable chemisorbed complexes and reacting species for which time-resolved measurements have been made.

The isomerization of cyclopropane on ZnNa-A has been followed using time resolved spectroscopy. From the intensity of the ν(C=C) stretch of the product, propene, the kinetics of the reaction have been followed and the reaction sites identified. The rate of isomerization was found to be very much faster than that previously reported for similar systems. In a separate study the adsorbed complex formed between propene and Na-A zeolite has been investigated.

On adsorption of carbon monoxide on Cu(I) containing Y zeolite, three different locations for the adsorbed CO have been observed. These experiments have been repeated for a variety of sample pretreatment conditions and the results used to explain the inconsistency in the scientific literature, where a range of ν(C≡O) stretching frequencies have been presented by different authors. In essence, it has been shown that the sample pretreatment has a marked effect on this cation distribution within the zeolite, and hence on the number and intensity of CO bands that are observed, since each site has a characteristic carbonyl stretching frequency. Copper containing Y zeolites were also investigated through the adsorption of ammonia and the reduction of the Cu(II) form by

CO and NH_3. The rationale for this work was to attempt to better understand the reduction process.

A study of ethyne adsorbed on ZnNa-A has revealed two adsorption sites within the framework. At one site C_2H_2 was found to be weakly π-bonding to the Na cations. The second site was identified as the Zn cations, at which the C_2H_2 was observed to lose hydrogen and form Zn-acetylide. The Zn-acetylide was observed to react slowly with zeolitic water to form ethanal. In separate studies ethanal was shown to be formed when C_2H_2 was adsorbed on Ag-A zeolite but no chemical reaction was observed on the Na-A form.

Ethanal adsorbed on some ion-exchanged type A zeolites (Zn, Na, Ag) has been observed to form complexes with the charge compensating cations and framework hydroxyl groups. On zeolite ZnNa-A three species were identified; a hydrogen bonding complex formed with the framework hydroxyl groups, and two coordinating complexes formed with the charge compensating cations; (one with the Na(I) ions and one with the Zn(II) ions). In contrast two complexes were found on Ag-A (one hydrogen bonding, the other with the Ag^+ cation) and one on Na-A, formed with the Na(I) ions. When adsorbed ethanal was heated, under vacuum, on ZnNa-A and Na-A new species were formed. These were tentatively identified as carboxylate species.

A study of ethene adsorbed on ZnNa-A has been made by infrared and inelastic neutron scattering spectroscopy (INS). The IR measurements clearly showed the formation of a π-bonded adsorption complex, by the observation of the formally inactive ν_2(C=C) stretching mode of ethene but no ν(C-H) stretching

vibrations were observed. In the INS data a number of vibrations of the adsorbed C_2H_4 with respect to the surface were seen, as well as a weak broad band due to the ν(C-H) stretching modes.

DECLARATION

The work described in this thesis has not been submitted for any other degree and is the original work of the author except where acknowledged by reference.

ACKNOWLEDGEMENTS

I would like to acknowledge the help and encouragement I have received from my many friends and associates during my years of study in Durham.

I am especially indebted to my supervisor, Dr. Joe Howard, for his valuable advice, encouragement and enthusiasm towards the work in this thesis.

I would like to thank the technical staff of Durham University for their help and assistance so freely given during the research of this thesis.

My thanks are expressed to Dr. Juergen Eckert for arranging my visit to P.8, WNR, Los Alamos National Laboratory, Los Alamos, New Mexico, during the Summer of 1984.

Finally I acknowledge the Science and Engineering Research Council for the provision of a research studentship and thank Mrs. Marion Wilson for her secretarial skill in typing this thesis.

J. M. Nicol

Durham, October 1985.

CONTENTS

Page No.

CHAPTER ONE

INTRODUCTION

1.1 Introduction

Vibrational spectroscopy of adsorbed molecules has been extensively used to achieve an understanding of the interactions between adsorbates and solid surfaces, at a molecular level. In this thesis vibrational spectroscopy, and in particular, infrared spectroscopy, has been applied to the study of the species formed when small molecules, such as carbon monoxide, ethyne and cyclopropane, are adsorbed on ion exchanged zeolites.

Zeolites, a group of aluminosilicate catalysts, are industrially important and scientifically interesting materials. They were chosen to be studied because of the above factors and others, such as the paucity of infrared data on the adsorption of molecules other than bases, on their surfaces.

Infrared spectroscopy of zeolite-adsorbate systems can be used to obtain a variety of information such as the nature of the adsorbed species, their number and location in the framework, and to some extent the strength of adsorption. Further, infrared measurements can be used to follow chemical reactions which are occurring on a short time scale, and to obtain details of the kinetics of such reactions. In the extreme case, it would be hoped to obtain information on the nature of the intermediates. Probe molecules, such as carbon monoxide and ammonia, may be used to obtain details of cation locations and the acidity of zeolite frameworks.

1.2 Zeolites

Zeolites are crystalline, hydrated aluminosilicates, with an open framework structure, based on an infinite three dimensional network of SiO_4 and AlO_4 units, in which charge compensating cations are located.[1] They are classified (Chapter Two) according to the structure of the aluminosilicate framework,[1] which may be thought of as a regular arrangement of cavities interconnected by channels, in which are found the cations and water molecules. Zeolitic water is, in general, easily removed and those zeolites which retain their structure on dehydration are termed molecular sieves.[1] Within the cavities of a dehydrated zeolite guest molecules may be adsorbed. The maximum size of a possible adsorbate is determined, in the first instance, by the dimensions of the cavities, but other factors (Chapter Two) such as the location and radii of the cations and temperature, are also important.

The charge compensating cations, which in synthesised or natural zeolites are usually alkali or alkaline earth cations, may be exchanged with other monovalent or polyvalent cations, *e.g.* transition metal ions. The degree of ion exchange obtained depends, very much, on the zeolite type and the cations involved. In some instances the complete exchange of the cations is difficult.

Protons may also provide the charge compensation of the zeolite lattice. These form hydroxyl groups in the framework which act as Brönsted acid sites, giving zeolites their acidic properties.

Protons can be introduced through ion exchange with ammonium ions and thermal treatment to liberate NH_3 and leave H^+ in the framework. For stable high silica zeolites direct ion exchange of H^+ with mineral acid may be used. In addition hydroxyl groups are always present in zeolite frameworks through the termination of the lattice. In those zeolites with polyvalent cations, coordinating water may dissociate, *viz.*

$$M(H_2O)^{n+} \rightleftharpoons MOH^{(n-1)+} + H^+$$

to form hydroxyl groups in the framework.

The acid sites in zeolites are important in giving zeolites their catalytic properties in hydrocarbon transformations and other reactions. In addition to the Brönsted acidity provided by the hydroxyl groups, the charge compensations and tri-coordinate aluminium atoms formed by the loss of framework oxygen and H^+ high temperature, provide Lewis sites in the framework. Both types of acidity are important in giving zeolites their catalytic properties.

In addition the unique nature of the zeolite framework is very often able to stabilize metal ions in unusual oxidation states. This property is also important catalytically, in such reactions as oxidation and reduction.

It is these adsorption, ion-exchange and catalytic properties of zeolites above, which give them their usefulness in the commercial world.

Historically, zeolites were first discovered by Cronstedt, when he identified the mineral Stilbite in 1756.[2] From the observation that the mineral lost water when heated, the name "Zeolite" was derived from the classical Greek meaning "boiling

stones". It was not until some 200 years later, with the introduction of synthetic zeolites,[3,4] that zeolites became commercially important. In the next Section some of the applications of zeolites will be briefly described. It is impossible here to give a complete review of the uses of zeolites, so only some of the most important and more interesting applications are featured.

1.3 Zeolite Catalysts and their uses

In 1980 there were 40 species of natural zeolites and over 150 synthetic types reported.[1] Of these, only a small number have found a use commercially as adsorbents, catalysts and ion exchangers, *etc.*, as listed in Table 1.1. In Table 1.2 some of the actual commercial and potential uses of zeolites are given.

TABLE 1.1 Zeolite types used in commercial applications in 1980, after ref. 5.

Zeolite Minerals	Synthetic Zeolites	
Mordenite	A	Na, K, Ca forms
Chabazite	X	Na, Ca, Ba forms
Erionite	Y	Na, Ca, NH_4, rare earth forms
Clinoptilolite	L	K, NH_4 forms
	Omega	Na, H forms
	Zeolan, Mordenite	H, Na forms
	ZSM-5	Various forms
	F	K form
	W	K form

TABLE 1.2 Summary of the commercial potential uses of Zeolites, after ref. 5,7

Adsorption	Ion Exchange	Catalysis
Regenerative separation based on sieving selectivity	Regenerative processes NH_4^+ removal Metal separations and removal from waste water	Hydrocarbon conversion - Alkylation, Cracking, Hydrocracking, Isomerization
Purification Bulk separations Non-regenerative Drying Windows Refrigerants Cryosorption Gas storage Carriers of Chemicals	Non-regenerative processes Radioisotope removal and storage, Detergent builder Artificial kidney dialysate regeneration, Aquoculture - NH_4^+ removal Ruminant feeding of non-protein nitrogen, Ion-exchange fertilizers	Hydrogeneration and dehydration Hydrodealkylation Methanation Shape-selective reforming Dehydration Methanol to gasoline Organic catalysis Inorganic reactions H_2S oxidation NH_3 reduction to NO CO oxidation $H_2O \rightarrow O_2 + H_2$
Other Agriculture Animal Culture Beverage carbonation Flame extinguishers Electrical conductors Ceramics Solar energy Weather modification Nuclear industry Paper making Toothpaste Brewing Construction industry Fish farming		

The major industrial use of zeolites is as cracking catalysts in the petrochemical industry, where zeolites such as Re-Y, H-Y and Mg-Y are used to produce gasoline from crude oil.[6] In 1979 this accounted for 95% of the free world use of zeolites.[6] All catalytic cracking has been carried out in the United States and Canada with zeolites since 1976.[6]

A second major use of zeolites, (*e.g.* Co, Mo, W or Pt-Pd on H-Y, mordenite, erionite or Z14-US), is as hydrocracking catalysts in the conversion of inferior crude fractions to more desirable products, such as heating oils, gasoline and petrochemical feedstocks.[6] The demands for such products as unleaded gasoline has increased the importance of the hydrocracking process. In 1979 it was reported that about 1,500,000 barrels/day of oil were processed using hydrocracking.[6]

With increasing world demands for oil, alternative methods of producing gasoline have been sought. The high silica zeolite ZSM-5 has been shown to be able to convert methanol to gasoline.[5] This reaction has given a new route for the conversion of natural gas and coal into petroleum products which will find increasing importance in the future.

Also in the energy area zeolites have been used in solar energy systems and gas storage mediums,[5] where their adsorption properties have been utilised.

In the nuclear industry, due to their ion-exchange and adsorption properties, zeolites are also finding increasing use. Zeolites have been suggested as a suitable storage media for long-lived radioisotopes, due to their stability in the presence of ionizing radiation, low solubility and dimensional stability.[5,7] For long term storage, the zeolite, containing

the radioisotopes, is encapsulated in cement or glass, or alternatively, at high temperatures, the zeolite is converted into a glass. One of the earliest uses of zeolites, in the nuclear industry, was in the separation of ^{137}Cs and ^{90}Sr ions from low level radioactive waste waters, created by nuclear reactors.[8] Recently, zeolites were used in the clean up of the radioactive water resulting from the Three Mile Island accident in the U.S.A.[9]

The separation of oxygen and nitrogen from air, by the pressure swing adsorption technique,[10] was made commercially viable with the introduction of zeolite molecular sieves as adsorbents. Small plants using 5A zeolites are commercially available with a capacity of about $50Nm^3/hr.$, and have been used to produce oxygen, of about 93% purity, for medical use at home and in hospitals, for welding units and sewerage treatment plants.[11] Nitrogen generators have been used to provide high purity nitrogen, about 99.5% purity, for sealing various materials during canning operations and for nitrogen blankets in some metallurgical operations.[11]

In agriculture zeolites exchanged with nutrient ions, such as ammonium and potassium, can be added to solids as an ionic fertilizer.[5,7] In animal rearing zeolites have been found to have a beneficial effect when added to the diets of pigs, chickens and ruminants.[5,7] Significant increases in gain of body weight per unit of feed were achieved. Sickness and mortality were also reduced. Zeolites are also utilized in controlling the malodourof animal farm units.

Increasingly now zeolites are being employed in the manufacture of detergents. They are used both as detergent builders and for water softening replacing environmentally unsatisfactory tripolyphosphates. Zeolite A and, to a lesser extent, zeolite X are the zeolites used.[7,9]

Finally, in this brief review, zeolites have found a use in the food industry. The large adsorption capacity of zeolites for carbon dioxide has been used as a novel method for preparing carbonated beverages at the time of consumption rather than by bottling under pressures.[5] More recently the use of a Crimean zeolite in beer production has been noted.[7] It was anticipated,in this article,that a wide market for zeolites would be found in the home brewing of beer and wine![7]

1.4 The Physical Characterization of Zeolites

Many different physical techniques, *e.g.* infrared, nuclear magnetic resonance, X-ray diffraction, neutron scattering, *etc.*, have been used to characterize zeolites and the adsorbed species which are formed in their cavities. Each technique provides both unique and complementary information, which, when collected together, give the zeolite chemist an overall picture of the structure and/or reactions which occur on zeolite surfaces. When studying zeolites the technique chosen depends very much on the type of information required. To give a full review of each technique would be inappropriate in this thesis, so here the type of information obtained from some spectroscopic and diffraction techniques will briefly be described. A much fuller review is given in reference 12 and the references therein.

X-ray diffraction has been applied both to the identification of zeolite structures[13-15] and to the location of cations and adsorbate molecules.[16-17] A limiting factor in studying adsorbate systems by X-ray diffraction is small sample size but the not so widely used technique of neutron powdered diffraction[19] offers a number of advantages; the main ones being the location of protons and the use of larger samples, typically 3-10g. Although in order to locate protons accurately, it is necessary to exchange D for H, to reduce background levels. The use of larger samples allows the accurate determination of the chemical composition of the zeolite and the amount of adsorbate coverage to be better controlled. Neutron diffraction like X-ray diffraction has been applied both to structural determinations[20,21] and studies of adsorbate molecules.[22,23]

^{29}Si and ^{27}Al Nuclear magnetic resonance (NMR) has been used mainly to study the framework structure and, in particular, the ordering of aluminium of silicon atoms in the zeolite framework.[12,24] In addition NMR spectroscopy, particularly proton, NMR, has been applied to study molecules adsorbed in zeolites.[12,25] The introduction, in recent years,[12] of the routine use of solid state magic angle spinning NMR has increased greatly the applicability of this very powerful technique in studying catalyst systems. But there are still a number of extremely challenging problems to be overcome, one of which is the simultaneous adsorption and heating of samples within the confines of the rotating unit of the NMR spectrometer.

Spectroscopic techniques such as electron spin resonance[12,26] uv-visible[27,28] and Mössbauer[12,29] have mainly been applied to the

study of transition metals and the environment of these cations, *e.g.* oxidation state and coordination, within the zeolite frameworks.

The other major techniques not so far mentioned are the vibrational spectroscopic methods of infrared, Raman and inelastic neutron scattering. Raman spectroscopy has not been so widely used as infrared spectroscopy, due mainly to problems associated with high fluorescence levels. This problem is often caused by impurities within the zeolite framework, but in some instances the zeolite-adsorbate systems themselves fluoresce. Reports have been made both of structural[30] and adsorbate[31] studies using the Raman technique.

Inelastic neutron scattering (INS) which provides information similar to infrared studies, but is not limited by optical selection rules, has not been widely used, due in part to limited access to neutron sources and to other restraints which have limited studies to stable systems. Vibrational information from INS measurements of adsorbate molecules has mainly been reported in the 1000-50 cm^{-1} region[32-34] but the importance of this spectral region in providing information on the strength of adsorbate-cation interactions should be noted. It is therefore envisaged that INS studies will become more important in the future.

Finally, infrared spectroscopy, with which this thesis is concerned, provides information in the *ca.* 4000-400 cm^{-1} region. Although studies of adsorbates are usually limited to the region above 1200 cm^{-1}, due to the strong vibrations of the zeolite framework. Infrared studies of zeolites are discussed in detail in the next chapter.

REFERENCES (Chap. 1)

1. Breck, D.W., "Zeolite Molecular Sieves. Structure Chemistry and Use", Wiley, New York, 1974.

2. Cronstedt, A.F., Akad.Handl Stockholm, 17, 120 (1756).

3. Milton, R.M., U.S.Pat., 2,882,433, 14 April 1959.

4. Milton, R.M., Mol.Sieves, Pap.Conf. 199, 1967 (pub.1968).

5. Breck, D.W., "Properties and Applications of zeolites", (ed. Townsend, R.P.), The Chemical Society, 1980, p.391 and references therein.

6. Vaughan, D.E.W., in reference 5, p.295 and references therein

7. Dyer, A., Chemistry and Industry, 241, 1984.

8. Ames, L.L., Amer.Mineral, 45, 689, 1960.

9. Townsend, R.P., Chemistry and Industry, 246 (1984).

10. Armand, J.W., in ref. 5, p.92.

11. Rees, L.V.C., Chemistry and Industry, 252 (1984).

12. Lechert, H., "Zeolites: Science and Technology", (ed. Ribelro, F.R., Rodrigues, A.F., Rollmann, L.D. and Naccache, C.), Nato ASI Series E; Vol.80, p.151.

13. Mortier, W.J., Compilation of Extra Framework Sites in Zeolites, Butterworth Scientific Ltd., Guildford, 1982.

14. Smith, J.V., "Zeolite Chemistry and Catalysis", ACS Monograph 171, 1976, p.3.

15. Meier, W.M., "Molecular Sieves, Advances in Chemistry Series 121, A.C.S., 1973, p.39.

16. Seff, K., Acc.Chem.Res., 9, 121 (1976).

17. Cruz, W.V., Leung, P.C.W., and Seff, K., J.Am.Chem.Soc., 100, 6997 (1978).

18. Amaro, A.A. and Seff, K., J.Phys.Chem., 77, 805 (1973).

19. Bacon, G.E., "Neutron Diffraction", Clarendon Press, Oxford (1975).

20. Cheetham, A.K. and Eddy, M.M., Intrazeolite Chemistry, ACS Symposium, Series Vol.218 (1983), p.131.

21. Pluth, J.J., Smith, J.V., and Kvick, A., Zeolites, 5, 74 (1985).

22. Adams, J.M. and Haselden, J., Solid State Chem., 55, 209 (1984).

23. Lahn, R., Cohen de Lara, E., Thorel, P. and Ginoux, J.L., Zeolites, 2, 260 (1982).

24. Thomas, J.M., Klinowski, J., Fyfe, C.A., Gobbi, G.C., Ramadas, S. and Anderson, M.W., Intrazeolite Chemistry, A.C.S. Symposium, Series, Vol.218, p.159.

25. Fraissard, J., Ito, T., de Menorral, L.C. and Springuel-Huet, "Metal microstructures in zeolites", Studies in surface science and catalysis, vol. 12, Elsevier, 1982,p.179.

26. Kasai, P.H. and Bishop, R.J., "Zeolite chemistry and catalysis", A.C.S. Monograph, 171, (1976), p.350.

27. Kovachera, P., Davidova, N. and Shopov, D., Zeolites, 3, 92 (1983).

28. Laysch, H., Moerke, W., Vogt, F., Z.Chem., 20, 307 (1980).

29. Fitch, F.R. and Rees, L.V.C., Zeolites, 2, 279 (1982).

30. Dutta, P.K. and Barco, B.D., J.Chem.Soc., Chem.Commun., 1297 (1985).

31. Angell, C.L., J.Phys.Chem., 77, 222 (1973).

32. Howard, J. and Braid, I.J., Zeolites, 5, 101, (1985).

33. Howard, J., Robson, K. and Waddington, T.C., Zeolites, 1, 175 (1981).

34. Howard, J. and Waddington, T.C., "Advances in Infrared and Raman Spectroscopy, (Ed. Clark, R.J.H. and Hester,R.E.), Vol.7, Hayden, London, 1980. p. 86.

CHAPTER TWO

STRUCTURAL STUDIES OF ZEOLITES

2.1 Introduction

Zeolites are a class of crystalline aluminosilicates, with an open lattice framework, based on a three-dimensional array of AlO_4 and SiO_4 tetrahedra linked together by the sharing of oxygen atoms.[1] The structure may be represented by the general formula:

$$M_{x/n}[(AlO_2)_x(SiO_2)_y].WH_2O \qquad (1)$$

where M is a cation of valence n, W is the number of water molecules, and [ ] represents the framework composition. The ratio of Si:Al is (usually) greater than 1. The actual value depends upon the type of zeolite and the conditions used during synthesis. The cations M are present in sufficient number to balance the negative charge of the framework.

The complexity of zeolite structures has meant that a number of different models have evolved to represent their frameworks and enhance the understanding of their structures.[1] In this thesis the model adopted is not a space filling model but one built on lines, where vertices represent Si or Al atoms and the linking oxygen atoms lie slightly off the straight lines joining two vertices.

The TO_4 tetrahedral (T=Al or Si) are known as primary building units.[2] These are linked together to form subunits or secondary building units (SBU) from which the zeolite frameworks are constructed.[1-3] The SBU, illustrated in Figure 2.1, are joined to form three dimensional polyhedra, which are in turn connected together by oxygen bridges to form the overall framework structure. Some polyhedra found in zeolites are illustrated in Figure 2.2.

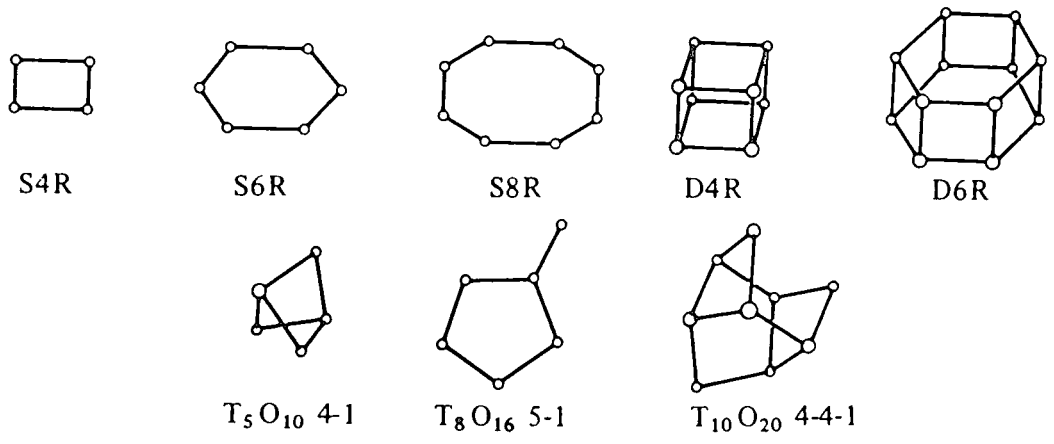

Figure 2.1 The secondary building units in Zeolite structures.[1,2] Linking oxygen atoms are not shown. Nomenclature that of ref. 1.

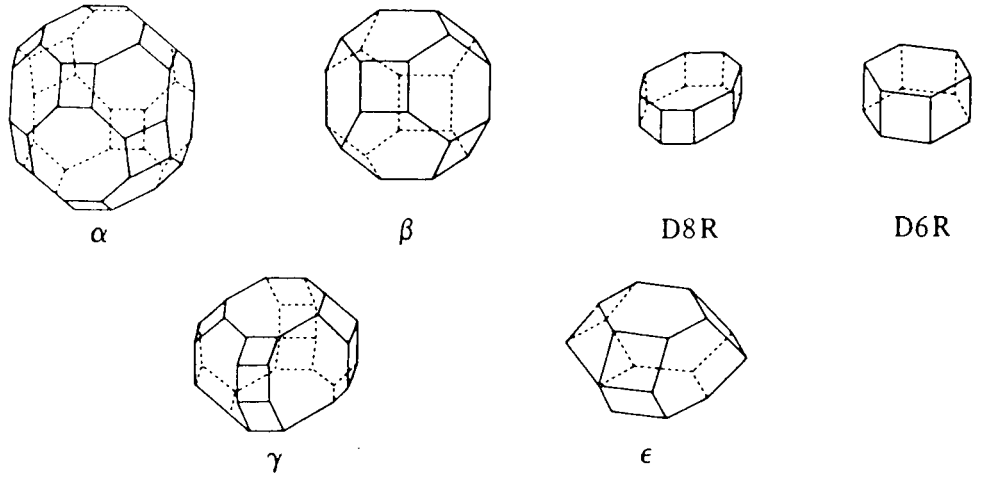

Figure 2.2 Some polyhedra in zeolite frameworks from ref.1.

α - truncated cubooctahedron; β - truncated octahedron or sodalite cage; D8R - double 8-ring; D6R - hexagonal prism (double 6-ring); ϑ - 18-hedron; ε - 11-hedron.

The structural classification of natural and synthetic zeolites into seven groups, based on SBU, have been proposed by a number of authors.[1-3] The classification is not completely unambiguous as many zeolite networks can be generated from several different SBUs, provided that the Si and Al atoms are regarded as indistinguishable. The classification according to Breck[1] is shown in Table 2.1.

TABLE 2.1 Zeolite Classification after Breck[1]

Group	Secondary building unit (Fig.2.1)	Example
1	Single 4-ring, S4R	Analcime, Zeolite P
2	Single 6-ring, S6R	Erionite, Sodalite hydrate
3	Double 4-ring, D4R	Zeolite A
4	Double 6-ring, D6R	Zeolite Y and X, Faujasite
5	Complex 4-1, T_5O_{10} unit	Thomsonite
6	Complex 5-1, T_8O_{16} unit	Mordenite, ZSM-S
7	Complex 4-4-1, $T_{10}O_{20}$ unit	Brewsterite

The work in this thesis is concerned with two synthetic zeolites A and Y, which belong to groups 3 and 4 respectively. Both zeolites contain the polyhedral sodalite unit in their frameworks (Figure 2.3a), but these units are arranged differently with respect to each other in the two structures, forming a series of larger cavities. The framework structures of zeolites A and Y and a number of other zeolites are illustrated in Figure 2.3. Within any zeolite structure, the largest cavity is labelled the α-cage, the second largest the β-cage, *etc.* For zeolites A and Y the α and β cages are labelled in Figure 2.3.

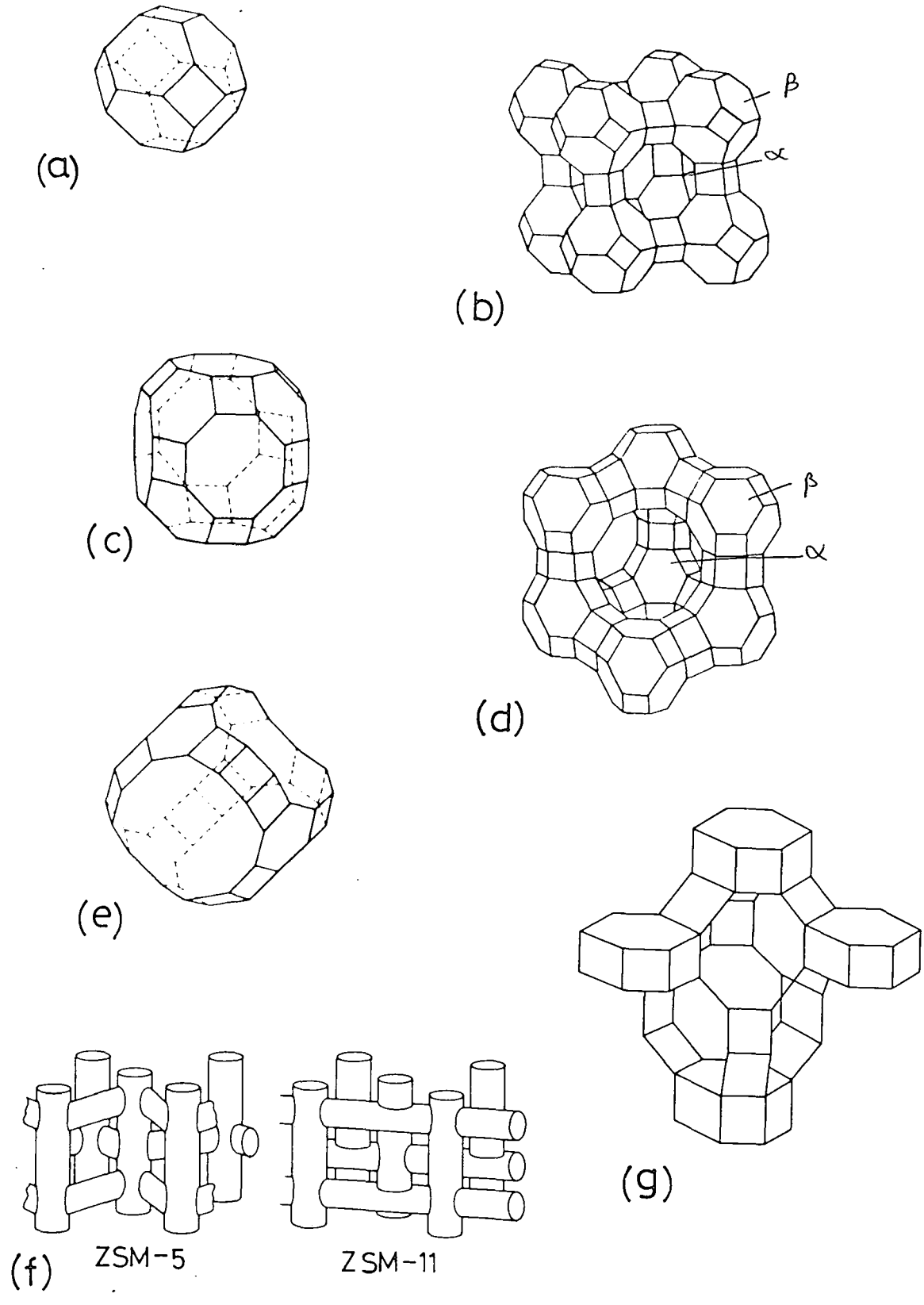

Figure 2.3 Some Structures of Zeolites and their cavities

(a) the sodalite cage, (b) Zeolite A, (c) the α-cage of zeolite A after Eberely[5], (d) Zeolite Y, (e) the α-cage of zeolite Y,[5] (f) ZSM-5 and ZSM-11, (g) erode

It is in the cavities formed by the polyhedra that adsorption and catalytic processes occur. The apertures to these cavities are formed by rings of tetrahedra and their size controls the type of adsorbate molecule which may enter. In the first instance the apperture size is governed by the number of tetrahedra in the ring (Table 2.2) but, to varying degrees, it is also changed by the framework topology and other factors such as the presence of cations and temperature.[1]

TABLE 2.2 Apertures formed by rings of tetrahedra found in zeolite structures.[4]

No. of tetrahedra in ring	Maximum free dimension (Å)
4	1.15
5	1.96
6	2.8
8	4.5
16	6.3
12	8.0

2.2 The structure and cation locations in zeolites A and Y

2.2.1 Zeolite A

The sodalite unit (Figure 2.3a) is a truncated octahedron consisting of 24 tetrahedra which has 8 hexagonal and 6 square faces. The free diameter of this cavity is 6.6Å. in zeolite A the sodalite units are linked together by bridging oxygen atoms between their square faces in a three dimensional array (Figure 2.4a). This generates a series of larger cavities, the free diameters of which are 11.4Å.[1] The tetra-

hedral centres of this cavity form the vertices of a truncated cubooctahedron (Figure 2.3b) comprising six octahedral, eight hexagonal and twelve square faces. In zeolite A the truncated cubooctahedron are α-cages and the sodalite units are β-cages. The α-cage in zeolite A is also referred to as the supercage, although strictly this term should be reserved for the larger α-cages of faujasite type zeolites (Section 2.2.2).

Entry into the α-cages of zeolite A can be made through the six 8-oxygen rings. These rings have a mean free diamter of 4.2Å defined by the ionic radius of the oxygen atoms.[6] Passage between an α- and β-cage is possible ∽ α the 6-oxygen rings of mean diameter 2.2Å. There are thus in zeolite A two interconnecting channel systems, one of diameter 11.4Å with 4.2Å constrictions, the other of alternate 11.4Å and 6.6Å cavities separated by 2.2Å constrictions. When fully hydrated in the sodium ion exchanged form Zeolite A has a pseudo unit-cell (see below) composition of $Na_{12}Al_{12}Si_{12}O_{48}.27H_2O$.[1] This structure is usually referred to as hydrated Na_{12}-A, where A refers to the framewave composition $[Al_{12}Si_{12}O_{48}]$. This form of notation will be used throughout this thesis.

Na_{12}-A zeolite, both in the hydrated and dehydrated form, has been extensively studied by X-ray and neutron diffraction.[7-14] Early powder X-ray diffraction studies[7] indicated Na_{12}-A to have a cubic structure. If the Si and Al ions were not differentiated, then the pseudo unit-cell of $Na_{12}Al_{12}Si_{12}O_{48}$ has a unit cell parameter of

12.3Å and a space group $Pm\bar{3}m$.[7] However, as the Si:Al ratio is 1:1, the Loewenstein electrostatic valence rule[15] requires a rigorous alternation of the AlO_4 and SiO_4 tetrahedra. This alternation is known as the 4:0 ordering scheme. In order to achieve this, the true unit cell constant must be 24.6Å and the symmetry is lowered to space group $Fm\bar{3}c$.[8-11]

Later, results from a series of techniques, namely electron diffraction,[14,16] neutron diffraction[14,13] and ^{29}Si n.m.r.[14,16,17], showed the Loewenstein rule to be violated in Na_{12}-A and the 3:1 ordering scheme was proposed. However, as the argument continues, more recent measurements have again come out in favour of the 4:0 ordering scheme.[18,19] There thus seems to be some uncertainty in the exact nature of the structure of zeolite A.

The true unit cell of Na_{12}-A contains 192 tetrahedra but, in common with many authors, we will hereafter discuss A-type zeolites in terms of the pseudo unit cell, *i.e.* $Na_{12}Si_{12}Al_{12}O_{48}.WH_2O$.

There are three crystallographically distinct types of oxygen ions in type A zeolites: O(1) ions are found bridging between sodalite units, O(2) and O(3) are at distinguishable sites in both the 6- and 8-oxygen rings.[20] The Si-O-Al bond angles reported for hydrated and dehydrated Na_{12}-A are listed in Table 2.3.

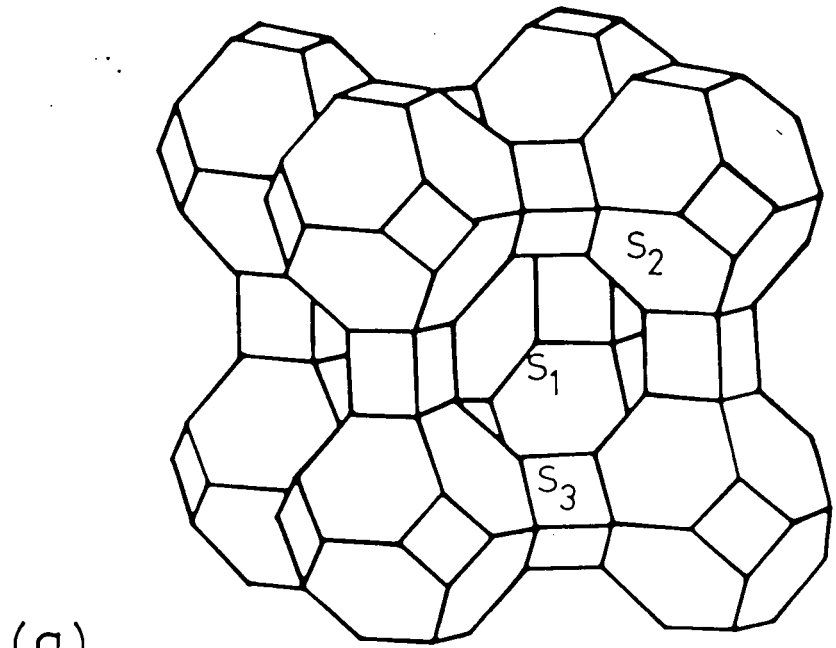

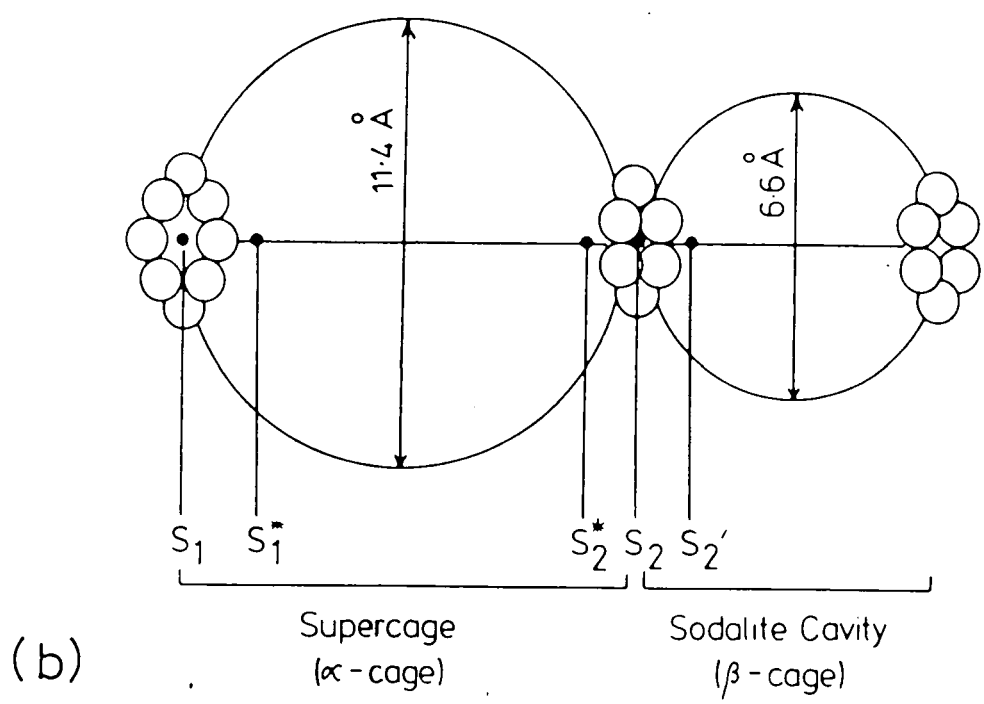

Figure 2.4 The structure and cation locations of Zeolite A

(a) the framework structure of Zeolite A showing cation locations

(b) Schematic representation of the cationic sites.

TABLE 2.3 Some reported bond angles in $Na_{12}A$ zeolite

Zeolite	Bond	Angle	Ref.
hydrated $Na_{12}A$	Si-O(1)-Al	145.5°	8
	Si-O(2)-Al	159.5°	8
	Si-O(3)-Al	144.1°	8
dehydrated $Na_{12}A$	Si-O(1)-Al	145.1°	21
	Si-O(2)-Al	165.6°	21
	Si-O(3)-Al	145.5°	21

Cation location in Zeolite A

The charge compensating cations of zeolite frameworks are, in dehydrated zeolites, generally held at specific sites. As the number of cations present is very often less than the total number of sites available, the cations tend to distribute themselves so as to minimise free energy. In a fully hydrated zeolite, the cations are themselves hydrated, and have only weak interactions with the framework. Hydrated cations are usually mobile.[20]

The cation locations in zeolite A, using the nomenclature of Barrer[20], are listed in Table 2.4 and illustrated in Figure 2.4. Also contained in Table 2.4 are the locations of the Na^+ ions in hydrated and dehydrated Na_{12}-A, as determined from X-ray diffraction studies.[7,8,21-26]

TABLE 2.4 Cation Locations in type-A zeolite

Position	Designation	No. of sites per pseudo unit cell	Location of Na^+ ions in Na_{12}^-A	
			Hydrated[8,17,22-24]	Dehydrated[21,25,26]
In an 8-oxygen ring	S1	3	3[a]	3
Adjacent to an 8-oxygen ring, but displaced into an α-cage	S1*			
In the centre of a 6-oxygen ring	S2	8	3[b]	8
Adjacent to a 6-oxygen ring, but displaced into an α-cage	S2*			
Adjacent to a 6-oxygen ring, but displaced into a β-cage	S2'			
Against a 4-oxygen ring, forming one of the ribs of an α-cage	S3	12		1
In the centre of the α-cage	S4	1	1[c]	
In the centre of the β-cage	SU	1		

a. not located with certainty.

b. coordinate tetrahedrally to 3 framework oxygens and 1 water molecule.

c. probably fully hydrated.

2.2.2 Zeolite Y and other related zeolites

Zeolites X and Y are synthetic analogues of faujasite, a naturally occurring zeolite of unit cell composition $Na_{12}Ca_{12}Mg_{11}[(AlO_2)_{59}(SiO_2)_{133}].235H_2O$.[1] The distinction between X and Y zeolites is based on the Si:Al ratio: those zeolites for which $1.0 \leq Si:Al < 1.5$ are classified as type-X zeolites, while those for which $1.5 \leq Si:Al$ 3 are classified as type-Y zeolites. A typical unit cell composition of type-Y zeolites is $Na_{56}[(AlO_2)_{56}(SiO_2)_{136}].250H_2O$.[1]

The aluminosilicate framework of faujasite-type zeolites is a diamond-like array of sodalite units (Figure 2.5a). Each sodalite unit is linked to four similar units by bridging oxygen atoms between their hexagonal faces.[1] The result is a very open structure, with nearly spherical supercages of *ca.* 12Å diameter (Figure 2.3c). Each supercage is surrounded tetrahedrally by four other supercages, which are separated by 12-oxygen rings of 8-9Å diamter. The entrances between the supercages and the sodalite units are of dimensions similar to those of Zeolite A.

X-ray diffraction has shown members of the faujasite group to have a cubic symmetry and a unit cell parameter of *ca.* 25Å.[27] If silicon and aluminium atoms occur at random over the zeolite framework, then the ideal space group is Fd3m.[27]

In faujasite-type zeolites four distinct types of framework oxygen atoms have been identified. These are described, together with some typical values, in Table 2.5.

TABLE 2.5 Some reported T-O-T bond angles in faujasite-type zeolites

Oxygen atom and description	BOND ANGLE		
	Hydrated NaX $Na_{88}Al_{88}Si_{104}O_{384}\cdot 220H_2O$ ref. 27	Natural faujasite (hydrated) ref. 28	Dehydrated NaY $Na_{57}Si_{135}Al_{57}O_{384}$ ref. 29
O(1): in ribs of hexagonal prisms	132.4°	140.6°	150°
O(2): between hexagonal faces of sodalite unit	141.5°	140.3°	156°
O(3): and O(4) form square faces of sodalite units	136.3°	145.1°	141°
O(4): see above	146.8°	140.6°	138°

Cation locations in faujasite-type zeolites

As with Zeolite A, cations are located in the framework of faujasite-type zeolites to balance the charge of the anionic framework. The cation locations after Barrer[20] are summarized in Table 2.6 and illustrated in Figure 2.5. The location of the Na^+ ions in hydrated Na-X and dehydrated Na-Y are summarised in Table 2.6.

2.3 Published crystal structures of ion exchanged Zeolites used in this thesis

2.3.1 Zinc exchanged type-A zeolite

The crystal structure of $Zn_{4-55}Na_{2.9}$-A used in this thesis has not been published. However, Seff *et al*[30,31] have reported the single crystal X-ray structure of hydrated and dehydrated Zn_5Na_2-A. A summary of the cation locations is given in Table 2.7.

TABLE 2.7 Cation Positions in Zn_5Na_2-A.

Site Designation[a]	Site occupancy	
	Hydrated[30]	Dehydrated[31]
S_1	2Na(I)	
S_2*	3Zn(II)	3Zn(II)
$S_2{}^1$		2Zn(II)
S_4	1Zn(II)	
S_u	1Zn(II)	

[a] See Table 2.4.

In the hydrated zeolite Zn(II) ions were located at three distinct crystallographic sites. One Zn(II) ion per pseudo unit cell was located at the centre of the sodalite

TABLE 2.6 Cation locations in faujasite type zeolites

Description of site	Designation[20]	Number of sites available per unit cell[20]	Hydrated Na-X[27] $Na_{88}Al_{88}Si_{104}O_{384}.220H_2O$	Dehydrated Na-Y[29] $Na_{57}[(AlO_2)_{57}(SiO_2)_{135}]$
In the centre of a hexagonal prism linking adjacent sodalite cages	S_I	16	9	7.5
In a sodalite cage, adjacent to a hexagonal prism	S_I'	32	8, 12 H_2O	19.5
In the centre of a sodalite cage	S_U	8		
In a 6-oxygen ring linking a sodalite cage and a supercage	S_{II}	)))	24, 8 H_2O	30.0
Near a 6-oxygen ring of site II, but displaced into the supercage	S_{II}^*	) 32)))		
Near a 6-oxygen ring of site II, but displaced into the sodalite cavity	S_{II}'	)))	26 H_2O	
In the supercage, adjacent to a square face of the sodalite cavity	S_{III}	48		
In the centre of a supercage	S_{IV}	8		
In the 12-oxygen window of a supercage	S_V	16		

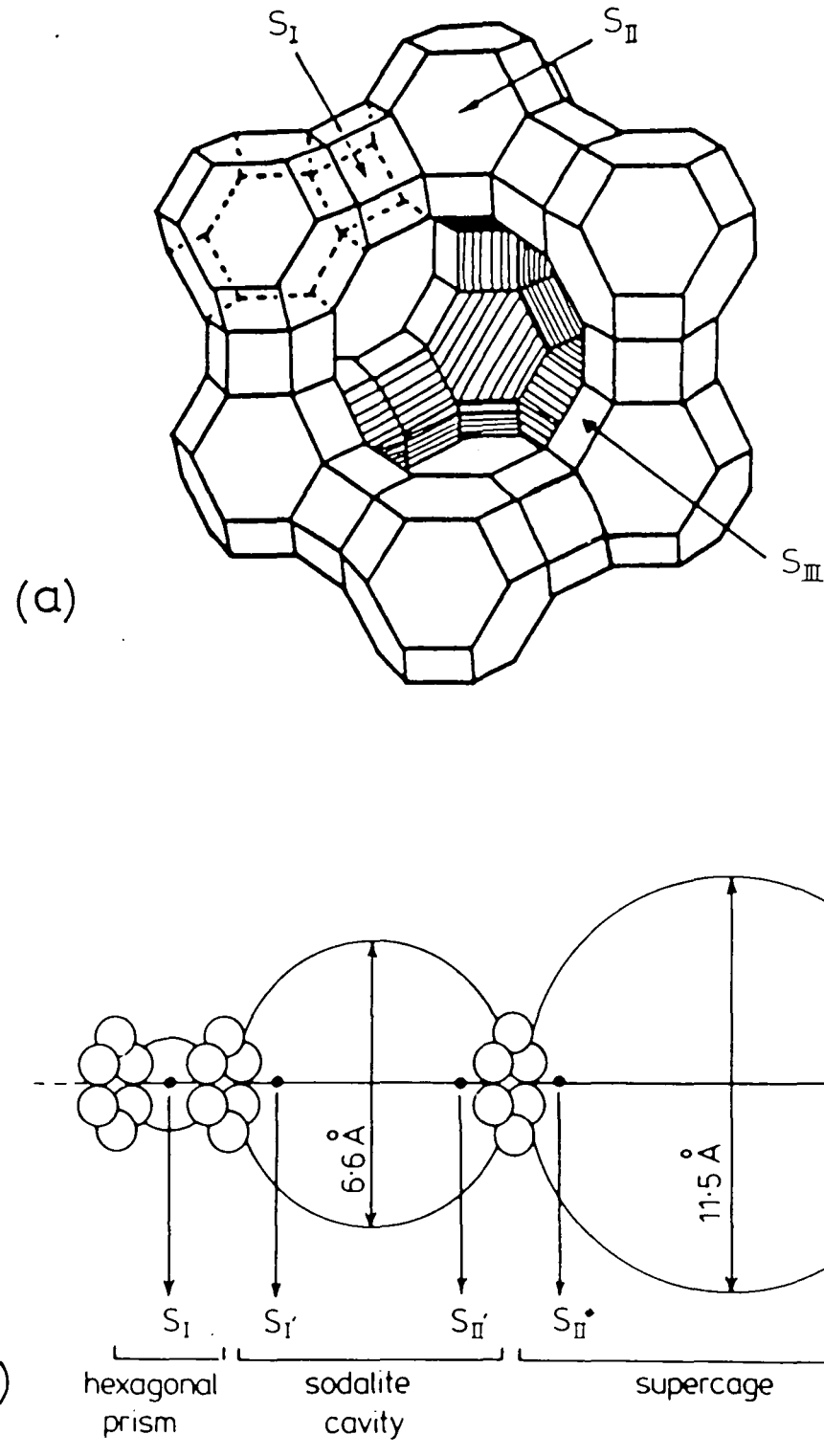

Figure 2.5 The structure and cation locations of Faujasite type Zeolites

(a) the framework structure showing cation locations;

(b) Schematic representation of cationic sites.

unit (S_u), coordinated by a distorted octahedron of water molecules. A second Zn(II) ion was also associated with a distorted octahedron of water molecules, but was sited towards the centre of the supercage (S_4). The three remaining Zn(II) ions lie just inside the large cavity at S_2^*, where they are coordinated tetrahedrally to three framework oxide ions and probably to a hydroxide ion. The two Na^+ ions per pseudo unit cell were associated each with 8-ring oxide ions and two water molecules at S_1.

After dehydration at 623K for 2 days under vacuum,[31] Zn(II) ions were located in two nonequivalent positions in the 6-oxygen rings. Three Zn(II) ions inside the large cavity at S_2^* are tetrahedrally coordinated to three framework oxide ions and one water molecule. The remaining two Zn(II) ions are bridged by a single water molecule inside the sodalite cavity at S_2'. No Na(I) ions were located but one would assume that they would lie in the 8-oxygen rings (S_1) as in the hydrated structure.

2.3.2 Copper exchanged type-Y Zeolites

Crystal structures have been published of hydrated[32] and dehydrated[33] Cu(II)Na-Y zeolite with varying degrees of ion exchange. The single crystal X-ray analysis of fully copper exchanged faujasite in both the hydrated and dehydrated state has also been reported.[34]

In the hydrated zeolites the Cu(II) cations were found to be rather mobile and were thus not all located. the cation distributions are summarized in Table 2.8(a).

TABLE 2.8 Cation locations in Copper(II) exchange Y zeolites

(a) Hydrated CuNaY

Site \ Sample	$Cu_7Na_{29}H_{13}Y$[32] .250 H_2O	$Cu_{12}Na_{21}H_{11}Y$[32] .250 H_2O	$Cu_{13}Na_{16}H_{10}Y$[32] .250 H_2O	Cu_{28}Faujasite[34] $[(AlO_2)_{56}(SiO_{136})xH_2O)$
S_I	4.5 Na^+	3.6 Na^+	0.8 Na^+	
S_I	14.9 Na^+	13.5 Na^+	15.5 Na^+	6.3 Cu^{2+}
S_{II}	1.9 Cu^{2+}	1.5 Cu^{2+}	3.0 Cu^{2+}	
S_{II}'	15.5 H_2O	15.6 H_2O	14.9 H_2O	
S_{II}^*	H_2O/cations	H_2O/cations	H_2O/cations	H_2O
S_{III}	9.7 Na^+	2.4 Na^+	6.5 Cu^{2+}	
Su or S_{IV}	5.4 Cu^{2+}	8.7 Cu^{2+}		H_2O

(b) Dehydrated CuNaY

Site \ Sample	$Cu_{16}Na_{24}Y$[32]	$Cu_{12}Na_5H_{29}Y$[32]	$Cu_{16}Na_{24}Y$[33] + NH_3	$Cu_{16}Na_{24}Y$[33] + Pyridine	Cu_{28}Faujasite[34] $[AlO_2)_{56}$-$(SiO_2)_{135}]$
S_I	3.2 Cu^{2+}	1.7 Cu^{2+}	2.1 Cu^{2+}	1.9 Cu^{2+}	1.5 Cu^{2+}
S_I	11.4 Cu^{2+}	9.9 Cu^{2+}	12.1 Cu^{2+}	2.3 Cu^{2+}	14.2 Cy^{2+}
S_{II}	20.5 Na^+	8.0 Na^+	17.8 Na^+	26 Na^+	3.8 Cu^{2+}
S_{II}'			9.4 NH_3		0.8 Cu^{2+}
S_{II}^*					1.5 Cu^{2+}
S_{III}					3.3 Cu^{2+}

The results of the X-ray studies for dehydrated Cu(II)Na-Y and Cu(II) exchanged faujasite are summarized in Table 2.8(b). This table also contains details of cation distributions in the presence of ammonia and pyridine. In all the zeolites, on dehydration, the cations are observed to prefer the sites in the small cavities (S_I and S_I'). In $Cu_{16}Na_{24}$-Y[33] the Cu(II) ions at Site I' are coordinated to six framework oxygen atoms. In contrast those cations in Site S_I were found to be coordinated to three framework oxygen atoms. In the presence of bases (NH_3 and C_5H_5N) a migration of the cations away from the hidden S_I site was observed. The migration of the copper cations has also been observed by ESR Spectroscopy (Chapter Five).

In fully exchanged faujasite Cu(II) ions were located in sites S_I, S_I', S_{II}, S_{II}' and S_{II}^*. Cations at S_I' (Cu(I'A), Figure 2.6a) were found to be mainly strongly bound to the zeolite framework, but a small number at Cu(I'B) were less firmly bound, presumably due to their interaction with residual water. A similar type of interaction is observed in the 6-oxygen rings at sites S_{II}(Cu(IIA)), S_{II}' (Cu(II')) and S_{II}^* (Cu(IIB)), (Figure 2.6b). The cations at site S_{III} (Cu(III), Figure 2.6c) are located in the supercages coordinated to two framework oxygens.

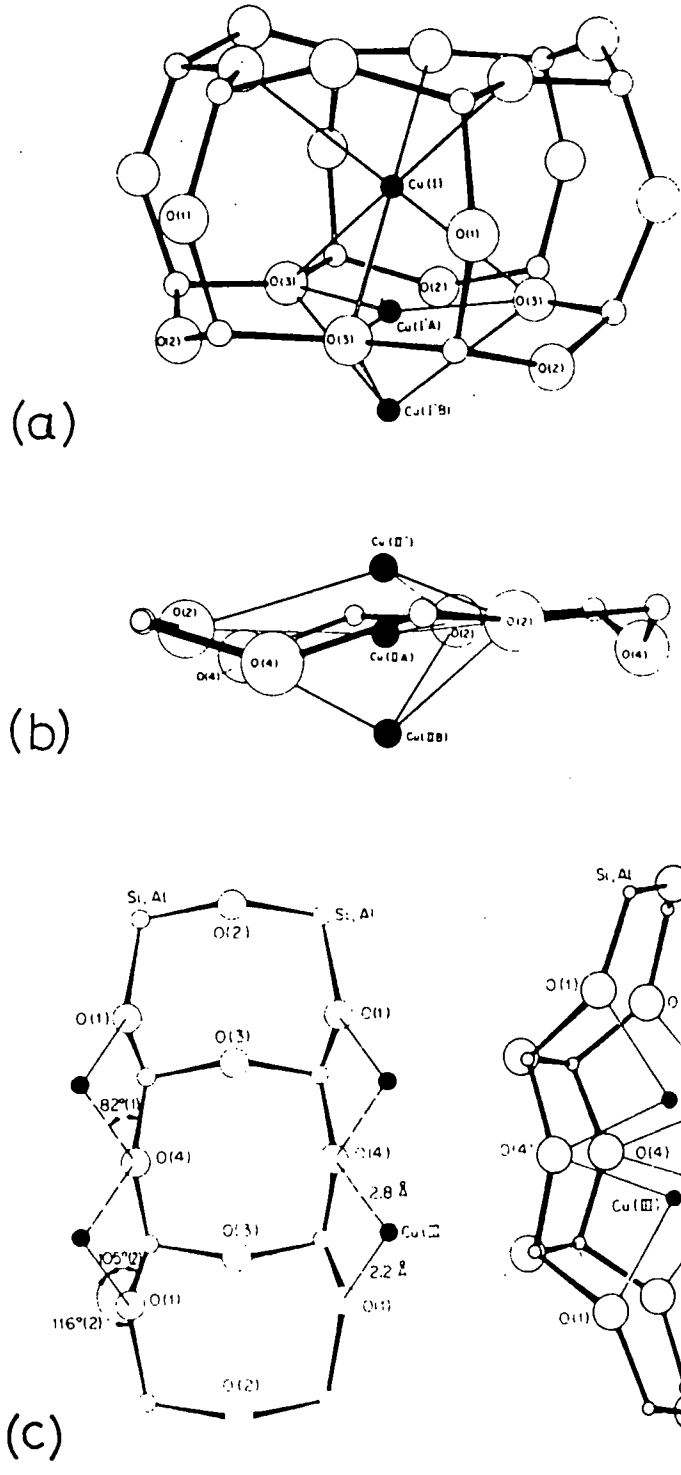

Figure 2.6 Perspective views of the coordination of the copper (II) ions in fully exahanged faujasite [33]

(a) In the hexagonal prisms
(b) In the 6-rings between the α and β cages
(c) In the supercages.

(Because of repulsive forces simultaneous occupancy of Cu(II) ions in adjacent sites in the above diagrams is not expected).

2.4 Vibrational analysis of Zeolite frameworks

2.4.1 Framework vibrations

IR spectroscopy,[35-46] and to a lesser extent Raman spectroscopy,[35,47-49] has been extensively applied to the structural analysis of zeolite frameworks. For all zeolites the fundamental vibrations of the TO_4 units are observed in the mid-infrared region (200-1300 cm^{-1}) while in the far-infrared region, below 300 cm^{-1}, modes associated with the vibrations of the cations are observed.

Flanigen *et al*[35] investigated the framework vibrations of a large number of synthetic zeolites. Although each zeolite exhibited its own characteristic IR spectrum (Figure 2.7), similarities between spectra could be correlated with known framework structures as determined by X-ray diffraction. According to the treatment of Flanigen *et al*[28] two classes of IR band arose in the 1300-200 cm^{-1} region: (1) those due to the internal modes of the TO_4 tetrahedra and which were insensitive to variations in the framework structure; and (2) those arising from vibrations of the external linkages between tetrahedra which depended upon the framework structure and were related to the presence of some types of SBU and building block polyhedra. Both classes of vibration were found to occur within characteristic frequency regions, these are summarized in Table 2.9 and illustrated for Na-Y zeolite in Figure 2.8.

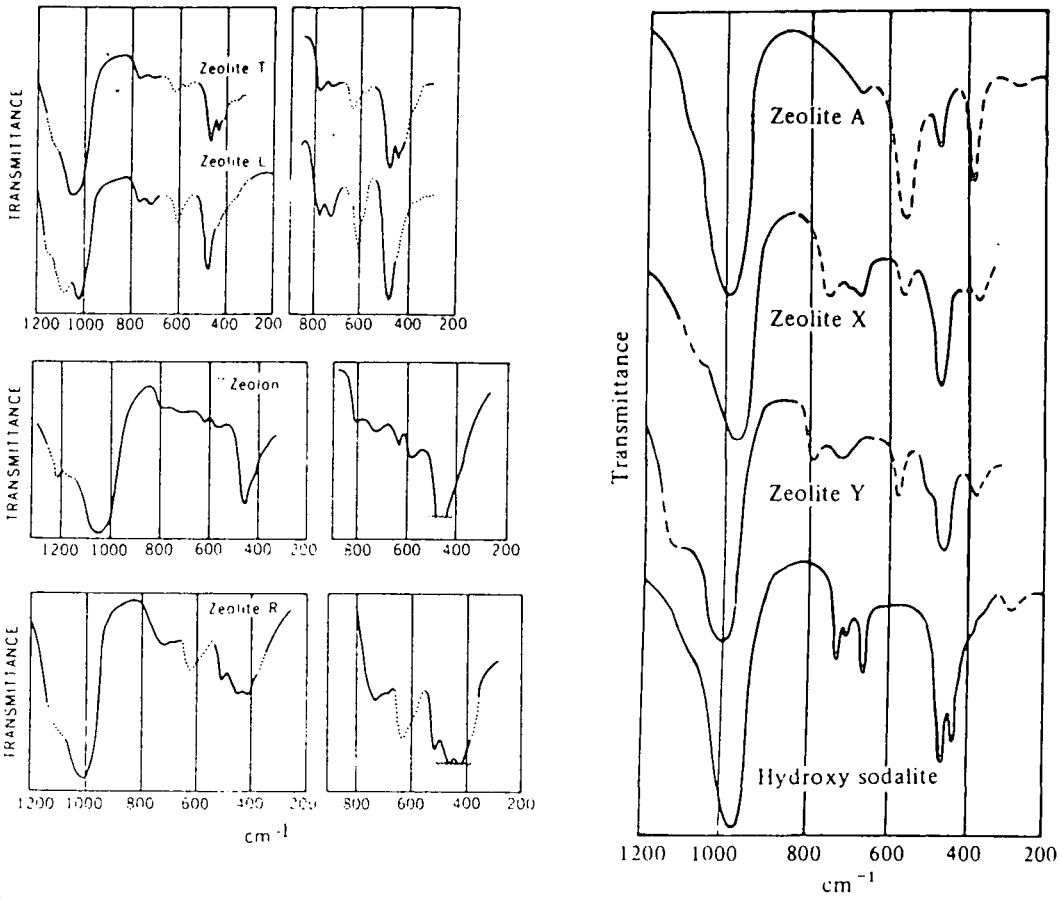

Figure 2.7 Infrared transmission spectra of some zeolites (KBr Discs) after ref. 35

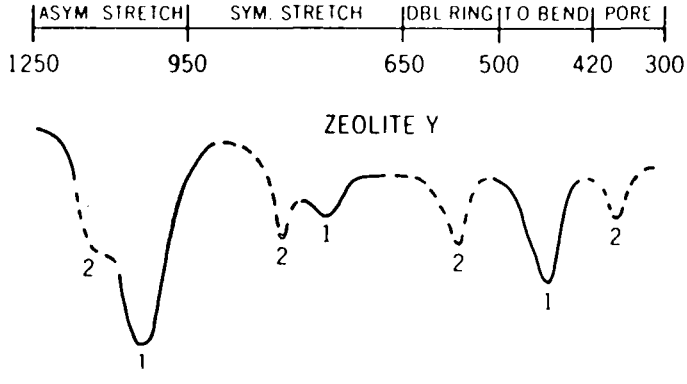

Figure 2.8 The assignment of Zeolite framework vibrations illustrated with the spectrum of zeolite Y (Si:Al=2.5) after ref. 35.

1 = internal tetrahedra - structure insensitive

2 = external linkages - structure sensitive.

TABLE 2.9 The characteristic frequencies (cm^{-1}) of zeolite skeletal vibrations after Flanigen *et al*[35]

Internal Tetrahedral		External linkages	
Antisymmetric stretch	1250-950	Double ring	650-500
Symmetric stretch	720-650	Pore opening	360-420
T-O bend	420-500	Symmetric stretch	750-820
		Antisymmetric stretch	1050-1150

Increasing the atomic fraction of Al atoms in the tetrahedral framework has been shown by a number of authors[35-37,50-5] to cause a shift to lower frequencies of the zeolite framework modes. For a series of X and Y zeolites Flanigen *et al*[35] reported a linear decrease in the bands associated with the ν_{asym}(T-O) (970-1020 cm^{-1}) and ν_{sym}(T-O) (670-725 cm^{-1}) internal stretching modes, the double 6-ring (D-6) (565-586 cm^{-1}) and the 12-ring pore opening modes (360-385 cm^{-1}). The observed trends are shown in Figure 2.9.

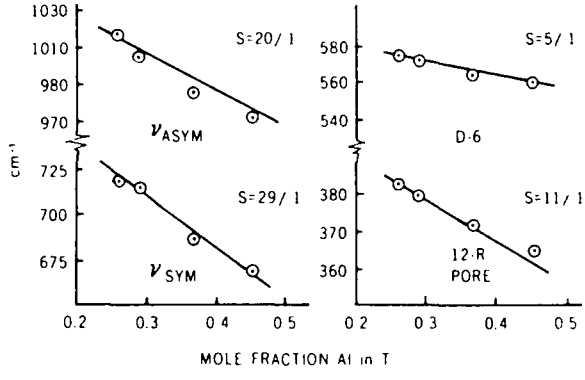

Figure 2.9 Frequency *versus* atom fraction of Al in the framework of Zeolites X and Y for several infrared bands after ref.35.
S = cm^{-1}/0.1 mole fraction of Al.

Similar shifts in the infrared spectra of X and Y zeolites were also observed by Kiselev *et al*[37] and Wright *et al*[51].

The data so far reviewed has been for hydrated zeolites containing univalent charge balancing cations. When these zeolites are dehydrated only minimal changes in the aluminosiliciate framework occur that give rise to minor changes in the IR spectra in the 200-1300 cm^{-1} region.[1,35] The situation is somewhat different for zeolites containing divalent cations.[35,37] In Figure 2.10 the data of Zhdanov *et al*[37] shows the strong sensitivity of framework IR vibrations to the cation-type and charge for a series of dehydrated X zeolites. Flanigen *et al*[35] have reported similar changes in the spectra of Ca-Y (Figure 2.11) after dehydration, dehydroxylation and rehydration. The spectral changes were interpreted as being due to the movement of the cations from sites inside the sodalite units to positions near the centre of the hexagonal prisms (S_I). Analogous spectral changes were reported for La exchanged Y zeolite.[35]

Mid IR spectroscopy has also been applied to the study of zeolite framework synthesis, modification and deposition. Flanigen[46] gives an excellent review of the type of information which may be obtained from such studies.

In the far-infrared region (<300 cm^{-1}) bands observed in the spectra of dehydrated zeolites have been assigned to the stretching modes of cations in specific sites in the aluminosilicate framework.[41-45] In conjunction with a knowledge of the cation distribution and the relationship $\nu_i \alpha M_i^{-\frac{1}{2}} R_i^{-3/2}$ (where ν_i is the cation vibrational frequency of a particular site i and M_i and R_i are the mass and ionic

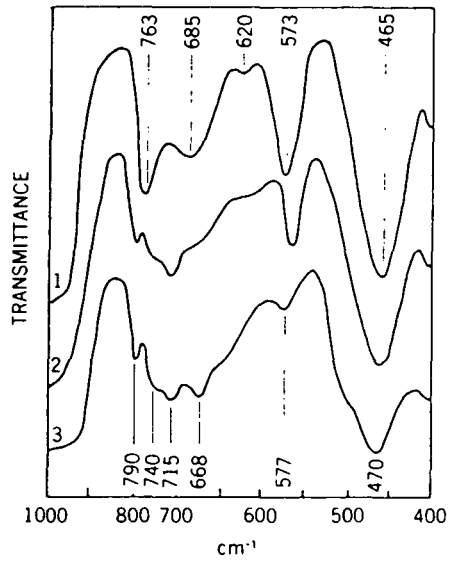

Figure 2.10 Framework infrared spectra for self supporting wafers of Zeolite X with different exchangeable cations after vacuum treatment at 673K for 4 hours after ref. 37.

(1) Na-X (2) Sr-X (3) Ca-X.

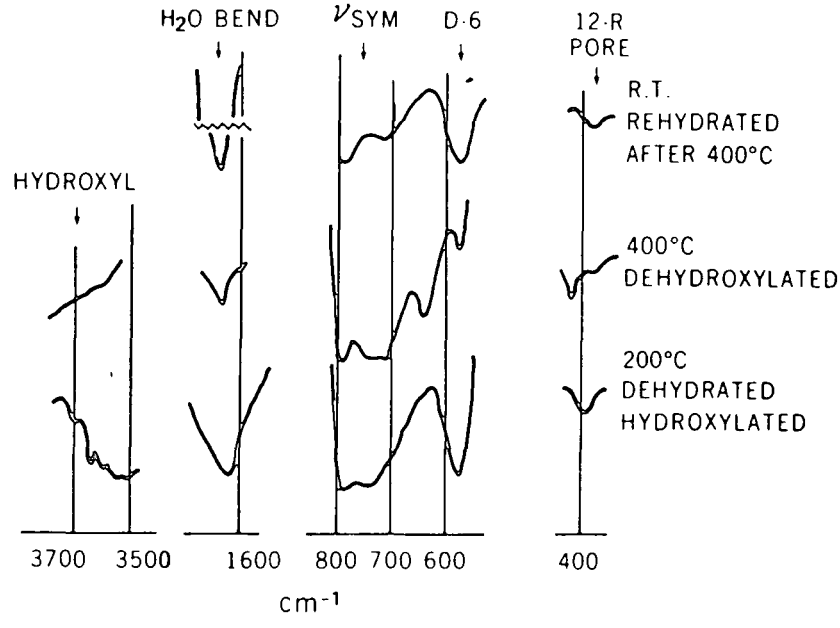

Figure 2.11 Infrared spectra for Ca exchanged Y zeolite (Si:Al=2.5) after dehydration, dehydroxylation and rehydration, after ref. 35.

radius of the cation) proposed by Brodskii *et al*,[44] the assignment of bands to cations at specific crystallographic sites is possible (Table 2.10).[41,43-45]

TABLE 2.10 Frequencies (cm^{-1}) assigned to vibrational modes of cations in dehydrated type-X and Y zeolites

(a) After ref. 43.

Assignment	Na-X	K-X	Ca-X	Cs-X	Na-Y	K-Y	Ba-Y
S_I	160		287		167	107	137
S_I',S_{II},S_{II}'	190	156	273	86	186	133	107
S_{III}	67	58		39			

(b) After ref. 41[a]

Assignment	Ca-Y	Mn-Y	Co-Y	Ni-Y	Cu-Y	Zn-Y
S_I	131	161	170	177	163	162
S_I'	91	116	104	116	103	100
S_{III}	173	140	142	148	137	126

[a] In all zeolites Na^+ cations gave rise to a band in the frequency range 200-190 cm^{-1}.

These cation modes were found by the authors[43] to shift to lower frequencies on hydrations, as the cation-framework interaction was weakened by the hydration of the cation. Ozin *et al*[41] for Co-Y investigated the effect of the Si/Al ratio on the spectrum below 300 cm^{-1}. A shift in the vibrational frequencies to lower wavenumbers with increasing Si/Al ratio was observed (Table 2.11).

TABLE 2.11 The observed dependence of the cation vibrational frequency for site I in Co^{2+} ion exchange faujasite zeolite on the Si/Al ratio[41]

Si/Al	frequency, cm^{-1}
1.25	175.5
2.5	170
3.8	168
20.0	164

As the Si/Al ratio was increased the spectrum became dominated by site S_I, as this became the only site occupied in the high silica zeolites.

2.4.2 Structural hydroxyl groups

Structural hydroxyl groups, because of their importance to the catalytic activity of zeolites, have been extensively studied by IR spectroscopy. A number of review articles describe in detail the positions of these bands and their interpretation.[52-56]

Although considerable variation in the number and position of zeolite hydroxyl groups in any particular zeolite is reported by various authors, the differences are probably due to different sample pretreatment, the extent of cation, deficiency and instrumentation used to carry out the IR measurements.[55] Most studies have concentrated on X and Y zeolites, from which the following interpretations of structural hydroxyl bands in the 3750-3500 cm^{-1} region have been made.[52-56]

(1) Bands at *ca.* 3750 cm^{-1}: this band assigned to SiOH groups is associated either with the termination of the zeolite lattice or with siliceous impurities.

(2) Bands at *ca.* 3690 cm^{-1}: hydroxyl groups in this region have been associated with AlOH groups or in zeolites containing divalent cations with H_2O interacting with the cations.
(3) Bands at *ca.* 3650, 3610 and 3550 cm^{-1}: in decationized (hydrogen form) zeolites these bands have been associated with OH groups in the supercages and in the hexagonal prisms respectively. For zeolites, particularly, those containing divalent cations, these bands have been associated with the dissociation of water during dehydration, induced by the localization of cations and their associated electrostatic fields *viz.* $Zeolite^{2-} + M^{2+} + H_2O \longrightarrow MOH^{+} + Zeolite\text{-}OH^{-}$. In this case the bands are then associated with the zeolitic OH groups and the MOH^{+} species.

The hydroxyl groups in zeolite frameworks act as Brönsted acid centres, while trigonal aluminium atoms and the charge compensating cations behave as Lewis acid centres. These types of acidity have been extensively probed by the adsorption of bases such as ammonia and pyridine.[54,47] The IR spectra of such molecules interacting with Brönsted or Lewis acid sites contain characteristic features which enable the identification of specific acid sites within zeolite frameworks. For example pyridine interacts with Brönsted sites forming the pyridinium ion, evidence for which is found at *ca.* 1545 cm^{-1} in the infrared spectrum:[54,57] whereas pyridine coordinated to Lewis acid sites gives rise to bands in the 1440-1450 cm^{-1} region.[54,57]

2.4.3 Adsorbates

Although there are numerous publications on the study of molecules adsorbed in zeolites using IR spectroscopy,

almost all the work has been on the adsorption of bases to identify particular acid sites. Relatively little work has been published on IR studies of zeolite catalysis, the adsorption of hydrocarbons and reacting species with which this thesis is concerned. Here a few general comments on the type of information which may be obtained from IR studies will be given. A full review of studies relevant to the work presented in this thesis will be given in each chapter as appropriate.

From the IR spectra of adsorbates the following information may be obtained:

(A) From band shifts, changes in relative band intensity and the absence of rotational structure in the spectrum compared to that of the free adsorbate molecule, one can identify that adsorption has taken place.

(B) Information can be obtained on the strength of bonding and to whether an adsorbate is physisorbed or chemisorbed by studying the dependence of the adsorbate IR band intensities as a function of gas overpressure, time of evacuation and heating, *etc.*

(C) One can obtain information on the geometry of the adsorbed species and its nature by looking at changes in the selection rules which occur on adsorption. The presence of new frequencies very often indicates the formation of new species (Chapter Seven).

(D) From the multiplicity of bands compared to the gas or solution phase the identification of multiple adsorption sites is possible (Chapter Four).

(E) Catalytic reactions which occur on zeolite surfaces may be identified from reaction products (Chapter Seven) and the rate and kinetics of chemical reactions may be followed (Chapter Four).

(F) Adsorbates may be used as probe molecules to identify cation locations (Chapter Five).

IR studies of species adsorbed in zeolites, particularly time resolved studies of reacting systems, can yield a wealth of information which is not readily available by any other means. These studies allow a molecular interpretation of the chemistry of Zeolite-adsorbate systems.

REFERENCES (Chap. Two)

1. Breck, D.W., "Zeolite molecular sieves: structure, chemistry and use", Wiley-Interscience, New York, (1974).

2. Meier, W.M., "Molecular Sieves", Society of Chemical Industry, London, (1968), p.10.

3. Gramlich-Meier, R. and Meier, W.M., J. Solid State Chem., 44, 41, (1982).

4. Brower, R.M., Chem.Ind., 1203, (1968).

5. Eberley, P.E., "Zeolite Chemistry and Catalysis", ACS. Monograph, 171, 1976, p.392.

6. Seff, K., Acc. Chem. Res., 9, 121, (1976).

7. Breck, D.W., Eversole, W.G., Milton, R.M., Reed, T.B. and Thomas, T.L., J.Am.Chem.Soc., 78, 5963, (1956).

8. Gramlich, V. and Meier, W.M., Z.Kristallogr., 133, 134, (1971).

9. Thoni, W., Z. Kristallogr., 142, (1975).

10. Pluth, J.J. and Smith, J.V., J.Phys.Chem., 83, 741 (1979).

11. Pluth, J.J. and Smith, J.V., J.Am.Chem.Soc., 102, 4704, (1980)

12. Pluth, J.J. and Smith, J.V., Nature, 291, 265, (1981).

13. Thomas, J.M., Bursill, L.A., Lodge, E.A., Cheetham, A.K. and Fyfe, C.A., J.Chem.Soc.,Chem.Commun., 276, (1981).

14. Bursill, L.A., Lodge, E.A., Thomas, J.M. and Cheetham,A.K., J.Phys.Chem., 85, 2409, (1981).

15. Loewenstein, W., Am.Mineral, 39, 92 (1954).

16. Engelhardt, G., Zeigeen, D., Lippmaa, E. and Magi, M.Z., Anorg.Allgem.Chem., 468, 35 (1980).

17. Klinowski, J., Thomas, J.M., Fyfe, C.A. and Hartman, J.S., J.Phys.Chem., 85, 2590, (1981).

18. Pluth, J.J. and Smith, J.V., ACS Symposium series, 218, 119 (1983).

19. Bennett, J.M., Blackwell, C.S. and Cox, D.E. ACS Symposium series, 218, 143 (1983).

20. Barrer, R.M., "Zeolites and Clay minerals as sorbents and Molecular Sieves", Academic Press, London, (1978).

21. Yanagida, R.Y., Amaro, A.A. and Seff, K., J.Phys.Chem., 77, 805 (1973).

22. Reed, T.B. and Breck, D.W., J.Am.Chem.Soc., 78,5972 (1956).

23. Howell, P.A., Acta.Cryst., 13, 737 (1960).

24. Broussard, L. and Shoemaker, D.P., J.Am.Chem.Soc., 82, 1041 (1960).

25. Smith, J.V. and Dowell, L.G., Z.Kristallogr., 126,135 (1968).

26. Subramian, V. and Seff, K., J.Phys.Chem., 77, 805 (1973).

27. Olson, D.H., J.Phys.Chem., 74, 2758 (1970).

28. Baur, W.H., Am.Mineral, 49, 697 (1964).

29. Eulanberger, G.R., Shoemaker, D.P. and Keil, T.G., J.Phys.Chem., 71, 1812 (1967).

30. Kim, Y. and Seff, K., J.Phys.Chem., 84, 2823 (1980).

31. Amaro, A.A., Kovaciny, C.L., Kunz, K.B., Riley, P.E., Vance, T.B., Yanagida, R.Y. and Seff, K., Mol.Sieves. Int.Conf. 3rd, P.113 (1975).

32. Martin, J., Sonia, J. and Cana, F.H., J.Phys.Chem., 80, 1776 (1976).

33. Gallezot, P., Ben Taarit, Y., and Imelik, B., J.Catal., 26, 295 (1972).

34. Maxwell, J.E. and de Boer, J.J., J.Phys.Chem., 79, 1874 (1975).

35. Flanigen, E.M., Katami, H. and Szmanski, H.A., Adv.Chem. Ser., 101, 201 (1971).

36. Milkey, R.G., Am.Mineral, 45, 990, (1960).

37. Zhadanov, S.P., Kiselev. A.V., Lygin, R.J. and Titova,I.I., Russ.J.Phys.Chem., 38, 1299, (1964).

38. Burragato, F., Mathias, F., Paradi, G., Rerd.Soc.Ital. Mineral Petrol., 34, 27 (1978).

39. Joshi, M.S. and Bhoskar, B.T., Indian J.Pure.Appl.Phys., 19, 560 (1981).

40. Oinuma, K. and Hayashi, J., J.Tokyo Univ., 8, 1 (1967).

41. Ozin, G.A., Baker, M., Godber, J. and Shihua, Wu., J.Am.Ehcm.Soc., 107, 1995 (1985).

42. Stock, T., Dombrowski, D., Fruwert, J. and Ratajazak, H., J.Chem.Soc., Faraday Trans.I, 79, 2773 (1983).

43. Butler, W.M., Angel, C.L., McAllister, W. and Risen, W.M., J.Phys.Chem., 81, 2061 (1977).

44. Brodskii, I.A., Zhadanov, S.P. and Stanevich, A.E., Op.Specktrosk, 30, 58 (1971).

45. Brodskii, I.A. and Zhadanov, S.P., Proc.5th Int.Conf. Zeolites (Naples, 1980), Ed. L.V.C.Rees, Heyden, London (1980), p.234.

46. Flanigen, E.M., "Zeolite Chemistry and Catalysis", ACS. Monograph, 171, 80 (1976), and references therein.

47. Dutta, P.K. and Del Barco, B., J.Phys.Chem., 89, 1861 (1985).

48. De Kanter, J.J.P.M., Maxwell, I.E. and Trotter, P.J., J.Chem.Soc., Chem.Comm., 733 (1973).

49. Angel, C.L., J.Phys.Chem., 77, 222 (1973).

50. Stubican, V. and Roy, R., Am.Mineral, 46, 32 (1961).

51. Weight, A.C., Rupert, J.P. and Granquist, W.T., Amer. Mineralogist, 53, 1293 (1968).

52. Basila, M.L., Appl.Spectr.Rev., 1, 289 (1968).

53. Yates, D.J.C., Catalysis Rev., 2, 113 (1968).

54. Kiselev, A.V. and Lygin, V.I., "Infrared Spectra of Surface compounds", John Wiley, New York, 1972.

55. Ward, J.W., "Zeolite Chemistry and Catalysis", ACS Monograph, 171, 118 (1976).

56. Kustav, L.M., Barovkov, V.Yu. and Kazansky, V.B., J.Catal., 72, 149 (1981).

57. Ward, J.W., J.Catal., 10, 34 (1968).

CHAPTER THREE

EXPERIMENTAL

3.1 Ion-exchange and analysis of zeolites

The zeolites described in this thesis were prepared, unless otherwise stated, from the binder free Na form by ion-exchange in aqueous solutions at ambient temperature. After ion-exchange the samples were filtered, washed with demineralized or distilled water and dried in an oven at 323K.

Elemental analysis was performed by atomic absorption spectroscopy (Perkin-Elmer 5000). Type A zeolites were dissolved in dilute nitric acid before measurement against an appropriate standard. For type Y zeolites, the sample was first digested with hydrogen fluoride and perchloric acid before dissolving in dilute nitric acid. This latter method did not allow analysis for silicon in type Y zeolites.

X-ray powder photographs were used to detect any sample decomposition during ion-exchange.

(A) ZnNa-Y

ZnNa-Y zeolite was prepared from Na-A (B.D.H.) by ion-exchange with 0.1M $ZnCl_2$ (B.D.H., S.L.R.) solution for seven days. The volume of solution was chosen, such that it contained the stoichiometric amount of Zn(II) ions necessary to produce the required degree of ion exchange. If the desired degree of exchange was not achieved after the first exchange, the sample was exchanged in the same manner for a further seven days.

(B) Cu(II)Na-Y

Na-Y (Union Carbide Corporation) was exchanged with 0.4M $CuCl_2$ (Fisons Scientific) solution, the volume of which

contained an excess of Cu(II) ions, for 24h. The sample was found to be 73.2% ion-exchanged with Cu(II) ions by this method. No structural breakdown was found to have occurred during ion-exchange.

3.2 Sampling method and activation of zeolites

Though more recent Fourier transform IR techniques of diffuse reflectance (DRIFT) and photoacoustic (PAS) spectroscopy offer the advantage of little sample preparation, the conventional technique of transmission IR spectroscopy on thin self-supporting discs was chosen. The main reason for this was that quantitative transmission measurements can be routinely made and used to calculate rate constants (see Chapter Four); whereas quantitative DRIFT and PAS is fraught with problems and nothing would have been gained in attempting these more difficult measurements.

To eliminate any effects due to a dilutant, the zeolites were studied in the form of thin self-supporting discs (7-15 mg cm^{-2}). These discs were pressed using a 1.5 cm diameter die at a pressure of 6.7-8.5 tons cm^{-2}, and have a maximum infrared transmission of *ca.* 30%. Though the use of a dilutant, *e.g.* KBr, would increase the transmission of the samples, zeolites have been observed to undergo solid state reactions with KBr as illustrated here for Cu(II)Na-Y. On stirring this zeolite with powdered KBr a brown discolouration of the sample was observed. This indicated the formation of bromine and presumably the reduction of Cu(II)→Cu(I). Figure 3.1 shows the DRIFT spectra of a neat and KBr mixed Cu(II)Na-Y

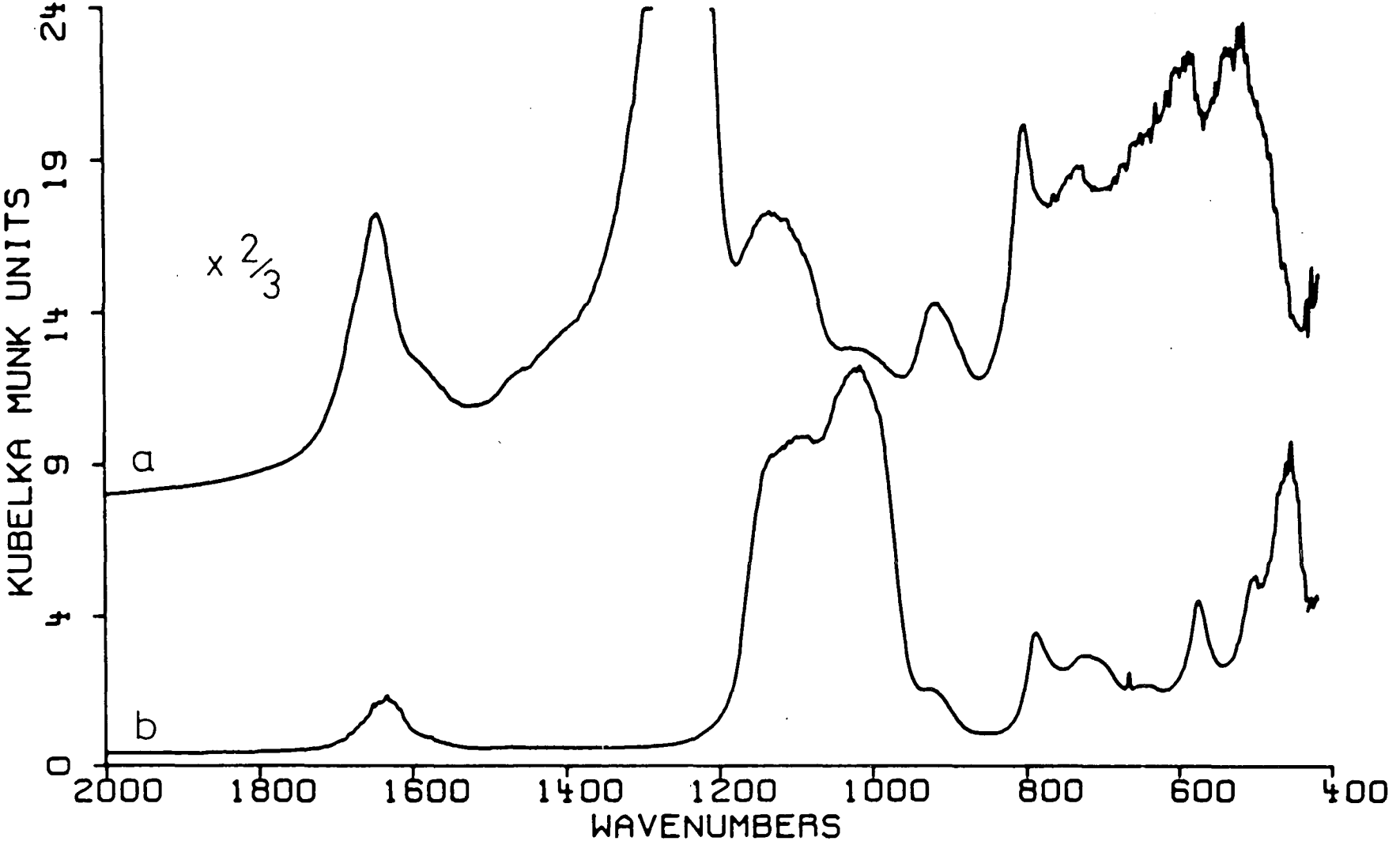

Figure 3.1 Diffuse reflectance spectra of Cu(II)Na-Y

(a) Neat zeolite; (b) Zeolite mixed with KBr. (Y axis displaced).

zeolite, in which shifts are observed in band positions due to the dilutant. Further the use of self-supporting discs eliminates the possibility of interactions between the adsorbate and the dilutant. No effects on the zeolites have been absorbed from the action of pressing the discs.

For adsorption studies of zeolites it is first necessary to activate the samples by heating under vacuum to remove adsorbed water and other impurities (*e.g.* organic residues from the synthesis). In the IR studies described in this thesis the following, *in situ*, procedure was adopted using the cell and vacuum line described in Section 3.3. The zeolite disc was mounted in the cell and placed in the sample compartment of the IR spectrometer, where it remained for the duration of the experiment. The sample was first evacuated to less than 10^{-4} torr, before slowly heating to the desired activation temperature (600-750K) over a period of 1.5-2 hr. After heating under vacuum at this temperature for a number of hours, the sample was cooled to ambient temperature where adsorption studies were undertaken. Full details of activation temperatures and times are given in each chapter.

3.3 The infrared cell and vacuum line

Apart from one glass socket joint used as a gas inlet, the whole system was constructed of high quality stainless steel. Periodically, it was necessary to bake out the system to remove impurities, mainly water, adsorbed on the line walls.

(A) The infrared cell

A diagram of the transmission cell designed by Howard and Kadir[1] is shown in Figure 3.2. This cell has an optical pathlength of 48 mm. The windows (A), which are made of KRS-5 (20mm x 4mm) are sealed with vitron O-rings and a knurled ring (B) and cooled *via* the water jacket (C).

The sample (D) is placed between stainelss steel rings and held in place by a third screw threaded ring (E). A molybdenum wire (F) (99.95%, 0.5mm diameter and 2m in length) insulated by refrasil sleeving is used to heat the sample holder. Electrical contact (G) to a transformer and variac, used to control the heating rate, is made through the feed-throughs in the 70mm flange, which is sealed *via* a copper compression ring (V.G. Scientific). The temperature is monitored *via* a chromel-alumel thermocouple (H), through this flange.

The cell fits into the sample compart of the spectrometer and is connected to the vacuum line *via* an Edward's pipeline valve and a length of flexible tubing at I.

(B) The vacuum line

The vacuum system is shown in Figure 3.3. It is based on a turbomolecular pump, A, (Leybold-Heraeus) with a rotary vane backing pump, B, which can routinely provide a pressure of 10^{-6} torr. All joints in the line, bar one, were made through flanges which are sealed *via* a copper compression ring. Pressure in the system is monitored by one of three gauges:

a = 46mm

b = 48mm

c = 52.5mm

d = 10mm

e = 6.8mm

f = 20mm

h = 74mm

i = 83mm

j = 63.5mm

k = 9mm

l = 12mm

m = 32mm

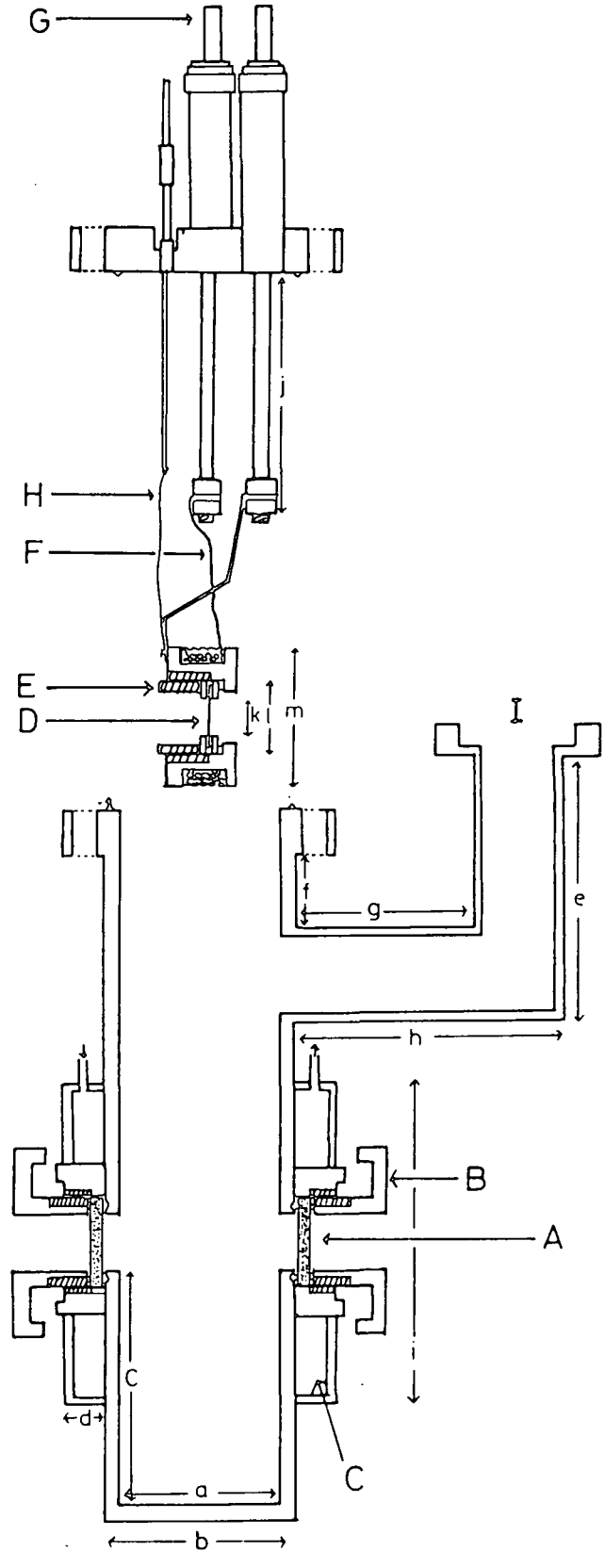

Figure 3.2 The infrared cell

A = Window, B = Knurled ring, C = Water jacket, D = Sample, E = Screw threaded ring, F = Heating wire, G = Electrical contact, H = Thermocouple, I = Connection to vacuum line.

(not to scale).

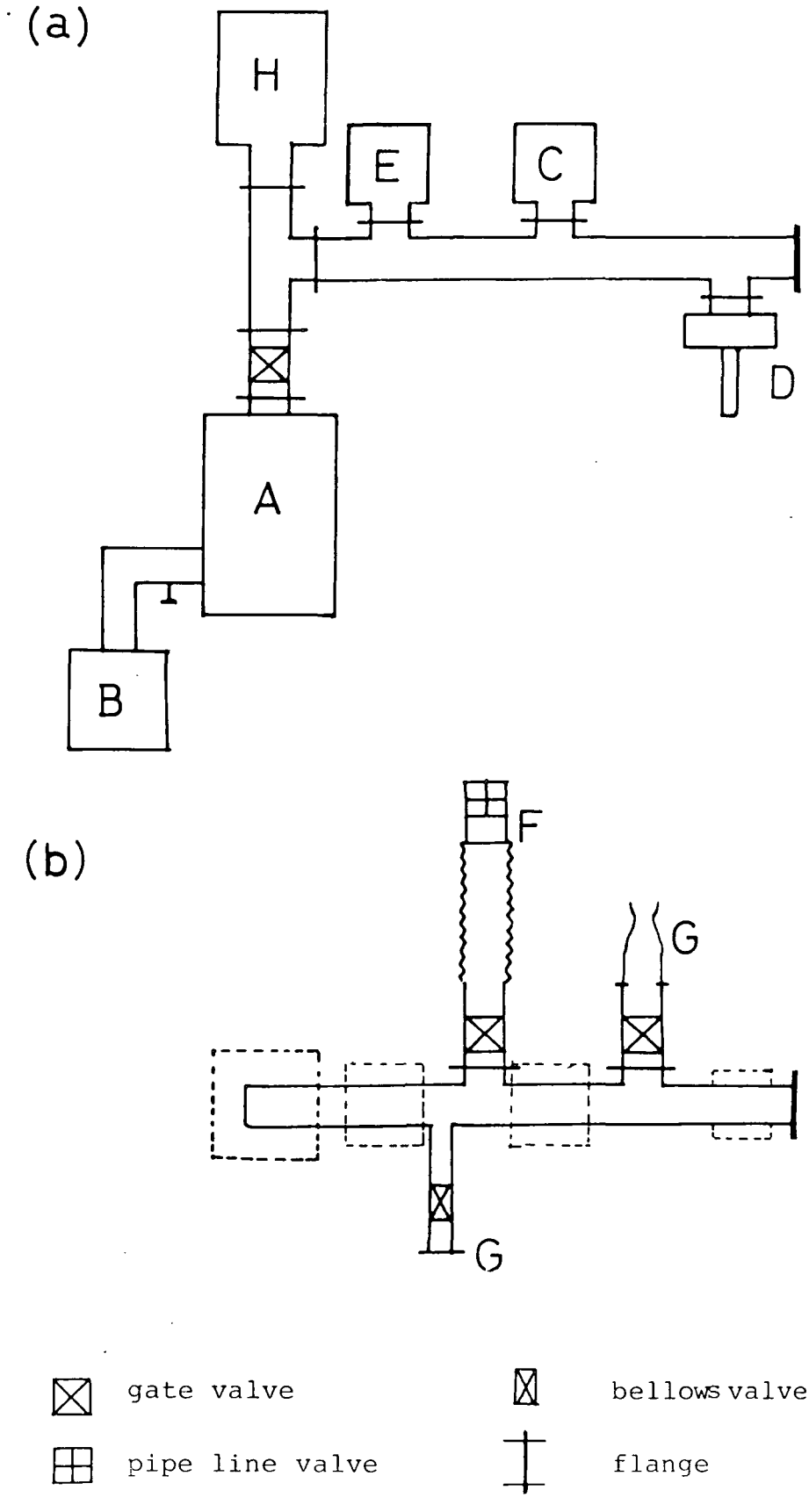

Figure 3.3 The Vacuum line

(a) top view; (b) side view.

A = turbomolecular pump, B = backing pump; C = ion gauge;
D = piranigauge, E = Baratron, F = cell attachment;
G = gas inlet. (not to scale).

(i) A hot cathode ionization gauge (Leybold-Heraeus) $10^{-3} \rightarrow 10^{-9}$ torr (C).

(ii) A Pirani gauge (U.G.) 0.75→760 torr (D).

(iii) A Baratron gauge (MSK Instruments Inc.) 0.1→1000 torr (E).

As the response of a Baratron gauge is independent of the nature of the gas, this gauge was used to measure the pressures of the adsorbate gases and vapours admitted to the zeolite samples.

The cell is attached to the line at F through a length of flexible tubing. Gases or vapours are admitted *via* valves at G.

A quadrupole mass spectrometer, H, (Spectromass 80, Spectrum Scientific) is invaluable in detecting small leaks and impurities in the system.

3.4 Infrared data collection and presentation

3.4.1 The infrared spectrometers

Two IR spectrophotometers were used to collect the data presented in this thesis. As these were both commercial instruments a full description with optical layouts is not given but can be found in the literature available from the manufacturers.[2,3]

(A) The Perkin-Elmer 580B

The PE 580B[2] is a double beam, ratio recording, dispersive IR spectrometer, which uses gratings to scan the IR region between 4000 and 180 cm^{-1}. The source and detector

are a Nernst Glower at 1473K and a vacuum thermocouple with a CsI window respectively. The spectrometer is connected to a Perkin-Elmer 3500 data station, through which it is controlled. The spectra are displayed on a visual display unit (VDU) and the spectral data saved on floppy disc. The data station's other function is to perform data manipulations, such as scale expansion *via* the ABEX command, smoothing, multiple scans and the subtraction of a reference spectrum from a sample spectrum.

The two most common manipulations used were the ABEX and smoothing commands. The ABEX command is used to expand a weak spectrum and is equivalent to running a spectrum with a sample of increased concentration. The smoothing routine is used to remove spectral noise. An investigation of the order of performing these two commands revealed that the same degree of expansion was not achieved in each case (Figure 3.4). A standard was adopted by which the ABEX command always preceded the smoothing command.

For studies of zeolites the spectrometer was operated with a scan time of 10 min. (4000-180 cm^{-1}) and a corresponding maximum resolution of 2.3 cm^{-1}.

Only a small fraction of the data collected by this instrument is presented in the following chapters, as the second instrument, a Nicolet 60SX, with the advantages of Fourier transform infrared spectroscopy (FTIR), allowed data of a higher quality to be obtained.

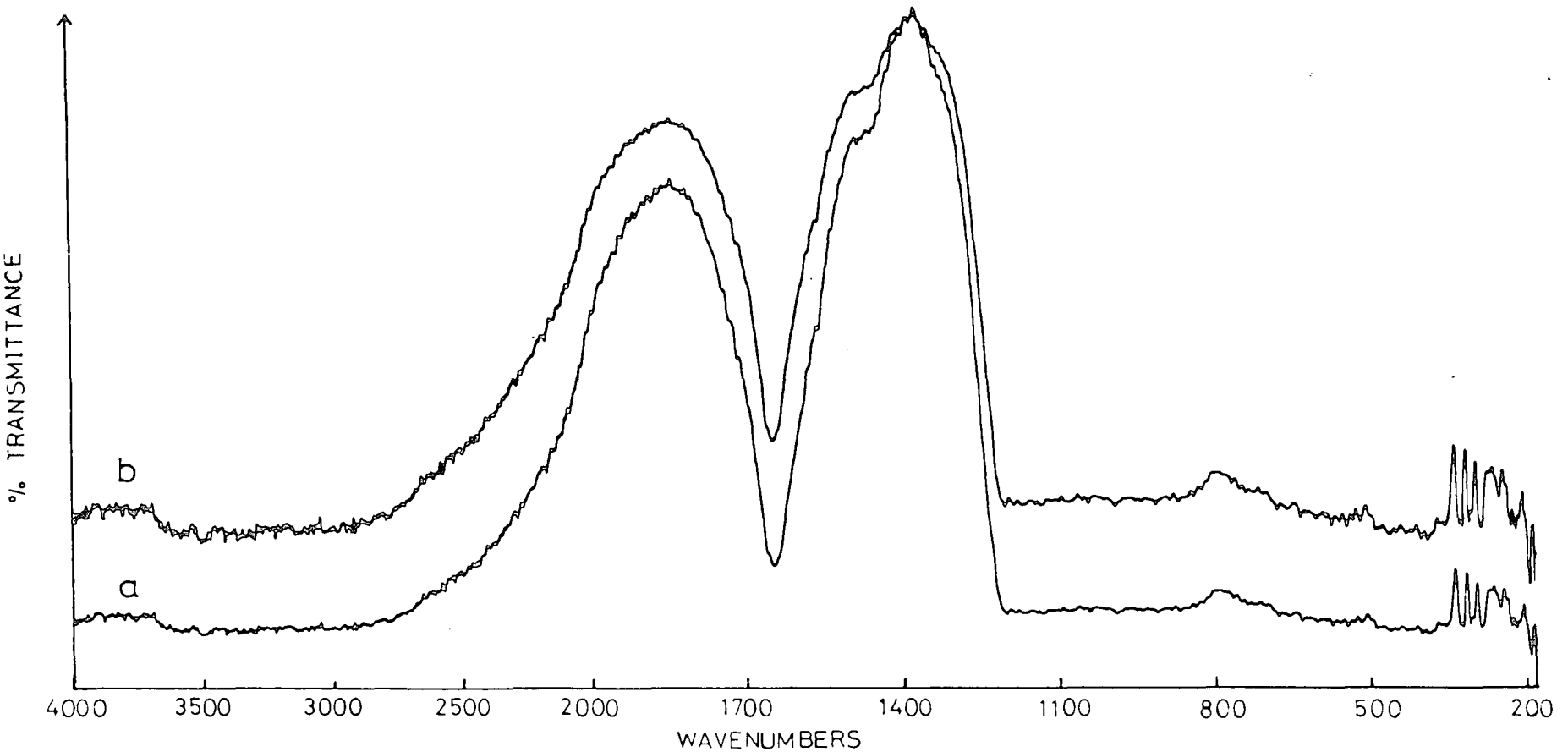

Figure 3.4 The effect of the ABEX and smoothing command order on spectral data

(a) ABEX then smooth;

(b) Smooth then ABEX.

(B) The Nicolet 60SX Fourier transform Spectrometer

The Nicolet 60SX FTIR Spectrometer[3] is a mid-IR instrument based on a Michelson interferometer, a simplified diagram of which is shown in Figure 3.5. The Michelson interferometer consists of three components: the beam splitter (B), a fixed mirror (C) and a moving mirror (D). Radiation from the Globar source impinges on the KBr beam splitter, which has the property of transmitting half the light to mirror (C), and reflecting the remainder to mirror (D). As the two beams are reflected from the mirror surfaces they recombine at the beam splitter where constructive and destructive interference occurs, depending on the position of the moving mirror relative to the fixed mirror. The resulting beam passes on through the sample to the liquid nitrogen cooled mercury-cadmium-telluride (MCT) detector.

Let us consider the detector output if a monochromatic source, *e.g.* a Laser, is used. When the moving mirror is in such a position that the distance between it and the beam splitter, B-D, is the same as that between the beam splitter and the fixed mirror, B-C, the two reflected beams would be in phase with each other and interfere constructively. At this point of zero path difference (ZPD), the detector signal would be a maximum. When the moving mirror moves to a position such that B-D is 1/4 wavelength (λ) greater than B-D, the total path difference between the two beams would be $\lambda/2$. The two beams would then be 180^{o} out of phase and would interfere destructively. The detector signal would then be a minimum. Thus, for monochromatic radiation as the position of the moving mirror changes, the signal reaching the

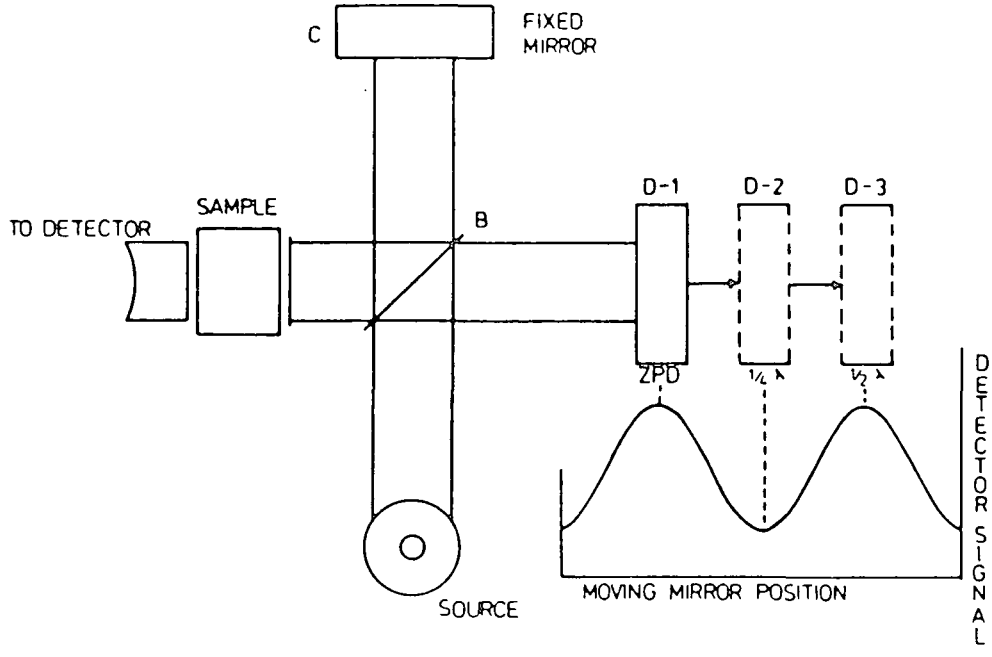

Figure 3.5 A Michelson interferometer

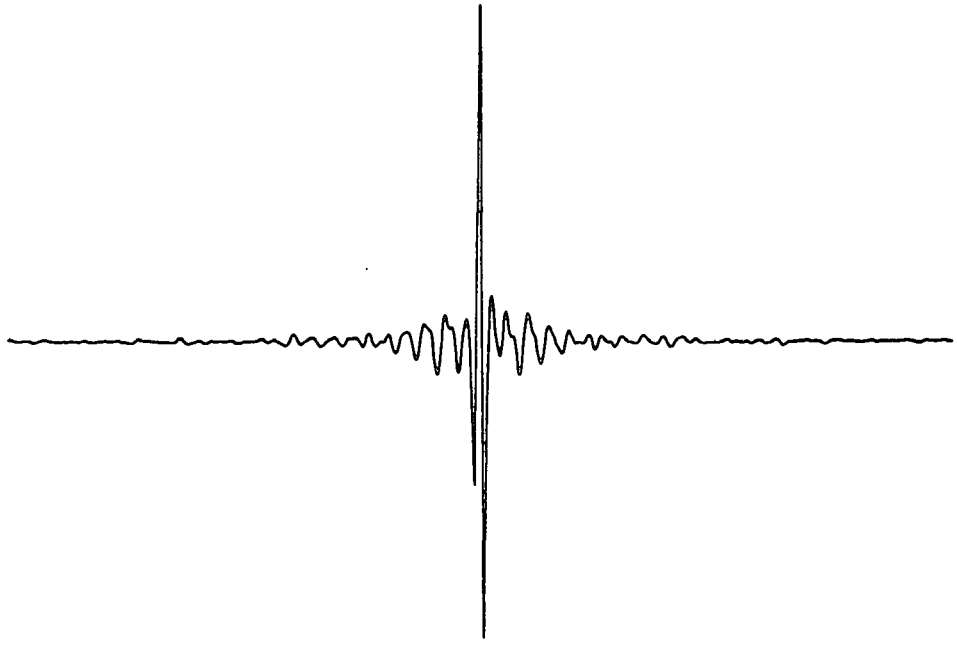

Figure 3.6 Typical interferogram

detector is a modulated sine wave (Figure 3.5), the frequency of which is determined by the velocity of the moving mirror.

This same process occurs for every frequency of the broadband IR source. The resultant detector signal for all the frequencies is called an interferogram (Figure 3.6), *i.e.* the summation of all of the modulated sine waves. A theoretical interferogram would be symmetrical about the point of zero path difference, but in practice, as shown in Figure 3.6, this is not the case.[4] The asymmetry arises because the refractive index of the beam splitter is a function of frequency which introduces a small but unique phase shift for each frequency.

The interferometer can be thought of as a means of encoding the initial frequencies into a form that the detector can observe. From the interferogram, $I(\alpha)$, the spectral intensity, $G(\tilde{\nu})$, at each wavenumber $(\tilde{\nu})$ is obtained by means of the Fourier transformation,[8]

$$G(\tilde{\nu}) = \int_{o}^{x_{max}} I(\alpha) \cos (2\pi\nu x) dx.$$

where x is the path difference between the two mirrors. This mathematical computation is carried out by the computer which controls the interferometer. Theoretically, the interferogram is infinitely long, but in practice it is truncated so that data outside the region of interest is ignored. In the Nicolet system[3] this is done by means of an apodization function. This minimizes the distortions in the spectrum, such as side bands due to the effects of truncation. The

Nicolet system routinely uses the Happ-Genzel function,

$$0.54 + 0.46 \cos \frac{\pi}{2} \frac{|n_i - Z|}{NDP-2}$$

where n_i is the displacement of point i from the start of the scan, Z is the location of ZPD and NDP the number of data points. Each point in the interferogram is multiplied by this function before the Fourier transform is calculated.

Once the Fourier transform has been calculated, a single beam spectrum (Figure 3.7) is obtained by a phase correction which allows for the fact that the refractive index of the beam splitter is frequency dependent and that the ZPD is not necessarily the first point in the spectrum.

An important feature of the interferogram is that every data point collected contains information over the entire IR region. In essence, the detector is observing all frequencies at all times. This, along with several other features of FTIR spectroscopy leads to some distinct advantages over dispersive instruments.[3,4] These are outlined below:

The Felgett or multiplex advantage.[3,4] In a dispersive instrument each resolution element (M) is only observed for a fraction of the scan time, whereas in an interferometer all frequencies are viewed by the detector simultaneously. The signal to noise ratio ($^{S}/_{N}$) of an interferometer is proportional to $T^{\frac{1}{2}}$, where T is the total observation time. In a dispersive instrument the $^{S}/_{N}$ ratio is proportional to $(^{T}/_{M})^{\frac{1}{2}}$. Thus an interferometer has an advantage of $M^{\frac{1}{2}}$ over a dispersive instrument. This can be viewed in two ways. Firstly a $^{S}/_{N}$ ratio equivalent to that of a dispersive instrument may be obtained in a fraction of the time, and secondly an improved

$^{S}/_{N}$ ratio may be obtained if scans are co-added for the time equivalent to the dispersive scan.

The Jaquinot or throughout advantage.[3,4] Because an interferometer has no slits to define the resolution, the energy reaching the detector is limited by the size of the mirrors and the interferometer. In a dispersive instrument the slits of few tenths of a millimeter mean that only a small fraction of the light incident on the sample reaches the detector.

The Connes advantage.[3] The internal reference Laser used to monitor the position of the moving mirror, is also used as an internal wavelength calibration. No external wavelength calibration standard is therefore needed.

The straylight advantage.[3] Because the interferometer modulates each IR frequency differently there is no equivalent of stray light in FTIR. This means that absorbance values remain linear even beyond three absorbance units.

No emission contributions.[3] The detector of the FTIR system responds to audio frequencies resulting from the modulation of the IR frequencies by the interferometer. Because the sample is located after the interferometer, any IR radiation emitted from the sample will not be modulated and consequently will not be detected.

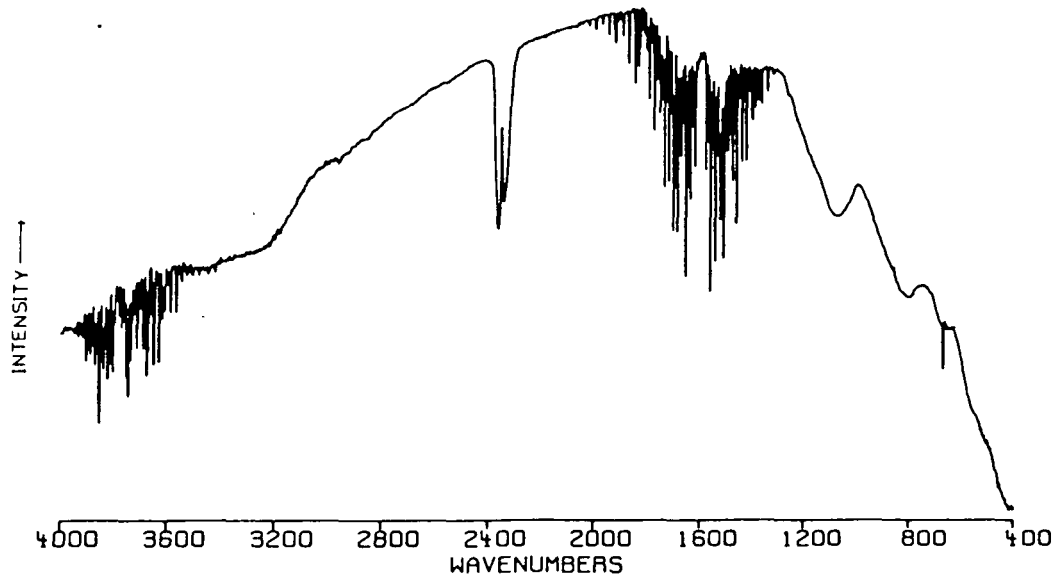

Figure 3.7 A FTIR single beam instrument background spectrum

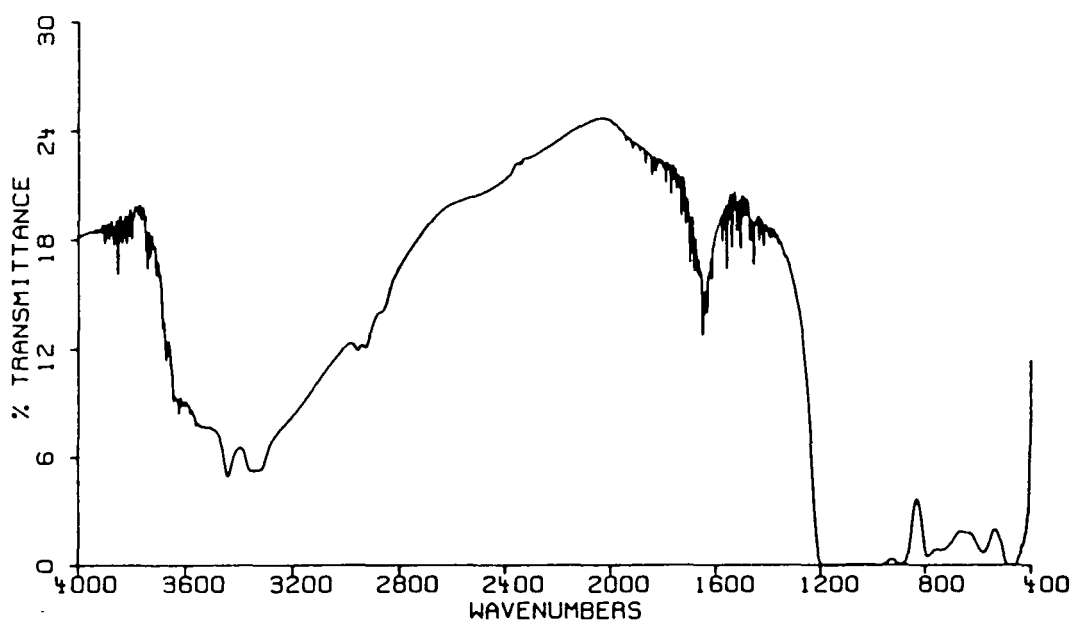

Figure 3.8 A FTIR transmittance spectrum of a hydrated zeolite

To obtain a spectrum in percentage transmittance from single beam data, the sample file is ratioed against a single beam background spectrum. In all the FTIR data presented in this thesis the background spectrum used was that of the spectrometer with no sample in the beam (Figure 3.7). This will give a sample spectrum in transmittance as shown in Figure 3.8 for a hydrated zeolite.

One disadvantage of a purged compared with an evacuable spectrometer is that in the purged instrument the concentrations of H_2O and CO_2 usually vary with time. Thus ratioed spectra will still contain contributions from these gases, since the data are necessarily collected at different times. These absorption bands may be removed by subtracting the spectrum of H_2O and CO_2 in absorbance units (Figure 3.9) from the sample spectrum in the same units, using the interactive subtraction routines supplied with the instrument. The results for a zeolite sample is illustrated in Figure 3.10. The computer attached to the instrument also allows many other data manipulations to be performed, such as peak-picking, deconvolution, background corrections, *etc.*[3]

One of the advantages of using FTIR spectroscopy to study catalytic systems is that the rapid scan rate of the instrument allows species which are undergoing change, to be followed as a function of time. The scan rate is governed by a number of parameters, principally the mirror velocity, the retrace time of the mirror and the detector response. The choice of these parameters affects the $^{S}/_{N}$ and the resolution of the spectra, such that a high scan rate will result in a trade-off in $^{S}/_{N}$ and resolution.

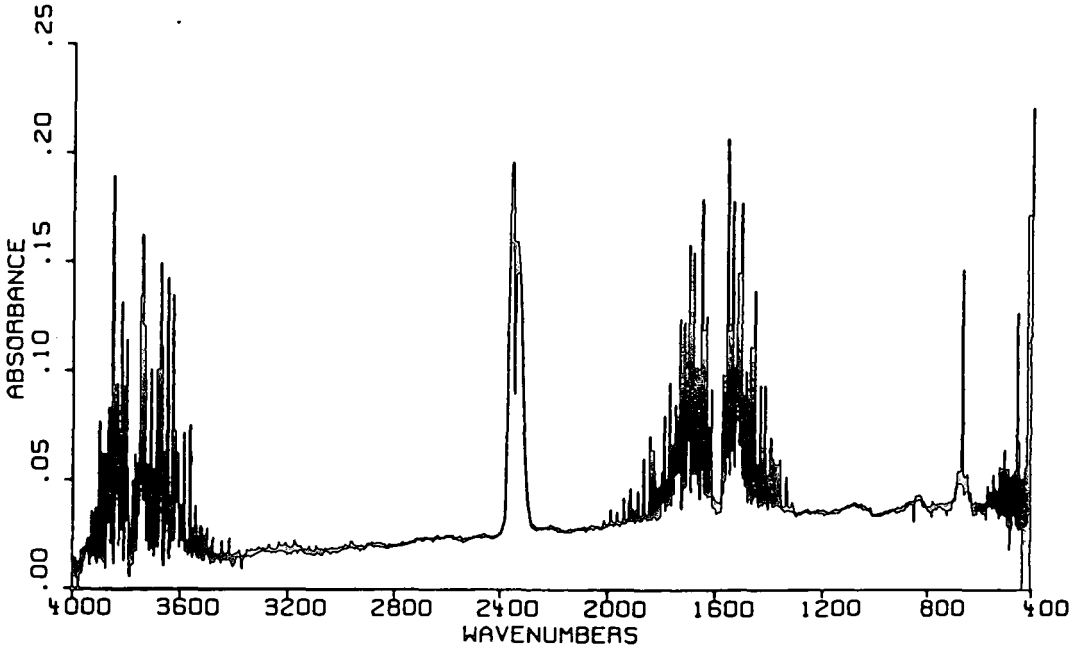

Figure 3.9 The FTIR spectrum of atmospheric water vapour and carbon monoxide

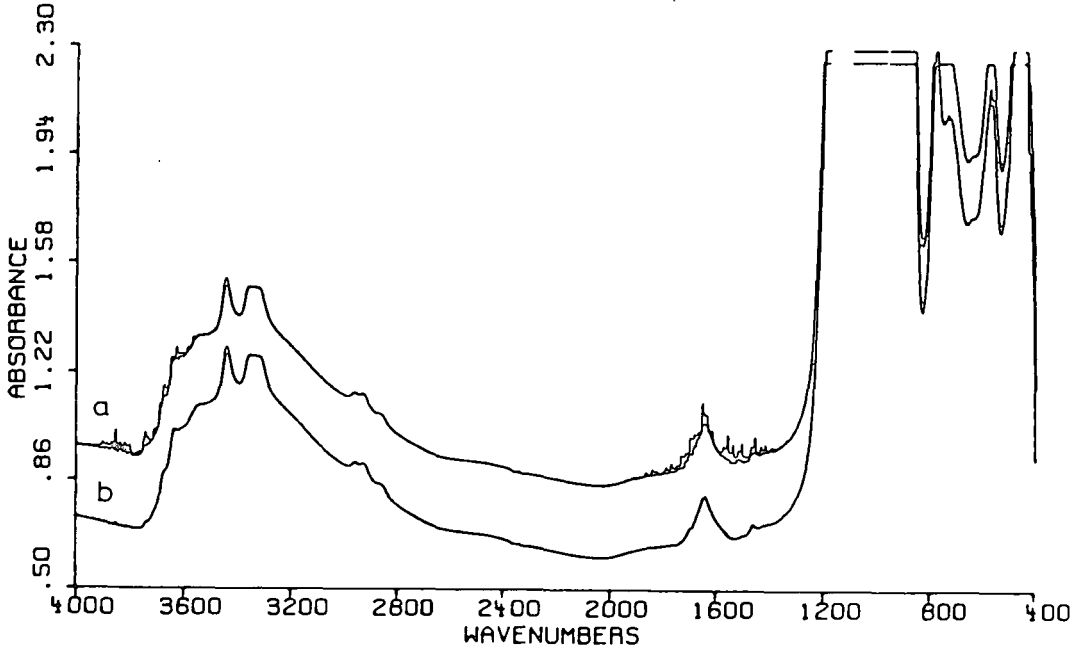

Figure 3.10 The subtraction of atmospheric water vapour and CO_2 from a sample spectrum

Hydrated zeolite (a) before subtraction of H_2O (vapour) and CO_2 and (b) after subtraction of H_2O (vapour) and CO_2.(Y axis displaced).

The mirror velocity (V) governs the modulation frequency (F) of the IR radiation of wavenumber $\bar{\nu}$, through the relationship:

$$F = 2V\bar{\nu}$$

Thus the modulation frequency range must be set, such that it falls within the range of maximum response from the detector. This will optimize the $^{S}/_{N}$ ratio in the spectrum. The broad band MCT detector used in the present study functions best at high audio-frequencies (900-50,000Hz), *i.e.* at high mirror velocities. The 60SX system was therefore routinely operated with a mirror velocity of 1.570 cm sec^{-1}. If slower mirror velocities had been used, a triglycine sulphate (TGS) detector would have been preferred. A TGS detector has maximum response at low audio frequencies (10-500Hz). If the scan rate chosen is too high, it is possible for some resolution to be lost, as the instrument will be unable to deal with the high rate of data conversion. Thus the scan rate (mirror velocity) must be chosen to optimize both $^{S}/_{N}$ and resolution.

The advantages of obtaining a spectrum with a good $^{S}/_{N}$ ratio in a reasonably short time is illustrated in Figure 3.11. Here the very weak absorption bands (*ca.* .015 abs. units) of the adsorbed species are clealy visible above the background. This means that FTIR spectroscopy enables the study of species present in very low concentration. This is very important in the study of reacting systems.

In an FTIR spectrometer the resolution is governed by how far the mirror travels from the point of ZPD. Under ideal conditions, the resolution is the inverse of the maximum

optical path difference.[3] In the Nicolet 60SX[3] an alternative approach is used. The resolution is defined by the number of data points taken. Using the sampling theorem,[3] two data points must be present for every resolution element, *i.e.* for a resolution of 4 cm^{-1} there would be a data point every 2 cm^{-1}. Thus the resolution is controlled by the file sizes through the computer, and not by the movement of the mirror which is fixed at a displacement greater than the maximum resolution available. The resolution in the Nicolet 60SX system may therefore be easily varied.

During the collection of data there exists the possibility that a bad interferogram will be collected. So that this interferogram is rejected, a correlation test is used to check the newly acquired interferogram against the signal averaged interferogram. This test preserves the S/N ratio of the spectrum.

In setting up the Nicolet 60SX to collect data, a number of parameters have to be chosen, such as iris, number of scans, resolution (no. of data points), electronic filters, mirror velocity, *etc.* Some parameters, such as the number of scans are chosen for each individual experiment, but others, *e.g.* electronic filters, mirror velocity are set to standard values to allow an accurate comparison between spectra. In the data presented in this thesis a scan rate of *ca.* 2 scans per second (mirror velocity = 1.570 cm sec^{-1}) was chosen. The electronic filter settings used (4 and 13) were those recommended by Nicolet[3] for the 4000-400 cm^{-1} range. The instrument resolution was fixed at 2 cm^{-1}. The iris setting used was that chosen during the alignment of the instrument.

The choice of the number of sample scans (NSS) was dependent upon how rapidly the system understudy was changing. To avoid a wide variation, a few standard values were used, which gave the following approximate scan times (start of scan to end of scan).

NSS	Scan time (sec.)	NSS	Scan time (sec.)
16	9	128	60
32	16	256	120
64	31	512	238

The number of scans chosen for the background spectrum (NSB), should give approximately the same noise level as in the sample spectrum. Unless otherwise stated, NSB=128 and NSS=512.

3.4.2 Data presentation

All the spectra presented in this thesis are in absorbance units *versus* wavenumber (cm^{-1}). The computers of both instruments calculate the absorbance (A) spectrum from the % transmission (T) spectrum using the relationship:

$$A = \log_{10} \left(\frac{T}{100}\right)$$

Absorbance units were chosen because they are proportional to concentration, *viz.*

$$A = -\varepsilon C \ell$$

where ε is the extinction coefficient, C is the concentration and ℓ is the thickness of the sample. Thus rate calculations may be performed from spectral intensities.

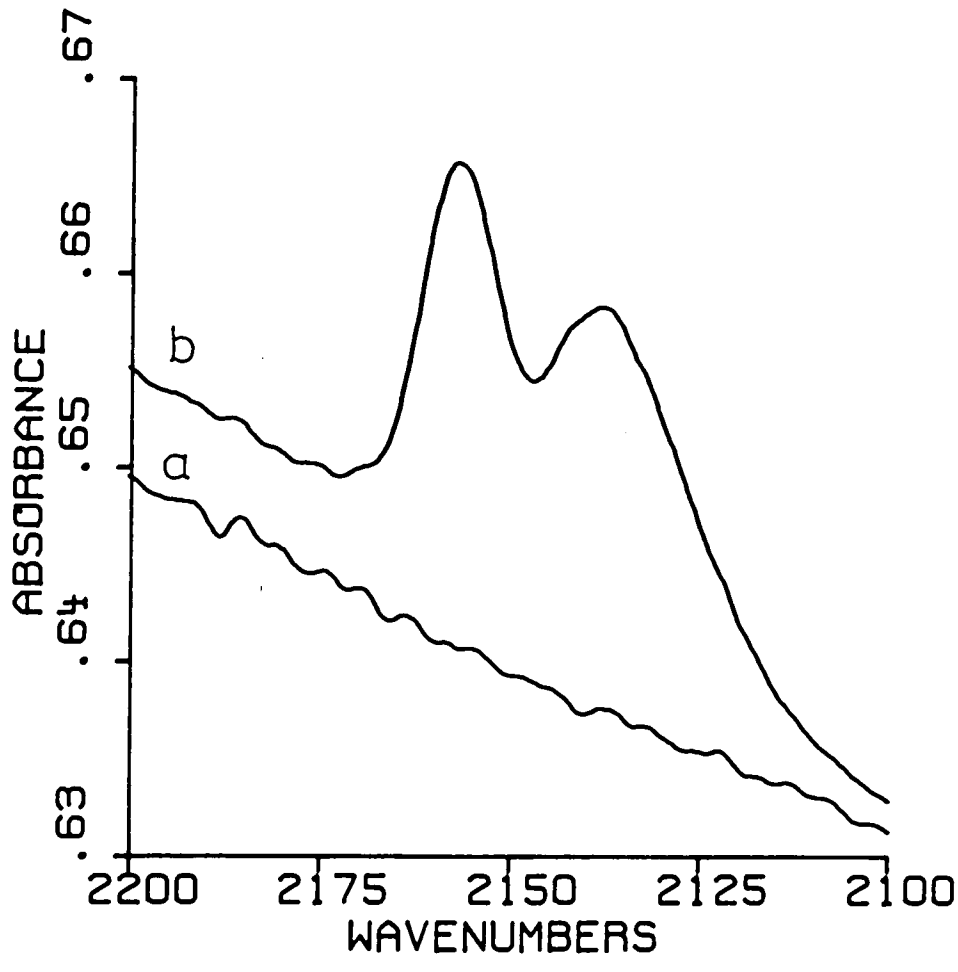

Figure 3.11 The FTIR spectrum of CO adsorbed on hydrated Cu(II)Na-Y zeolite

(a) Zeolite background;

(b) Zeolite with adsorbed CO.

The spectra of a hydrated zeolite in transmission and absorbance units were shown in Figures 3.8 and 3.10. From these spectra it can be seen that zeolites are highly absorbing materials. Typically, even for very thin discs, in the region 4000-1200 cm^{-1} only between 10-30% of the incident radiation is transmitted. Below 1200 cm^{-1} very strong absorptions due to framework vibrations occur. These are far more intense than vibrations due to adsorbed species and in fact even in very thin discs often lead to regions of total absorptions of light. Thus in the data presented only the 4000-1200 cm^{-1} region will generally be discussed.

In the spectra of zeolite-adsorbate systems the contribution from the adsorbed species varies considerably. An example (Figure 3.11) has already been given of very weak adsorbate bands, which are only just observable above the background. In contrast examples of zeolite-adsorbate spectra are given in Figure 3.12, to show the more usual band intensities encountered in studies of adsorbed species.

In some spectra, *e.g.* Figures 3.12 (i) and (ii) both the zeolite background and adsorbed species spectra have hydrocarbon band at *ca.* 2850, 2918 and 2960 cm^{-1}. These bands are due to the detector and not to species adsorbed within the zeolite framework. They arise because the alignment of the IR beam in the sample and reference beams are not identical and hit the detector in two slightly different positions. The absorptions from hydrocarbons in the anti-reflection coating on the detector window and from the detector support glue which creeps around the detector with ageing, are not therefore ratioed out. When the C-H stretching region of adsorbed

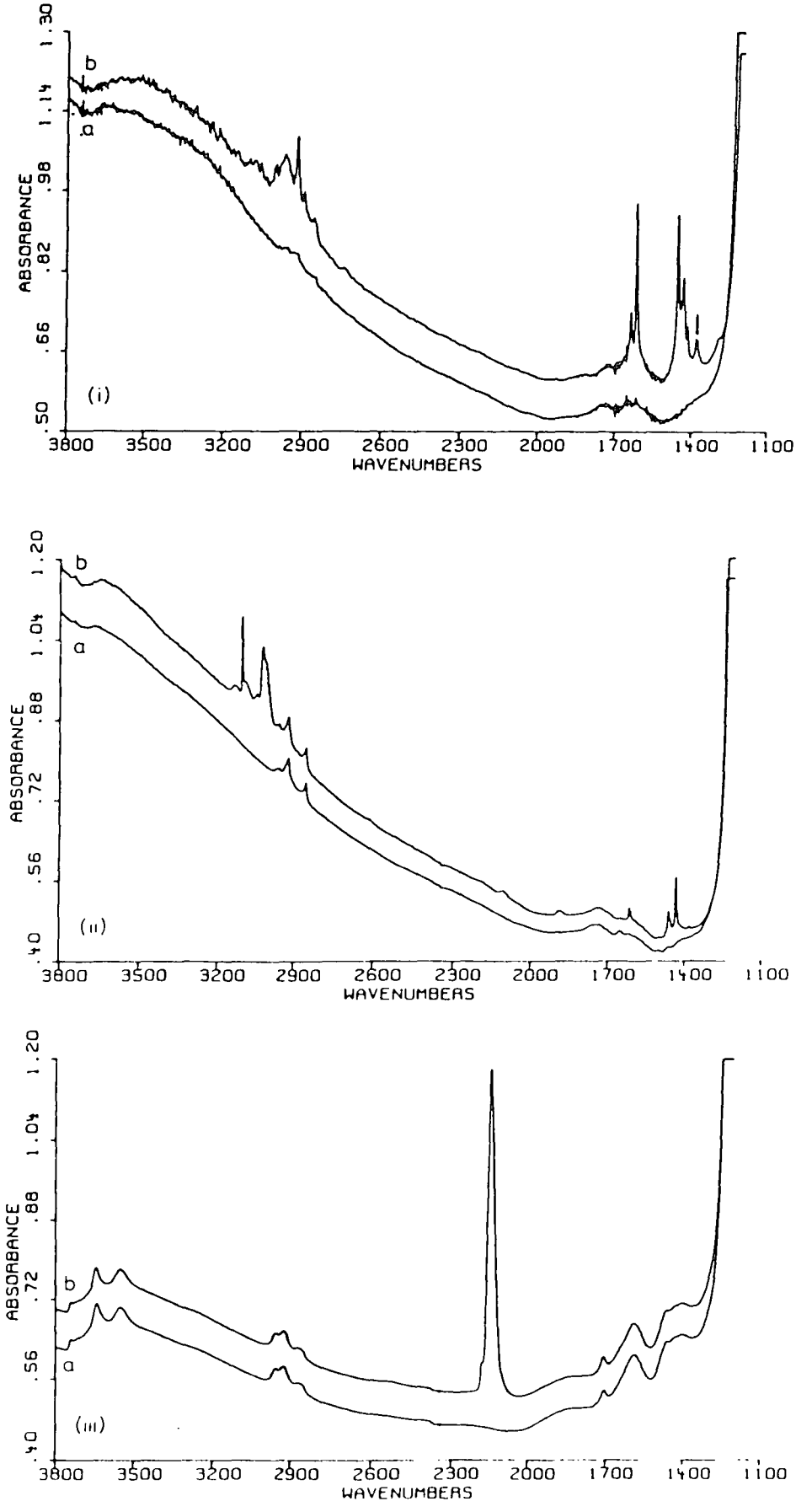

Figure 3.12 The FTIR spectra of Zeolite adsorbate systems

(i) ZnNa-A + propene, (ii) ZnNa-A + Cyclopropane,

(iii) Cu(II)Na-Y + CO.

(a) degassed Zeolite; (b) Zeolite + adsorbate.
(Y axis offset).

species needs to be examined, the zeolite background is subtracted from the spectrum of the adsorbed species to remove these absorption bands.

REFERENCES

1. Howard, J and Kadir, Z.A., unpublished work.

2. Model 580B Infrared spectrophotometer operators manual, Perkin-Elmer Ltd., England (1977).

3. Model 60SX instruction manuals, Nicolet Instrument Corporation, Madison, Wisconsin, U.S.A.

4. Griffiths, P.R., "Chemical Infrared Fourier Transform Spectroscopy", John Wiley, New York, 1975.

CHAPTER FOUR

CYCLOPROPANE ISOMERIZATION OVER Zn EXCHANGED A ZEOLITE

4.1 Introduction

4.1.1 Cyclopropane Adsorption

The isomerization of cyclopropane (c-C_3H_6) is a commonly used test reaction for the catalytic activity of oxides[1-7] and zeolites,[8-13] as in the simplest case, structural isomerization occurs with the formation of only one reaction product, propene (C_3H_6).

Brönsted acid sites have been proposed in many studies as the active centers,[6-10] the reaction occurring *via* "edge-on" or "face-on" protonation of c-C_3H_6 to form the non-classical carbonium ion, *viz.*

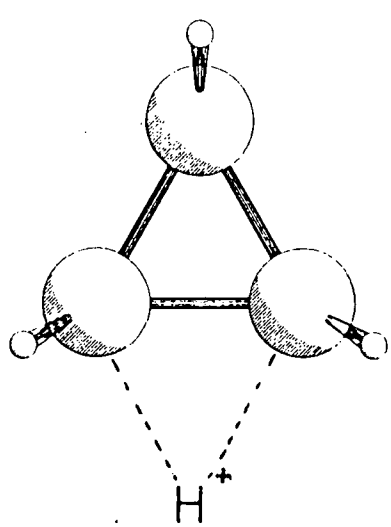

"EDGE-ON"

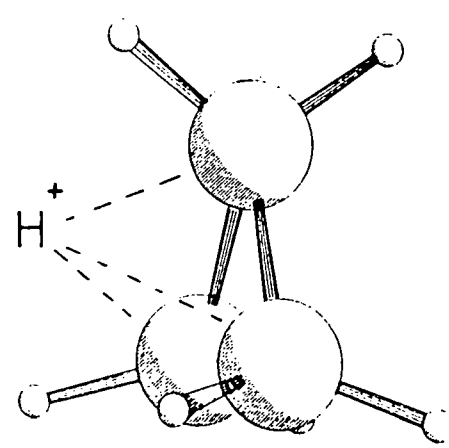

"FACE-ON"

In agreement with this Basset and Habgood[11] showed that on Na-X zeolite the rate of c-C_3H_6 isomerization to C_3H_6 was influenced by the degree of sample dehydration. An increase in the dehydration temperature caused a loss of catalytic

activity, which was restored by exposing the samples to water vapour at lower temperatures. This showed that water or more probably protons, in the form of hydroxyl groups (Brönsted acid sites) are essential to the formation of the reaction intermediate.

For type A zeolites, in which Brönsted sites are either absent or in very low concentrations, Lewis acid sites, *i.e.* the cations, have been shown to be the active centres.[14,15] Propene was identified as the only isomerization product. In contrast different workers studying $c\text{-}C_3H_6$ isomerization on Y type zeolites, which contain a large number of Brönsted centres, have identified a variety of reaction products and proposed a number of mechanisms (Table 4.1). An explanation of this lies in the different zeolite batches, sample pre-treatments and reaction conditions employed which influence the Brönsted acidity of the samples.

In a recent study, using IR spectroscopy, Förester and Seebode showed that $c\text{-}C_3H_6$ was sorbed face-on to the cations in some partially ion-exchanged type A zeolites (Ca^{2+}, Co^{2+}, Mg^{2+}, Zn^{2+}).[14] By following the appearance of the ν(C=C) stretching vibration of adsorbed C_3H_6, the rate of isomerization was found to be greatest for those zeolites containing cations with the greatest polarizing power ($Ca^{2+}<Mg^{2+}<Zn^{2+}<Co^{2+}$). Thus, in the absence of Brönsted sites and reaction by-products, they proposed that the cations were acting as Lewis acids, polarizing the electron density of the sorbed $c\text{-}C_3H_6$ and activating it towards isomerization. Furthermore the rate of isomerization was found to be increased by the co-adsorption of SO_2.

TABLE 4.1 A summary of the isomerization products of Cyclopropane on Y type zeolites

Zeolite	Technique	Reaction temperature	Products	Reference	Comments and Mechanisms
H-Y	IR	RT	isobutane	8	Participation of structural OH groups established. 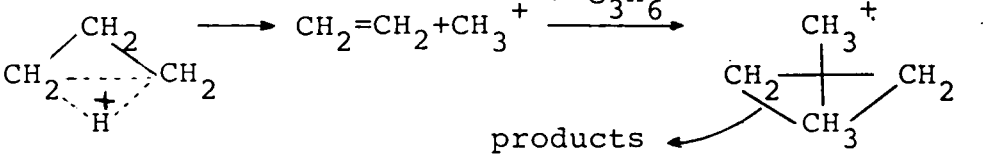 Ethyne was not identified in the reaction products.
		473K	C_3H_6 + aromatics		
Na-Y and HNa-Y	Mass spectrometry and NMR	558K	C_3H_6 only product	9	Deuterium labelling of acid sites. 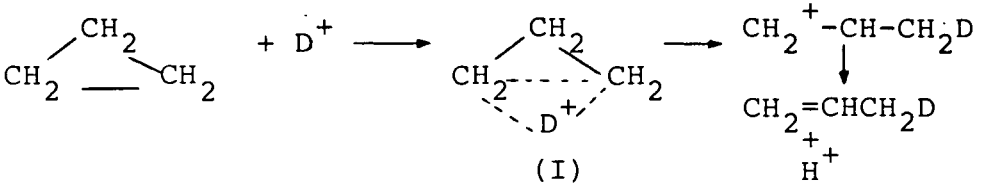 ((I) is in equilibrium with all its isomers)
NaH-Y	Gas chromatography	398K	isobutane major product. (2-Methylpentane, heptane and C_3H_6 identified if long reaction times used)	10	Concentration of propene found to reach a maximum and then decrease, showing that it was a reaction intermediate. The Oligomerization-isomerization-cracking mechanism was proposed.

Although Förester *et al*[14] observed the formation of C_3H_6 within 30 minutes of c-C_3H_6 adsorption on $Co_{4.5}Na_3$-A zeolite using IR spectroscopy, studies by X-ray diffraction[16] and inelastic neutron scattering[17] have shown stable c-C_3H_6 adsorption complexes to be formed in partially Co and Mn ion-exchanged Na-A zeolite. A rationalization of these apparently contradictory results is needed. In the case of the inelastic neutron scattering studies,[17] known quantities of c-C_3H_6 were always adsorbed at submonolayer coverages. Adsorption was therefore always on selective sites within the supercages. This, coupled with the experimental conditions of cooling the samples to temperatures of 77K or below in under 1 hour, could explain the observation of stable c-C_3H_6 complexes. The IR data in contrast was collected at ambient temperatures with an excess of gaseous c-C_3H_6 always in contact with the samples. Important features in the single crystal X-ray diffraction work of Seff *et al*[16] were the extremely large thermal ellipsoids of the carbon atoms, the very long metal-carbon distances obtained (Mn-C and Co-C, 3.09 and 2.81Å respectively) and the apparent shortening of the C-C bonds to 1.1Å on adsorption (1.51Å in the gas phase). This, together with the c-C_3H_6 pressures of one atmosphere which were in contact with the samples for several days, and the location of eight c-C_3H_6 ligands in each supercage, leads us to doubt the validity of this work especially considering the rapid isomerization observed by IR spectroscopy.

4.1.2 Propene Adsorption

Unlike c-C_3H_6, C_3H_6 frequently forms stable sorption complexes on catalyst surfaces.[14,18-27] Adsorption occurs either through the formation of a σ or π bond between C_3H_6 and a surface site or by the loss of H^+ or H^- to form an allyl complex. Infrared spectroscopy may be used to distinguish between these two species, by the shift of the ν(C=C) vibrations of C_3H_6 from its gas phase value (1647 cm^{-1}) and the appearance of surface hydroxyl groups.

For an allyl species (dissociative adsorption) the (C=C) mode of C_3H_6 is replaced by a (C---C---C) vibration which is observed below 1600 cm^{-1}. This is accompanied by the appearance of hydroxyl groups at *ca.* 3600 cm^{-1}. For example on ZnO[20] these modes are observed at 1545 cm^{-1} (ν(C---C---C)) and 3985 cm^{-1} (ν(OH)).

Weakening of the C_3H_6 double bond by σ or π bonding (non-dissociative adsorption) to the surface sites (usually a metal cation) causes the ν(C=C) vibration to shift[14,20-23] to between 1630 and 1540 cm^{-1}.

A number of IR studies of C_3H_6 adsorbed on zeolites have been reported,[14,18,19] showing complex formation with the charge compensating framework cations. Förester *et al*,[14] at high degrees of pore filling on ion exchanged A type zeolites (Co^{2+}, Mg^{2+}, Zn^{2+}), identified a Na^+-C_3H_6 complex in addition to the transition metal-C_3H_6 complex. A similar result has also been observed on CoNa-X zeolite.[19] On these A type zeolites adsorption was always non-dissociative.

In the work reported here, we have investigated the adsorption of C_3H_6 and c-C_3H_6 on partially Zn-exchanged type A zeolite. The aim of this study was to examine the complex formed between C_3H_6 and the cations (Zn^{2+} and Na^+) and to investigate the effect of pressure on the rate of c-C_3H_6 isomerization. This work was started before the report of a similar study on A type zeolites, by Förester and Seebode,[14] appeared in the literature.

4.2 Experimental

$Zn_{4.5}Na_{3.0}$-A zeolite was prepared and analysed as described in Chapter Three and is referred to here after as ZnNa-A. Na-A, for the propene adsorption experiments was obtained from BDH.

Cyclopropane (99.7%, Matheson Ltd., U.S.A.) and propene (99% Argo International Ltd., U.K.) were purified by the freeze-pump-thaw technique before use.

Dehydration, adsorption, *etc.*, were carried out *in situ* (see Chapter Three). A summary of the experimental conditions is given in Table 4.2. In the c-C_3H_6 isomerization experiments the gas pressure in contact with the sample was not altered after the initial adsorption. Data collection for the first spectrum (16 scans, 8.4 seconds) was completed within 30 seconds of the c-C_3H_6 adsorption. Where relevant, in the spectra which follow, the data collection time is shown in brackets after the time at which data collection was started.

TABLE 4:2 A Summary of Dehydration and Adsorption Conditions used for the ZnNa-A and Na-A Zeolites

Sample	Maximum Temperature (K)	Dehydration time * (hours)	Pressure of adsorbate (t'orr)	
			C_3H_6	c -C_3H_6
NaA	738	33	5-40	-
NaA	753	15.5	7-40	-
ZnNaA	738	13.3	5-20	-
ZnNaA	743	39	-	5.2
ZnNaA	748	36.5	-	32.5

* Total time at maximum temperature.

4.3 The Crystal Structure of ZnNa-A

No crystal structure of dehydrated $Zn_{4.5}Na_{3.0}$-A has been published. However, the X-ray structure of $Zn_{5.0}Na_{2.0}$-A has been reported.[28] The cation locations are summarized in Table 2.7 and will be similar in our zeolite.

4.4 Results and Discussion

4.4.1 Dehydration

Typical spectra obtained during the dehydration of ZnNa-A and Na-A zeolites are shown in Figures 4.1 and 4.2 respectively. Before dehydration two sets of features are observed,

(i) a broad intense band at 3750-3000 cm^{-1};

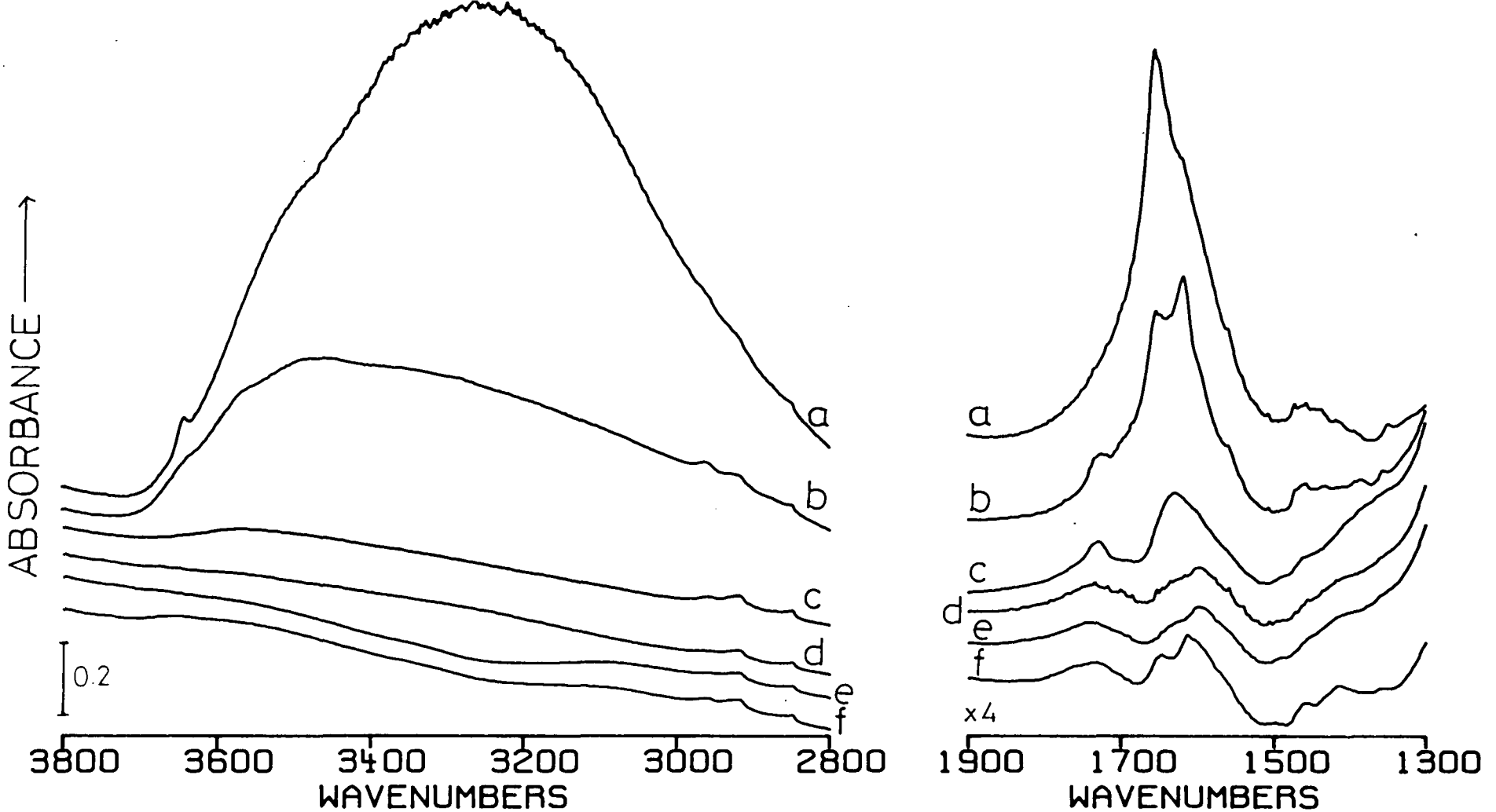

Figure 4.1 The dehydration of ZnNa-A zeolite

(a) Zeolite at ambient temperature under vacuum. Sample heating at (b) 473K, (c) 728K, (d) 748K for 15 hours and (e) 748K for 36 hours, (f) sample cooled to ambient temperature. (Y axis offset)

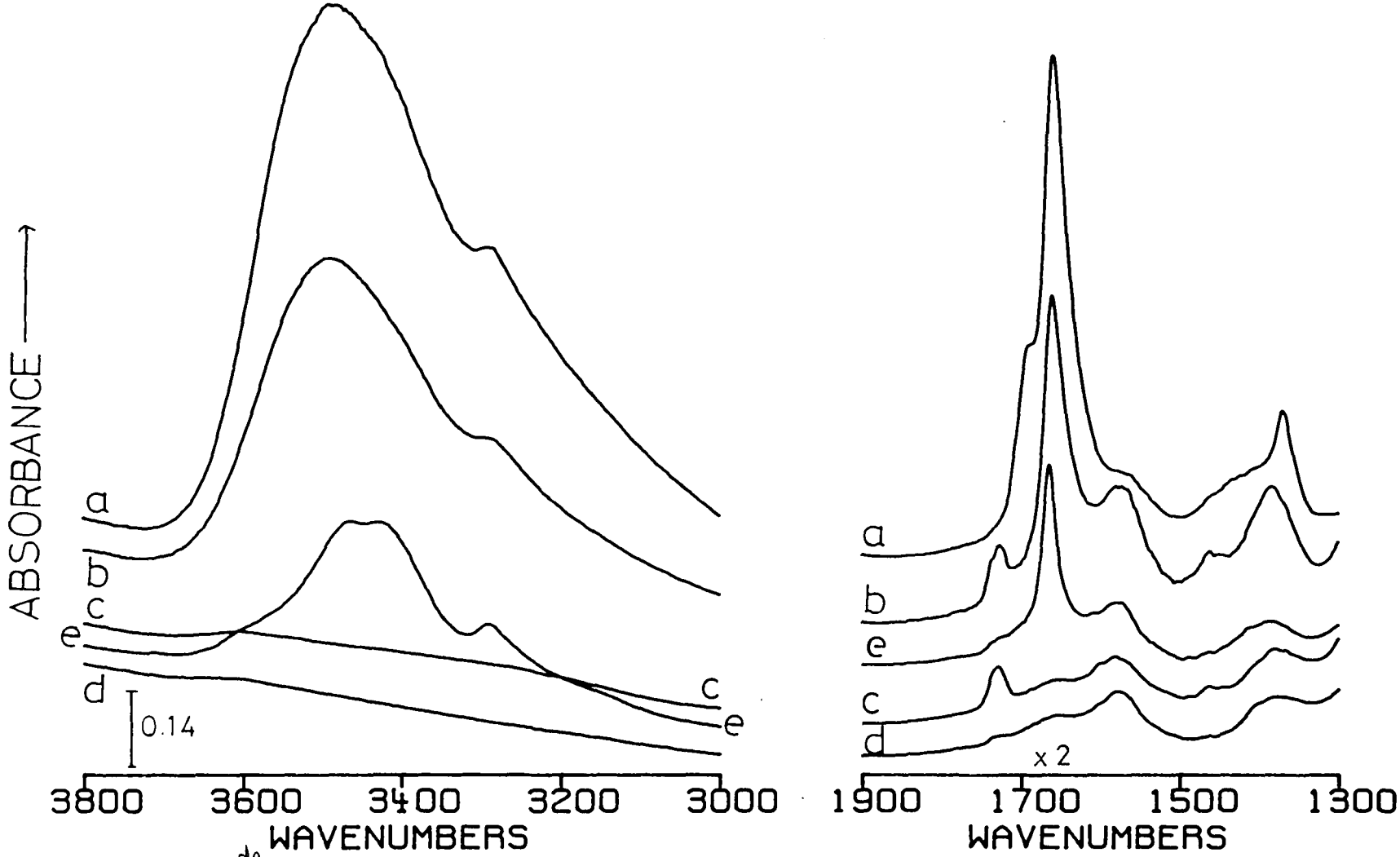

Figure 4.2 The dehydration of Na-A zeolite

(a) zeolite at ambient temperature under vacuum. Sample heating at (b) 513K, (c) 743K and (d) 753K for 15.5 hours; (e) sample cooled to ambient temperature. (Y axis offset)

(ii) weaker but sharper band(s) at 1650 and 1620 cm^{-1} for ZnNa-A and 1658 cm^{-1} for Na-A.

These bands are due to the stretching and bending modes of water molecules associated with the zeolite framework and cations and can be seen to be lost on dehydration.

Features to note in the spectra of ZnNa-A are the sharp band at *ca.* 3640 cm^{-1} (Figure 4.1(a)) and the two $\sigma(H_2O)$ vibrations at 1650 and 1620 cm^{-1} (Figure 4.1(b)). The former band can be assigned to the ν(OH) mode of free hydroxyl groups (no hydrogen bonding) within the zeolite framework.[29] The two $\sigma(H_2O)$ vibrations show that water molecules are coordinated at two different sites (*e.g.* the cations and the framework oxygens) in the zeolite framework.

In Figure 4.2(a) (Na-A) a shoulder is observed at *ca.* 1689 cm^{-1}. This band is too high to be assigned to the ν_2 bending mode of water. Tentatively, it may be assigned to the antisymmetric bend (ν_4) of the hydronium ion (H_3O^+). Evidence for H_3O^+ has been reported by Corma *et al*,[30] who observed ν_4 at 1690 and 1685 cm^{-1} for HNa-Y and NH_4-RhO respectively.

Weak features observed in the region 1800-1300 cm^{-1} (other than $\delta(H_2O)$ modes) are associated with structural vibrations (overtone and combination band) and included carbonates.[31]

On cooling the zeolite samples to room temperature an increase in intensity in the ν(OH) and $\sigma(H_2O)$ regions show that readsorption of water has occurred. This water could originate from at least two sources:

(i) the surface of the vacuum system;

(ii) from dissociated water in the zeolite framework.

Although there is a known tendency for the dissociation of water at high temperatures in transition metal zeolites[32] we did not observe any features associated with metal hydroxides and Brönsted acid sites. The source of water was therefore concluded to be the surface of the vacuum system.

4.4.2 Adsorption of Propene

As C_3H_6 is the product of the isomerization of $c\text{-}C_3H_6$ on ZnNa-A zeolite, we first undertook a study of C_3H_6 to allow the identification of product bands.

The adsorption of C_3H_6 by ZnNa-A and Na-A zeolites (Figures 4.3 and 4.4) leads to intense narrow bands in the IR spectra. By comparing the spectra of the adsorbed C_3H_6 complexes with the literature assignments[33] for gaseous C_3H_6, we can assign, using the same nomenclature,[33] the transitions of the adsorbed species (Table 4.3). A spectrum of gaseous C_3H_6 is shown for comparison in Figure 4.5. Recently Förester and Seebode reported data for C_3H_6 adsorbed on the same zeolites.[14] On comparing their data (Table 4.4) with our results (Table 4.3), we observe that although agreement of band positions and assignments is good in the 1700-1200 cm^{-1} region, this is not the case in the 3100-2700 cm^{-1} region. Although an explanation for the extra bands observed in this latter region cannot be found for Na-A, this is not the case for ZnNa-A. Here the presence of two different adsorption complexes is probably responsible (see below). In agreement

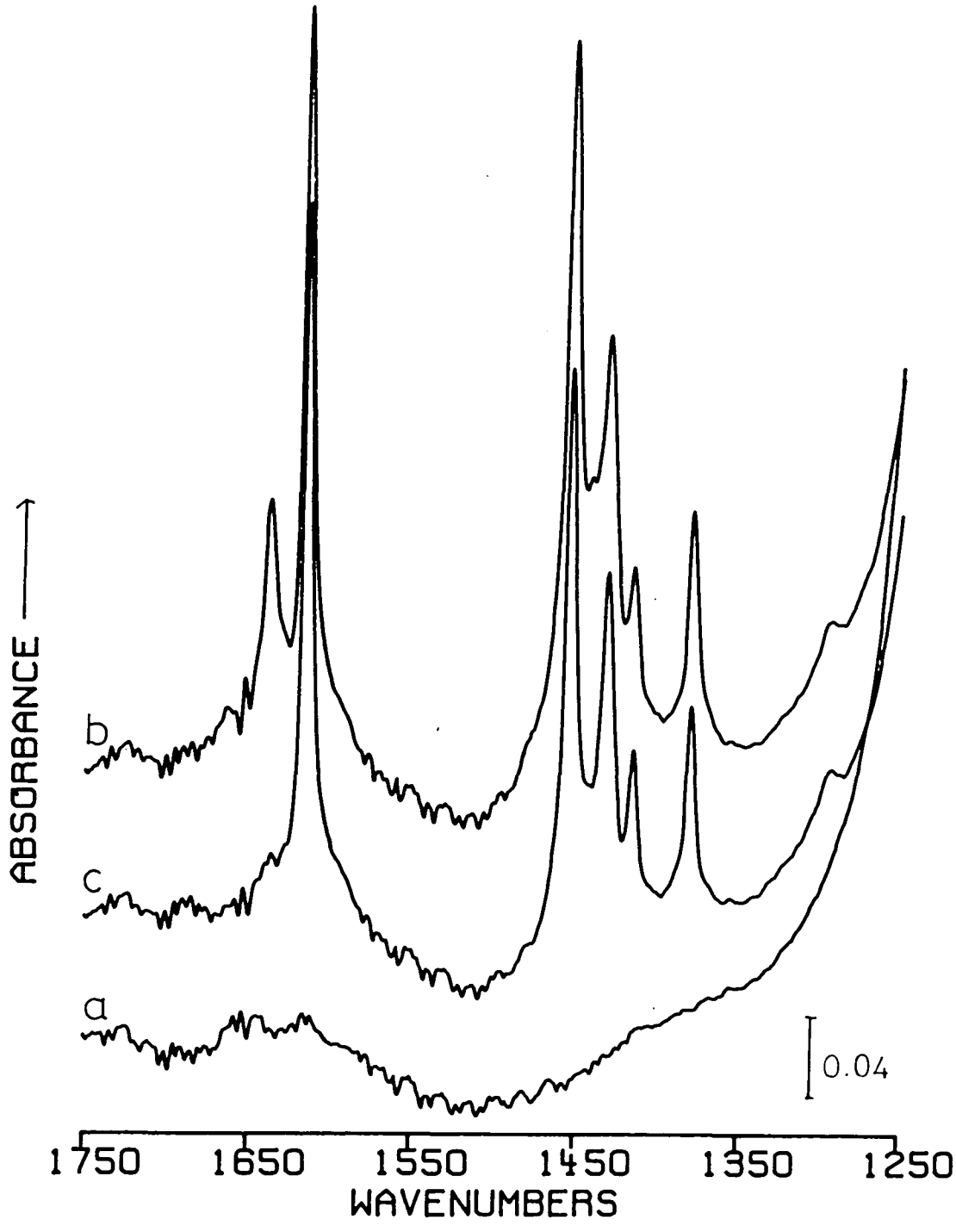

Figure 4.3(i) The infrared spectrum of propene adsorbed on ZnNa-A zeolite dehydrated for 53.3 hours at 738K. The 1750-1250 cm^{-1} region

(a) dehydrated zeolite background.
(b) adsorption of 5.7 torr of C_3H_6.
(c) on evacuation of C_3H_6.

(Y axis offset)

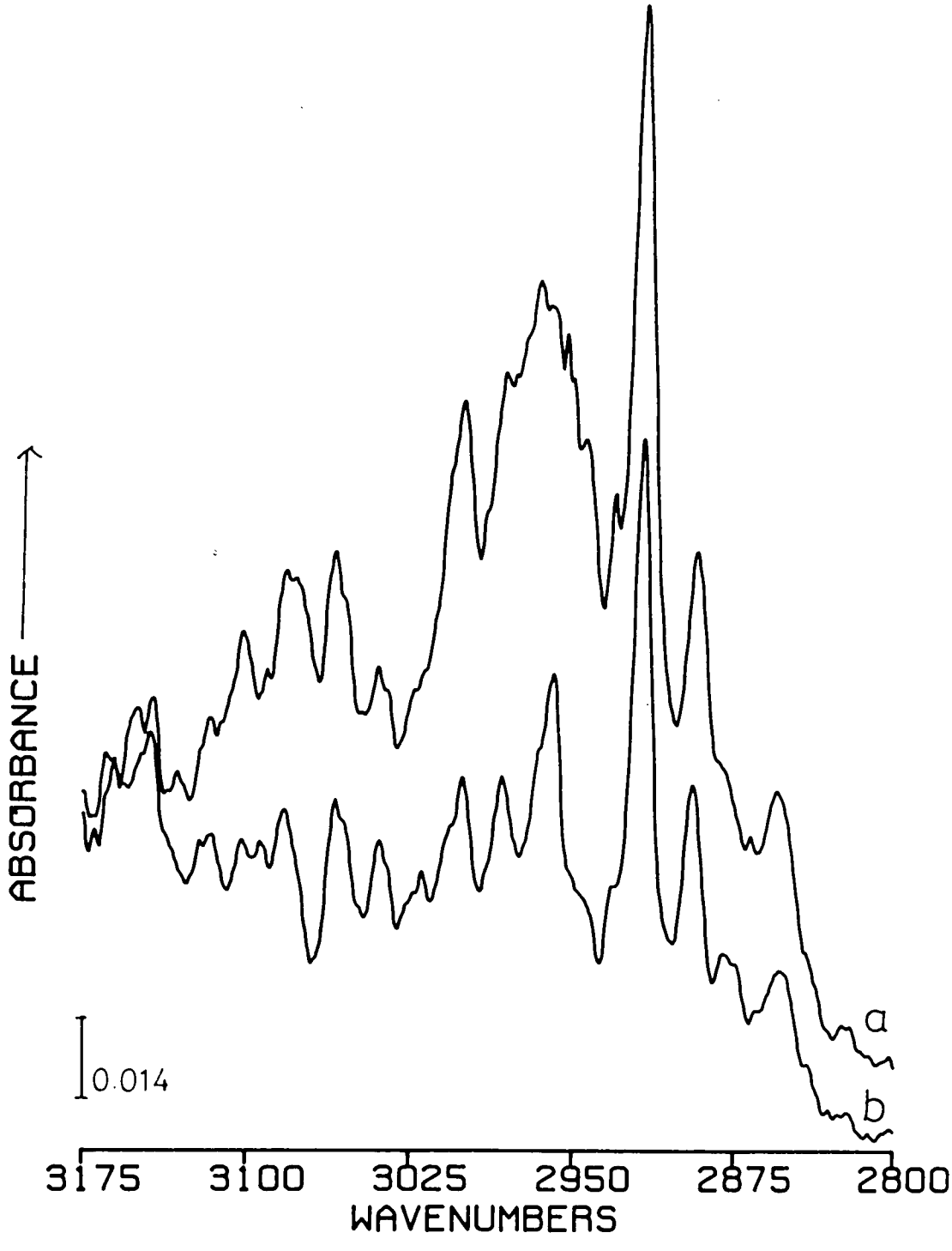

Figure 4.3(ii) The infrared spectrum of propene adsorbed on ZnNa-A zeolite dehydrated at 738K for 13.3 hours: the 3175-2800 cm^{-1} region.

(a) adsorption of 5.7 torr of C_3H_6.

(b) on evacuation of C_3H_6.

Dehydrated zeolite background subtracted from spectra.

(Y axis offset)

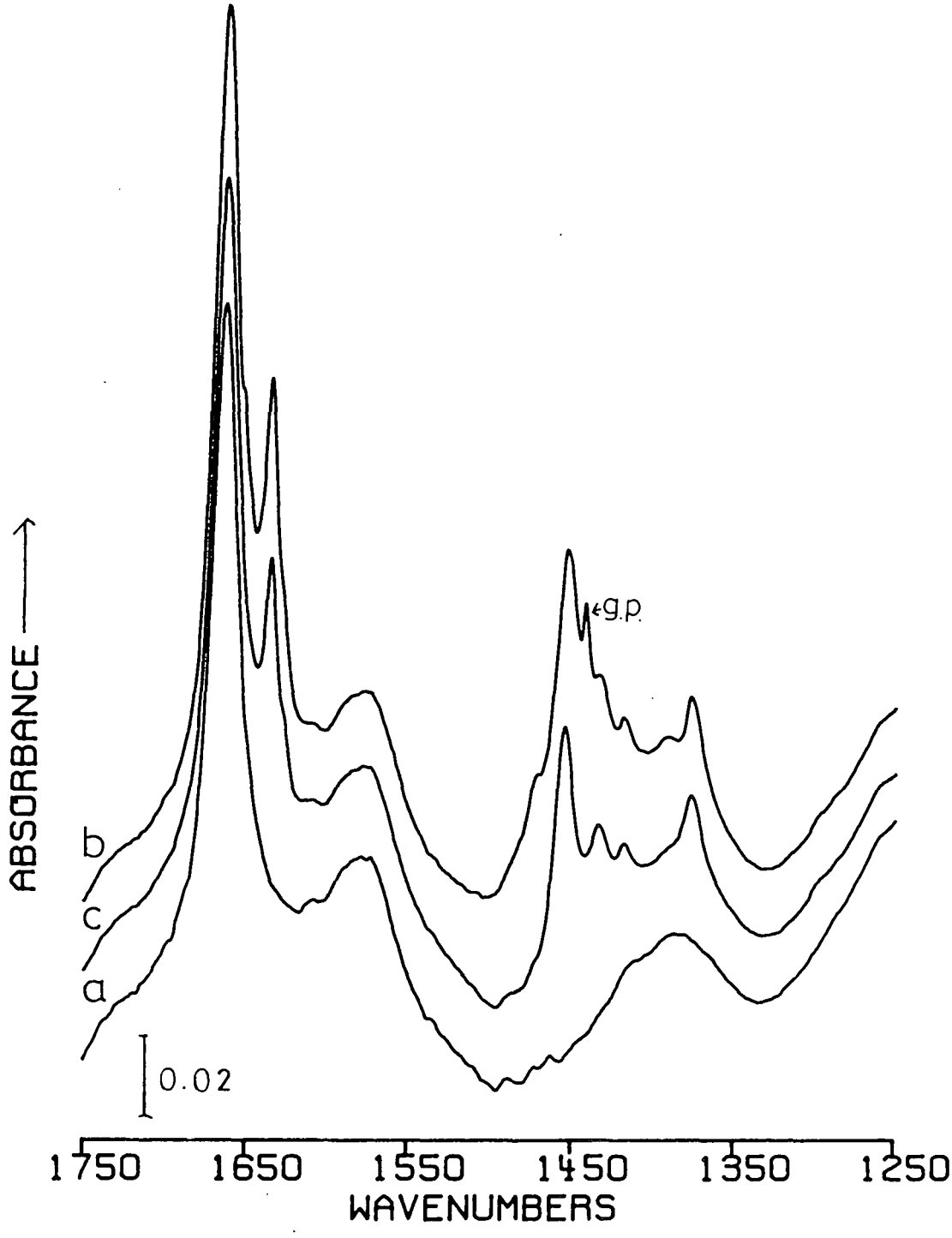

Figure 4.4(i) The infrared spectrum of Propene adsorbed on Na-A zeolite dehydrated for 15.5 hours at 753K: the 1750-1250 cm^{-1} region

(a) dehydrated zeolite background.
(b) adsorption of 9.8 torr of C_3H_6.
(c) on evacuation.

g.p.=gas phase

(Y axis offset)

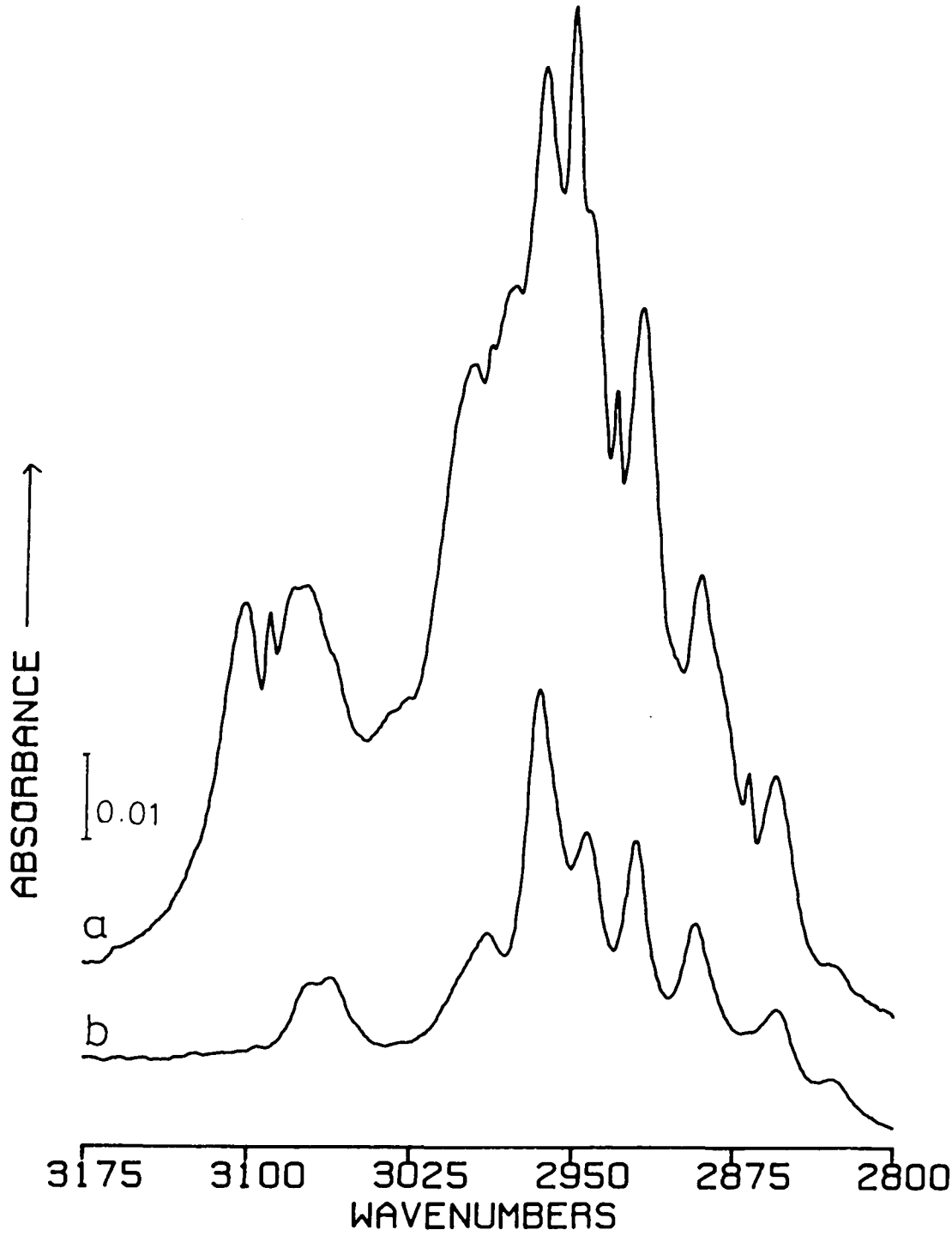

Figure 4.4(ii) The infrared spectrum of propene adsorbed on Na-A zeolite dehydrated for 15.5 hours at 753K: the 3175-2800 cm^{-1} region.

(a) adsorption of 9.8 torr of C_3H_6.

(b) on evacuation.

Dehydrated zeolite background subtracted from spectra.

(Y axis offset)

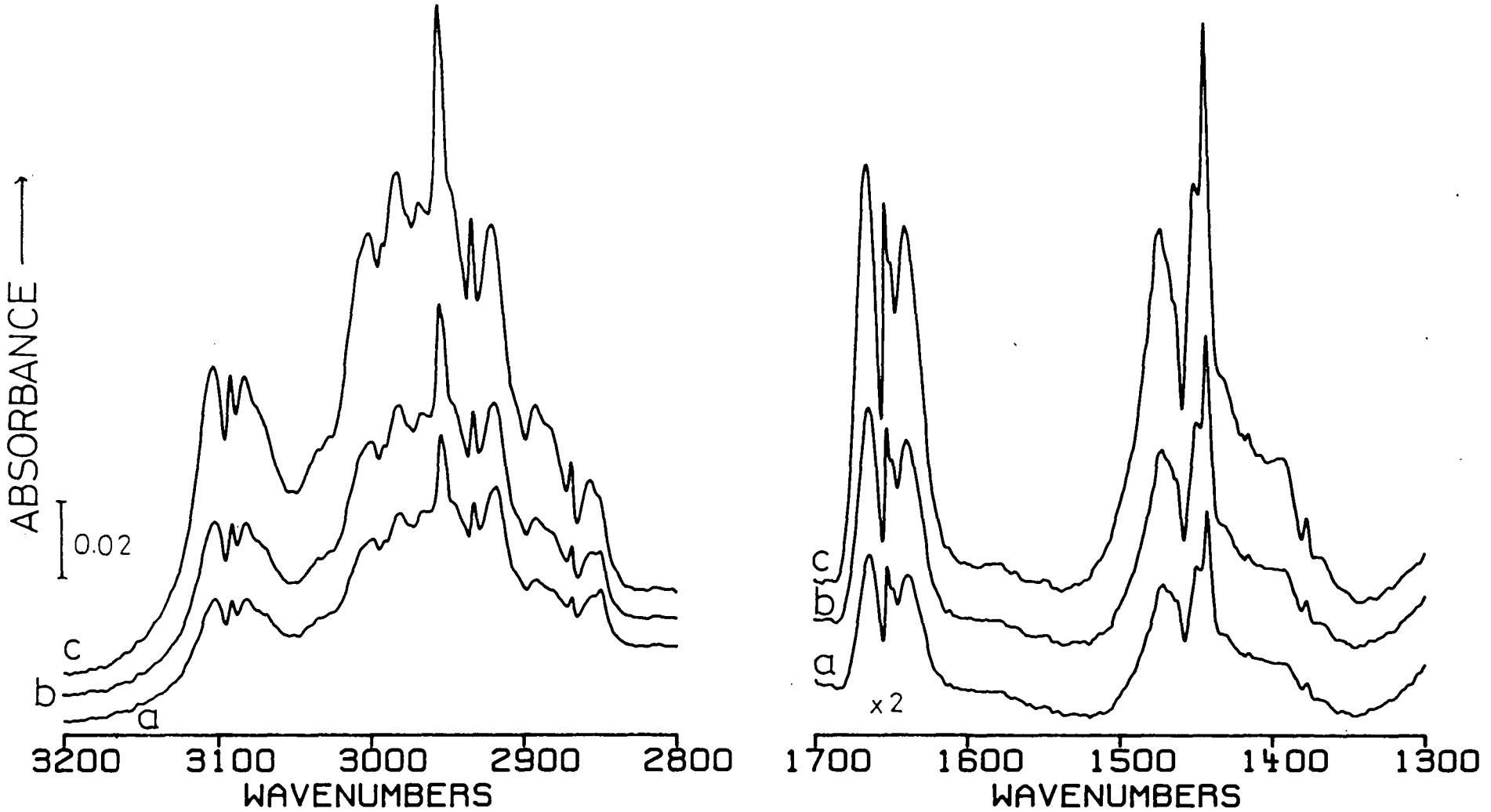

Figure 4.5 Gas phase infrared spectrum of propene in the sample cell (path length 48mm)

(a) 6.8 torr, (b) 10.6 torr and (c) 20.0 torr. (Y axis offset)

TABLE 4,3 The vibrational bands (cm^{-1}) and assignments of propene adsorbed on ZnNa-A and Na-A zeolites observed in the present work

ZnNa-A	Na-A	Gas Phase[33]	Assignment[a] (nomenclature that of ref. 33)
3074	3073	3081	) ν_1 CH_2 stretch
3060	3062	3067	) $\nu_6 + \nu_8$
3039			)
3008		3012	) ν_2 CH_3 stretch
3002	3002(sh)[b]		)
2984	2990		)
			) ν_3 CH_2 sym. stretch
2976		2979	)
2967(sh)	2967	2960	) ν_{15} CH_3 asym. stretch
2959		2942	) $2\nu_{16}$
2944	2944		) ν_4 CH_3 asym. stretch
2919	2921	2916	)
2895	2893	2884	$2\nu_7$
2855	2855	2852	ν_5 CH_3 sym. stretch
	2929	2825	$2\nu_8$?
2746		2732	$\nu_7 + \nu_{10}$?
1638	1636		)
		1647	) ν_6 C=C stretch
1616			)
1454	1454	1472	ν_{16} CH_3 asym. deform.
1431	1433	1448	ν_7 CH_3 asym. deform.
1415	1416	1416	ν_8 CH_2 deform.
1379	1376	1399	ν_9 CH_3 sym. deform.
1293	1298	1317	)
			) ν_{10} C-H band
		1287	)

[a] sym. = symmetric, asym. = asymmetric, deform. = deformation

[b] sh = shoulder.

TABLE 4.4 Band Positions (cm^{-1}) of propene adsorbed on $Zn_{4.4}Na_{3.2}$-A and Na-A zeolites after Förester and Seebode[14]

Zn_4-A	Na-A	Assignment [a]
3070	3070	ν_1 CH_2 asym. stretch
3042		$\nu_6 + \nu_8$
3000	3000	ν_3 CH stretch
2970	2970	ν_4 CH_2 sym. stretch
2960	2950	ν_{15} CH_3 asym. stretch
2918	2930	$2\nu_{16}$
2893	2900	ν_4 CH_3 asym. stretch
2860	2865	ν_5 CH_3 asym. stretch
2825		$2\nu_8$
2740		$\nu_8 + \nu_{10}$
1638	1636	ν_6 C=C stretch
1616		ν_6 C=C stretch
1455	1456	ν_{16} CH_3 asym. deform.
1431	1435	ν_7 CH_3 asym. deform.
1415	1420	ν_8 CH_2 deform.
1379	1375	ν_9 CH_3 sym. deform.
1298	1298	ν_{10} CH band

a. See Table 4.3

with this explanation, on close scrutiny of the data some of the bands, *e.g.* the 2944, 2967 and 3002 cm^{-1}, are observed to be lost preferentially on evacuation. This does not though explain why Förester *et al* did not observe the same number of bands in this region.

In the case of ZnNa-A zeolite, a problem arises in that when there is an overpressure of C_3H_6, two bands are observed in the region of the C=C stretching vibration at 1638 and 1616 cm^{-1}. By comparing Figure 4.3(i)(b) with Figure 4.3(i)(c) we observe that the band at 1638 cm^{-1} disappears completely on evacuation, whereas all other bands are only reduced in intensity. This suggests that there are two different adsorbed species, one of which is characterized by a C=C stretching vibration at 1638 cm^{-1} and the other by the same mode at 1616 cm^{-1}. As expected, it is the species with its transition frequency closest to the gas phase value which is removed first. We have observed that the species which has a C=C stretching vibration at 1616 cm^{-1} is only desorbed by heating the zeolite to over 473K under evacuation. For Na-A zeolite adsorption of C_3H_6 leads to only one transition at 1636 cm^{-1} in the C=C stretching region (Figure 4.4(i)). In this case the single adsorbed species is only slowly desorbed by evacuation at room temperature. We interpret these results as indicating that the species which is easily desorbed from ZnNa-A is adsorbed on the Na(I) ions, whereas the more strongly adsorbed species is associated with C_3H_6 coordinated to the Zn(II) ions.

The different values for the C=C stretching vibrations of the Zn(II) and Na(I) C_3H_6 complexes may be ex-

plained in terms of the nature of the cations. For Na(I) ions, which have no filled orbitals of the correct symmetry, donation of electron density may occur only from the C_3H_6 π-orbitals into the vacant Na(I) 3s orbital. This forms a σ-bonded Na(I)-C_3H_6 complex. In the Zn(II)-C_3H_6 complex, the cations are able to form a σ-bond with the C_3H_6 and to participate in back-bonding by donating electron density from their filled 3d orbitals into the antibonding π^* orbital of C_3H_6. The π-bonding of this complex weakens the C_3H_6 double bond to a greater degree than the σ-bonding of the Na(I)-C_3H_6 complex. Hence a larger shift in the ν(C=C) vibration relative to the gas phase value of 1647 cm^{-1}, is observed for the Zn(II)-C_3H_6 complex.

On adsorption, shifts are observed in most of the C_3H_6 bands relative to the gas phase. A notable exception is the ν_8, CH_2 deformation mode, at *ca.* 1416 cm^{-1}. We would expect a large shift in this band due to the interaction of the double bond with the cations. Therefore our assignments in terms of pure vibrational modes may be incorrect. The coupling of vibrational bands in organometallic complexes is well known,[34,35] and has been shown to occur in the C_3H_6 analogue of Zeise's salt,[35] $K[C_3H_6PtCl_3].H_2O$. Bands observed in its infrared spectrum at 1504 and 1365 cm^{-1} were assigned to the coupled C=C stretch and CH_2 deformation modes (Table 4.5). It seems reasonable to assume that such coupling may occur in complexes formed in zeolite frameworks. Therefore by comparing the spectrum of $K[C_3H_6PtCl_3].H_2O$ with that of our Zn(II)-C_3H_6 complex, an alternative assignment of the bands in the 1620-1200 cm^{-1} region, in terms of the coupling of the C=C stretch and CH_2 deformation modes is seen to exist (Table 4.6).

TABLE 4.5 Assignment of the IR Spectrum of $K[C_3H_6PtCl_3].H_2O$.[35]

Band (cm^{-1})[a]	Assignment[b]
1504 (s)	CH_2 deformation + C=C stretch
1449 (s)	CH_3 asym. deformations
1429 (s)	
1392 (m)	CH_3 sym. deformation
1365 (s)	C=C stretch + CH_2 deformation
1252 (w)	not assigned.

[a] s = strong, m = moderate, w = weak.

[b] see Table 4.3.

TABLE 4.6 The Alternative Assignment of the Spectrum of Zn(II)-C_3H_6 in the 1620-1200 cm^{-1} region

Band (cm^{-1})	Assignment
1616	C=C stretch + CH_2 deformation
1454	CH_3 Asym. deformations
1431	
1415	CH_3 Sym. deformations
1379	CH_2 deformation + C=C stretch
1293	C-H bend.

A full normal coordinate analysis of the complex is needed to confirm this alternative assignment and to consider further coupling which has been reported for gaseous C_3H_6.[36]

Although we recognize this alternative assignment, in terms of mixed modes, we will continue, for simplicity, to use the pure mode description (Table 4.3).

While the C_3H_6 is quickly desorbed from the Na ions in the ZnNa-A zeolite (Figure 4.3(i)(c), this is not the case for Na-A (Figure 4.4(i)(c). This difference in behaviour was not reported by Förester and Seebode[14] in their studies of the same systems. We propose that three factors may be responsible for the different Na(I)-C_3H_6 complex stabilities in the two zeolites:

(i) the presence of Zn(II) ions in ZnNa-A;

(ii) the presence of zeolitic water in Na-A;

(iii) cation location differences.

We observe that in ZnNa-A the ν(C=C) band of the Na(I)-C_3H_6 complex is at 1638 cm^{-1}, whereas in Na-A it is at 1636 cm^{-1}. Even though the shift of 2 cm^{-1} indicates the bonding to be slightly stronger in Na-A, it is too small to explain the very different complex stabilities observed, especially considering that we may not be dealing with pure modes. The presence of the Zn(II) cations seems unlikely to be the reason for the different complex stabilities.

Considering the second factor, some of the water readsorbed by Na-A after dehydration would be associated with the cations. Hydrated Na(I) ions at site S_I would cause partial blocking of the 8-ring aperture, which may increase

the complex stability by hindering its desorption from the cavities. This effect would not be important in ZnNa-A where little readsorption of water occurred.

To test the above factor, C_3H_6 was adsorbed onto a sample of Na-A that had been dehydrated for 33 hrs. and which re-adsorbed less water on cooling (Figure 4.6), than the sample in figure 4.4 Comparing this data, with the results for the shorter dehydration (Figure 4.4), we observe the intensities of the bands due to the adsorbed C_3H_6, relative to the gaseous C_3H_6 band at 1442 cm^{-1}, to be greater for the longer dehydration. On evacuation though, (Figure 4.6(c)), the Na(I)-C_3H_6 complex is seen not to be easily desorbed from this sample. From this data we conclude that, though water can block the C_3H_6 adsorption sites, it is not responsible for the different complex stabilities.

The third factor, cation locations then perhaps offers the best explanation. In ZnNa-A zeolite the Na(I) ions are located only in the S_1 sites, whereas in Na-A zeolite Na cations are also located at the S_2^* and S_3 sites within the framework. We may then explain the stronger complex formation in Na-A zeolite in terms of a C_3H_6 complex formed at the S_2^* or S_3 sites.

4.4.3 Adsorption and Isomerization of Cyclopropane

In a previous study of c -C_3H_6 adsorbed on ZnNa-A, Kadir[37] showed the isomerization rate to be dependent upon the severity of the zeolite pretreatment. We therefore chose, in the present study, to employ the most severe conditions used in this previous work (723K for 36 hrs.) to minimise the in-

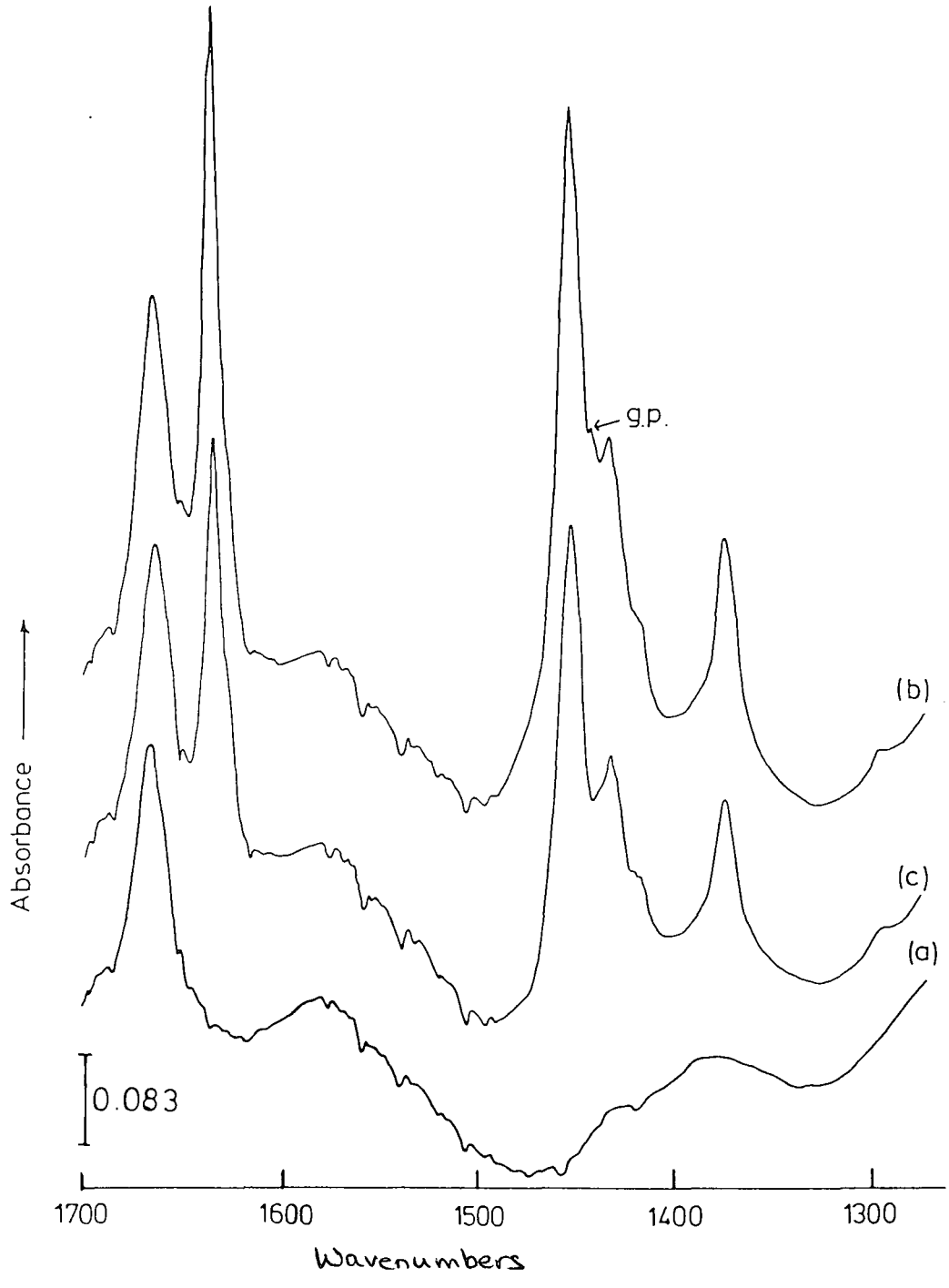

Figure 4.6 The infrared spectrum of propene adsorbed on Na-A dehydrated for 33 hours at 723K.

(a) dehydrated zeolite background.
(b) adsorption 10.3 torr of C_3H_6.
(c) on evacuation.

g.p. = gas phase. (Y axis offset).

fluence of water on the isomerization rate. No Brönsted acid sites were detected on the adsorption of pyridine onto a sample dehydrated under these conditions.

So that an investigation of the effect of pressure on the rate of isomerization could be made, $c\text{-}C_3H_6$ was adsorbed at overpressures of 5.2 and 32.5 torr. Spectra collected during the isomerization at these two pressures are shown in Figures 4.7-4.9. The assignments and spectrum of gaseous $c\text{-}C_3H_6$ are shown, for comparison, in Table 4.7 and Figure 4.10. The assignment of bands due to the adsorbed species is given in Table 4.8, together with the data recently reported by Förester and Seebode on the $Zn_{4.4}Na_{3.2}$-A+$c\text{-}C_3H_6$ system.

The 1700-1300 cm^{-1} region

In this region vibrations due to adsorbed $c\text{-}C_3H_6$ are observed at 1461 and 1431 cm^{-1}. The latter band, assigned to the ν_9 scissoring mode, overlaps with the ν_7 vibration of adsorbed C_3H_6. In Figure 4.3(i) the relative intensity of the ν_7 mode (1431 cm^{-1}) is observed to be less than the ν_{16} mode (1454 cm^{-1}) of adsorbed C_3H_6. In the case of the $c\text{-}C_3H_6/C_3H_6$/-ZnNa-A system (Figure 4.7), the 1431 cm^{-1} is of greater intensity than the 1461 cm^{-1} band. It is therefore concluded that the major contribution to the 1431 cm^{-1} band is from adsorbed $c\text{-}C_3H_6$.

Although the band at 1461 cm^{-1} is due only to adsorbed $c\text{-}C_3H_6$, its assignment is uncertain; three different assignments have been prepared:

(i) Förester *et al*[14] assigned it to the ν_2 CH_2 scissoring mode in the ion exchanged A zeolites they studied.

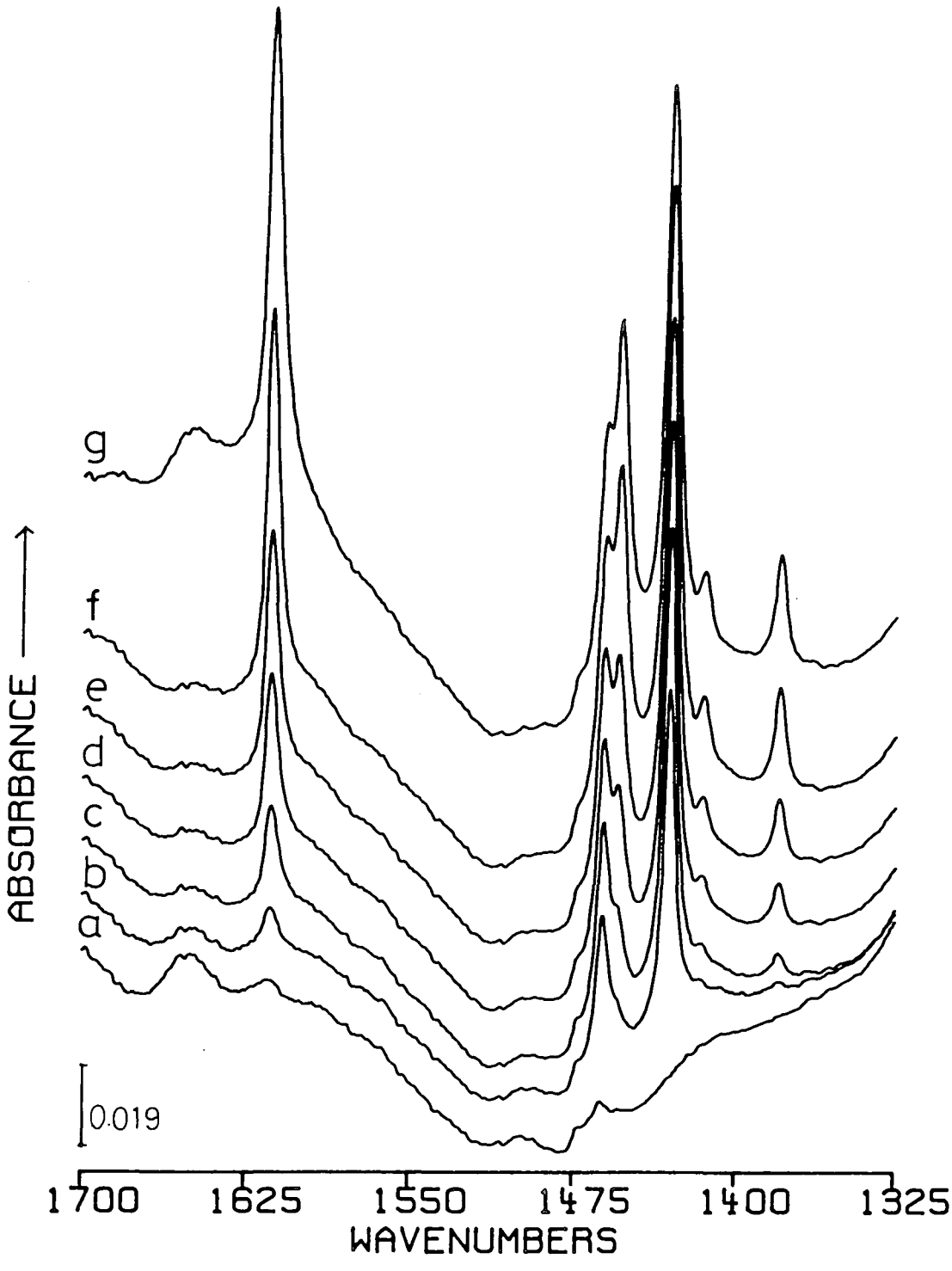

Figure 4.7 The isomerization of Cyclopropane (5.2 torr) on ZnNa-A zeolite in the region below 1700 cm⁻¹

(a) dehydrated zeolite background (31 sec.), (b) 20 seconds after adsorption of $c\text{-}C_3H_6$ (8 sec.), (c) 2.5 minutes after adsorption (8 sec.), (d) 10 minutes after adsorption (31 sec.), (e) 20 minutes after adsorption (31 sec.), (f) 1 hour after adsorption (31 sec.), (g) 6.5 hours after adsorption (31 sec.).

(Y axis offset)

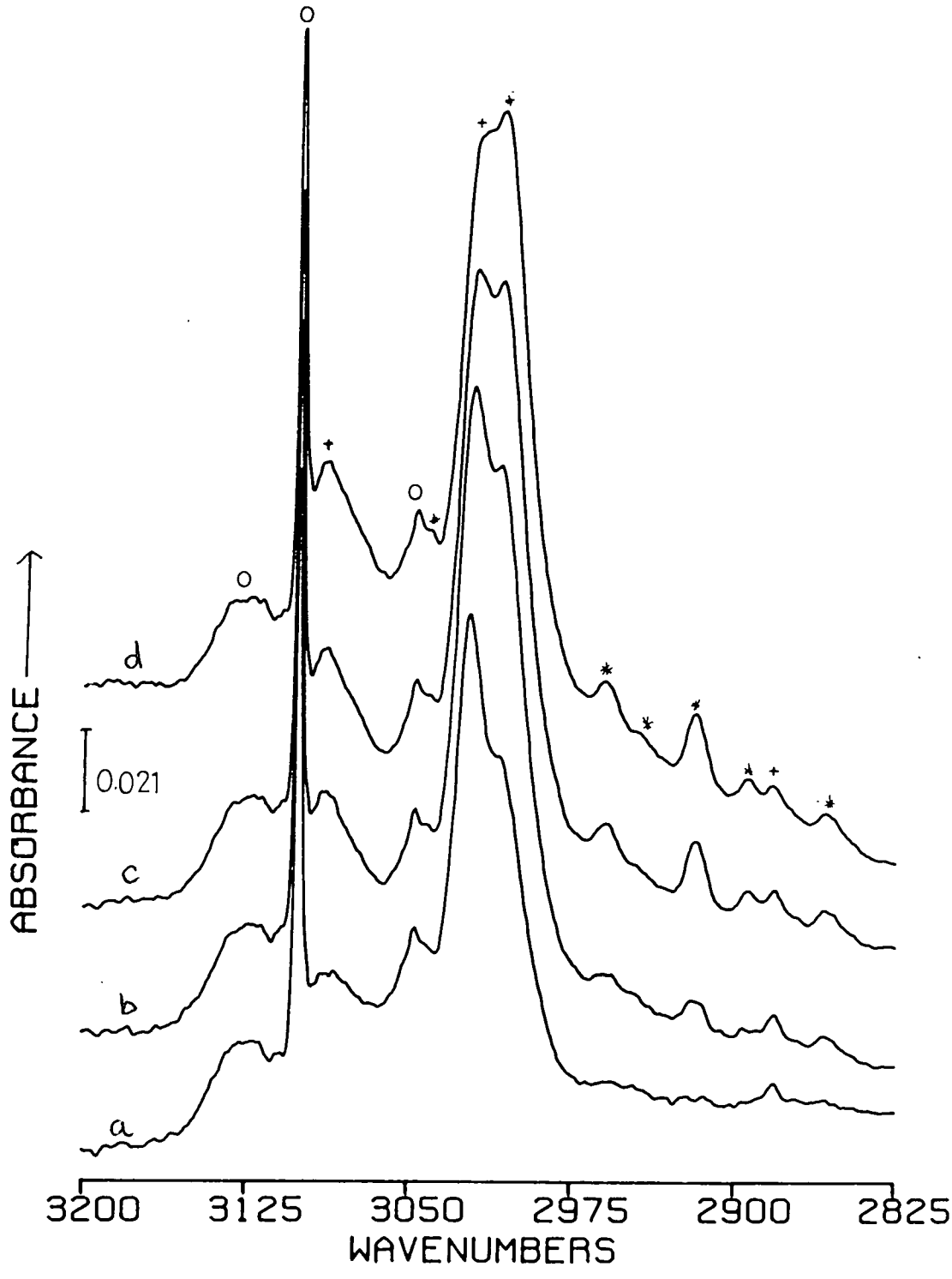

Figure 4.8 The isomerization of Cyclopropane (5.2 torr) on ZnNa-A zeolite in the ν(CH) region

(a) 20 seconds after adsorption (31 sec.), (b) 10 minutes of adsorption (31 sec.), (c) 1 hour after adsorption (31 sec.), (d) 6.5 hours after adsorption (31 sec.).
Background subtracted from spectra.
+ adsorbed cyclopropane; * adsorbed propene; O gaseous cyclopropane.

(Y axis offset)

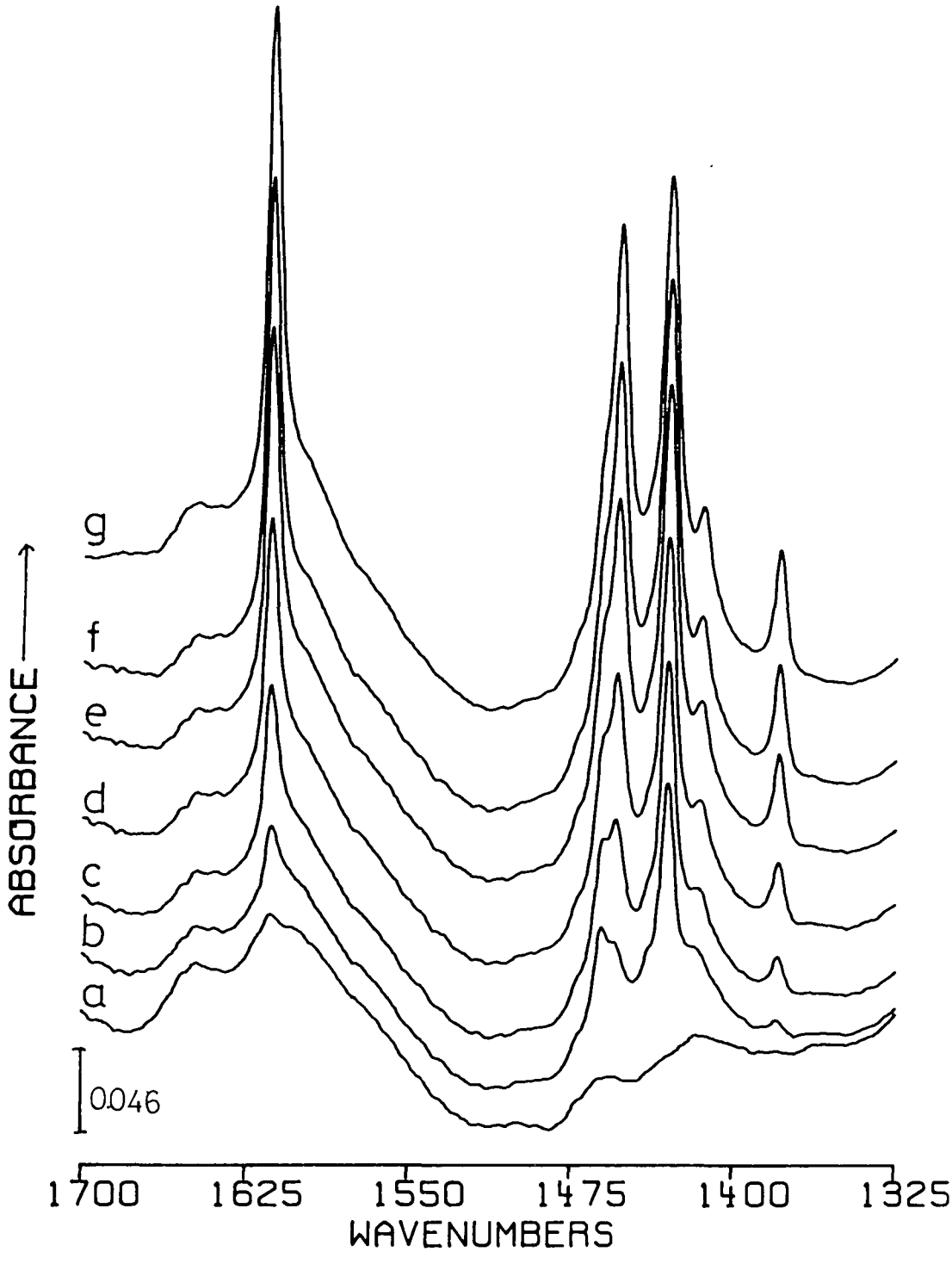

Figure 4.9 The adsorption of Cyclopropane (32.5 torr) on ZnNa-A

(a) dehydrated zeolite background (31 sec.), (b) 10 seconds after adsorption (8 sec.), (c) 1 minute after adsorption (8 sec.), (d) 2.7 minutes after adsorption (8 sec.), (e) 20 minutes after adsorption (31 sec.), (f) 1 hour after adsorption (31 sec.), (g) 4 hours after adsorption (31 sec.).

(Y axis offset)

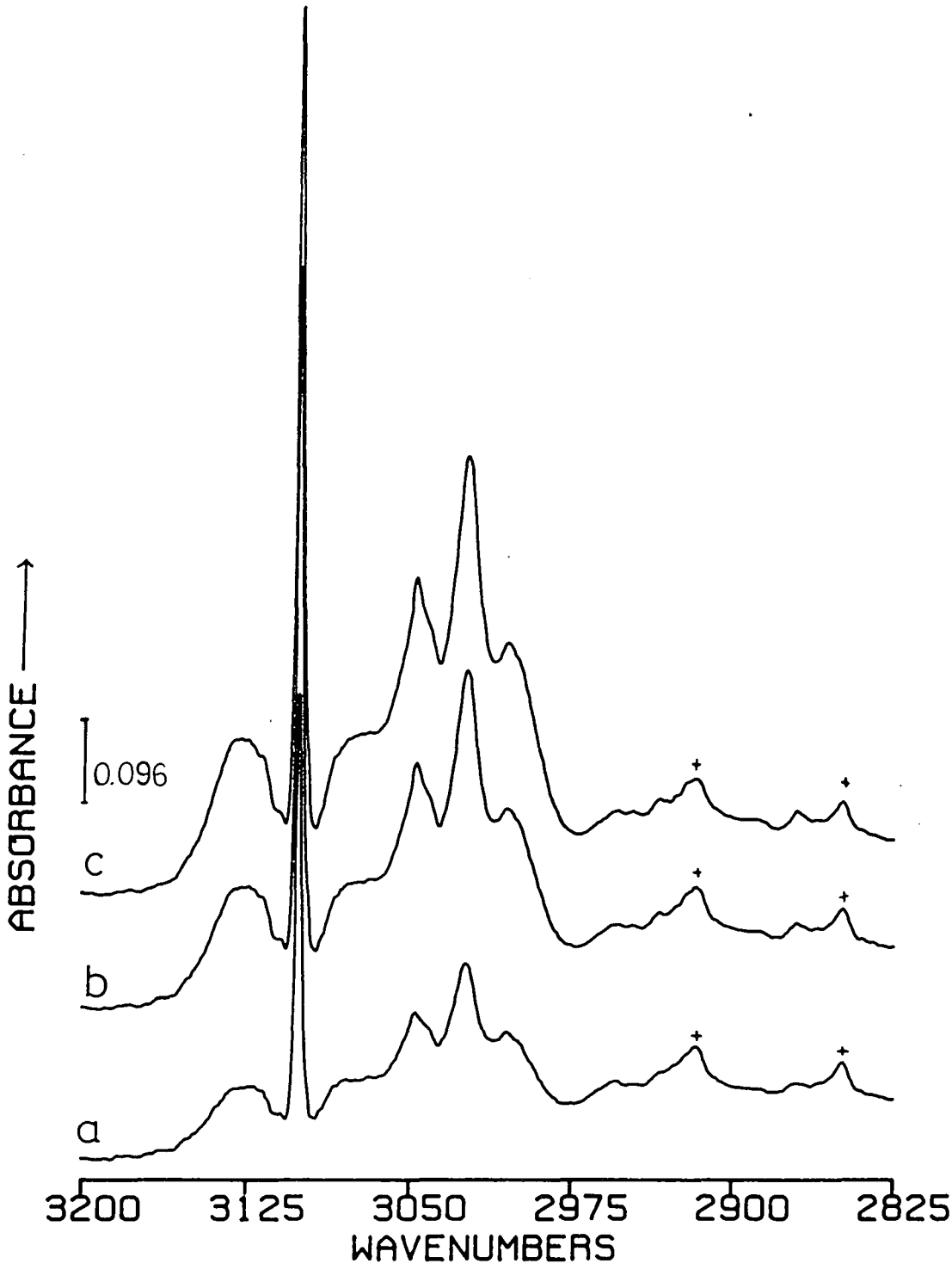

Figure 4.10. The infrared spectrum of gas phase cyclopropene in the sample cell. (path length 48mm).

(a) 5.6 torr; (b) 10.6 torr; (c) 16.1 torr.

(+ due to instrument) !Y axis offset)

TABLE 4.7 Fundamental frequencies (cm^{-1}) of gaseous cyclopropane as reported in the literature[38]

Symmetry Species (D_{3h})	Activity[a]	Approximate mode[b]	Selected valvue	Infra red	Raman
A_1	R	ν_1 CH_2 sym. stretch	3038	ia	3038
	R	ν_2 CH_2 scissors	1479	ia	(1504) FR[a] (1453) ($2\nu_{14}$)
	R	ν_3 ring stretch	1188	ia	1188
A_1''	ia	ν_4 CH_2 twist	1126	ia	ia
A_2'	ia	ν_5 CH_2 wag	1070	ia	ia
A_2''	IR	ν_6 asym. stretch	3103	3103	ia
	IR	ν_7 CH_2 rock	854	854	ia
E'	R+IR	ν_8 CH_2 sym. stretch	3025	3025	3020
	R+IR	ν_9 CH_2 scissors	1438	1438	1442
	R+IR	ν_{10} CH_2 wag	1029	1029	1023
	R+IR	ν_{11} ring deform.	866	866	866
E''	R	ν_{12} CH_2 asym. stretch	3082	ia	3082
	R	ν_{13} CH_2 twist	1188	ia	188
	R	ν_{14} CH_2 rock	739	ia	739

[a] R = Raman active, IR = infra red active, ia = inactive

[b] Sym = symmetric, asym. = antisymmetric, deform. = deformation

[c] Fermi resonance.

TABLE 4.8 Assignment of the observed bands for cyclopropane adsorbed on ZnNa-A zeolite

Förester *et al* [a,14]	Present work[b]	Species	Assignment of the cyclopropane bands
	3120 3101	)c-C_3H_6 (g.p.)[d])	)ν_6 CH_2 asym. stretch)
3100		c-C_3H_6	ν_6 C-H stretch
	3089	c-C_3H_6	ν_{12}/ν_6 CH_2 asym. stretch
3080		c-C_3H_6	ν_{12} C-H stretch
	3047	c-C_3H_6 (g.p.)	ν_1 CH_2 asym. stretch
	3041	C_3H_6	ν_{11} CH_2asym.stretch or $\nu_6+\nu_8$
	3020	c-C_3H_6	ν_1 CH_2
3020		c-C_3H_6	ν_1 C-H stretch
3010		c-C_3H_6	ν_8 C-H stretch
	3008	c-C_3H_6/C_3H_6	ν_1 CH_2 stretch
	2960 2947 2919	))C_3H_6)	
2883	2882	c-C_3H_6	$2\nu_2 + \nu_9$
	2894 2858	))C_3H_6	
	1892	c-C_3H_6 (g.p.)	$\nu_{10} + \nu_{11}$
1882		c-C_3H_6	$\nu_{10} + \nu_{11}$
	1614	C_3H_6	
1463[e]	1461	c-C_3H_6	$2\nu_{14}/\nu_2$ Fermi diad
	1454	C_3H_6	
1431	1431	c-C_3H_6/C_3H_6	ν_9 CH_2 scissors
	1414	C_3H_6	
	1380	C_3H_6	

[a] only cyclopropane data quoted.

[b] assignments apply to bands observed in presence of gas phase.

[c] see Table 4.3 for assignment of propene bands.

[d] g.p. = gas phase.

[e] Förester *et al* assign this to the ν_2(CH_2 deformation)

(ii) For Co, Mn and Zn ion exchanged A zeolites, the vibration was assigned to the $2\nu_{14}$ overtone band.[16,39]

(iii) Reanalysis of the work of Al Noami[39] on CoNa-A, by Howard and Braid [17] who considered the band intensity and the gas phase data[40] resulted in an assignment of this band to the lower frequency component of the $2\nu_{14}/\nu_2$ Fermi diad.

In the present case, considering the intensity of the 1461 cm^{-1} band, an assignment to the lower frequency component of the $2\nu_{14}/\nu_2$ Fermi diad is preferred.

In the c-C_3H_6/C_3H_6/ZnNa-A system the ν(C=C) vibration of adsorbed C_3H_6 is observed at 1614 cm^{-1}, compared to 1616 cm^{-1} in the C_3H_6/ZnNa-A system. This small shift may be due either to the presence of the c-C_3H_6 or to changes in the mixing of the C_3H_6 modes.

The 3200-2800 cm^{-1} region

The data from this region are shown in Figure 4.8 for the 5.2 Torr c-C_3H_6 adsorption. The results for the 32.5 Torr adsorption were identical, except the absolute intensities were greater.

In this spectral region Förester *et al*[14] observe five bands due to adsorbed c-C_3H_6, while we observe only four (Table 4.8). The difference occurs for the ν_6 and ν_{12} C-H stretching vibration, where, even after subtraction of gaseous c-C_3H_6 we see only one broad band at 3089 cm^{-1}, due to the two modes. The two bands were reported at 3100 and 3080 cm^{-1} respectively by Förester *et al*. We feel that the spectral manipulation employed by Förester *et al* may be the cause of this difference. But as full details were not provided in

their report, we are unable to make a definite conclusion.

The band at 3608 cm^{-1} is observed to increase in intensity during the course of the isomerization (Figure 4.8), due to the formation of the isomerization product C_3H_6.

4.4.4 Geometry of the Complex

On adsorption c-C_3H_6 may form a complex with either C_{2v} (edge-on) or C_{3v} (face-on) symmetry (Figure 4.11). In the gas phase c-C_3H_6 has D_{3h} symmetry under which those modes transforming as A_2' and A'', are Raman and IR inactive. On lowering the symmetry these modes remain inactive for C_{3v} but become active under C_{2v} (Table 4.9). Thus using IR spectroscopy, we may distinguish between C_{2v} and C_{3v} symmetry by the observation of an A_2' (D_{3h}) mode, (the A'', (D_{3h}) mode being IR inactive for C_{2v} and C_{3v}). Only the CH_2 wag (1070 cm^{-1} in the gas phase[42]) has this symmetry, but unfortunately strong vibrations of the zeolite framework in this region make conclusive observations by IR spectroscopy impossible.

Förester and Seebode[14] concluded that adsorption of c-C_3H_6 was 'face-on', by examination of the C-H stretching and CH_2 deformation regions. Here a splitting of the E' and E'' modes into A_1+B_2 and A_2+B_1 occurs only for C_{2v} symmetry (ν_8, ν_{12} and ν_9). In our data there is no indication of any splitting of the C-H stretching modes but these bands are broad, so this is inconclusive. The absence of splitting of the ν_9 (E') vibration (1431 cm^{-1}) though, indicates that adsorption is probably 'face-on' to the cations.

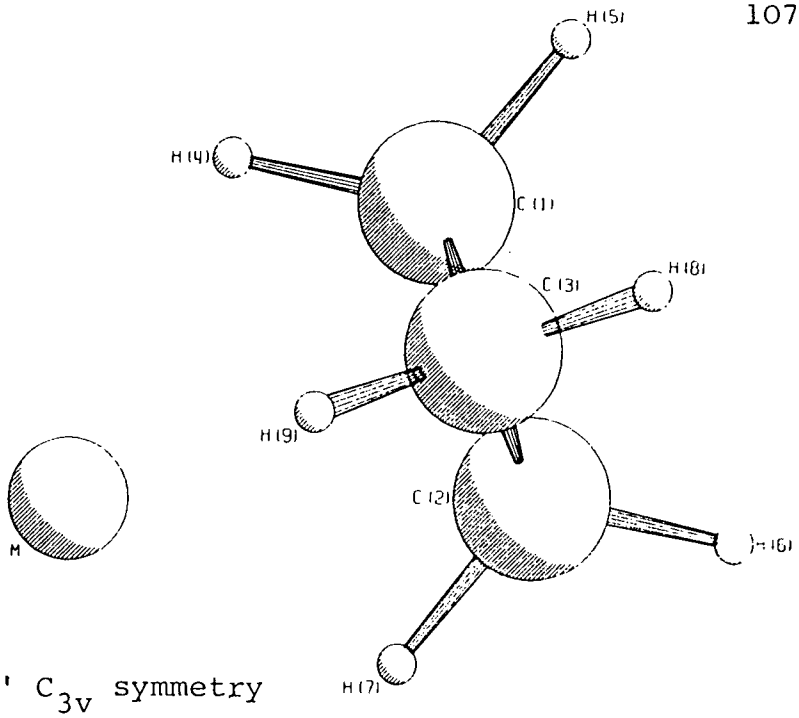

(a) 'face-on' C_{3v} symmetry

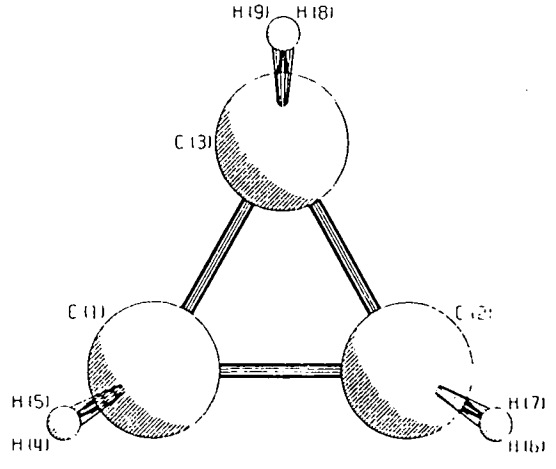

(b) 'edge-on' C_{2v} symmetry

Figure 4.11 Two possible cation-cyclopropane adsorption complexes in zeolites

TABLE 4.9 (a) Correlation of the D_{3h}, C_{3v}, C_{2v} point groups[41]

A_1	R + i.r.	A_1'	R	A_1	R+i.r.
A_2	R	A_1''	ia	A_2	ia
B_2	R + i.r.	A_2'	ia		
B_1	R + i.r.	A_2''	i.r.	A_1	R+ i.r.
$A_1 + B_2$	R + i.r.	E'	R+i.r.	E	R + i.r.
$A_2 + B_1$	R + i.r.	E''	R		

(b) Symmetries of the normal modes of cyclopropane under various point groups

(1) gas phase $\Gamma_{vib.}(D_{3d}) = 3A_1 + A_2' + 4E' + A''_1 + 2A''_2\ 3E''$

(2) face bonded adsorption complex $\Gamma_{vib.}(C_{3v}) = 5A_1 + 2A_2 + 7E$

(3) edge bonded adsorption complex $\Gamma_{vib.}(C_{2v}) = 7A_1 + 4A_2 + 5B_1 + 5B_2$

Although we doubted the validity of the X-ray diffraction study[16] on $c\text{-}C_3H_6$ adsorbed on Co^{2+} and Mn^{2+} ion exchanged A zeolites, a 'face-on' adsorption complex was reported. This was in agreement with the assignment of Forester *et al*[14] for $c\text{-}C_3H_6$ adsorbed on type A zeolites. Tam *et al*,[43] however, reported a cation sensitive splitting of ν_{11} (866 cm^{-1}, E´) mode in the Raman spectra of $c\text{-}C_3H_6$ adsorbed on X type zeolites and interpreted this in terms of a C_{2v} ('edge-on') structure.

4.4.5 Adsorption sites

Since C_3H_6 is observed in the first spectrum collected after the adsorption of $c\text{-}C_3H_6$ (Figure 4.7(b)), the isomerization must have an induction of at most a few seconds.

During the first hour, the 1461 cm^{-1} band of adsorbed $c\text{-}C_3H_6$ increases in intensity, but after this period it decreases. On evacuation (Figure 4.12) the remaining $c\text{-}C_3H_6$ was not immediately desorbed. These data lead us to conclude that adsorption occurs by two slightly different mechanisms, which give the same $c\text{-}C_3H_6$ complex.

The position of the "ν(C=C)" stretch at 1614 cm^{-1} show the product to be adsorbed on the Zn(II) cations. As the rate of intensity increase of this band decreases with time, we conclude that the $c\text{-}C_3H_6$ is adsorbed also on the Zn(II) cations. In our sample, Zn(II) cations are located at two sites, S_2^* and S_2' (Section 4.3). As the $c\text{-}C_3H_6$ is unable to enter the sodalite cages, we associate the first mechanism with site S_2^* in the supercage, where adsorption can occur immediately.

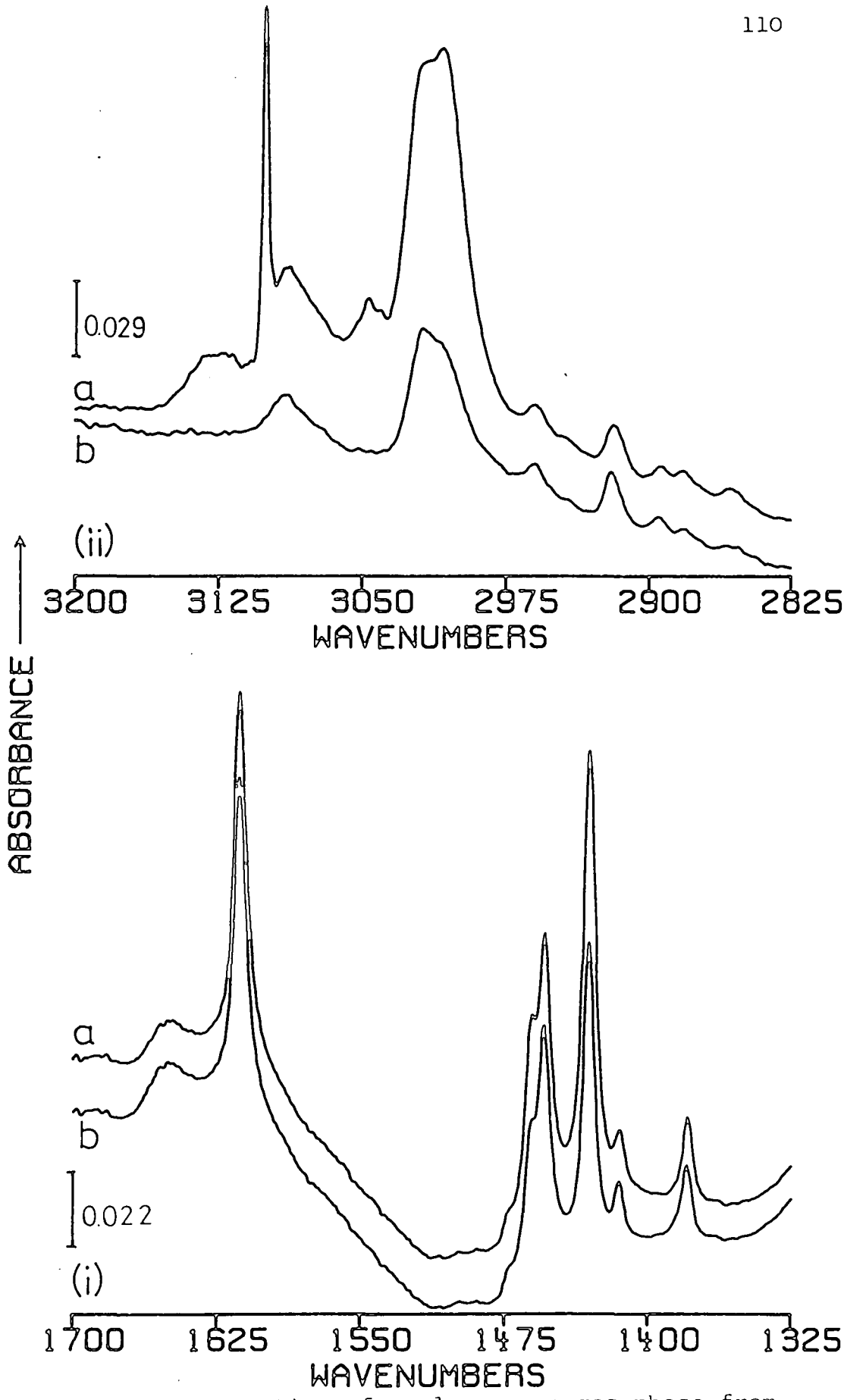

Figure 4.12 Evacuation of cyclopropane gas phase from ZnNa-A after 6.5 hours

(a) ZnNa-A + 5.2 torr of c-C_3H_6 after 6.5 hours

(b) evacuation of gas phase from sample (a).

Zeolite background subtracted from spectra in (ii).

(Y axis offset)

The second mechanism is characterized by the gradual increase in the 1461 and 3020 cm^{-1} in the initial period (*ca.* 1 hr.). The position of these bands show the adsorption complex to be formed at the same type of site as for the first process. We propose the second mechanism to involve the migration of the Zn(II) ions from site S_2' in the sodalite cages to site S_2^* in the supercages, where they become accessible to the $c\text{-}C_3H_6$ molecules. In support of this, cation movement of Mn(II) ions have been reported in type A zeolite on the adsorption of $c\text{-}C_3H_6$.[16] Thus the adsorption site of $c\text{-}C_3H_6$ is the Zn(II) cations at site S_2^*.

4.4.6 The rate of isomerization

The rate of isomerization of $c\text{-}C_3H_6$ to C_3H_6 can be followed using the intensity of the ν(C=C) band of the product at *ca.* 1616 cm^{-1}. This band is isolated from $c\text{-}C_3H_6$ and other C_3H_6 bands and of sufficient intensity for quantitative evaluation. Although the *ca.* 1616 cm^{-1} band overlaps with the deformation mode of zeolitic water, only after periods of several hours does water readsorption become a problem, when measuring band intensities.

In order to quickly characterize the catalytic activity of Ca^{2+}, Mg^{2+}, Zn^{2+} and Co^{2+} ion-exchanged A zeolites, Förester and Seebode[14] measured the 'appearance time' of the ν(C=C) band of C_3H_6. They defined this as the time taken for a 5% dip in the transmission of the band to occur. Because percentage transmission is not directly proportional to concentration, a comparison of samples using the 'appearance time' will only be valid if each sample has the same

background transmittance level. This condition is, however, unlikely to be achieved due to the difficulties of pressing self-supporting zeolite discs with specific concentrations and the probable optical differences between the different samples. We note, in addition, that comparison, particularly between samples of the same zeolite, should be undertaken with the same reactant concentration. If this latter condition is not fulfilled, different reaction rates will result in large errors in the 'appearance times'. In this respect, as reactant concentrations were expressed in terms of the number of molecules of $c\text{-}C_3H_6$ per cavity and no adsorption isotherms have been published for $c\text{-}C_3H_6$ adsorbed on ZnNa-A, a comparison with Förester *et al's* data is difficult. In conclusion, we note that the 'appearance time' may have some qualitative significance when a comparison is made between zeolites of very different catalytic activity, when the above problems are not critical.

No attempt is therefore made in the present study to compare the catalytic activity of our samples of ZnNa-A with those of Förester *et al* using the 'appearance time' parameter. Instead we make a comparison using rate constants, obtained from measurement of the intensity of the ν(C=C) band of the product.

(A) The derivation of a rate constant from IR measurements

In contrast to the indirect method of evaluating kinetics data for heterogeneous catalytic reactions from gas phase compositions,[6,7,9,10] the IR approach of Förester and Seebode[14] directly monitors the isomerization in the zeolite cavities.

On the basis that the jump frequency from one sorption site to another was much higher than the reaction rate, the probability of conversion was assumed by Förester *et al*[14] to be equal for all molecules regardless of adsorption site. From the observations that diffusion into the zeolite cavities, adsorption and desorption were fast, compared to the surface reaction, they concluded the isomerization itself should be the rate determining step.

The isomerization of $c\text{-}C_3H_6$ on $Zn_{4.4}Na_{3.2}$-A in the presence of SO_2 cocatalyst was found[14] to be well described by the integrated form of the first order equation:

$$\ln(X_\infty - X) = \ln X_\infty - kt. \qquad \text{(eqn. 1)}$$

where X = absorbance of the C=C mode of C_3H_6 at time t, X_∞ = absorbance after full conversion and k = rate constant for the disappearance of $c\text{-}C_3H_6$. This equation is valid if (i) the Beer-Lambert law is obeyed, (ii) full conversion is reached, and (iii) the product concentration at time zero is zero. From measurements of adsorbance uptake and the absorbance of the band due to the ν(C=C) mode, the authors showed the Beer-Lambert law to be strictly valid only at low product concentrations ($\lesssim 2$ C_3H_6 molecules per cavity). At high concentrations deviations occur, as C_3H_6 is adsorbed in front of the Na(I) ions.

To obtain a value of X_∞, Forester *et al*[14] extrapolated their data points to full conversion, which gave a X_∞ value 30-40% higher than the highest measured value of $X_\infty (X_{max})$. They calculated that the uncertainty in X_∞ led to errors of 10-15% in the slope of the $\ln(X_\infty - X)$ *versus* time plots, from which the rate constants were obtained.

Using the same approach as Förester and Seebode, we have calculated a rate constant for the isomerization of c-C_3H_6 on $Zn_{4.55}Na_{2.9}$-A in the absence of a co-catalyst. This approach is valid for our data as no absorption of C_3H_6 in front of the Na(I) ions was observed. In addition it is assumed that C_3H_6 is not desorbed. As shown earlier, this assumption is valid since C_3H_6 forms strong adsorption complexes with the Zn(II) ions.

(B) The calculation of the rate plots

Figure 4.13 shows a plot of the absorbance of the ν(C=C) C_3H_6 band *versus* time, for c-C_3H_6 overpressures of 5.2 and 32.5 Torr. Some difficulty was experienced in determining the baseline of this band, due (in part) to the slow readsorption of water with time. In order to determine the baselines from which the band heights were to be measured the following procedure was adopted:

(i) In the region of interest (1650-1550 cm^{-1}) the gradient of the relatively flat background (degassed zeolite disc) was measured;

(ii) for the adsorbed species data, a line with this gradient was drawn on the spectra, in the same region, where it touched wings of the absorption band. This line served as the baseline.

Due to the readsorption of water by the zeolite discs it is not simple to measure a value of X_∞ from the spectra. A value for X_∞ was therefore obtained by the extrapolation of the data points in the X *versus* time curves (Figure 4.13).

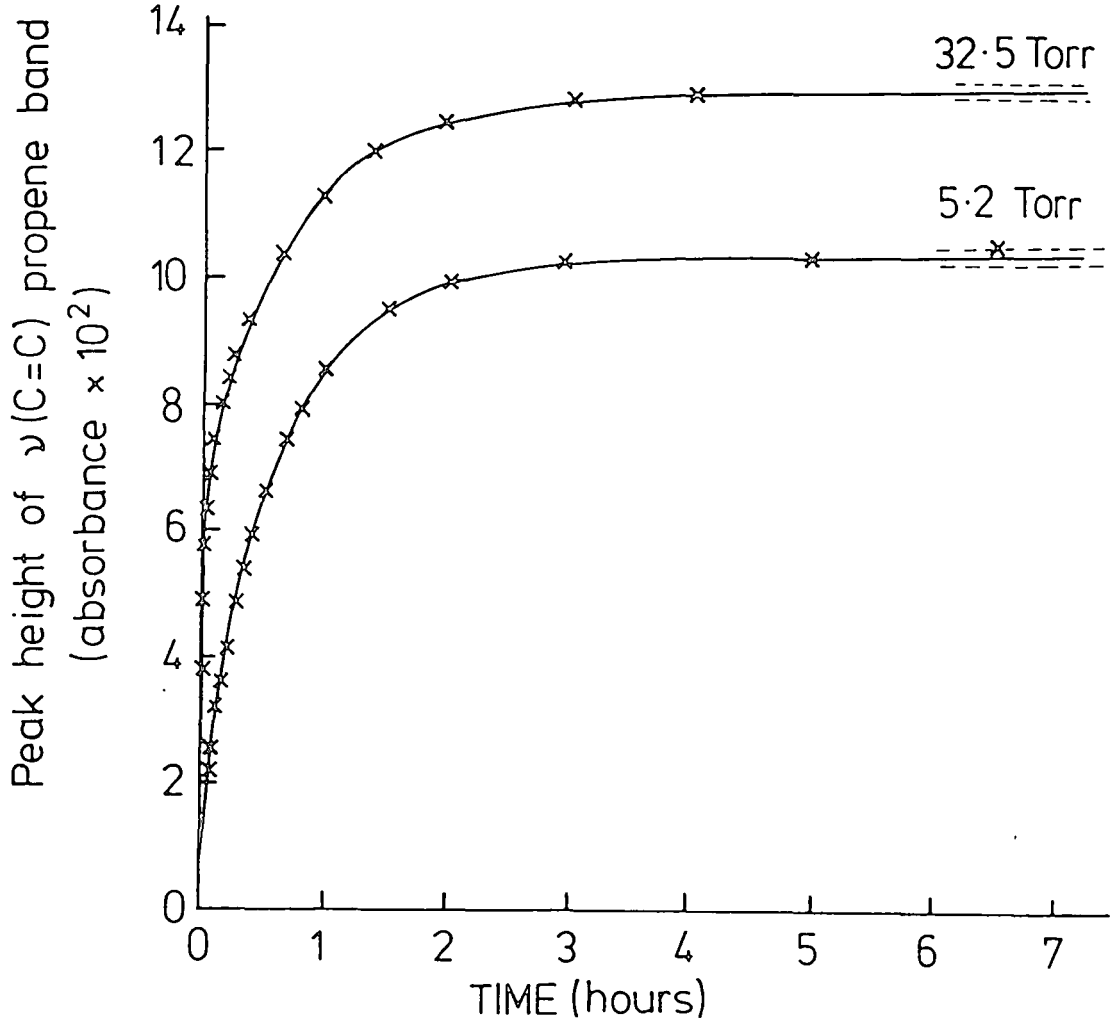

Figure 4.13 The isomerization of cyclopropane on ZnNa-A zeolite. Height of the ν(C=C) peak of propene *versus* time for two cyclopropane overpressures

As will be shown later, this procedure leads to reasonable estimates of X_∞, as data points were collected for periods of 4 hours or more. Once an infinity value had been estimated for each ^{c}-C_3H_6 pressure, this and two other infinity absorbances of $X_\infty \pm 0.2 \times 10^{-2}$ were used to calculate three values of $\ln(X_\infty - X)$ for each data point. The X_∞ values are marked on Figure 4.13. For each ^{c}-C_3H_6 pressure, three first-order rate curves of $\ln(X_\infty - X)$ *versus* time were plotted, as shown in Figures 4.14 and 4.15. A gradient was obtained for each line by a least squares fit of the data points in the time intervals 5-55 minutes for Figure 4.14 and 10-60 minutes for Figure 4.15. The data points outside these intervals were omitted because of their obvious deviation from the first order rate equation. From equation (1) the gradients of these plots are equal to -k, where k is the observed rate constant for the isomerization of ^{c}-C_3H_6 in the zeolite cavities. A summary of the three rate constants obtained for each pressure, and the X_∞ values used, is given in Table 4.10.

TABLE 4.10 A summary of the rate constants obtained from the $\ln(X_\infty - X)$ *versus* time plots for the two cyclopropane pressures

5.2 Torr ^{c}-C_3H_6		32.5 Torr ^{c}-C_3H_6	
10^2 X_∞ (absorbance units)	k (s^{-1})	10^2 X_∞ (absorbance units)	k (s^{-1})
10.8	3.98×10^{-4}	13.4	2.81×10^{-4}
10.6	4.18×10^{-4}	13.2	2.98×10^{-4}
10.4	4.39×10^{-4}	13.0	3.20×10^{-4}
Average k = 4.18×10^{-4} s^{-1}		Average k = 3.00×10^{-4} s^{-1}	

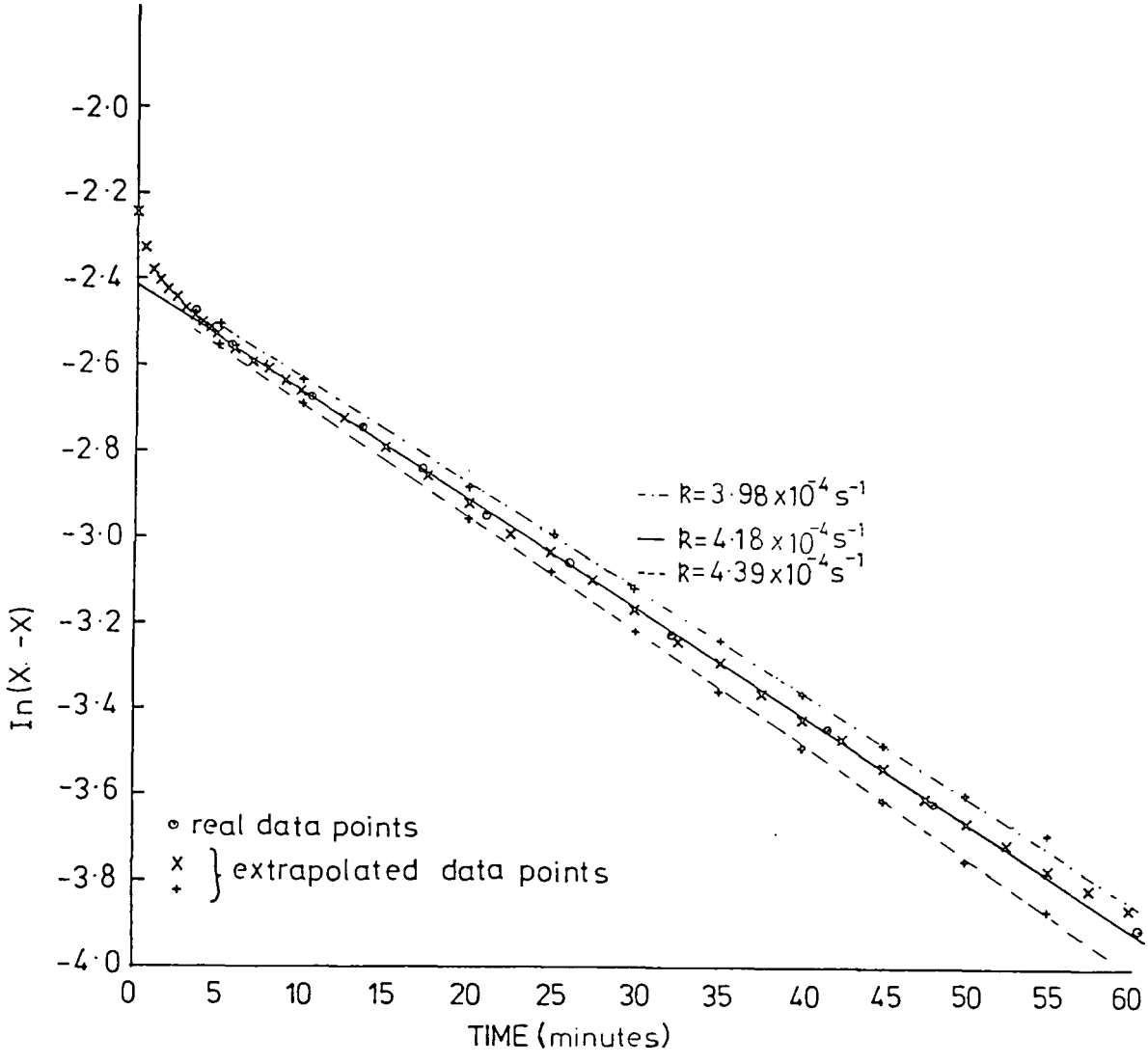

Figure 4.14 The isomerization of cyclopropane on ZnNa-A zeolite at a pressure of 5.2 torr. Determination of the first order rate constant.

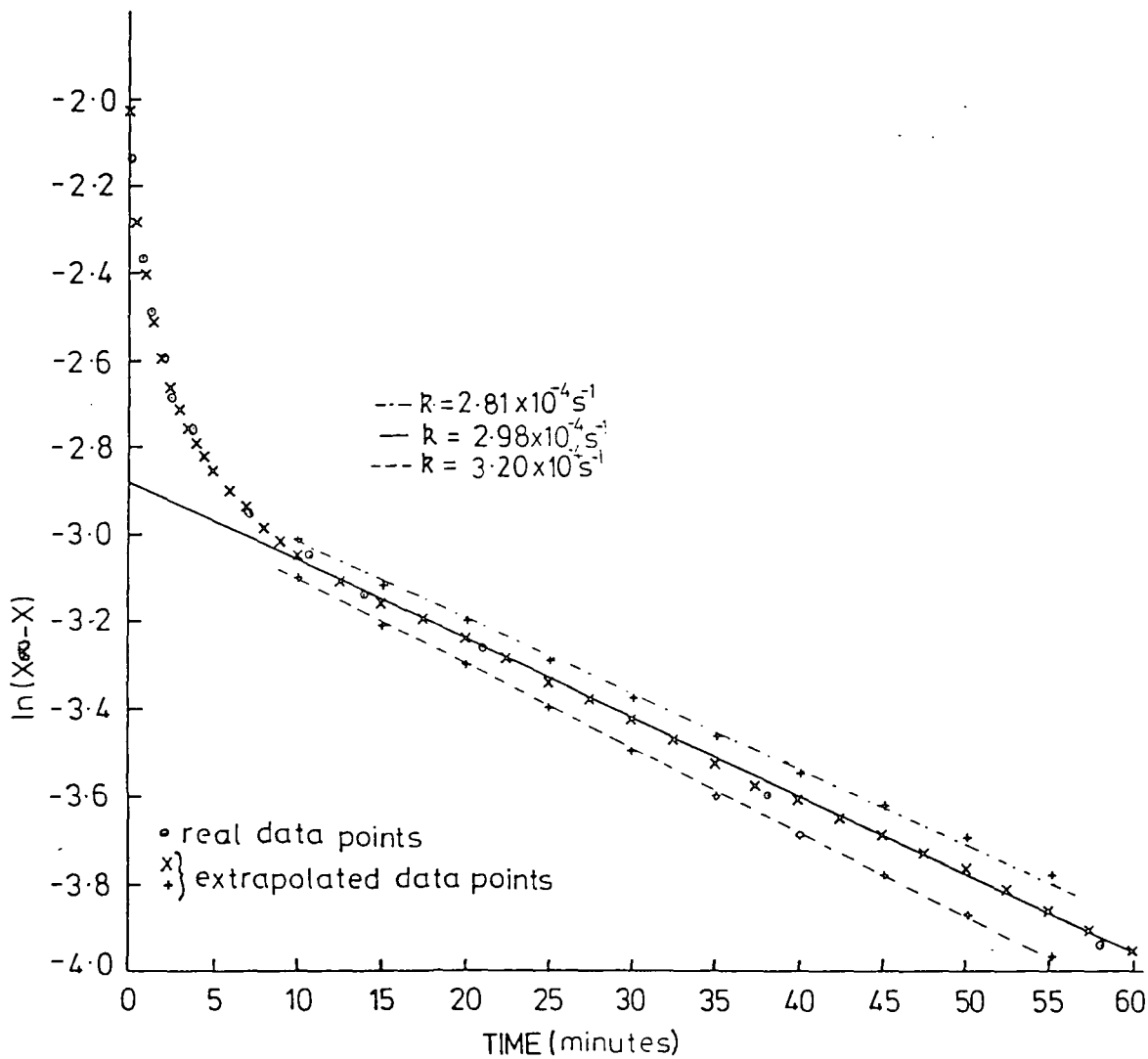

Figure 4.15 The isomerization of cyclopropane on ZnNa-A zeolite at a pressure of 32.5 torr. Determination of the first order rate constant.

It is seen, from Table 4.10, that the different X_∞ values used to calculate the rate plots cause no significant variation in the rate constant observed for each ^{c}-C_3H_6 pressure. An average value of the gradients can therefore be taken to represent a reasonable value for k at each pressure (Table 4.10). From a comparison of these average k values, a likely pressure dependence of the rates is noted. This will be considered later.

In Figures 4.14 and 4.15 it is observed that the data points in the initial stages deviate markedly from the first order rate curve. The most likely explanation of this is that the rate of diffusion of the ^{c}-C_3H_6 into the cavities is fairly slow and so equilibrium is not obtained immediately. Once equilibrium is obtained the data is observed to obey equation (1). Förester *et al*[15] reported a similar deviation in rate data (at high temperature) for ^{c}-C_3H_6 isomerization on type A zeolites (Li^+, Na^+, Mg^{2+}, Ca^{2+} and Co^{2+}), obtained from gas phase composition measurements; no deviation was observed in their (ambient temperature) IR measurements.[14,44]

(C) The half-life of the isomerization

The half-life for a first order reaction is given by:

$$\frac{\ln 2}{k}$$

From the average k values a half-life for the isomerization of 28-38 minutes is obtained. It is well known in reaction kinetics that infinity values are normally taken after ten half-lives. For the isomerization reaction, this point will be reached after *ca.* 4.6-6.3 hours. We can therefore assume

that the extrapolated values of X_∞ are reasonable, as the values were obtained at around this time after the start of the isomerization, and data points were collected in this interval.

(D) The alternative rate equation

It was noted earlier that there was a likely pressure dependance on the observed rate constant. This dependance cannot be accounted for by the first order rate equation (1) used to fit the data, since its derivation ignores any equilibrium between the gaseous and adsorbed $c\text{-}C_3H_6$. We have therefore attempted a more detailed analysis of the data allowing for (a) the strong chemisorption of the reaction product, C_3H_6, on the isomerization sites and (b) an equilibrium between the adsorbed $c\text{-}C_3H_6$ and the gas phase. Thus we make the reasonable assumption that the product is not desorbed under the conditions used (see earlier section on C_3H_6 adsorption).

Using the Langmuir isotherm model[45] for the adsorption of $c\text{-}C_3H_6$, the rate of adsorption (r_a) and desorption (r_d) may be expressed as:

$$r_a = k_a P[\text{no. of vacant sites}] = k_a P(S_T - C_c - C_p) \qquad \text{(eqn. 2)}$$

where k_a = constant for adsorption, P = pressure of $c\text{-}C_3H_6$, S_T = the total number of surface sites, C_c = number of sites occupied by adsorbed $c\text{-}C_3H_6$ at time t, C_p = number of sites occupied by adsorbed C_3H_6 at time t: and

$$r_d = k_d C_c \qquad \text{(eqn. 3)}$$

where k_d = constant for desorption.

At equilibrium $r_a = r_d$ then

$$k_d C_c = k_a P[S_T - C_c - C_p] \qquad \text{(eqn. 4)}$$

rearranging and letting $k_1 = k_d/k_a$

$$\therefore \quad C_c = \frac{S_T - C_p}{\left(\frac{k_1+1}{P}\right)} \qquad \text{(eqn. 5)}$$

For the isomerization of c-C_3H_6 on a surface the first order rate equation is given by

$$\frac{-dC_c}{dt} = kC_c = \frac{dC_p}{dt} \qquad \text{(eqn. 6)}$$

where k is the rate constant for the isomerization of adsorbed c-C_3H_6.

Substituting for C_c in equation (6)

$$\frac{k(S_T - C_p)}{\left(\frac{k_1+1}{P}\right)} = \frac{dC_p}{dt} \qquad \text{(eqn. 7)}$$

By rearranging this expression and integrating, the following integrated rate equation is obtained

$$\frac{k}{\left(\frac{k_1+1}{P}\right)} t = -\ln(S_T - C_p) + Z \qquad \text{(eqn. 8)}$$

where Z is a constant.

Now at $t = 0$, $C_p = 0$

$$\therefore \quad Z = \ln S_T \qquad \text{(eqn. 9)}$$

$$\text{Thus } \left(\frac{k}{\frac{k_1+1}{P}}\right) t = \ln S_T - \ln(S_T - C_p) \qquad \text{(eqn. 10)}$$

Now the total number of surface sites, S_T, is proportional to X_∞ and the number of adsorbed C_3H_6 molecules at time t is equal to X.

The rate equation (10) can therefore be written in the form

$$\ln(X_\infty - X) = \ln(X_\infty) - \left(\frac{k}{\frac{k_1+1}{p}}\right) t \qquad \text{(eqn. 11)}$$

This equation can now be compared to equation (1). The only significant difference between these two equations is the gradient of a $\ln(X_\infty - X)$ *versus* time plot. According to equation (11) the gradient will be dependent upon pressure, whereas equation (1) predicts it to be proportional to k. For the new model, equation (11) predicts that as the $c\text{-}C_3H_6$ pressure becomes very large, the gradient will approach k, and become independent of pressure. At low pressures, the gradient will be pressure dependant, with a value less than k.

Unfortunately the predicted pressure dependance of the gradient of the $\ln(X_\infty - X)$ *versus* t plots is actually opposite to that which is observed experimentally. This new model therefore does not account for the observed behaviour in the gradient of the $\ln(X_\infty - X)$ *versus* time plots. There are a number of other effects which if considered, may perhaps explain the experimental observations:

(i) the value of ΔH for the adsorption of $c\text{-}C_3H_6$ may change as a function of coverage, in which case the Langmuir Model for the adsorption is not applicable. Other isotherms, such as the Frendlich and Tempkin which allow the ΔH of adsorption to vary as a function of coverage[45] may better describe the adsorption behaviour of $c\text{-}C_3H_6$;

(ii) we have already proposed that there was some cation movement on $c\text{-}C_3H_6$ adsorption. There exists then the possib-

ility that the pressure of the reactant affects the cation positions within the zeolite cavities;

(iii) a final possibility is, of course, that the rate constant itself is actually pressure dependant.

(E) A comparison with published rate constants

We have observed the gradient of the $\ln(X_\infty - X)$ *versus* time plot to be different at the two pressures studied. This makes a direct comparison with the work of Förester *et al*[14] on the same system difficult, particularly as no over-pressures were stated in their work. If, however, we do as Förester *et al* did and simply equate the gradient with the first order rate constant (equation (1)), then some useful information can be obtained. This arises because the measured gradients of our two plots are not too different (*viz.* 4.18 and $3.0 \times 10^{-4} s^{-1}$).

Förester and Seebode[14] have only published a rate constant for c.-C_3H_6 isomerization on ZnNa-A in the presence of the co-catalyst SO_2, which has been observed to enhance the isomerization rate by factors of *ca.* 20 times. In the presence of between 3-10 SO_2 molecules/supercage the rate constant was found to vary between $1.5\text{-}3.2 \times 10^{-3}$ s^{-1} g^{-1}. The maximum value was obtained at between 8-9 SO_2 molecules supercage, above this concentration partial blocking of the catalytic sites occurred.

The units chosen by the authors to describe their rate constants (s^{-1} g^{-1}) also makes a direct comparison with our data difficult. In our experiments the mass of zeolite in the beam will not exceed 10 mg. Thus the average rate con-

stant in our isomerization experiments is 0.0358 s^{-1} g^{-1}. This rate constant clearly indicates that our isomerization rate is considerably faster than that observed by Förester *et al*[14]. As the compositions and activation of the zeolites, and the amount of adsorbed $c\text{-}C_3H_6$ were comparable in our work and that of Förester *et al*, there is no obvious reason for the extremely large variation in the catalytic activity of the sample.

More recently Förester *et al*[15] have published rate constants for $c\text{-}C_3H_6$ isomerization on a number of other type A zeolites (Li^+, Na^+, Mg^{2+}, Ca^{2+} and Co^{2+}). The rate constants were determined from studies in a recirculatory flow reactor at 473K, using gas chromatography (g.c.) for analysis of the gas phase composition. A rate constant of 5 x 10^{-4} s^{-1} was reported for the most active zeolite, $Co_{4.4}Na_{3.2}$-A at 473K. This zeolite, from the previous study by the authors,[14] was shown to have a higher catalytic activity towards $c\text{-}C_3H_6$ isomerization than ZnNa-A. It is therefore surprising considering the higher temperature, that the rate constant for the reaction on Co-A is of the same magnitude as the rate constant we have found for ZnNa-A at room temperature. In further IR and g.c. studies of the CoNa-A + $c\text{-}C_3H_6$ system (to be published by Förester *et al*[44]) a rate constant of *ca*. 2 x 10^{-5} s^{-1} was reported for the isomerization at beam temperature (345K) by the IR technique. From reactor/g.c. studies in the temperature range 420-480K, an Arrhenius plot was made, from which a rate constant at beam temperature (345K) was calculated (1.19 x 10^{-5} s^{-1}), in agreement with the value obtained from the IR measurements. When we substitute into the Arrhenius equation given in this paper the temperature of 473K, a rate constant of

3.1×10^{-3} s^{-1} is obtained.[1] This value differs significantly from that actually reported (5×10^{-4} s^{-1}).[15] This raises doubts in the reliability of the rate constants reported by these authors.

It is of interest to note that the rate constant we obtain for the isomerization of $^{c}-C_3H_6$ on Zn-exchange A zeolite is of the same order of magnitude as that for the gaseous isomerization of $^{c}-C_3H_6$ at 773K, for which Atkins[46] has reported a k value of 6.7×10^{-4} s^{-1} at the high pressure limit. This illustrates how effective zeolites are as catalysts.

4.5 Conclusions

In agreement with Förester *et al*,[14] we observe the isomerization of $^{c}-C_3H_6$ on ZnNa-A zeolite to be well described by a first order rate equation. We have, however, found the isomerization to occur at a very much faster rate in our samples of ZnNa-A.

An apparent pressure dependance in the gradient of the $\ln(X_\infty - X)$ *versus* time plots (the gradient is equal to the rate constant in the treatment of Förester) has also been observed. An alternative analysis based on the Langmuir isotherm model was unable to explain the observed decrease in the gradient at higher pressures.

A deeper consideration of the assignments for C_3H_6 adsorbed on ZnNa-A has led us to propose an alternative assignment scheme, involving the mixing of the $\nu(C=C)$ and $\delta(CH_2)$ modes, as has been observed in Zeise's salt. Without

a full normal coordinate analysis this alternative assignment cannot be verified. It is proposed to undertake this in the future.

Clearly further work is required to clarify the discrepancies between our results and those of Förester *et al.* In addition it is proposed that neutron diffraction studies are undertaken to obtain structural data on the location of $c\text{-}C_3H_6$ complexes in Co and Mn exchanged type A zeolites.

REFERENCES (Chap.4)

1. Roberts, R.M., J.Phys.Chem., 63, 1400, (1959).

2. Hall, W.K., Lutinski, F.E. and Gerberich, H.R., J.Catal., 3, 512, (1964).

3. Gerberich, H.R., Hightower, J.W. and Hall, W.K., J.Catal., 8, 39, (1967).

4. Hightower, J.W. and Hall, W.K., J.Am.Chem.Soc., 90, 851, (1968).

5. Hall, W.K., Larson, J.G. and Gerberich, H.R., J.Am.Chem. Soc., 85, 3711, (1963).

6. Larson, J.G., Gerberich, H.R. and Hall, W.K., J.Am.Chem. Soc., 87, 1880, (1965).

7. Hightower, J.W. and Hall, W.K., J.Phys.Chem., 72, 4555, (1968).

8. Tam, N.T., Cooney, P.R. and Curthorys,G., J.Catal., 44, 81, (1976).

9. George, Z.M. and Habgood, H.W., J.Phys.Chem., 74, 1502, (1970).

10. Kiricsi, I., Hannus, I., Varga, K. and Fejes, P., J.Catal., 63, 501, (1980).

11. Basset, D.W. and Habgood, H.W., J.Phys.Chem., 64, 769, (1960).

12. Flockhart, B.D., McLoughlin, L. and Pink, R.C., J.Chem. Soc.Chem. Commun., 818, (1970).

13. Bartley, B.H., Habgood, H.W. and George, Z.M., J.Phys. Chem., 72, 1689, (1968).

14. Förester, H. and Seebode, J., Zeolites, 3, 63, (1983).

15. Fejes, P., Kiricsi, I., Förester, H. and Seebode, J., Zeolites, 4, 259 (1984).

16. Cruz, W.V., Leung, P.C.W. and Seff, K., J.Am.Chem.Soc., 100, 6997, (1978).

17. Howard, J. and Braid, I.J., Zeolites, 5, 101, (1985).

18. Coudurier, G., Decamp, T. and Pralianol, H., J.Chem.Soc., Faraday Trans.I., 78, 2661, (1982).

19. Kubelková, L., Nová-ková, J., Kriványek, M., and Jírú, P., React.Kinet.Catal.Lett., 5, 479, (1976).

20. Efremov, A.A. and Davydov, A.A., Kinet.Katal., 21, 488, (1980).

21. Drent, A.L. and Kokes, R.J., J.Am.Chem.Soc., 92, 6709, (1970).

22. Davydov, A.A., Mikhaltchenko, V.G., Sokolovskii, V.D. and Boreskov, G.K., J.Catal., 55, 299, (1978).

23. Efremov, A.A., Lokhov, Yu.A. and Davydov, A.A., Kinet. Katal., 22, 702, (1981).

24. Gordymara, T.A. and Davydov, A.A., Kinet.Katal., 20, 733, (1979).

25. Tam, N.T. and Shepherd, N., J.Chem.Soc., Chem.Comm., 868, (1978).

26. John, C.S., Marsden, C.M. and Dickinson, R., J.Chem.Soc., Faraday Trans.I, 72, 2923, (1976).

27. Förester, H., Franke, S. and Seebode, J., J.Chem.Soc., Faraday Trans.I., 79, 373, (1983).

28. Kim, Y. and Seff, K., J.Phys.Chem., 84, 2823 (1980).

29. Kiselev, A.V. and Lygin, V.I., "Infrared Spectra of Surface Compounds", Wiley, New York, 1972.

30. Corma, A., Lopezagudo, A. and Fornes, U., J.Chem.Soc., Chem.Commun., 17, 942 (1983).

31. Förester, H. and Seelemann, R., React.Kinet.Catal.Lett., 17, 149, (1981).

32. Breck, D.W., "Zeolite Molecular Sieves", Wiley, New York, 1974, pp. 462-463 and references therein.

33. Herzberg, G., "Infrared and Raman Spectra of Polyatomic Molecules", Van Nostrand, New York, 1945.

34. Hiraishi, J., Spectrochim.Acta A., 25, 749, (1969).

35. Ševčicha, R. and Čapka, M., Collection Czechoslov.Chem. Commun., 39, 2221, (1974).

36. Silvi, B., Labarb, P. and Perchard, J.P., Spectrachim. Acta A, 29, 263, (1973).

37. Kadir, Z.A., Ph.D. Thesis, University of Durham, 1983.

38. Shimanouchi, T., "Tables of Molecular Vibrational Frequencies, Consolidated Volumn I", NSRDS, 1972.

39. Al Noami, A.N., M.Sc. Thesis, University of Durham, 1981.

40. Butcher, R.J. and Jones, W.J., J.Mol.Spectrosc., 47, 64, (1973).

41. Califano, S., "Vibrational States", Wiley, London, 1976.

42. Levin, I.W. and Pearce, R.A.R., J.Chem.Phys., 69. 2196, (1978).

43. Tam, N.T., Tasai, P. and Cooney, R.P., Aust.J.Chem., 31, 255 (1978).

44. Fejes, P., Förester, H., Kiricsi, I., Seebode, J. and Varga, K. (in press).

45. Bond, G.C., "Catalysis by metals", Academic Press, London, 1962, p.70-71.

46. Atkins, P.W., "Physical Chemistry", Oxford University Press, p.857, 1978.

CHAPTER FIVE

FTIR STUDIES OF COPPER CONTAINING Y ZEOLITES

Part I. The location of Copper(I) - carbonyl complexes

5.1 Introduction

Copper(II)Na-Y zeolites are important catalysts in a number of reactions, *e.g.* oxidation,[1-3] cracking[4] and isomerization.[5] It has been proposed for some reactions, *e.g.* the oxidation of ammonia, important in the manufacture of nitric acid,[3] that the reversible reduction of Cu(II) $\longrightarrow$ Cu(I) is an important step in the mechanism. An interest in this step and the paucity of vibrational spectroscopic studies of species adsorbed on reduced Cu(II)Na-Y zeolite provided the motivation for the present work.

Published studies[6-8] of copper exchanged Y zeolites show that only the Cu(I) ions form complexes with carbon monoxide. Therefore CO may be used as a probe for copper ions in the +1 oxidation state. As the stretching vibration ($\nu(C\equiv O)$) of adsorbed CO occurs in a region (2000-2200 cm^{-1}) free of other zeolite vibrations, it may easily be monitored by IR spectroscopy. We have, using FTIR spectroscopy and CO as a probe, been able to locate Cu(I) in different sites in the zeolite framework and to observe cation migration. In addition the adsorbtion of CO on framework atoms has been observed. From the data obtained, we have been able to propose an explanation of the inconsistency in the published $\nu(C\equiv O)$ band positions, for CO adsorbed on Cu(I)Na-Y.

Samples of Cu(I) containing Y zeolites were, in the present study, prepared by partial autoreduction of Cu(II)Na-Y during dehydration. In some instances samples were treated with oxygen during dehydration to reduce the Cu(I) content in the zeolite. Cu(I)Na-Y zeolite may also be prepared by the

reduction of Cu(II)Na-Y with suitable reducing agents (*e.g.* CO)[6,7]. In Chapter Six the reduction of Cu(II)Na-Y by CO and NH_3 will be discussed. In reference to the current chapter, it is important to note that when CO is adsorbed on to Cu(I)Na-Y the relative intensity and positions of bands due to adsorbed CO is the same as for CO adsorbed on to autoreduced samples prepared without oxygen treatment.

5.2 Structural Studies of Cu(II)Na-Y and Cu(I)Na-Y

5.2.1 Cu(II)Na-Y

X-ray diffraction studies of hydrated[9] and dehydrated[10,11] Cu(II)Na-Y zeolites with varying degrees of ion-exchange have been published. The structures which were discussed in detail in Chapter Two, showed that while the Cu(II) ions preferred the α cage sites (S_{II}^* and S_{III}) in the hydrated zeolite, migration of the cations to the small cavity sites (S_I and S_I') occurred on dehydration.

As Cu(II) ions are paramagnetic a number of authors have used electron spin resonance (ESR) spectroscopy[12-16] to study the location of Cu(II) ions in Y zeolites. In hydrated zeolites (0.2-70% exchanged) Soria *et al*[12,13] found two types of Cu(II) ions; one a distorted octahedral complex $[Cu(H_2O)_6]^{2+}$ was tumbling in the large cavities, while the other Cu(II) ions were localized on the cavity walls.

ESR studies of dehydrated Cu(II)Na-Y zeolite have revealed Cu(II) ions in a number of environments. Mörke *et al*[16] for $Cu(II)_{4.5}Na_{44.5}$-Y and $Cu(II)_{18.5}Na_{16.5}$-Y found

Cu(II) ions in sites S_I' and S_{II} and in a cluster in the supercage.

Soria *et al*[12,13] dehydrated Cu(II)Na-Y (7.5-57% exchanged) under vacuum at temperatures up to 873K and recorded the ESR spectrum at intermediate stages of the dehydration. They observed, firstly the removal of loosely held water molecules immobilizing the Cu(II) ions in the S_{II} (or S_{II}^*) positions in the supercages. Later as these cations gradually lost water some of them entered the sodalite cavities. In the final dehydrated state, the Cu(II) ions were mainly located in sites S_I' and S_{II}, and some water was found to be retained rigidly inside the sodalite units. With increasing copper content, coupling of the Cu(II) ions in oxygen bridged pairs was favoured. Coordinative geometries of the Cu(II) species were proposed from the spin-Hamiltonian parameters to include distorted octahedral, square-pyramidal and distorted trigonal environments.

In another study of the dehydration of Cu(II)Na-Y Herman and Flentge[15] found that a rapid dehydration of low exchanged zeolites (2-17% exchanged) left most of the Cu(II) ions in the α cages, but slow dehydration by a long evacuation at room temperature prior to heating gave a higher number of Cu(II) ions in the small cavities. As the copper content increased, rapid dehydration tended to yield Cu(II) ions in both the supercage and small cavity sites.

The adsorption of bases, such as NH_3 and C_5H_5N, have been observed to cause a redistribution of the cations in dehydrated Cu(II)Na-Y. From the X-ray work of Gallazot *et al*[11] the presence of such ligands resulted in the with-

drawal of the cupric ions from the inner sites (S_I and S_I') to the zeolite supercages (Table 2.8). Similar results have been recorded by ESR spectroscopy.[17,18]

5.2.2 Cu(I)Na-Y

Although no X-ray structural data has been published on Cu(I)Na-Y, the behaviour of this zeolite towards oxygen suggests that the Cu(I) ions are located in the small cavities.[6] Unlike Cu(I) ions in aqueous solution, which are very unstable to oxidation, Huang detected no ESR signal due to Cu(II) ions when oxygen was adsorbed onto Cu(I)Na-Y at room temperature. However, when NH_3 was adsorbed prior to oxygen exposure a strong ESR signal due to Cu(II)-ammine complexes was detected immediately oxygen was adsorbed. In other experiments Huang[6] observed the white dehydrated Cu(I)-Na-Y zeolite to turn gradually light blue when exposed to the atmosphere, as conceivably oxidation took place (Cu(II)Na-Y is light green/blue in colour). These results indicated that in dehydrated Cu(I)Na-Y the Cu(I) ions were located in the small cavity sites (S_I and S_I') which, at room temperature, oxygen cannot enter. Similar to the situation with Cu(II)Na-Y, the adsorption of NH_3 or H_2O affects the migration of the Cu(I) ions towards the supercages, where aquo or ammine complex are formed. Once in the supercages the Cu(I) ions are observed to be readily oxidized to Cu(II) ions.

5.2.3 Summary

Overall these previous structural studies have shown in hydrated Cu-Y zeolites (Cu(II) or Cu(I)), the cations prefer sites in the supercages, where they may readily co-

ordinate to water molecules. On dehydration the mobile Cu cations, migrate to the remote S_I and S_I' sites, ~~within the sodalite cages~~, though in high exchange sample some cations are still located in the S_{II}' sites. In the presence of bases (*e.g.* NH_3) the mobile Cu(II) and Cu(I) ions have been observed to migrate back into the supercages where they form complexes.

5.3 The autoreduction of Cu(II)Na-Y and other reduction mechanisms

Jacobs *et al*[19] showed that when Cu(II)Na-Y (68% exchanged) was dehydrated above 623K, the autoreduction of Cu(II) ⟶ Cu(I) occurred. This was accompanied by the loss of loosely held oxygen from the zeolite framework and the formation of true Lewis acid sites. The existence of true Lewis acid sites was confirmed by the adsorption of pyridine. For the reverse process the oxidation of Cu(I) ions was found to be most effective at 613K.

Reduction mechanisms

Studies of the reduction mechanism of Cu(II) ions in Y zeolites have been undertaken by a number of authors using a variety of reduction techniques, details of which are given in Section 6.2.

With CO as the reducing agent Naccache and Taarit[1] proposed the reduction to occur according to the following scheme (eqn. 1).

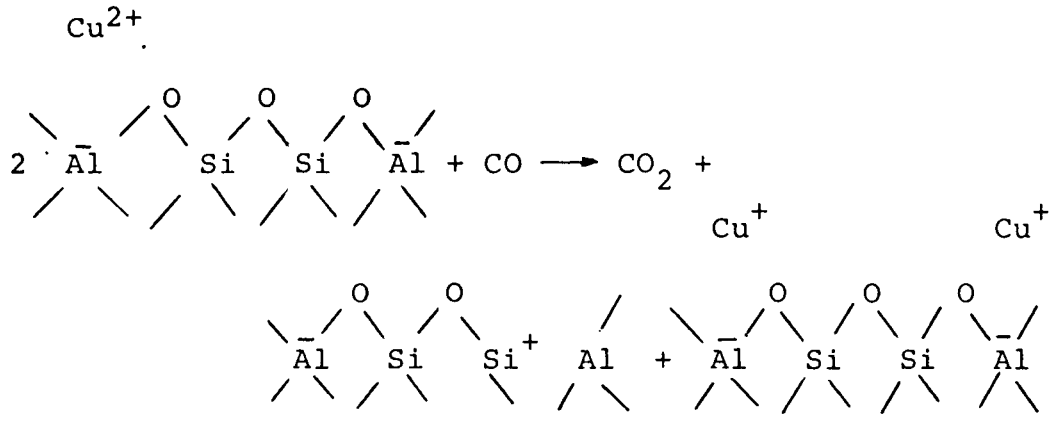

(eqn.1)

A similar mechanism was proposed by Jacobs *et al*[19] for the autoreduction of Cu(II) ions during dehydration (eqn. 2).

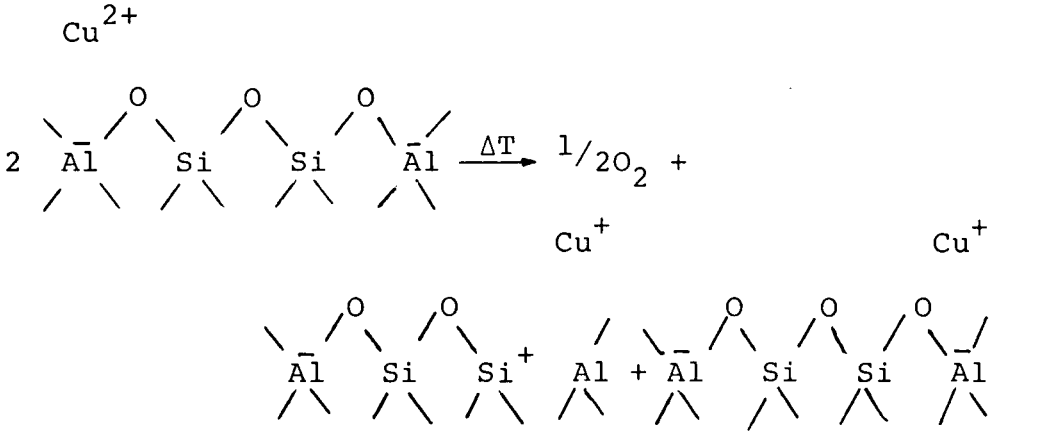

(eqn.2)

In both of these mechanisms oxygen is lost from the framework forming trigonal aluminium atoms which act as true Lewis acid sites.

A kinetics study of the reduction of Cu(II)Na-Y by hydrogen[20] showed the cupric ions in the α and β cages to be reduced by two first order processes. One, the faster process involved the Cu(II) ions in the α-cages. The second, slower mechanism, had as its rate determining step the migration of the Cu(II) ions into the α-cage from the β-cages. As a result of the reduction, protons are fixed in the zeolite lattice, *viz*:

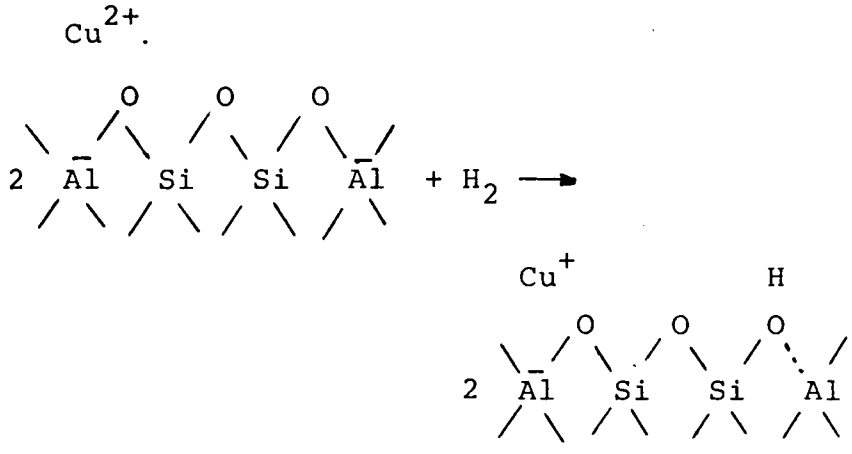

(eqn. 3)

This equation (3) represents the overall reduction mechanism. The further reduction of Cu(I) ⟶ Cu(O) was investigated by the authors,[20] the rate being dependent upon the diffusion of the reactant.

The above work[20] showed that the ease of reduction is a function of the location of the Cu(II) ions in Y zeolites with S_I ions being the more difficult to reduce.

The nature of the true Lewis acid sites in Y zeolites formed by the reduction of Cu(II) ions was investigated further by Jacobs and Beyer.[21] They reinvestigated the reduction of Cu(II)Na-Y (68% exchanged) by CO and by H_2 after the oxidation of the Cu(I)Na-Y. As a result of their studies, it was proposed that the true Lewis acid sites were $[AlO]^+$ species external to the zeolite lattice, in accord with the model proposed by Kühl.[22] On reoxidation the $[AlO]^+$ species remained unchanged and $(Cu\text{-}O\text{-}Cu)^{2+}$ species are formed.

Experimental evidence was presented for the existence of the $[AlO]^+$ sites in the oxidized zeolite from the IR spectra of adsorbed pyridine and from the reduction of the oxidized zeolite by H_2. In the latter case H^+ is not incorporated into the zeolite but water is formed, as seen by the presence

of $\delta(H_2O)$ at 1640 cm^{-1} in the IR spectrum. These proposed mechanistic steps are shown diagrammatically in Figure 5.1.

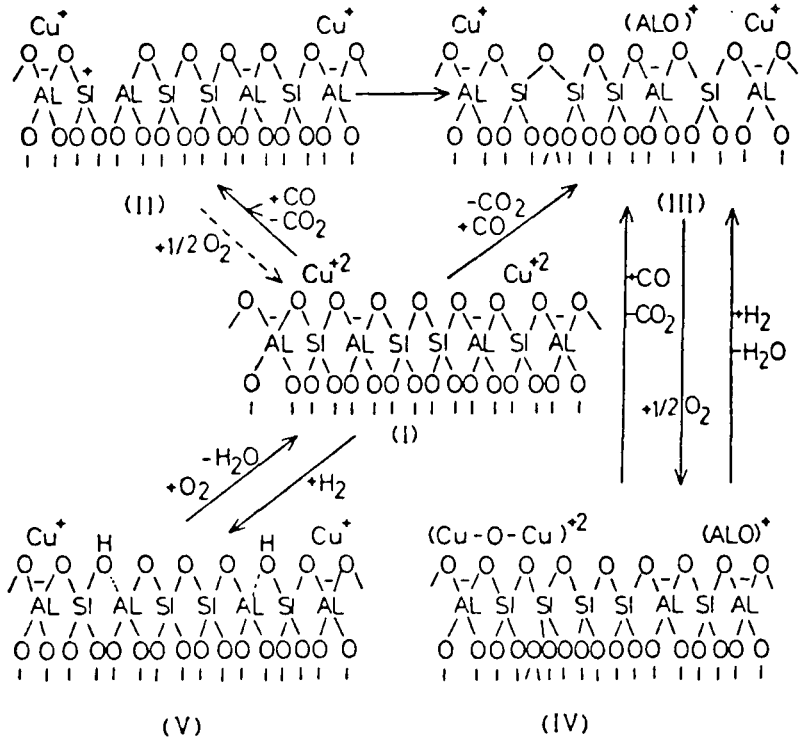

Figure 5.1 Schematic representation of several redox reactions occurring in Cu(II)-Y zeolites.[21]

In Figure 5.1 species (I) ⟶ (II) and (I) ⟶ (V) represent equations (1) and (2) for autoreduction and hydrogen reduction respectively. It was suggested that structure (II) may well be a metastable intermediate to the final $[AlO]^+$, product (III) in the proposed mechanisms.

5.4 A review of previous studies of CO adsorbed on to Copper containing Y zeolites

A number of authors have studied the adsorption of CO by copper containing Y zeolites using IR spectroscopy. When these studies are compared, a number of inconsistencies are noted. In the present work we will show that this is due to different populations of the cation sites by the Cu(I) ions, as a result of slightly different pretreatment conditions.

The interaction of CO with CuNa-Y zeolites has also been studied by a number of other techniques including adsorption isotherm and calorimetric measurements.

5.4.1 Infrared Studies

The infrared spectrum of CO adsorbed on Cu(I)Na-Y zeolite was first reported by Huang.[6,7] Fresh samples of Cu(I)Na-Y, prepared by reduction of the Cu(II) zeolite with NH_3 and CO, showed a weak band at 2140 cm^{-1} due to residual adsorbed CO. When CO (40 torr) was adsorbed onto the samples, a very strong band was observed at 2160 cm^{-1} (Figure 5.2a), which remained on evacuating the sample for 10 minutes. These bands were assigned to Cu(I)-CO complexes formed within the zeolite framework.

Since Huang reported the characteristic $\nu(C\equiv O)$ band of Cu(I)-CO complexes, a number of authors have used this band to characterize samples of CuNa-Y zeolites. In Table 5.1 a summary of these is given. A number of spectra are reproduced in Figure 5.2. From Table 5.1 it is apparent that there is significant variation both in the value of $\nu(C\equiv O)$ for Cu(I)-CO complexes reported by the various authors and in the number of bands observed. Two authors[8,19] who clearly from their spectra (Figure 5.2b and c), observe a second band or shoulder, reported neither a position nor an assignment for the feature. We will shortly illustrate, using the more sensitive technique of FTIR spectroscopy, that the different positions and number of bands are associated with Cu(I)-CO complexes formed at different cationic sites in the framework. The distribution of cations in these sites is influenced by sample pretreatments.

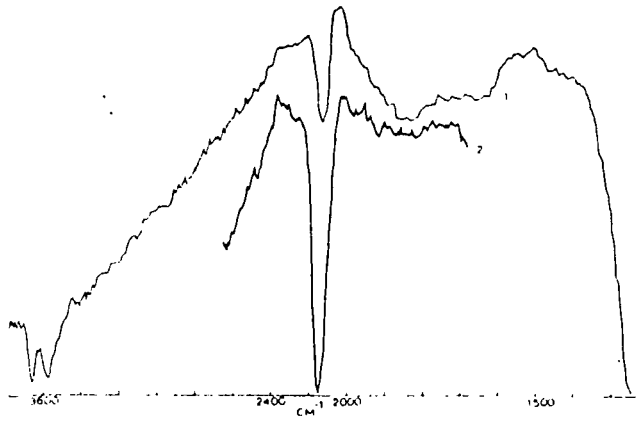

(a) Infrared spectra of CO absorbed in Cu(I)Y (75%) zeolite: (1) Freshly prepared sample; (2) with the addition of 40 torr of CO at 25°. [6,7]

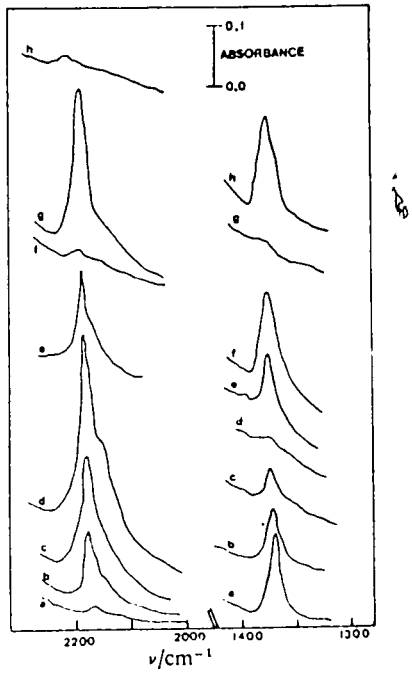

(b) Room temperature adsorption of CO (2180 cm^{-1}) and CO_2 (1370 cm^{-1}) on CuNaY68 pretreated as follows: (a), (b), (c) and (d) vacuum degassed for 2 hours at 593, 693, 773 and 823K respectively: (e), (f), O_2 adsorption at 673 and 613K on sample outgassed at 823K; (g) outgassing of (f) at 323K; (h) readsorption of O_2 on (g) at 613K. [8]

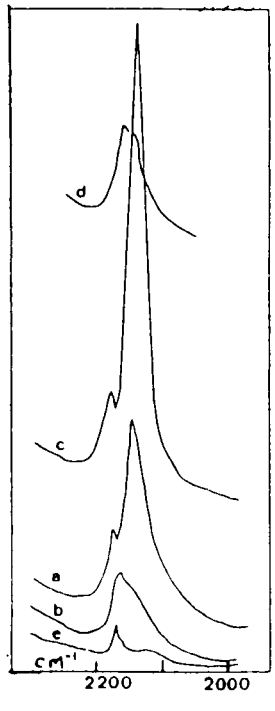

(c) Addition of 40 torr of CO at room temperature after the following successive treatments: (a) outgassing in vacuo at 350°C, (b) addition of 150 torr O_2 at 230°C for 25 min., (c) re-addition of hydrogen (160 torr at 230°C for 25 min.), (d) addition of 150 torr of O_2 at 230°C, (e) room temperature adsorption of CO on Na-Y. [19]

Figure 5.2 Some published spectra of CO adsorbed on Cu(I) Na-Y zeolites

TABLE 5.1 A summary of ν(CO) frequencies observed by various authors for CO adsorbed on CuNaY zeolites

Sample exchange and reducing agent	Comments	ν(CO) cm^{-1}	Ref.
CO/NH_3 reduced	Freshly prepared Cu(I)Na-Y (residual band): Cu(I)-CO	2140	6,7
73% exchange	40 Torr of CO Adsorbed: Cu(I)-CO	2160	
Autoreduced 68% exchanged	No CO pressure given Shoulder visible below 2180 cm^{-1} Not assigned by authors: Cu(I)-CO	2180	19
H_2 reduced 52 and 75% exchange	No details of how many bands or pressure: Cu(I)-CO	2135-2145	24
H_2 reduced 68% exchange	40 Torr of CO band visible above 2145, not assigned by authors	2145	8
Autoreduced? 14.3 —— 80.7% exchange	No detail of number of bands: Cu(II)-CO	2140-2180	23
H_2 reduced 68 and 32% exchange	Nujol mull Cu(I)-CO	2145	25

5.4.2 Other Studies

A comparison has been made by Huang[6] of the adsorption isotherms for CO adsorbed on Cu(II) and Cu(I) containing Y zeolites. The uptake of CO at 298K and 100 torr by Cu(II)Na-Y (75% exchanged) was less than 0.2 mmole/g(close

to the value of Na-Y),whereas in the reduced sample a much greater uptake of 1.65 mmole/g was recorded. This latter value corresponds to the adsorption of about one CO molecule per Cu(I) ion (below 375K and at 100 Torr). These results show there is specific adsorption of CO by Cu(I) ions but not by Cu(II) ions in Y zeolites. This was supported by infrared studies of CO adsorption during oxidation-reduction cycles of CuNa-Y zeolites (Figure 5.2b).[6,19] Here an adsorption band in the $\nu(C\equiv O)$ region was only observed for reduced samples, showing that carbonyl complexes were only formed between Cu(I) ions and CO. The value of the heat of adsorption of CO on reduced CuNa-Y and the strength of the $\nu(C\equiv O)$ vibration led Huang to conclude that interaction was distinctly chemisorption.

Furthermore the adsorption measurements of Huang[6] revealed that below 373K the diffusion of CO into the sodalite cavities was possible. This is a rather surprising observation since CO has a Van der Waals diameter (3.16Å) which is larger than the free openings of the hexagonal windows (2.2Å). Huang[26] rationalized this observation in view of the strong Cu(I)-CO interaction which could somewhat change the shape of the CO molecule. This, coupled with a slight vibrational enlargement of the hexagonal window at higher temperatures, would enable CO to enter the sodalite cages. He therefore proposed,that Cu(I)-CO complexes may form inside the sodalite cages.

Despite the conclusive observation above that Cu(II)Na-Y does not interact strongly with CO, a number of authors have reported Cu(II)-CO interactions from calorimetric[23] and IR measurements.[27,28] A common characteristic in these

studies was that the authors dehydrated their zeolites without oxygen treatment at temperatures greater than 613K. In view of the findings of Jacobs *et al*[19] that autoreduction of Cu(II) ions may occur at dehydration temperatures above 613K, we propose that the interactions observed were actually due to Cu(I) ions in the framework produced by the autoreduction mechanism.

5.4.3 Summary

From these previous studies the following postulates arise, which will be used in interpreting the data obtained in the present study.

(1) CO only interacts strongly with Copper ions in the +1 oxidation state.

(2) Cu(I)-CO complexes in Y zeolites are of a 1:1 stoichometry.

(3) The diffusion of CO into the sodalite cavities is possible below 373K.

5.5 Experimental

Cu(II)Na-Y was prepared as described in Chapter Three. The sample, which was 73% exchanged ($Cu_{20.5}Na_{15.1}$-Y), is referred to hereafter as Cu(II)Na-Y. This zeolite was stored in air at room temperature.

Carbon Monoxide (99.0%, British Oxygen Company) was purified by passing it through a liquid nitrogen trap before use. Oxygen (99.9%, British Oxygen Company special gases) was used without further purification.

Samples were dehydrated under vacuum by the standard technique (Chapter Three). The temperatures used and periods held at the maximum temperature are given in Figure 5.3, together with other experimental details. Sample 1 was used in additional studies described in Chapter Six. Samples 2 and 3 were treated with oxygen during dehydration to decrease the number of Cu(I) ions formed by autoreduction.

Figure 5.3 A summary of the experimental conditions used for the CO + Cu-Y experiments

Sample 1

Cu(II)Na-Y

↓ Evacuated for 18 hr at R.T.

Dehydrated at 697K for 18 hr.

↓ Cooled to RT

Adsorption of CO 0.3 ⟶ 22.4 torr

↓

Evacuation for 1 hr

↓

Desorption of CO by heating at 573K for 30 mins.

↓

Sample used in Chapter Six for the adsorption of NH_3

Sample 2

Cu(II)Na-Y

↓ Evacuated for 20 hr. at R.T.

Adsorbed CO (0.1 ⟶ 18.1 Torr)

↓ Evacuated for 40 min.

Dehydration at 673K for 80 min.

↓ Adsorption of O_2 (32.5 Torr) for 3 hr. at 673K.

Evacuation of O_2 at 673K for 11 hr.

↓ Cool to R.T.

Adsorption of CO 0.8 ⟶ 22.2 Torr

↓

Evacuation for 2.5 hr.

Sample 3

Cu(II)Na-Y

↓ Evacuation for 14.3 hr.

Dehydrated at 693K for 2 hr.

↓ Cooled to R.T.

Adsorption of CO 1.1 ⟶ 10.3 Torr

↓ Evacuation for 0.5 hr.

Heated to 613K

↓ Adsorption of O_2 at 613K for 30 min.

Cooled to RT in presence of O_2

↓ Evacuation of O_2

Adsorption of CO 3.3 ⟶ 31.9 Torr

↓

Evacuation of O_2

Sample 4

Cu(II)Na-Y

↓

Dehydration at 673K for 10 hrs.

↓ Cooled to R.T.

Adsorption of CO 3.9 Torr

↓ CO in contact with sample for 4.3 hr.

Evacuation for 110 Min.

↓

Desorption of CO by heating.

5.6 Results

When CO is adsorbed onto autoreduced Cu(II)Na-Y zeolite (sample 1) (Figure 5.4(i)) two bands and a shoulder are observed at *ca.* 2178, 2141 and 2153 cm^{-1} respectively. On evacuation of gaseous CO (Figure 5.4(ii)) the 2178 cm^{-1} band is immediately removed and the lower frequency features now centred at 2156 and 2142 cm^{-1}, though decreased, in intensity are better resolved.

The 2178 cm^{-1} band is clearly associated with a weakly adsorbed species, whereas the desorption behaviour (Figure 5.4(ii)) of the remaining two bands indicates that they are better described as chemisorbed CO. The 2178 cm^{-1} will be shown to be due to CO adsorbed on framework sites and will be discussed after the chemisorbed species.

5.6.1 The bands in the 2160-2130 cm^{-1} region

The intense bands at 2142 and 2156 cm^{-1} due to chemisorbed CO can be assigned from Table 5.1 to the $\nu(C\equiv O)$ vibration of Cu(I)-CO complexes. As on desorption (by evacuation and heating) of CO from sample 1 (Figure 5.4(ii)) the 2142 cm^{-1} band is more readily desorbed, the two bands must be due to Cu(I)-CO complexes at different locations in the zeolite framework. This observation differs from those reported in the literature, where only <u>one</u> strongly adsorbed Cu(I)-CO complex has been reported.

For comparison of the spectra presented here it should be noted that within any figure all of the spectra are plotted on the same absorbance scale, but that this scale is not necessarily the same for each figure.

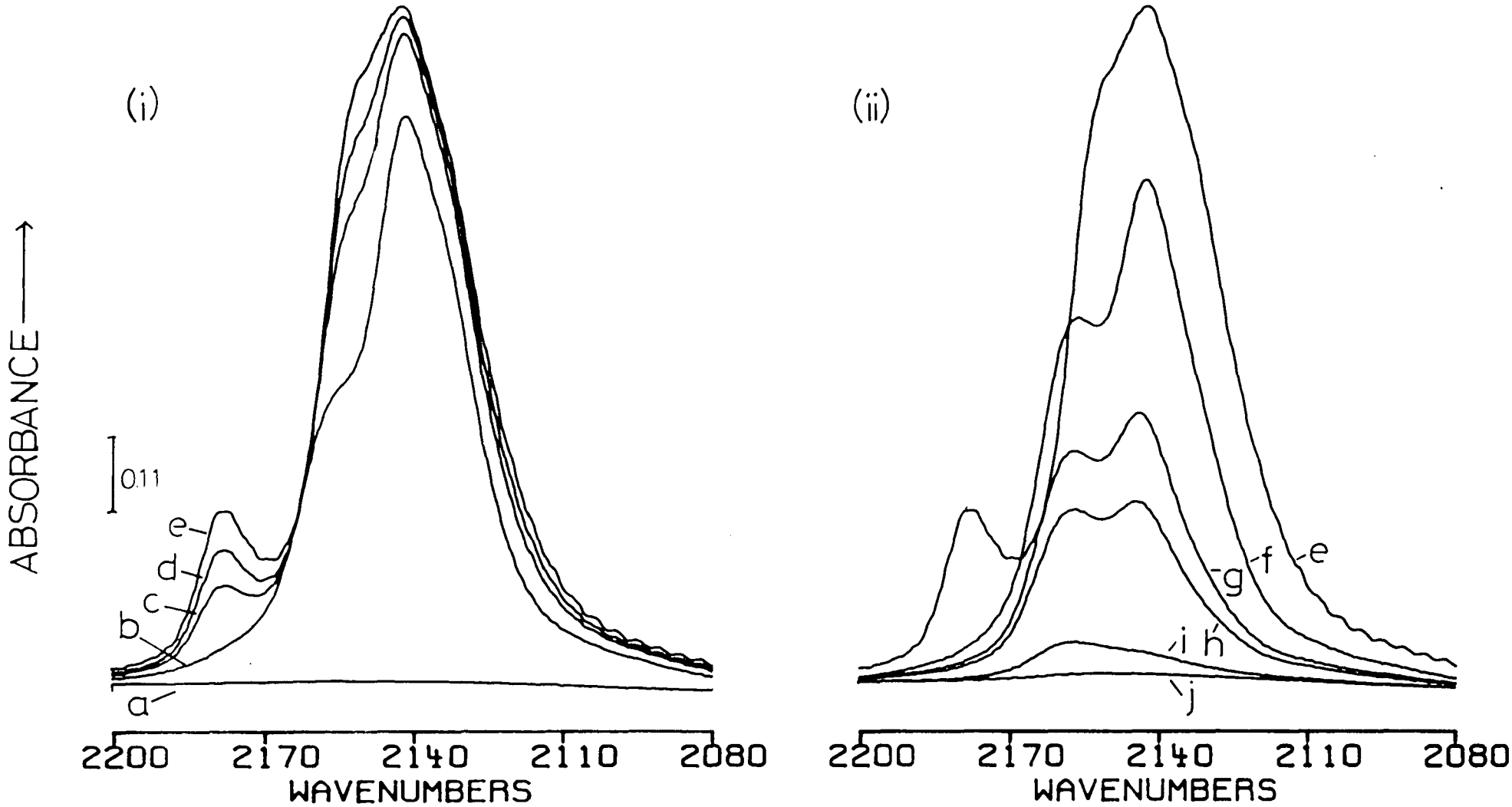

Figure 5.4 The adsorption of CO on autoreduced Cu(II)Na-Y (sample 1)

(i) The adsorption of CO at various pressures; (a) dehydrated zeolite background, sample (a) with CO; (b) 0.3 torr, (c) 5.2 torr, (d) 10.4 torr and (e) 22.5 torr.

(ii) The desorption of CO by evacuation and heating; (e) as in (i), (f) evacuation of gas phase, (b) evacuation for 1 hour at 293K, sample heated at (h) 348K, (i) 444K and (j) 523K.

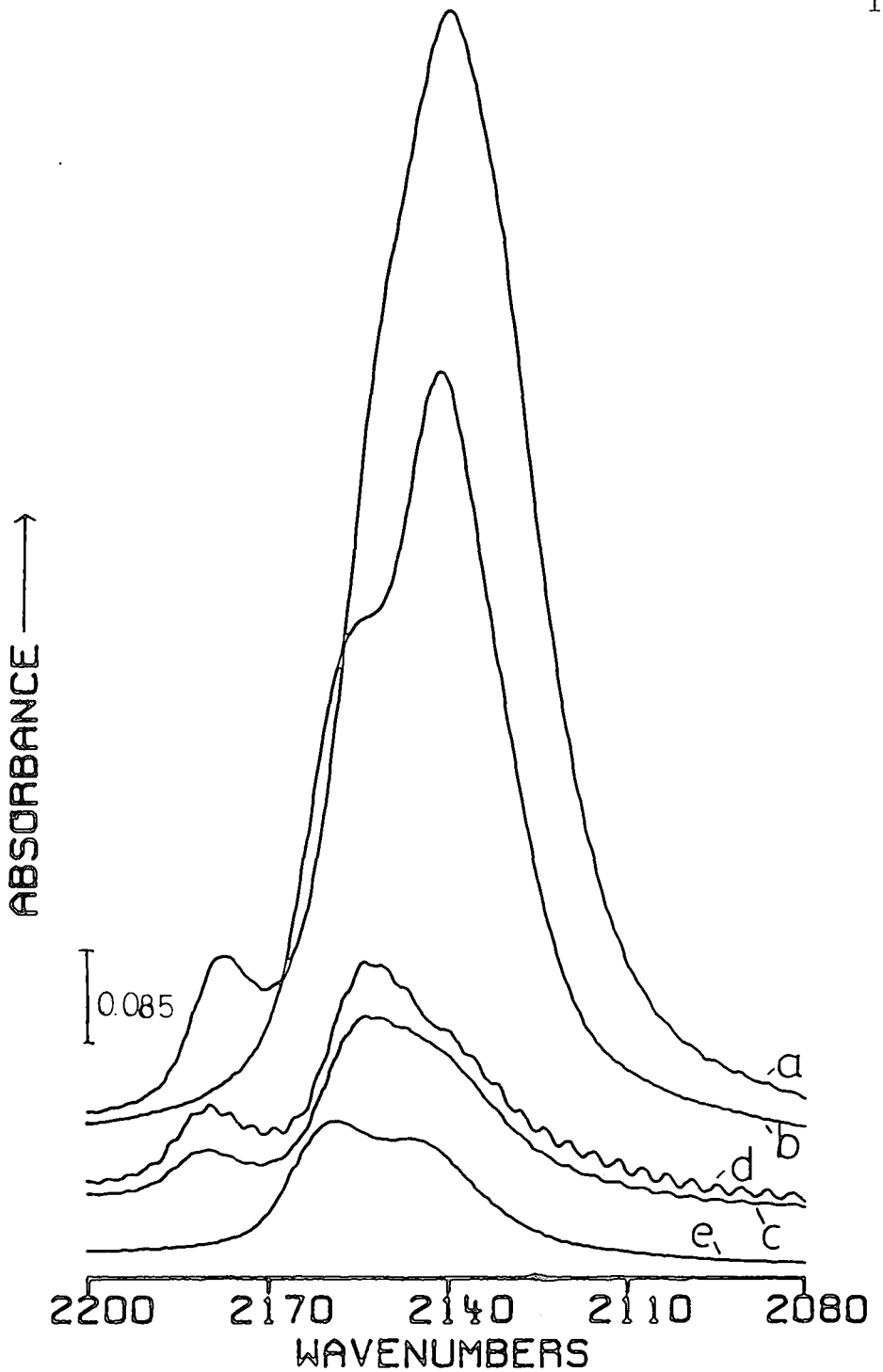

Figure 5.5 The adsorption of CO onto autoreduced and oxygen treated Cu(II)Na-Y (sample 3)

(a) Adsorption of CO (10.3 torr) onto autoreduced Cu(II)Na-Y;

(b) Evacuation of sample (a);

(c) Adsorption of CO (7.9 torr) onto sample 3 after oxygen treatment (see Figure 5.3);

(d) Sample (c) after pressure increased to 31.9 torr;

(e) Evacuation of sample (d).

(all spectra plotted on same absorbance scale. Curves d-e y axis displaced with respect to curved a and b).

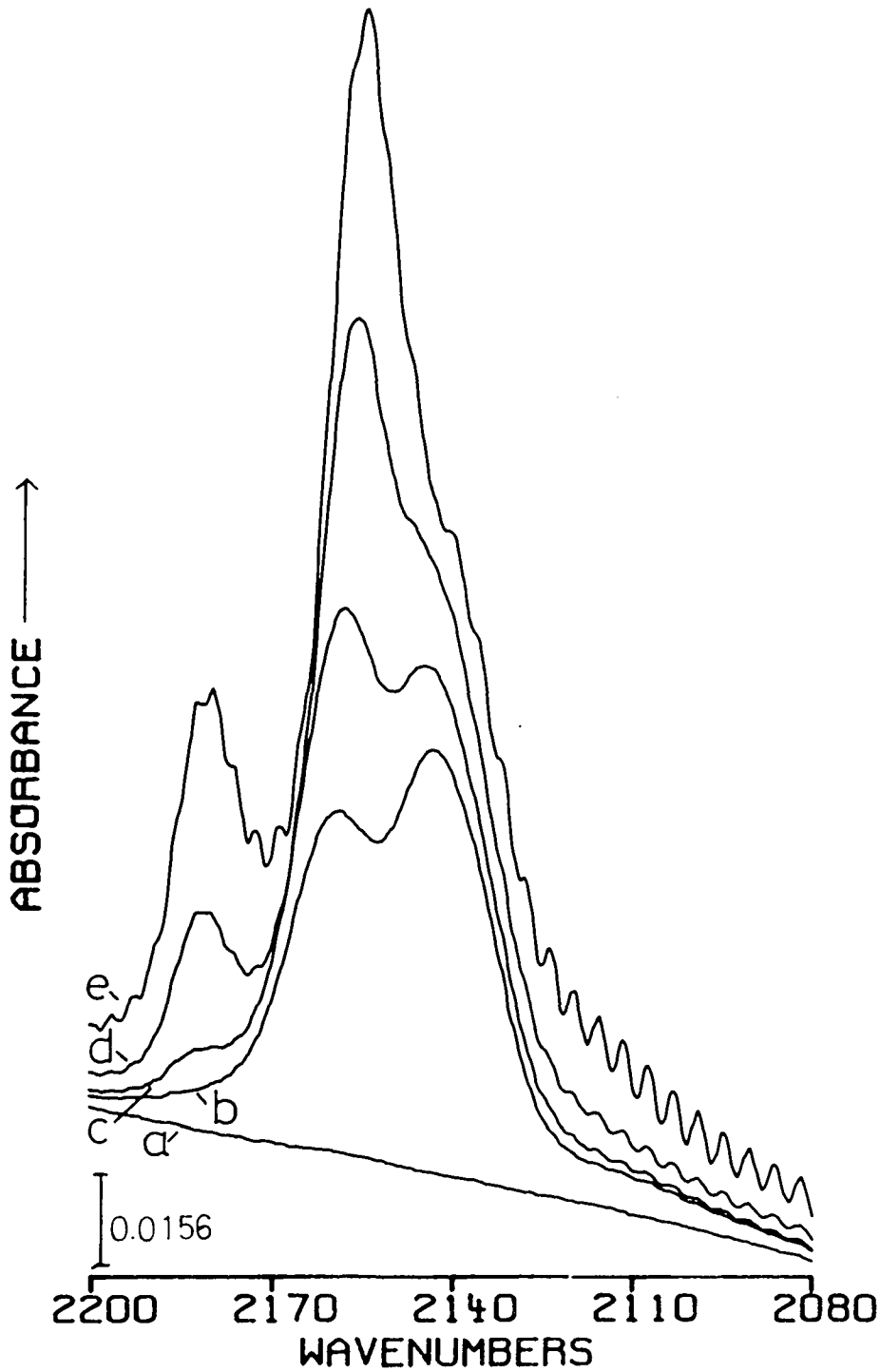

Figure 5.6 The adsorption of CO on to Cu(II)Na-Y treated with oxygen at 673K (sample 2).

(a) Zeolite background after O_2 treatment described in Fig.5.3
Sample (a) with CO; (b) 0.1 torr;
(c) 0.8 torr, (d) 5.0 torr and (e) 22.2 torr.

In Figure 5.5a and b the spectra obtained when CO (10.3 torr) was adsorbed and evacuated from autoreduced Cu(II)Na-Y (Sample 3) are shown. The same sample was subsequently treated with oxygen at 613K before cooling in O_2 and CO(31.3torr) readsorbed (Figure 5.5c-e). As expected oxygen treatment is seen from the reduced absolute intensities of the $\nu(C\equiv O)$ bands to significantly decrease the number of Cu(I) ions in sample 2. Secondly we observe that after oxygen treatment the relative intensities of the 2142 cm^{-1} band (band A) is less than that of the 2156 cm^{-1} band (band B) (Figure 5.5e), whereas in the autoreduced zeolite (Figure 5.4f and 5.5b) the reverse was true.

It is clear already from these two experiments that the relative populations of the two different chemisorption sites can be altered by sample pretreatment conditions. Naturally we assume here and throughout that the dipole moment of adsorbed CO at a particular adsorption site is independent of the sample pretreatment so that relative intensities can be interpreted with some significance.

The effect of oxygen treatment on band intensities is seen more clearly in sample 2,which was treated less severely than sample 3 with oxygen (Figure 5.6). At a CO pressure of 0.1 torr (Figure 5.6b) band A dominated the spectrum as in the autoreduced samples, but as the pressure of CO was raised (Figure 5.6c-e) band B was observed to grow more rapidly and become the most intense band in the spectrum. On evacuation of CO band B remained the most intense band in the spectrum. The greater intensity of band A at 0.1 torr of CO is probably due to the initial adsorption of CO at the

most accessible sites, *i.e.* those sites nearest to the supercages (see below).

Oxygen is expected to oxidize more readily those Cu(I) ions in the more accessible sites, *i.e.* in the sites nearest to the supercages. As we observe band A to be less intense relative to band B after oxygen treatment of autoreduced samples, it is proposed that the Cu(I)-CO complex responsible for band A is formed between CO and Cu(I) ions in sites nearest to the supercages, *i.e.* in the S_{II} sites. Band B is then assigned to Cu(I)-CO complexes formed with Cu(I) ions in the more remote S_I and S_I' sites.

In addition to the features already mentioned above, there appears to be additional intensity lost from *ca.* 2130 cm^{-1} on evacuation of the gas phase (Figure 5.4(ii)). This intensity will be shown later to be due to a fourth species.

5.6.2 The adsorption of CO onto hydrated Cu(II)Na-Y

From the above results it is clear that Cu(II) ions are readily reduced to Cu(I) ions during dehydration, but some Cu(I) ions are more readily oxidized than others. The small cavity S_I and S_I' sites have been shown to provide a stable environment for the Cu(I) ions at room temperature.[6] We decided to investigate whether Cu(I) ions were already present in our hydrated zeolite.

In Figure 5.7 the spectra are shown of CO adsorbed on to hydrated Cu(II)Na-Y (sample 2), that had been evacuated at room temperature (beam temperature) for 20 hrs. to remove the loosely coordinate water from the zeolite

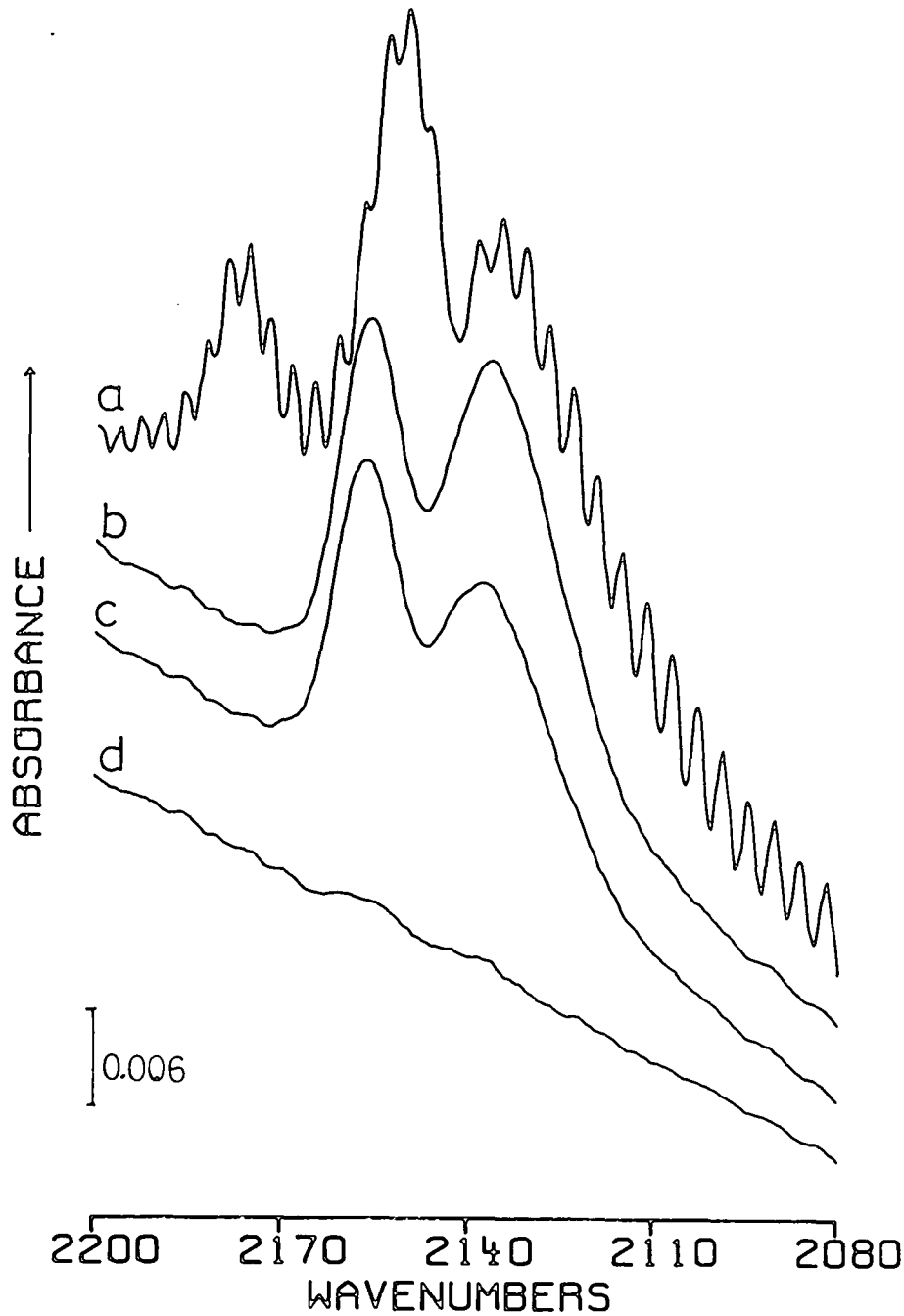

Figure 5.7 The desorption of CO from hydrated Cu(II)Na-Y (sample 2)

(a) adsorption of 18.1 torr of CO

(b) evacuation of sample (a)

(c) evacuation for 40 minutes

(d) sample (e) heated to 393K.

framework. It is apparent from the figure that two very weak bands are observed at 2157 and 2138 cm^{-1} after the removal of gaseous CO from the cell. These bands must, in agreement with the previous results, be assigned to Cu(I)-CO complexes.

An ESCA analysis of the hydrated Cu(II)Na-Y zeolite[29] showed no Cu(I) ions to be present. Therefore from the above results evacuation at ambient temperature can autoreduce Cu(II) ⟶ Cu(I) in the zeolite framework. Autoreduction thus appears to take place under much milder conditions than previously reported.

In the spectrum of the hydrated sample it is important to note that the band at 2178 cm^{-1} is absent. This site is therefore not available in the hydrated form.

5.6.3 The band at 2178 cm^{-1}

In samples of autoreduced Cu(II)Na-Y a band was observed at 2178 cm^{-1}, the intensity of which was found to be strongly dependent upon the pressure of CO in contact with the sample. On evacuation of the gas phase the band is immediately removed. It is therefore associated with weakly adsorbed CO.

The intensity of the band was very much decreased when samples were treated with oxygen (*e.g.* Figure 5.6). This indicates the band to be associated with an adsorption site formed by the autoreduction of Cu(II)⟶ Cu(I), but as the species is physisorbed the site cannot be associated with the cupric ions as these chemisorb CO.

It has previously been shown (Figure 5.7) that the band is absent in hydrated Cu(II)Na-Y and in spectra to be shown in the next chapter, the band is observed to be absent in a sample on which NH_3 had been preadsorbed.

The above findings lead us to propose that the 2178 cm^{-1} band is associated with CO adsorbed on the true Lewis acid sites. These sites are formed during dehydration of Cu(II)Na-Y by autoreduction (Section 5.3) and will be blocked by bases as observed.

5.6.4 The effects of time on band intensities and positions

To eliminate the possibility that the different $\nu(C\equiv O)$ band intensities observed in samples 1-3 were due to the slow diffusion of CO into the cavities, a quantity of CO (3.9 torr) was adsorbed onto autoreduced Cu(II)Na-Y (Sample 4) and the spectrum was monitored as a function of time. The spectra obtained over a four hour period are shown in Figure 5.8, from which the following observations are made:

(1) As the changes observed in Figure 5.8 do not involve any major alterations in the relative intensities of bands A and B, the effects observed in Figures 5.4-5.6 must be attributed to variations in the Cu(I) ion populations of the cationic sites caused by different sample pretreatments.

(2) The intensity of all bands increases considerably over the period of observation. This is due to the slow diffusion of CO into the zeolite cages, as reported by Huang.[6]

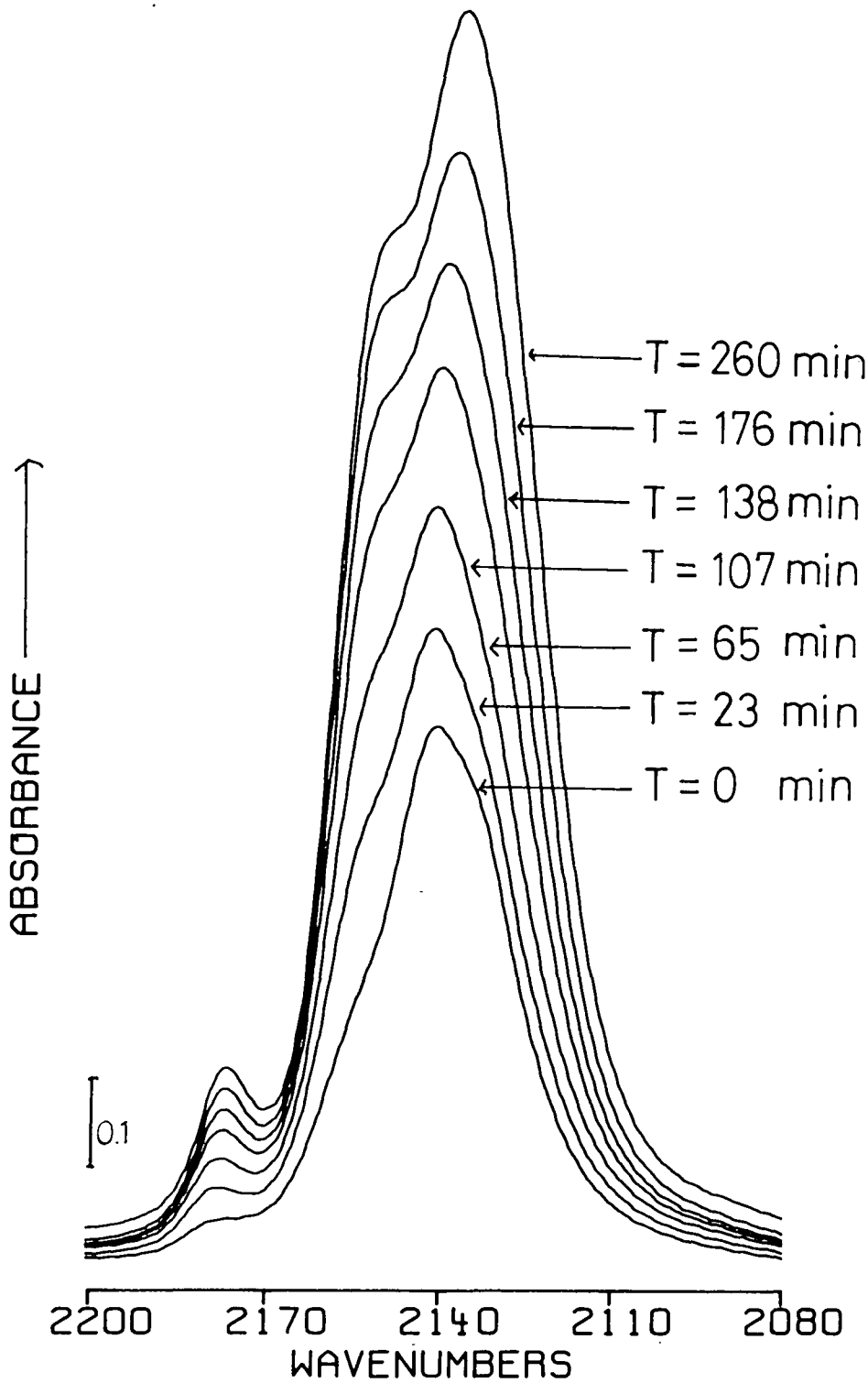

Figure 5.8 The adsorption of CO (3.9 torr) at constant pressure as a function of time on autoreduced Cu(II)Na-Y (sample 4)

(T = 0 is the time the first spectrum was started after adsorption).

(3) There is a gradual shift of the band centres to lower wavenumbers (except the 2178 cm^{-1} band). In the spectrum T = 260 minutes (Figure 5.8) the band centres occur at 2178, 2149 and 2136 cm^{-1}. This will be linked in the next section to the movement of the cations to more accessible sites.

5.6.5 The examination of subtraction spectra: evidence for cation movement

To investigate the possibility of cation movement spectral subtractions were preformed. The technique, using software provided with the Nicolet 60SX spectrometer,[30] allows the point by point subtraction of a reference spectrum from a sample spectrum. This allows the identification of very small changes in two spectra, *i.e.* before and after evacuation of gaseous CO. Negative bands obtained in such spectra are due to a greater band intensity in the reference spectrum. As the background level in our spectra was constant, a subtraction factor of 1 was used in each case.

Firstly, the spectrum of CO adsorbed on sample 4 at T=0 was subtracted from the spectra at times >T=0 in Figure 5.8. The results in the $\nu(C\equiv O)$ region are shown in Figure 5.9. From spectra (a) or (b) in Figure 5.9, the fourth species we suspected in Section 5.6.1, at *ca.* 2130 cm^{-1} is clearly visible as a shoulder at 2127 cm^{-1}. The four $\nu(C\equiv O)$ vibrations occur at 2178, 2152, 2138 and 2127 (Band C) cm^{-1} in these figures.

At later times (Figure 5.9) the growth of the 2127 cm^{-1} band appears to be responsible for the shift of the band centres to lower wavenumbers observed in Section 5.6.4.

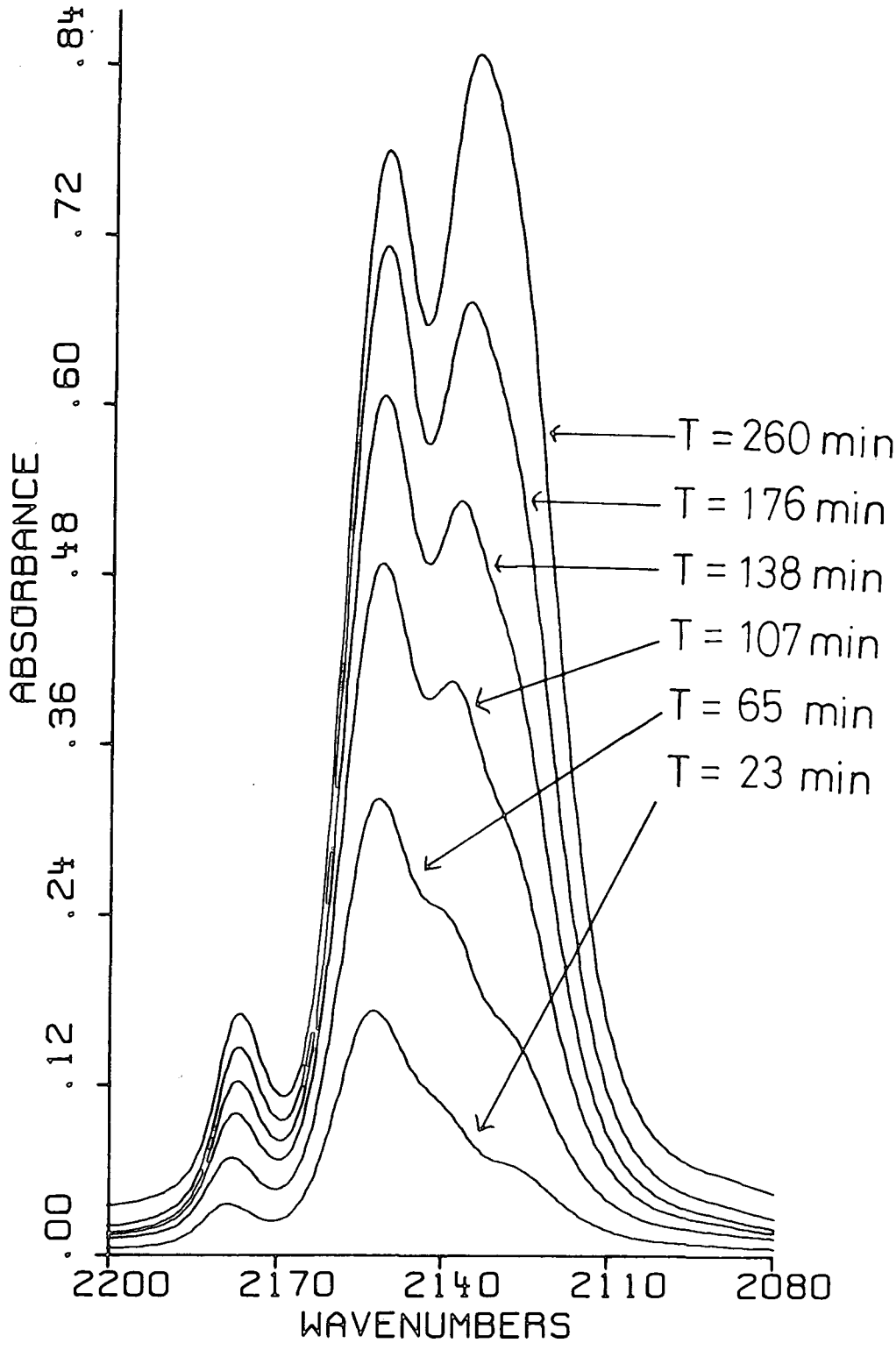

Figure 5.9 Subtraction of the spectrum at T=0 from the spectrum at time T, for CO adsorbed on to sample 4 as shown in Figure 5.8

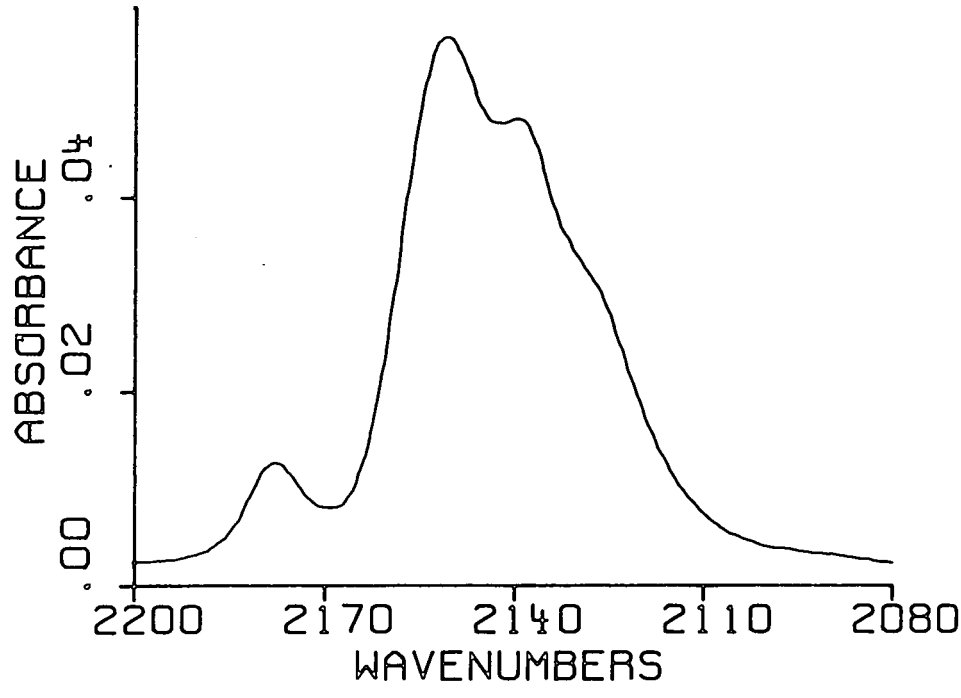

(a) 40-23 minutes

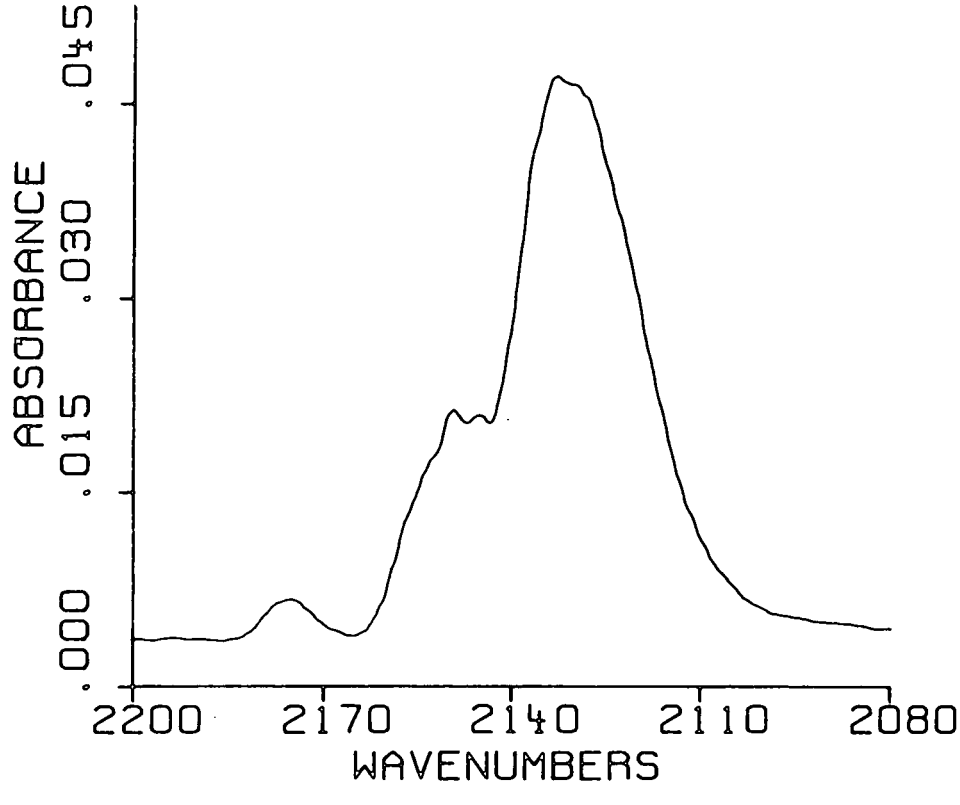

(b) 212-194 minutes

Figure 5.10 Subtraction spectra of constant time intervals for CO adsorbed on sample 4

(a) in the initial stages of adsorption, and

(b) after several hours contact.

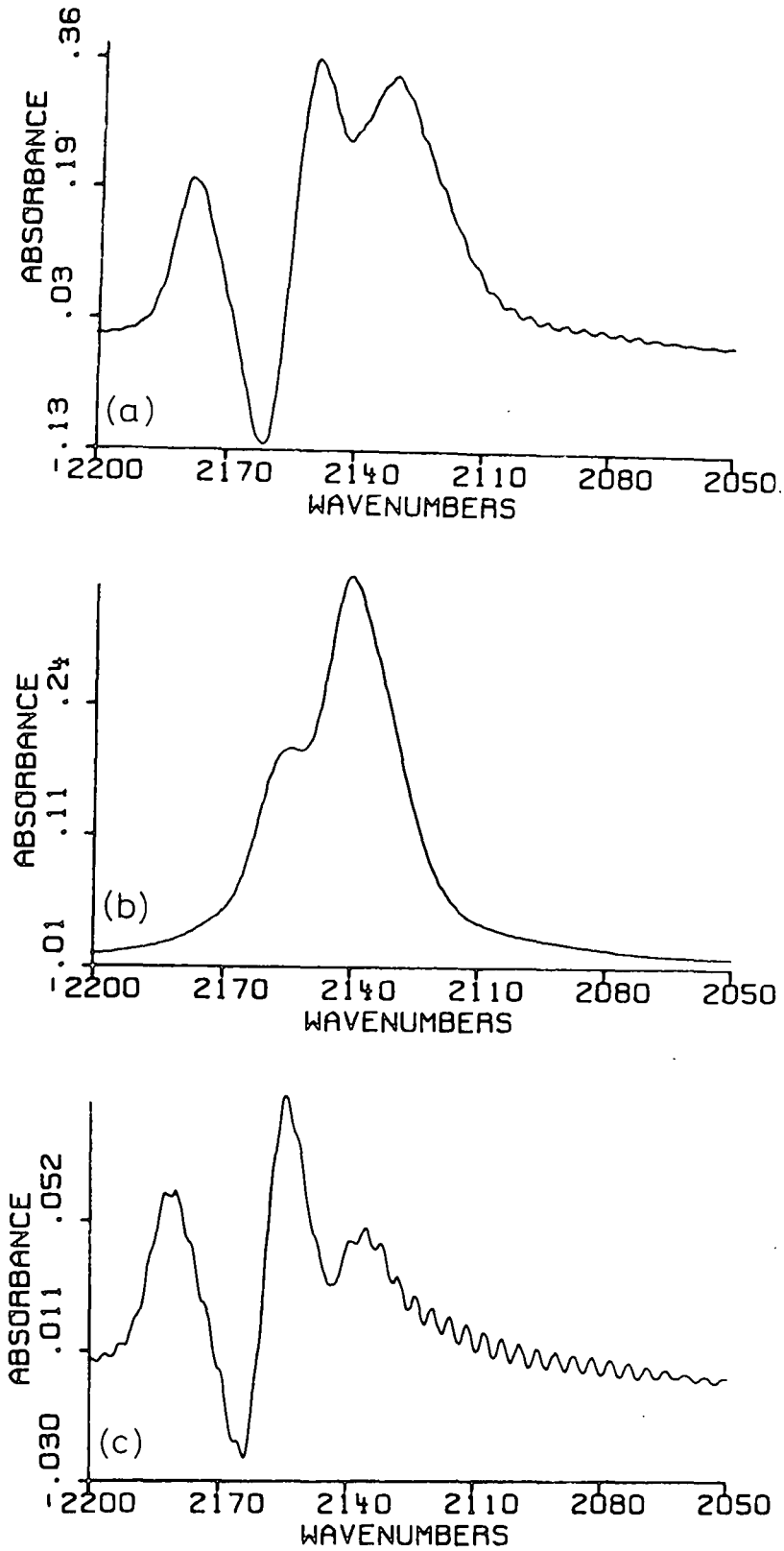

Figure 5.11 Subtraction spectra for CO adsorbed on to Cu(II)Na-Y (samples 1 and 2)

(a) Sample 1: subtraction of spectrum 5.4 (f) from 5.4 (e).

(b) Sample 1: subtraction of spectrum 5.4 (g) from 5.4 (f).

(c) Sample 2: subtraction of spectrum after evacuation from spectrum 5.6 (e).

This was confirmed by subtraction spectra for the time intervals 40-23 minutes and 212-194 minutes (Figure 5.10). These spectra show conclusively,that in the initial stages of adsorption the higher frequency bands show most growth, while after CO has been in contact with the zeolite for some time, it is the lower frequency bands which exhibit most intensity change. The higher frequency bands at *ca.* 2156-2150 cm^{-1} were associated in Section 5.6.1 with sites S_I and S_I', while those at lower wavenumbers were associated with sites near the supercages. The growth of the lower frequency band with time would thus indicate a migration of the Cu(I) ions towards the supercage sites. The initial growth in the high frequency band is probably attributed to the slow diffusion of CO into the cavities.

In the subtraction spectra performed in Figure 5.9 a negative feature was observed at 3633 cm^{-1} when CO was initially adsorbed onto sample 4. This feature is indicative of a perturbation of the OH groups by adsorbed CO. This feature was also observed in similar subtraction spectra of data shown in Figures 5.4-5.6. The very weak perturbation of the OH groups is likely to be associated with the adsorption of CO on the Lewis acid sites (Section 5.6.3).

The subtraction results have,so far,revealed the migration of the cations towards supercage sites. If we subtract the spectrum after removal of CO gas from that of CO in contact with Cu(II)Na-Y (Sample 1) (Figure 5.11a), a negative feature at *ca.* 2160 cm^{-1} and positive features at 2178, 2150 and 2130 cm^{-1} are observed. The negative band indicates an increase in the amount of CO adsorbed at the hidden Cu(I) sites

in the small cavities and shows that on evacuation there is a migration of cations back towards these sites. Subtractions performed later in the evacuation (Figure 5.11b) show only bands at 2156 and 2142 cm^{-1}, as seen initially on CO adsorption. This clearly shows that the general shift of bands to lower wavenumbers with time and the band at *ca.* 2127 cm^{-1} are due to the migration of the cations to sites nearer the supercages.

Finally a subtraction spectrum of the oxidized sample (sample 2) during evacuation (Figure 5.11a) shows the same features due to cation movement.

In Table 5.2 a summary of the observed results is given.

5.7 Discussion

The above results have shown a number of Cu(I)-CO carbonyl complexes to be formed at different cation sites within reduced Cu(II)Na-Y zeolites. These species are characterized by unique $\nu(C\equiv O)$ stretching vibration, such that a lower frequency indicates a complex formed in a more accessible site. The distribution of the Cu(I) cations in these sites has been found to be dependent upon the pretreatment of the samples. Finally the adsorption of CO on the Lewis acid sites within the framework has been identified.

5.7.1 The location of Cu(I)-CO complexes

As previously discussed the Cu(I) ions in dehydrated Cu(I)Na-Y are located in sites S_I and S_I' , and the

TABLE 5.2 A summary of $\nu(C\equiv O)$ frequencies (cm^{-1}) for CO adsorbed on variously pretreated copper zeolites

Bands observed in the presence of the gas phase			After evacuation of the gas phase	
autoreduced	oxidized	after long contact times on autoreduced	hydrated	autoreduced and oxidized
2178	2178	2178		
2156	2156[a]	2149	2156	2156
2142[a]	2142	2136	2138	2142
2127[b]				

a. most intense band in spectrum.

b. revealed from subtraction spectra.

adsorption of bases cause their migration towards sites in the supercages. Also Huang[26] noted that in the presence of adsorbed C_2H_4, no ESR signals due to Cu(II) ions were observed when the sample was exposed to oxygen. As C_2H_4 is unable to enter the β-cages, the adsorption must have been at S_{II} sites, but the Cu(I) ions so placed that they were unable to react with oxygen. The situation was found to be similar with CO.[26] Therefore in considering the location of our Cu(I)-CO complexes, sites actually inside the α-cages need not be considered.

Huang in his work[7] proposed a number of locations which are summarized in Figure 5.12. He considered all complexes in the absence of ligands (Ln in Figure 5.12), to be characterized by a ν(C≡O) vibration at 2160 cm^{-1}. In our work, the more sensitive FTIR technique (as opposed to the dispersive instruments he used), has shown the complexes to be characterized by slightly different ν(C≡O) frequencies. The bands observed at *ca.* 2156, 2142 and 2127 cm^{-1} we therefore assign to cations located at S_I or S_I', S_{II}' and S_{II} respectively (Table 5.3).

TABLE 5.3 A summary of the ν(C≡O) vibration of Cu(I)-CO species correlated to cation locations

Band (cm^{-1})	Cation location
2156	S_I or S_I'
2142	S_{II}'
2127	S_{II}

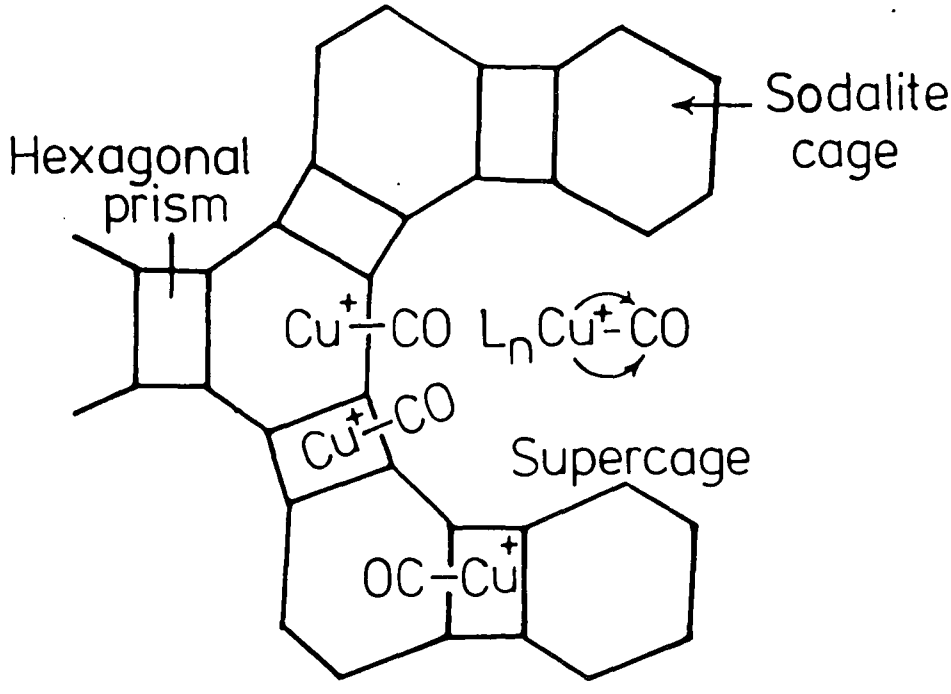

Figure 5.12 Schematic view of Cu(I)-CO complexes in Y zeolites after Huang.[7]

When CO is left in contact with the sample we find that there is a gradual migration (over periods of hours) of the Cu(I) ions towards the S_{II} sites. A very much slower (over periods of 1 month) migration of the Cu(I) ions towards the S_{II} sites has been reported by Strome and Klier[31] using luminescence spectroscopy.

The slightly different frequency observed for the complexes at different sites are due to the influence of the environment of the cation on the bonding, as will be discussed later.

5.7.2 True Lewis acid sites

A band in the region of 2180 cm^{-1} due to physisorbed CO has previously been observed by only a limited number of authors[8,19] for copper containing Y zeolites and has never been assigned.

Angell and Schaffer[32] reported bands at 2170 and 2120 cm^{-1} for CO (200 torr) adsorbed on ion-exchanged X and Y zeolites (Na^+, Li^+, Mg^{2+}, Ca^{2+}, Ba^{2+}, Sr^{2+}, Mn^{2+}, Fe^{2+}, Co^{2+}, Ni^{2+}, Zn^{2+} and Cd^{2+}). These bands were assigned to the interaction of CO with the framework oxide ions through either its oxygen (2170 cm^{-1}) or carbon end (2120 cm^{-1}). In later studies of Na and Ca exchanged A, X and Y zeolites a number of authors[33-35] attributed bands in the same region to P, Q and R branches of CO rotating in the zeolite cavities. Characteristically in these later experiments CO was adsorbed at temperatures below 200K. No bands assignable to rotational structure were observed above 273K. Therefore at room temperature the assignments of Angell and Schaffer seem more likely.

In the present work an alternative assignment of the band due to physisorbed CO at 2178 cm^{-1} is preferred. This band has been assigned (Section 5.7.2) to the co-ordination of CO with the true Lewis acid sites [$\geqslant Al^{+}$] in the zeolite framework. These sites were shown by Jacobs *et al*[19] to be formed during dehydration of Cu(II)Na-Y by an autoreduction mechanism (Section 5.3). In support of this assignment the site was observed to be blocked by adsorbed bases. It is proposed that a dipole induced in the CO molecule by the zeolite framework allows the $\geqslant Al^{+}$ species to coordinate to the oxygen end of the CO molecule.

Evidence in support of this assignment is found from reports[36] of the interaction of Lewis acids such as $AlBr_3$ with transition metal carbonyls such as $Cp_2Ru_2(CO)_4$.[37] In these adducts the Al of $AlBr_3$ is found to interact with the oxygen of a bridging carbonyl. In addition reports have been made of a similar interaction of transition metal carbonyls with the Lewis acid sites of Alumina.[37,38] Due to the influence of the transition metal complex the $\nu(C\equiv O)$ frequency of the Lewis acid coordinated carbonyl occurs well below 2000 cm^{-1}. Therefore a direct comparison with our work cannot be made.

If the bonding of the CO to the Lewis acid is assumed to be:

$$\geqslant Al^{+} \leftarrow {}^{\delta-}O \equiv C^{\delta+}$$

then electron density will be transferred from the carbonyl to the Al atom. The loss of electron density from the CO molecule will make it more like CO^{+}. The stretching

vibration of this species has been reported at 2183 cm^{-1}.[39] The high $\nu(C\equiv O)$ vibration of this complex is therefore explained.

Reversability of the true Lewis acid sites

In the study by Jacobs *et al*[19], gravimetric measurements showed that the true Lewis acid sites were fully reversible in autoreduced samples when treated with oxygen at 623K. This is in agreement with the observations in the present work.

However, as discussed in Section 5.3, Jacobs and Beyer[21] later in a study of the reduction of Cu(II)Na-Y by H_2 or CO, proposed that the true Lewis acid sites were not trigonal Al atoms but $[AlO]^+$ species. On oxidation the $[AlO]^+$ species remained in the framework and $[Cu\text{-}O\text{-}Cu]^{2+}$ pairs were formed. Therefore, if our proposal of the adsorption of CO on the true Lewis acid sites is correct a sample of oxidized Cu(I)Na-Y should show a band due to the $[AlO]^+$-CO species at 2178 cm^{-1}. We do not observe this to be the case for the oxidized autoreduced sample.

If $[AlO]^+$ species are responsible for the true Lewis acid sites in autoreduced Cu(II)Na-Y, then the non-observation of these sites in the oxidized sample may be due to the blocking of the $[AlO]^+$ sites by the $(Cu\text{-}O\text{-}Cu)^{2+}$ pairs. Conclusive evidence of this is not available from our IR measurement and will probably only be obtained from an NMR study.

5.7.3 Bonding in Cu(I)-CO complexes

In transition metal carbonyls[40] and for CO adsorbed on metal surface[41] the $\nu(C\equiv O)$ vibration is usually observed well below the gas phase value of 2143 cm^{-1} (<2125 cm^{-1}). This shift to lower wavenumbers reflects a weakening in the C≡O bond, as a result of the bonding interaction with the metal. For transition metal carbonyl compounds this shift is explained by (a) the formation of a σ bond by the overlap of the filled carbon σ orbital with a similar empty orbital of the metal, and (b) the overlap of a metal dπ or dpπ hybrid orbital with an empty antibonding pπ orbital of CO (πbonding/back bonding). The greater the degree of back-bonding the more the C-O bond is weakened.

In the work of Angell and Schaffer[32] on X and Y zeolites containing divalent cations, the $\nu(C\equiv O)$ bond was observed at 2200 cm^{-1}. This high frequency shift was explained in terms of an electrostatic interaction of CO with the cations which causes the movement of electron density to the cation from the carbon atom strengthening the C≡O bond as observed in CO^{+}.[39]

For Cu(I)Na-Y zeolites the large shift to higher wavenumbers is not so pronounced. In our zeolites, and in others reported in the literature the $\nu(C\equiv O)$ vibration of Cu(I)-CO complexes occurs in the range 2160-2130 cm^{-1}. This range overlaps well with the $\nu(C\equiv O)$ vibration of cuprous carbonyls in coordination compounds and in solution when no amine ligands are coordinated to the cuprous ion (Table 5.4).

TABLE 5.4 The infrared C-O stretching frequencies of Copper(I) carbonyls

Compound	C-O frequency (cm^{-1})	Ref.
$Cu(CO)CF_3SO_3$	2128	42
$Cu(CO)CH_3SO_3$	2130	42
$Cu(CO)C_2H_5SO_3$	2117	42
$Cu(CO)$-p-$CH_3C_6H_4SO_3$	2113	42
$Cu(CO)AsF_6$	2180 ± 5	43
$Cu(CO)CF_3CO_2$	2155	44
Cu(CO)Cl in water	2112	45
Cu(CO)Cl in pyridine	2069	45
Cu(CO)Cl in methanol	2090	44
$[Cu(dien)CO]BPh_4$	2080	46
[Cu(en)(CO)]Cl	2080	44
$[(en)Cu(CO)_2Cu(en)]Cl_2$	1905	44

Huang,[7] interpreted the bonding of Cu(I)-CO complexes in Y zeolites in terms of a σ bond formed by the interaction of the carbon lone pair electrons with empty metal orbitals. π-bonding was proposed not to be effectively involved,due to the coordination of the Cu(I) ions to the oxide ions of the zeolite lattice.

However, when amines are coordinating to the Cu(I) ion the situation is somewhat different, as the Cu(I) ions are now located in the supercages, with the result that lower ν(C≡O) frequencies are observed (Table 5.5) caused by backbonding between the Cu(I) ions and CO.

TABLE 5:5 ν(CO) frequencies in the presence of presorbed bases and C_2H_4 for CO adsorbed on Cu(I)Na-Y (75% exchange)

pre-adsorbate	presence of adsorbate	ν(CO) cm^{-1}	Ref.
NH_3	40 torr of CO	2080	7
ethylene diamine	40 torr of CO	1916 2090	
pyridine	40 torr of CO	2120	

This π-bonding is perhaps better explained in terms of the effect of the coordinating NH_3 ligand on the electron density at the cation. The σ bond formed between NH_3 ligand and the Cu(I) ion increases the electron density at the cation which prompts it to π bond to the CO molecule. A similar weakening of the $\nu(C\equiv O)$ bond is observed in Cu(I)-carbonyl complexes in solution with basic ligands present (Table 5.4).

In our zeolites we observe a range of $\nu(C\equiv O)$ vibrations, which with time shift to lower wavenumbers as migration of the cations towards the S_{II} sites occurs. Huang[7] suggested that the coordination of the Cu(I) ions to the oxide ions of the zeolite lattice may prevent π-bonding in the carbonyl complexes. The lower $\nu(C\equiv O)$ frequencies which we observe must reflect an increase in π-bonding in the complexes. As the S_{II} sites will be less well shielded by the framework oxygens than the S_I or S_I' sites, Huang's suggestion seems plausible in interpreting the spread of $\nu(C\equiv O)$ frequencies

observed in the present work. Even so, we presume that a very small amount of π-bonding will occur even in these complexes with ν(C≡O) very close to the gas phase value of CO, otherwise a larger shift to higher frequencies would be expected.

5.7.4 An explanation of previously reported ν(C≡O) values of Cu(I)-CO complexes in Y zeolites

In the present work the ν(C≡O) vibrations of Cu(I)-carbonyls formed in autoreduced Cu(II)Na-Y were found to be centred initially at 2142 cm^{-1} with a shoulder at 2156 cm^{-1}. These two features were found to (a) change with time, as cation movement occurred to form more species near the supercages, and (b) to vary initially in relative intensity depending on whether the sample was treated with oxygen during dehydration. These results were interpreted in terms of the movement of the cations from the hidden S_I and S_I' sites to more accessible sites (S_{II} and S_{II}') and secondly, in terms of the effect of pretreatment on the distribution of Cu(I) ions in these sites.

From the conclusion that sample treatment influences the distribution of cations in the S_I, S_I' and S_{II}' sites and hence the positions of the ν(C≡O) vibration of adsorbed CO the widely varying values of ν(C≡O) reported in the literature for Cu(I)-CO complexes in Y zeolites (Table 5.1) may be interpreted in terms of different cation distributions. It would appear that subtle changes such as evacuation for long periods at ambient, rate of dehydration, *etc.* are responsible for these changes as reported in ESR

measurements,[15] we are unable from the information supplied by the authors in their publication to propose which factors influence most strongly the cation distributions. We can, though, conclude that those authors who report a band centred at *ca.* 2160 cm^{-1} have a higher number of Cu(I) ions in the S_I and S_I' sites. Whereas those with a $\nu(C\equiv O)$ vibration nearer *ca.* 2140 cm^{-1} have more Cu(I) ions in S_{II} sites.

5.8 Conclusions

Using FTIR spectroscopy we have been able to locate Cu(I)-CO complexes in a number of different sites within the framework of Y zeolites. Over periods of hours the gradual migration of the Cu(I) ions in hidden sites towards the supercages has been observed. As a result of locating complexes with different $\nu(C\equiv O)$ values in the same zeolite, an explanation of the widely varying $\nu(C\equiv O)$ values reported in the literature has been given in terms of the cation distribution in the zeolites. Sample pretreatments have been proposed to cause these variations.

In addition it has been proposed that CO forms a weakly held species with the true Lewis acid sites in the framework. This species was characterized by a vibration at *ca.* 2178 cm^{-1}.

REFERENCES (Chap. 5)

1. Naccache, C. and Ben Taarit, Y., J.Catal., 22,171 (1971).

2. Mochida, I., Hayata, S., Kato, A. and Seiyama, T., Bull.Chem.Soc.Jpn., 44, 2282 (1971).

3. Williamson, W.B., Flentge, D.R. and Lunsford, J.H., J.Catal., 37, 258 (1975).

4. Tsutsumi, K., Fuji, S. and Takahashi, H., J.Catal., 24, 14 (1972).

5. Dimitrov, C. and Leach, H.F., J.Catal., 14, 336 (1969).

6. Huang, Y.Y., J.Catal., 30, 187 (1973).

7. Huang, Y.Y., J.Am.Chem.Soc., 95, 6036 (1973).

8. Herman, R.G., Lunsford, J.H., Bayer, H., Jacobs, P.A. and Uytterhoeven, J.B., J.Phys.Chem., 79, 2388 (1975).

9. Marti, J., Soria, J. and Cano, F.H., J.Phys.Chem., 80, 1776 (1976).

10. Gallezot, P., Ben Taarit, Y. and Imelik, B., J.Catal., 26, 295 (1972).

11. Gallezot, P., Ben Taarit, Y. and Imelik, B., Compt.Rend. Acad.Sci., C272, 261 (1971).

12. Turkevich, J., Ono, Y. and Scria,J., J.Catal., 25, 44 (1972).

13. Soria, J. and Conesa, J.C., J.Chem.Soc., Faraday Trans.I, 75, 406 (1979).

14. Chao, C.C., Lunsford, J.H., J. Chem.Phys., 57, 2890, (1972).

15. Herman, R.G. and Flentge, D.R., J.Phys.Chem., 82, 720 (1978).

16. Mörke, W., Vogt, F. and Bremer, H.Z., Anorg.Aug.Chem., 422, 273 (1974).

17. Vansant, E.F., Lunsford, J.H., J.Phys.Chem., 76, 2860 (1972).

18. Naccache, C. and Ben Taarit, Y., Chem.Phys.Lett., 11, 11 (1971).

19. Jacobs, P.A., de Wilde, W., Schoonheydt, R.A. and Uytterhoeven, J.B., J.Chem.Soc., Faraday Trans.I., 72, 1221 (1976).

20. Jacobs, P.A., Tielen, M., Linart, J. and Uytterhoeven, J., J.Chem.Soc., Faraday Trans.I., 72, 2793 (1976).

21. Jacobs, P.A. and Beyer, H.K., J.Phys.Chem., 83, 1174 (1979).

22. Kühl, G.H., "Molecular Sieves", Leuven University Press, p.227, (1973), ed., Uytterhoeven,J.

23. Miwa, Y., Tsutsumi, K. and Takahashi, H., Zeolites, 1, 3 and 98 (1981).

24. Iwamoto, M., Nagano, H., Furukawa, H. and Kagawa, S., Chem.Lett., Chem.Soc.Jpn., 471 (1983).

25. Gentry, S.J., Hurst, N.W. and Jones, A., J.Chem.Soc., Faraday Trans.(I), 75, 1688 (1979).

26. Huang, Y.Y., J.Catal., 61, 461 (1980).

27. Bremer, H., Mörke, W., Schödel, R. and Vogt, F., "Molecular Sieves", Advances in Chem.Series, 121, ACS. (1973), p.249.

28. Bregadze, T.A., Seleznev, V.A., Kadushin, A.A. and Krytov, O.U., Izvest.Akad.Nauk.SSSR., Ser.Khim., 12, 2701 (1973).

29. J.G. Eaves, Private Communication.

30. Model 60SX Instruction Manuals, Nicolet Instrument Corporation, Madison, Wisconsin, U.S.A.

31. Strome, D.H. and Klier, K., J.Phys.Chem., 84, 981 (1980).

32. Angell, C.L. and Schaffer, P.C., J.Phys.Chem., 70,1413 (1966)

33. Fenelon, P.J. and Rubalcava, H.E., J.Chem.Phys., 51, 961 (1969).

34. Paukshtis, E.A., Soltanov, R.I. and Yurchenko, E.N., React.Kinet.Catal.Lett., 22, 147 (1983).

35. Förster, H., Frede, W. and Schuldt, M., J.Mol.Structure, 61, 759 (1980).

36. Horwitz, C.P. and Shriver, D., Adv. in Organometallic Chemistry, vol.23, p.193, (1984).

37. Alick, A., Nelson, N.J., Strome, D. and Shriver, D.F., Inorg.Chem.11, 2967 (1972).

38. Tessier-Youngs, C., Correa, F., Pioch, D., Burwell, R.L. and Shriver, D.F., Organometallics, 2, 898 (1983).

39. Herzberg, G., "The Spectra of Diatomoic Molecules", Van Nostrand, 1950, p.522.

40. Cotton, F.A., and Wilkinson, G., "Advanced Inorganic Chemistry", 3rd ed., p.693, J. Wiley, New York, 1972.

41. Sheppard, N., and Nguyen, T.T., Advances in Infrared and Raman Spectroscopy, vol.5, 1978, Ed. Clark. R.J.H. and Hester, R.E., p.276.

42. Doyle, G., Eriksen, K.A. and Van Engen, D., Inorg.Chem., 22, 2892 (1983).

43. Desjardins, C.D., Edwards, D.B. and Passmore, J., Can. J.Chem., 57, 2714 (1979).

44. Scott, A.F., Wilkening, L.L. and Rubin, B., Inorg.Chem., 8, 2533 (1969).

45. Stewart, R. and Evans, D.G., Anal.Chem., 35, 1312 (1965).

46. Pasquali, M., Marchetti, F. and Floriani, C., Inorg.Chem., 17, 1684 (1978).

CHAPTER SIX

FTIR STUDIES OF COPPER CONTAINING Y ZEOLITES

Part II. Dehydration, Reduction and the adsorption of ammonia

6.1 Introduction

The work reported in this chapter forms the second part of a study of copper containing Y zeolites. Here we report:

(a) the effects of dehydration,

(b) the adsorption of ammonia,

(c) the coadsorption of CO and NH_3,

(d) the reduction of Cu(II)Na-Y with NH_3 and CO, and

(e) the adsorption of CO on Cu(I)Na-Y.

6.2 The preparation of Cu(I)Na-Y zeolites

Although standard ion exchange techniques can be used to prepare Cu(II)Na-Y zeolite, difficulties arise in the preparation of Cu(I)Na-Y due to the instability of Cu(I) ions in aqueous solution. Direct ion-exchange may be accomplished in the absence of oxygen with CuI[1] in liquid NH_3, though the preferred route is by the reduction of Cu(II)Na-Y zeolite. Reducing agents such as CO[2], H_2[3], NH_3[4,5] and olefins[6,7] may be used.

The most frequently used reducing agent is CO in the presence of NH_3 first described by Huang.[2,8] The adsorption of NH_3 relocates the Cu(II) ions in sites in or near the supercages where reduction by CO may be accomplished in 1 hour at 673K. Without NH_3 reduction times of *ca.* 30 hours are required. On evacuation of the reducing gases and products, the Cu(I) ions migrate to sites in the small cavities.

For reduction with hydrogen lower temperatures are required[3] but the Cu(I) ions formed are susceptible to further reduction to Cu(O), if the temperature exceeds 473K. Reduction with NH_3 or butadiene was shown by Maxwell and Drent[6] to occur at 373K. Residual water in the zeolite framework was found to dissociate during reduction, with the formation of hydroxyl groups (Brönsted acid sites).

Cu(I) ions are also introduced into Cu(II)Na-Y zeolites by autoreduction during dehydration.[9] This and other reduction mechanisms were discussed in Section 5.3.

6.3 Copper-Ammine complexes

The formation of copper-ammine complexes in Y zeolites has been studied by a number of techniques, *e.g.* adsorption measurements,[2,10] X-ray diffraction,[11] ESR[5,12,13] and IR[12] spectroscopy.

The adsorption of NH_3 on to dehydrated Cu(II)Na-Y was shown by ESR spectroscopy[5,13] and X-ray diffraction[11] (Chapter Two) to cause the migration of the Cu(II) ions into the large cavities where copper ammine complexes could be formed. From the ESR[5] parameters, the authors concluded that at room temperature the Cu(II)-ammine complex was square planar. On partial desorption of the ammonia at 373K, the symmetry of the complex was found to change to a distorted tetrahedron; the complex being formed by a Cu(II) ion coordinated to three lattice oxygens and one ammonia molecule. Upon increasing the desorption temperature (473-573K) the original signal due to the Cu(II) ions in the supercages was observed.

Huang and Vansant[10] measured the adsorption isotherms of ammonia adsorbed on 13, 48 and 75% exchanged Cu(II)Na-Y zeolites. These measurements showed that complex formation was completed at pressures of less than 20 torr. From the uptakes, in agreement with ESR results,[5] complexes of $[Cu(NH_3)_4]^{2+}$ stoichiometry were shown to be formed. In high copper content samples, it was felt that not all the Cu^{2+} ions were involved in complex formation.

For Cu(I)Na-Y zeolites adsorption measurements[2] showed the cuprous ammine complexes to be mainly $[Cu(NH_3)_2]^{+}$. As with Cu(II)Na-Y zeolites ammonia was shown, by the behaviour of the Cu(I) cations towards oxygen, to pull the cations into the supercages at room temperature (see Section 5.2).

Infrared measurements have only been published[12] for NH_3 adsorbed on Cu(II)Na-Y zeolites. By a comparison with the infrared spectrum of $Cu(NH_3)_4.SO_4$,[14] which above 1200 cm^{-1} has absorption bands at 3270 [ν(N-H)], 1610 [$\sigma(NH_3)_d$] and 1270 and 1240 [$\delta(NH_3)_s$] cm^{-1}, a band at 1275 cm^{-1} in the spectrum of Cu(II)Na-Y + NH_3 was assigned to the $[Cu(NH_3)_4]^{2+}$ complex. The remaining band assignments are summarized in Table 6.1. On desorption of NH_3 the 1275 cm^{-1} band was found to shift to 1260 cm^{-1} which led the authors to assign it to the tetrahedral complex described earlier. A plot of the intensity of the 1275 cm^{-1} band *versus* the amount of NH_3 adsorbed confirmed the complex to be $[Cu(NH_3)_4]^{2+}$ at room temperature.

TABLE 6.1 The infrared bands (cm^{-1}) and their assignments for NH_3 adsorbed on Cu(II)Na-Y after Flenge *et al*[12]

Before adsorption of NH_3	
3650 - 3660)	
)	OH stretch vibrations; weak
3550 - 3560)	
1640	H_2O bend ; weak, broad.
After adsorption of NH_3	
3400)	
)	
3380)	N-H stretch vibrations
)	
3320)	
)	
3270)	
)	
3220)	
)	
3190)	
1675)	
)	
1485)	Deformation of NH_4^+
)	
1435)	
1632)	doubly degenerate antisymmetric deformation
)	
1618)	deformation vibration of NH_3
1275	symmetric deformation of NH_3 coordinated to Cu^{2+}

6.4 Experimental

The carbon monoxide used is as described in Section 5.4. Ammonia (99.98%, British Oxygen Company), was dried with sodium metal and purified by the freeze-pump-thaw technique.

For the present studies of the adsorption of NH_3 and reduction the sample used was sample 1 of the previous chapter. This sample had been pretreated as shown in Figure 5.3 and was used after the desorption of CO. The treatments applied to the sample in the present chapter are summarized in Figure 6.1. In the previous chapter it was shown that sample 1 contained a number of Cu(I) ions introduced by autoreduction.

Figure 6.1 A summary of the experimental condition applied to Sample 1.

SAMPLE 1

Cu(II)Na-Y

(autoreduced by treatments given in Figure 5.3)

↓

Adsorption of NH_3 at RT (1.2 torr)

↓ evacuation for 15 mins.

Adsorption of CO (0.5 and 8 torr)

↓ evacuation for 10 mins.

Adsorption of NH_3 (10.7 torr) and CO (146 torr)

↓ reduction

At 362K for 13 hrs.

↓

673K for 1 hr

↓ evacuation for 3 hours at 673K

Adsorption of CO at room temperature (0.3-9.4 torr)

↓ evacuation.

6.5 Results and Discussion

The results will be presented in four sections:

(1) the dehydration of Cu(II)Na-Y,

(2) the adsorption of NH_3 on Cu(II)Na-Y,

(3) Cu(I)-carbonyl complexes in the presence of NH_3;

(4) the reduction of Cu(II)Na-Y,

(5) adsorption of CO on Cu(I)Na-Y.

6.5.1 The dehydration of Cu(II)Na-Y

Spectra of Cu(II)Na-Y (Sample 1) in the region above 1200 cm^{-1} during dehydration are shown in Figure 6.2. In the spectrum at 323K (Figure 6.2a) and at temperatures below this the intense band at *ca.* 1640 cm^{-1} and the broad feature at *ca.* 3700-3000 cm^{-1} (beneath the sharp bands) are due to adsorbed water, which on evacuation and heating is desorbed. Features in the 1600-1200 cm^{-1} region which are observed to change during dehydration are probably due to overtone and combination bands of the framework vibrations and/or to carbonates formed during ion exchange. The asymmetric and symmetric stretch of CO_3^{2+} in $Na_2[Cu(CO_3)_2].3H_2O$ has been reported at 1529 and 1326 cm^{-1} respectively.[15]

Superimposed on the broad water stretching band (3700-3000 cm^{-1}) are a number of sharp bands, which become better resolved as water is removed during dehydration (Figures 6.2a-c). These bands occur at *ca.* 3680, 3640, 3550, 3444 and 3345 (3360 and 3318 at <450K). At dehydration temperatures greater than 530K the bands at 3680, 3444 and 3345 cm^{-1} are removed, while the remaining bands and a new band at *ca.* 3740cm^{-1} are still observed even after heating at 698K for 15 hours. The assignment of the above bands is unclear because one of several species may be responsible, *viz.* structural hydroxyl groups and copper hydroxyl species.

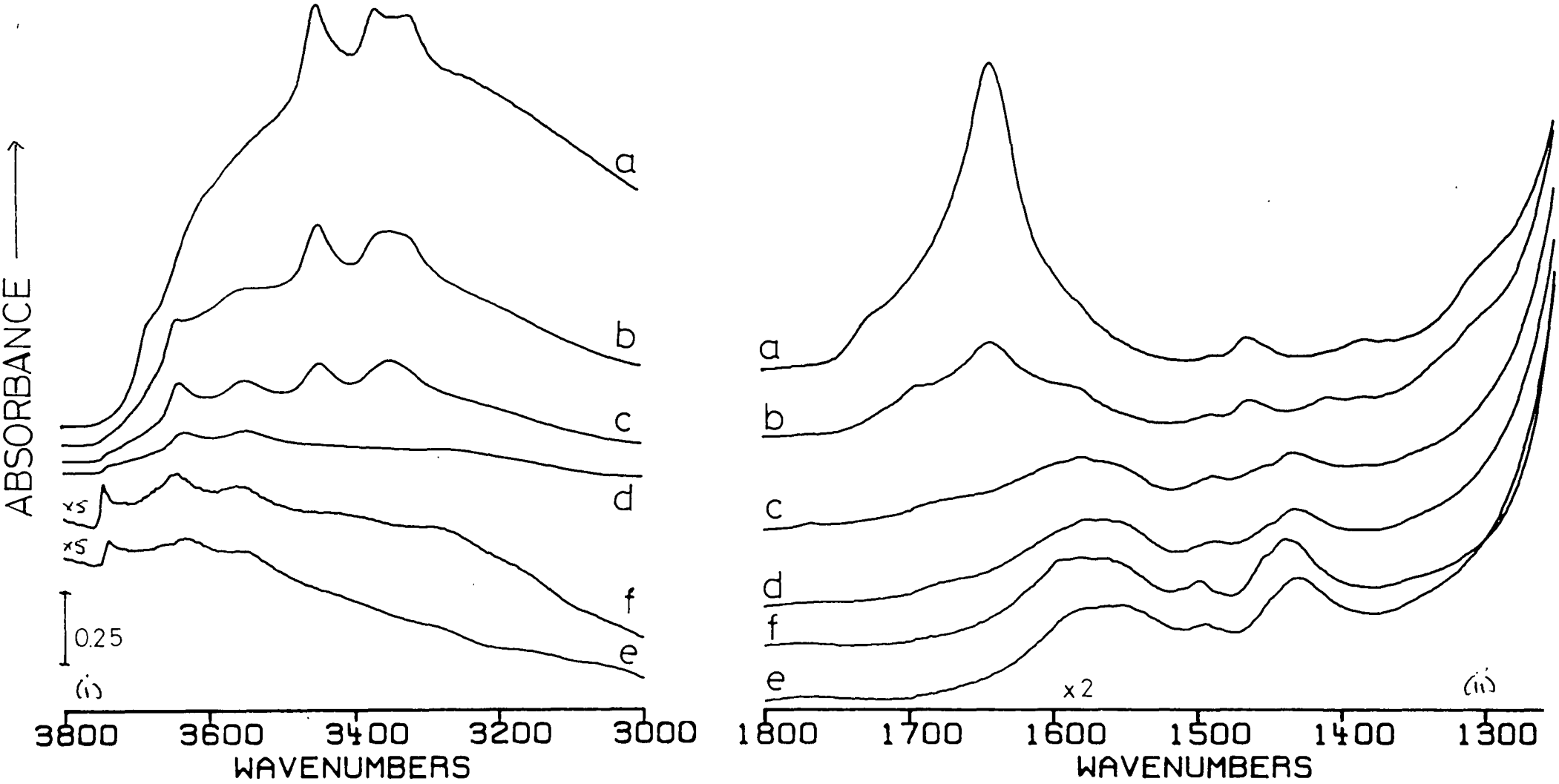

Figure 6.2 The dehydration of Cu(II)Na-Y (sample 1) under vacuum

Sample heated under vacuum at (a) 323K, (b) 473K, (c) 528K, (d) 618K, (e) 698K for 15 hours and (f) cooled to room temperature. ((a) ⟶ (d) in (i) plotted on smaller Y expansion). (Y-axis offset).

The bands at 3740 cm^{-1} and 3680 cm^{-1} may be assigned from the discussion in Chapter Two to Si-OH and Al-OH groups respectively.[16]

In previous reports of the dehydration of Cu(II)-Na-Y bands in the 3650-3500 cm^{-1} region were proposed to be generated by the reaction:[17,18]

$$Cu(OH_2)^{2+} \longrightarrow Cu(OH)^{+} + H^{+}.$$

These bands disappeared when the samples were heated above 573K. In agreement with this assignment copper hydroxide compounds are found to have vibrations in this region (Table 6.2). As in the present work the bands observed at 3640 and 3550 cm^{-1} were <u>not</u> lost on dehydration above 573K (Figure 6.2a-f), they are unlikely to be due to copper hydroxyl species. We therefore assign these bands to structural hydroxyl groups similar to those found in decationized zeolites.[16]

The bands at *ca.* 3444 and 3345 cm^{-1} were not observed in the previous reports[17,18] of the dehydration of Cu(II)Na-Y. By comparison with the ν(OH) adsorption frequencies of copper hydroxide compounds reported in the literature (Table 6.2) these bands would appear to be due to copper hydroxyl complexes in the zeolite framework. At elevated temperatures these species disappear, probably with the formation of coupled copper pairs, $(Cu\text{-}O\text{-}Cu)^{2+}$, which have been detected by ESR spectroscopy.[21,22] These copper hydroxides were probably formed during ion exchange.

A summary of all band assignments in the 4000-1200 cm^{-1} region is given in Table 6.3.

TABLE 6.2 The infrared adsorption frequencies of ν(OH) in copper complexes

Complex	Ref.	ν(OH) cm^{-1}
$Cu(SO_4).\ 3Cu(OH)_2$	19	(3586, 3564 (3390, 3270
$Cu(SO_4)_2.2Cu(OH)_2$	19	(3578, 3570 (3486
$Cu(NO_3)_2.3Cu(OH)_2$	19	(3543, 3522 (3428
Cu(OH)F	19	3185
Cu(OH)Cl	19	3400
$Cu_2(OH)_3Cl$	19	(3448, 3366 (3317
$Cu_2(OH)_3Br$	19	3516, 3424 ∿3410,∿3320?
$[2\text{-ampy})_2\ Cu(OH)ClO_4]_2$	20	3590
$[(2\text{-ampy})_2\ Cu(OH)NO_3]_2$	20	3642, 3620
$[(2\text{-ampy})_4\ Cu_2(OBu^n)(OH)(NO_3)_2]$	20	3630
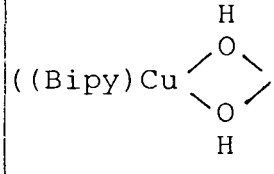	21	
where x = SO_4		3400
Br_2		3430
$(ClO_4)_2$		3440
Cl_2		3430
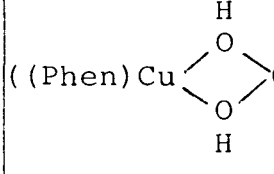	21	
where X = I_2		3480
Br_2		3350
$(ClO_4)_2$		3400, 3340

TABLE 6.3 Summary of bands (cm^{-1}) and their assignments observed during the dehydration of Cu(II)Na-Y

3740	ν(OH) of Si-OH
3700 ⟶ 3000[a]	ν(OH) of adsorbed H_2O
3680[a]	ν(OH) of Al-OH
3640	)
	) ν(OH) of framework hydroxyl groups
3550	)
3444[a]	)
	) ν(OH) of copper
3345[a] (3360)[a,b]	) hydroxides
(3318)	)
1640[a]	$\delta(OH_2)$ of adsorbed H_2O
1600-1200	framework vibrations.

a. Lost on dehydration.

b. Above 450K the 3345 cm^{-1} band splits into two components as indicated.

The region below 1200 cm^{-1}

More evidence for the presence of copper hydroxides should be found in the region below 1200 cm^{-1}, where the δ(OH) band has been reported[19,21] to occur (1000-670 cm^{-1}). Therefore as the ν(OH) bands are lost in the 3450-3300 cm^{-1} region, we would expect a band to be lost below 1000 cm^{-1}.

Unfortunately the very intense vibrations of the zeolite framework make observations below 1200 cm^{-1} of pure zeolite discs very difficult. Data collected in this region for sample 1 is shown in Figure 6.3. In spectrum 6.3a the bands, except the 900 cm^{-1} band, may be assigned to the vibrations of the internal and external tetrahedral linkages of the zeolite framework (Table 6.4) as described by Flanigen[24]

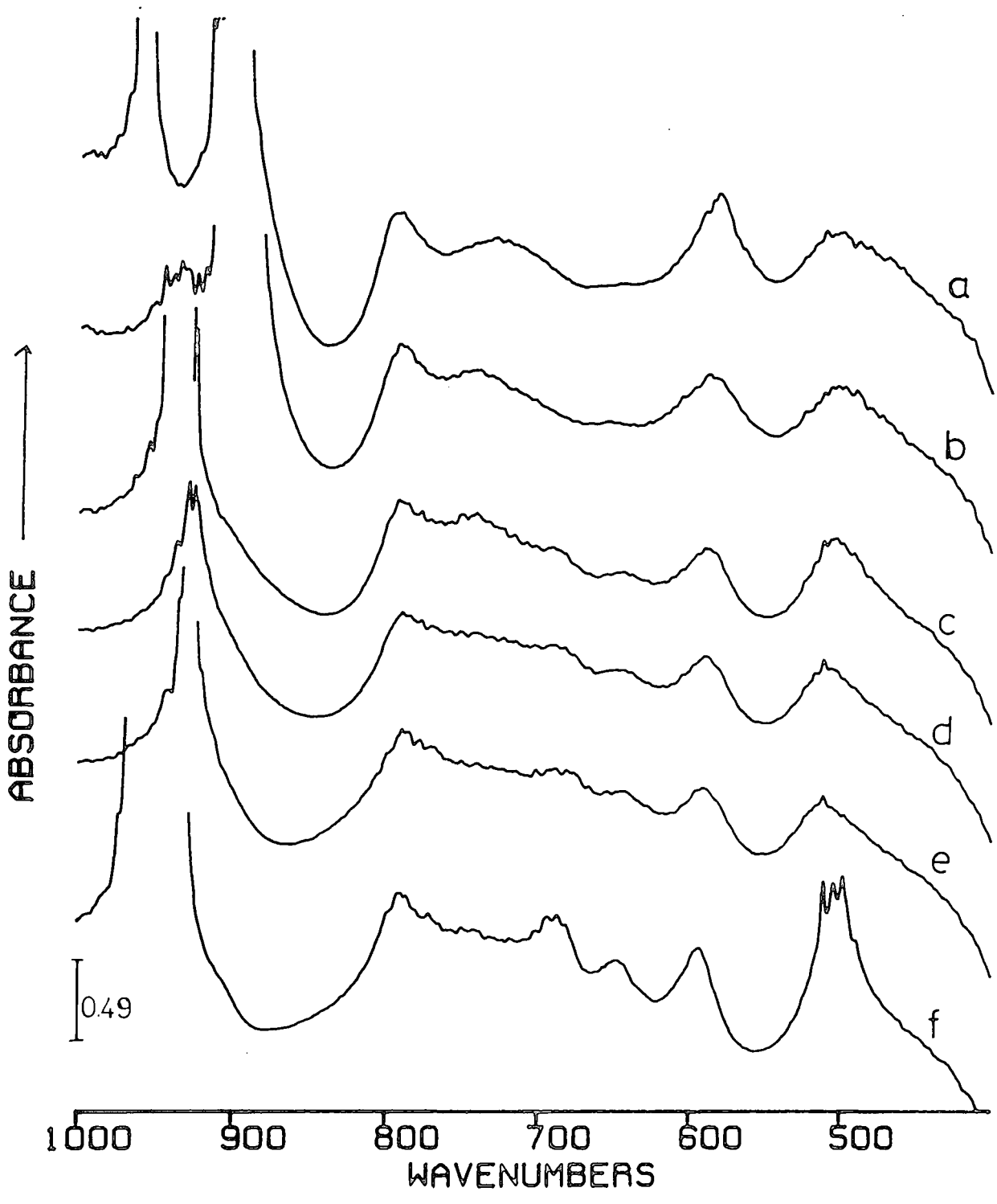

Figure 6.3 Spectra in the 1200-400 cm^{-1} region for Cu(II)Na-Y during dehydration under vacuum (sample 1)

Sample heated at (a) 323K, (b) 437K, (c) 528K, (d) 618K, (e) 698K for 15 hours and (f) cooled to room temperature. (Y-axis offset).

(Chapter Two). As the 900 cm^{-1} band cannot be assigned to any of these vibrations, this band is a candidate for the copper hydroxyl band .

TABLE 6.4 The assignment of the framework vibrations below 1200 cm^{-1}

Band (cm^{-1})	Assignment
1150	Asymmetric stretch (I)
970	Asymmetric stretch (E)
900	Copper hydroxyl band ?
795	Symmetric stretch (E)
725	Symmetric stretch (I)
580	double-ring (E)
500	T-O bend (I)

E = External Linkage, I = Internal Linkage.

ESR measurements[23,25] have shown that on dehydration of Cu(II)Na-Y, the Cu(II) ions migrate to sites in the sodalite cages. Changes in the framework vibrations should reflect this cation migration. In Figure 6.3 the external linkage band at 970 cm^{-1} is seen to shift to 950 cm^{-1} on dehydration and more structure is observed in the 700-600 cm^{-1} region which are likely to be due to overtone and combination bands. These changes probably reflect the migration of the cations into the sodalite cages and the formation of $(Cu\text{-}O\text{-}Cu)^{2+}$ pairs.

The band at 900 cm^{-1}, which gradually decreased in intensity and is lost above 523K, correlates well with the behaviour of the 3444 and 3360 cm^{-1} bands. As the δ(OH)

modes of copper hydroxides have been reported to occur in the region 1000-670 cm^{-1},[19,21] the assignment of this to δ(OH) of the copper hydroxides is feasible.

Though two pieces of evidence have been found for copper hydroxide complexes, we are unable to determine whether the species are bridging or linear.

6.5.2 The adsorption of NH_3 on Cu(II)Na-Y

The spectrum of ammonia adsorbed on to dehydrated (autoreduced) Cu(II)Na-Y is shown in Figure 6.4. Intense bands are observed in the 3800-3000 cm^{-1} and 1700-1200 cm^{-1} regions due to ν(NH) and δ(HNH) vibrations of ammine complexes in the zeolite framework. After 30 minutes the bands due to adsorbed NH_3 were observed to have increased in intensity as equilibrium was attained. At 309K an equilibration time of 30 minutes has been reported.[12]

The bands observed may be assigned by comparison with published data on gaseous NH_3 [26] (Table 6.5), $Cu(NH_3)_4.SO_4$ [27,28] (Table 6.6) and the previous study of NH_3 adsorbed on Cu(II)Na-Y (Table 6.1). A description of the normal modes of gaseous NH_3 and $Cu(NH_3)_4.SO_4$ is given in Figures 6.5 and 6.6 respectively.

TABLE 6.5 Assignment of the normal modes of gaseous NH_3.[26]

	Description	Selected value
ν_1	Symmetric stretch	3337
ν_2	Symmetric deformation	950
ν_3	Degenerate stretch	3444
ν_4	Degenerate deformation	1627

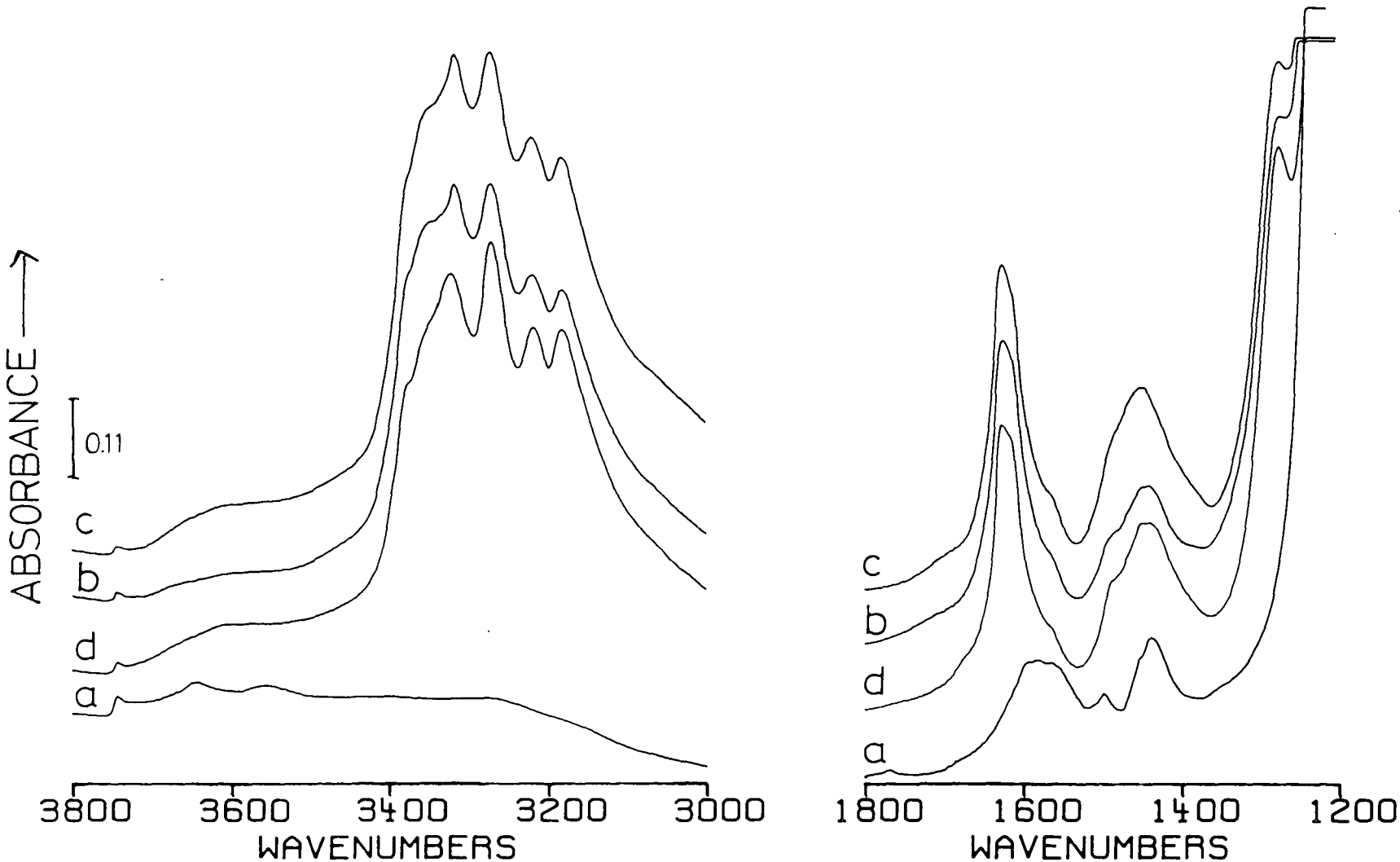

Figure 6.4 The adsorption of Ammonia on Cu(II)Na-Y (sample 1)

(a) Zeolite background, (b) adsorption of 1.2 torr of NH_3, (c) sample (b) after 30 minutes, (d) after evacuation for 15 minutes. (all spectra are offset).

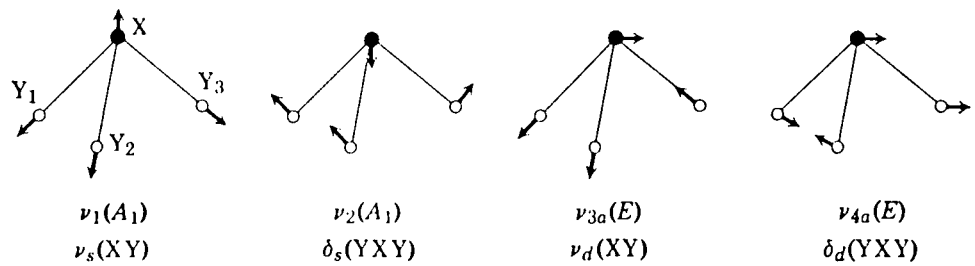

Figure 6.5 The normal modes of vibration of NH_3.[29]

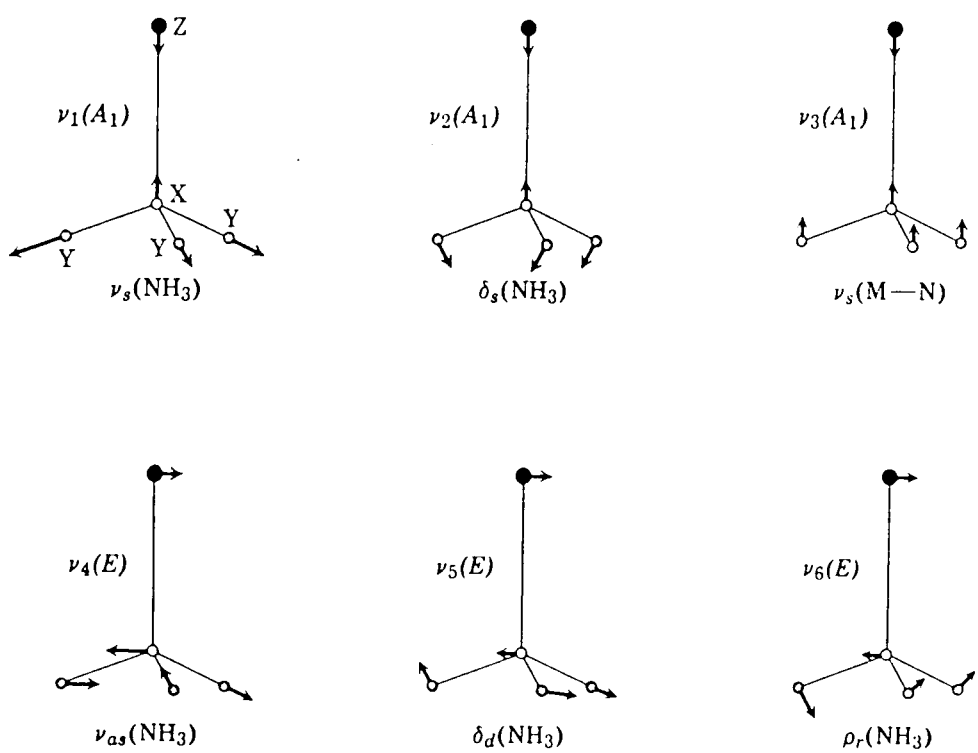

Figure 6.6 The normal modes of vibration of M-NH_3 groups.[29]

TABLE 6.6 Assignment of the normal modes of $[Cu(NH_3)_4]^{2+}$

	ν(NH)	$\delta_d(NH_3)$	$\delta_s(NH_3)$	Pr(NH_3)	ν(Cu-N)
observed[27]	3270	1610	1270) 1240)	713	420
calculated[27] value	3310) 3232)	1610	1251	708	419
observed[28]	3330 3260 2178	1640 1670	1280	735	426

The 1700-1200 cm^{-1} region

In the 1700-1200 cm^{-1} region the band at 1273 cm^{-1} may be assigned to the symmetric deformation of $[Cu(NH_3)_4]^{2+}$ complexes. The other bands in this region are assigned in Table 6.7.

TABLE 6.7 Assignment of the bands in the 1700-1200 cm^{-1} region of ammonia adsorbed on Cu(II)Na-Y observed in the present work

Band (cm^{-1})	Assignment
1627	Coordinately bound NH_3
1610 (sh)	$\delta_d(NH_3)$ of $[Cu(NH_3)_4]^{2+}$
1580	Framework vibration
1475))	Deformation of NH_4^+
1420)	
1273	$\delta_s(NH_3)$ of $[Cu(NH_3)_4]^{2+}$

On evacuation of gaseous NH_3 for 15 minutes at room temperature (Figure 6.4d), the intensity of the 1273 cm^{-1} band is observed to increase. This would, in contrast to the previous study,[12] infer that the number of $[Cu(NH_3)_4]^{2+}$

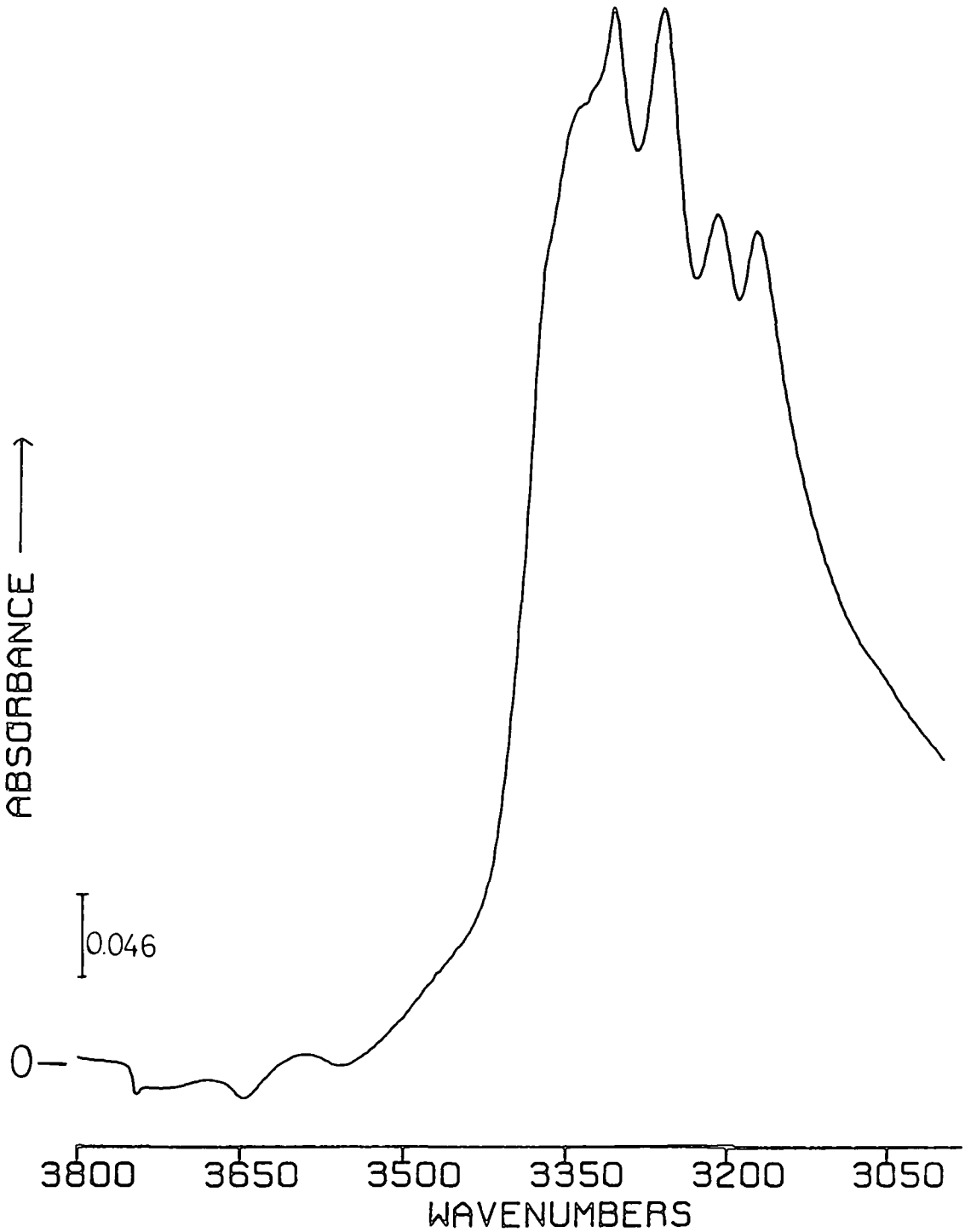

Figure 6.7 Subtraction of background (Figure 6.4a) from spectrum after adsorption of NH_3 (Figure 6.4b).

complexes had increased on evacuation. The only reasonable explanation of this behaviour is that NH_3 molecules which are hydrogen bonding to the structural OH groups (see below), hinder the formation of $[Cu(NH_3)_4]^{2+}$ species. This would imply that on evacuation when the NH_3 molecules are removed from the H bonding sites, they move to coordinate with the Cu(II) ions to form $[Cu(NH_3)_4]^{2+}$ complexes in the supercages.

The 3800-3100 cm^{-1} region

In this region bands due to ν(N-H) vibrations and structural hydroxyl groups are observed (Figure 6.4, Table 6.8).

A subtraction of the background spectrum from spectrum 6.4(b) revealed that an adsorption of NH_3 bands observed in the background spectrum at *ca*. 3740, 3640 and 3550 cm^{-1} were shifted in frequency or lost (Figure 6.7). These bands which were assigned to structural hydroxyl groups (Section 6.5.1) may be assumed to be either hydrogen bonding to an NH_3 molecule, as characterized by the broad band at *ca*. 3700-3500, or to have formed NH_4^+ species, which are observed at *ca*. 1475 and 1420 cm^{-1}. On evacuation another subtraction spectrum revealed these bands to reappear as the coordinating NH_3 molecules were removed. This data is the basis for the previous proposal that on evacuation the removal of the loosely coordinated NH_3 molecules, allows the formation of more cupric ammine complexes.

The bands observed below 3400 cm^{-1} may clearly be assigned to ν(N-H) vibrations. There are though several possible species which are expected to have ν(N-H) vibration in the 3400-3100 cm^{-1} region, *viz*. copper ammine complexes, NH_3 hydrogen bonding to framework hydroxyl groups and NH_4^+ species.

A comparison with published work has shown that no unique assignment may be made from the data available. Therefore the most likely assignments are given below and summarized in Table 6.8.

TABLE 6.8 Assignment of bands in the 3800-3100 cm^{-1} region due to NH_3 adsorbed on Cu(II)Na-Y observed in the present work

Band (cm^{-1})	Assignment
3700-3500 (broad)	Hydrogen bonding hydroxyl groups
3400 (broad sh.)	Hydrogen bonding ν(N-H)
3374 (sh)	ν(NH) of NH_4^+ or hydrogen bonding NH_3
3319	
3319	ν(NH) of $[Cu(NH_3)_4]^{2+}$
3269	
3216	
3181	

The bands at 3269, 3216 and 3181 cm^{-1} are probably best associated with the $[Cu(NH_3)_4]^{2+}$ complexes (Table 6.6), whereas the assignment of the 3319 cm^{-1} band is unclear. This latter band could be associated with either the copper-ammine complex, the NH_4^+ species or the NH_3 hydrogen bonding to the zeolite framework. The shoulder at *ca.* 3374 cm^{-1} and the general broad band beneath the sharper features in the 3400-3000 cm^{-1} region are best assigned to hydrogen bonding NH_3 and the NH_4^+ species.

An alternative assignment for the 3319 and 3269 cm^{-1} bands proposed by Kadir[30] was to $Cu(OH)_2$ and Cu(OH) species respectively. As in the present study there was no evidence

in the background spectrum (Figure 6.4a) for these complexes or water which could react with NH_3 to form copper-hydroxide species, *viz.*

$$2\ H_2O + Cu^{2+} + 2NH_3 \longrightarrow NH_4^+ + Cu(OH)_2,$$

the explanation of Kadir must be discounted in assigning these bands in the present work.

Further in assigning bands to copper-ammine complexes we have assumed the stoichiometry of the complex to be $[Cu(NH_3)_4]^{2+}$ as indicated from ESR[5] and gravimetric[10] measurements. There exists the possibility that we may be observing mixed species, as the compounds $Cu(NH_3)_5(BF_4)_2$ [31] and β-$CuCl_2(NH_3)_2$ [32] both have ν(N-H) vibrations in the same region as those of $[Cu(NH_3)_4].SO_4$. It was also shown in Chapter Five that sample 1 contained Cu(I) ions, therefore some bands may be due to $Cu(I)-(NH_3)_n$ complexes, which must be assumed to have vibrations in the same region.

6.5.3 Cu(I)-Carbonyl complexes in the presence of NH_3

After the removal of NH_3 from sample 1 by evacuation for 15 minutes CO was adsorbed (Figure 6.8). This sample was shown in Section 5.6 to contain Cu(I) ions and the desorption of CO at temperatures of 573K is expected to have increased this number. Although no direct evidence for $Cu(I)-(NH_3)_2$ complexes was obtained from the IR spectra (Section 6.5.2), published adsorption measurements[2] have shown ammonia to cause the migration of the Cu(I) ions towards the supercage sites.

In a previous study of CO adsorbed on Cu(I)Na-Y with NH_3 present Huang[8] observed the $\nu(C\equiv O)$ vibration of a $Cu(I)CO(NH_3)_n$ complex at 2080 cm^{-1} (40 torr), which almost disappeared on evacuation for 5 minutes. After partial desorption of the NH_3 (evacuation for 2 hours at 298K) a band was observed at 2125 cm^{-1} with a shoulder at 2080 cm^{-1}. Further evacuation for 2 hours at 393K, followed by CO adsorption at room temperature resulted in a band at 2150 cm^{-1} with a shoulder at 2135 cm^{-1}. The 2150 cm^{-1} band was not removed on evacuation.

In the present study when CO (0.5 torr) was adsorbed onto autoreduced Cu(II)Na-Y with preadsorbed NH_3 one weak band was observed at 2111 cm^{-1}. On increasing the pressure to 8 torr the intensity of the 2111 cm^{-1} band increased and a second band appeared at 2069 cm^{-1}. Both bands were removed by evacuation for 5 minutes. These two bands must reflect Cu(I) ions in different sites or complexed to different numbers of NH_3 molecules.

Huang explained the lower $\nu(C\equiv O)$ frequency of Cu(I)-carbonyl complexes in the presence of NH_3 to the relocation of the Cu(I) ions in the supercages. As the Cu(I) ions were no longer coordinated to the framework oxide ions, they were able to π-bond to the CO molecules which weakens the $C\equiv O$ bond and lowers the $\nu(C\equiv O)$ vibration to below 2100 cm^{-1}.

The cause of the π-bonding is perhaps better explained in terms of the effect of the coordinating NH_3 molecule on the electron density at the cation as explained in Section 5.7.3.

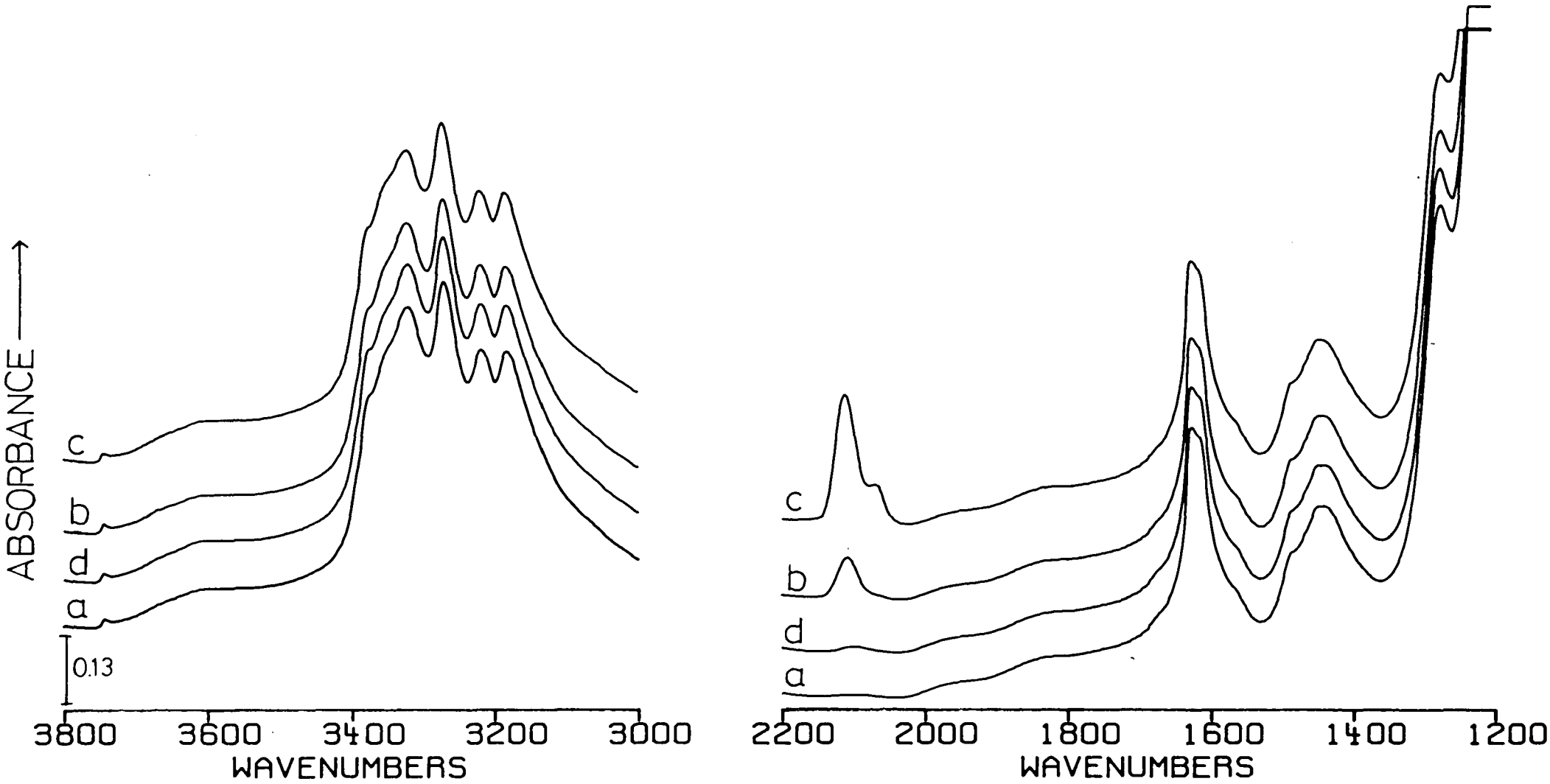

Figure 6.8 The adsorption of CO onto autoreduced Cu(II)Na-Y with preadsorbed NH_3 (sample 1)

(a) background; evacuation of NH_3 for 15 minutes; (b) 0.5 torr of CO; (c) 8.0 torr of CO; (d) evacuation. (all spectra are offset).

In Chapter Five we correlated the different $\nu(C\equiv O)$ values observed for CO adsorbed on autoreduced Cu(II)Na-Y to Cu(I)-carbonyl complexes in different cation sites in the zeolite framework. When amines (NH_3, pyridine and ethylenediamine) were partially desorbed from Cu(I)Na-Y zeolites Huang[8] found the C-O stretching frequency to shift gradually towards the value observed in the dehydrated zeolite (Table 6.9). The observed values can be interpreted in terms of the loss of the amine ligands which (a) decreases the effective π-bonding between the Cu(I) ions and the CO ligand, and (b) to the gradual withdrawal of the Cu(I) cations into the small cavity sites. The two values of $\nu(C\equiv O)$ we observe at 2111 and 2069 cm^{-1} in the presence of NH_3 must therefore be due to Cu(I) ions in different sites. The species with the value at 2069 cm^{-1} probably represents a complex formed in the centre of the supercage, with full coordination of the Cu(I) ions to NH_3 molecules. Only at high pressures are the CO molecules able to displace an NH_3 ligand to form the $Cu(I)CO(NH_3)_4$ carbonyl species. The higher wavenumber band we associate with Cu(I) ions which are still partially coordinated to the framework oxygens.

Of the bands due to adsorbed NH_3 only the band at 1273 cm^{-1} is observed to be affected by the adsorption of CO as on adsorption of CO its intensity decreases. This band was previously assigned to the $\delta_s(NH_3)$ mode of $[Cu(NH_3)_4]^{2+}$ complexes. Two possible explanations are available to account for the behaviour of the 1273 cm^{-1} band;

TABLE 6.9 Effect of Desorption Temperature of the Ligands on the C-O Stretching Frequency of Carbonyls in Cu(I)Y (75%) Zeolite (with CO at 25° and 40 Torr)[8]

Ligand	Desorption temperature, °C				
	25	120	200	300	400
NH_3	2080, 2125	2135, 2150			2160
en	1916, 2090	1918, 2110	2120	2150	2170
py	2130, 2190 (?)	2120	2130	2140	2155

(a) the formation of $Cu(I)\text{-}CO(NH_3)_n$ species causes a reduction in the overall number of the $[Cu(II)(NH_3)_4]^{2+}$ species in the supercages;

(b) the symmetric deformation mode (ν_2) of the Cu(II)-ammine complex is perturbed by the presence of CO and Cu(I) complexes in the supercages so that its position is shifted to lower wavenumbers. From IR measurements alone it is not possible to distinguish between these two possibilities.

6.5.4 The reduction of Cu(II)Na-Y

The reduction of Cu(II)Na-Y with CO in the presence of ammonia has been shown to occur in 1 hour at 673K.[2,8] The reduction of sample 1 by this method is discussed here. This sample already contained a quantity of Cu(II) ions introduced by autoreduction (Section 5.6, 5.3 and 5.7).

For reduction 10.7 torr of NH_3 and 146 torr of CO were adsorbed at room temperature. The spectra, which are shown in Figure 6.9, display bands assignable to Cu-ammine and $Cu(I)CO(NH_3)_n$ complexes as discussed in Sections 6.5.2 and 6.5.3.

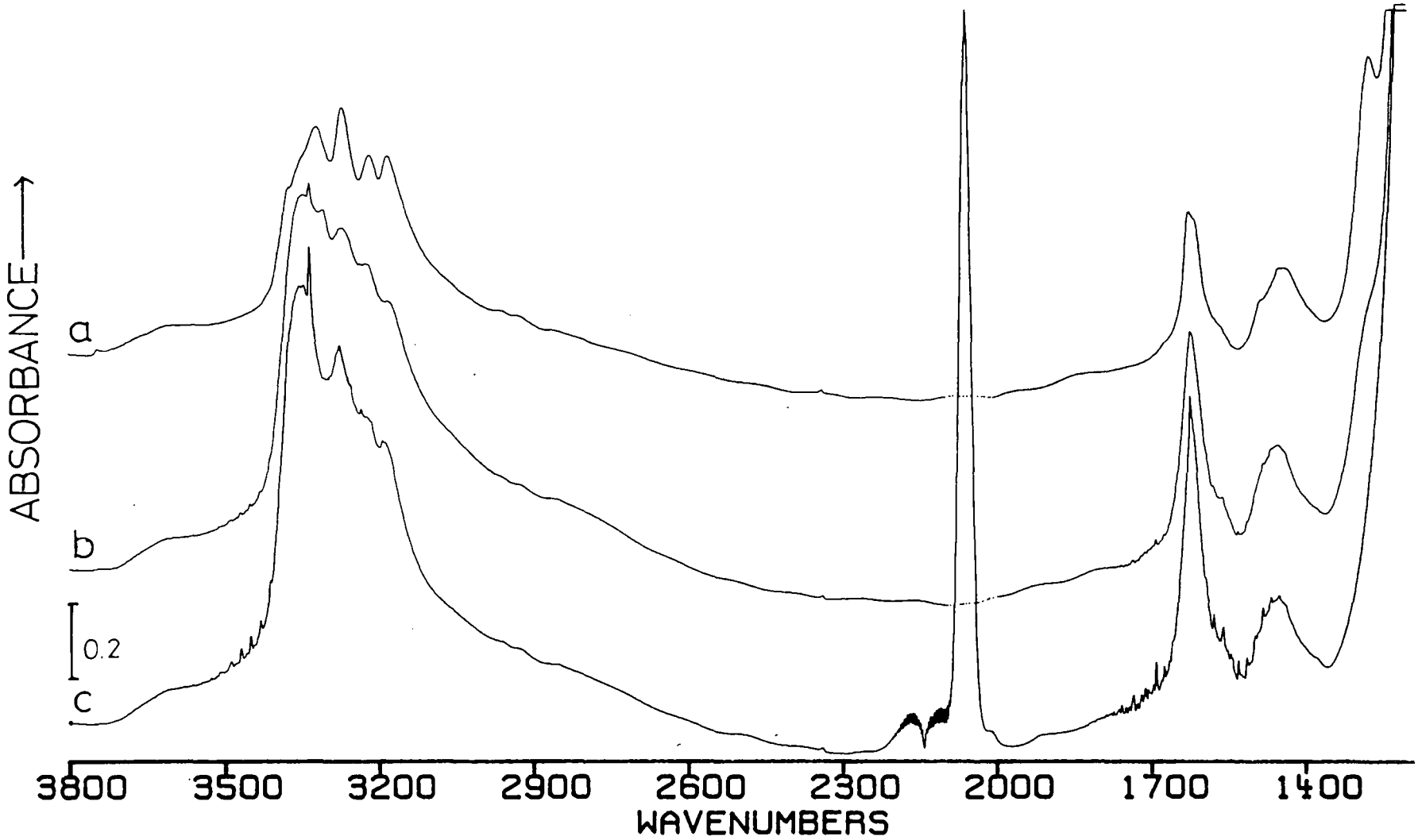

Figure 6.9 The adsorption of NH_3 and CO on to Cu(II)Na-Y

(a) background (spectrum 6.8d); (b) sample (a) + 10.7 torr of NH_3; (c) sample (b) + 146 torr of CO. (Y axis offset).

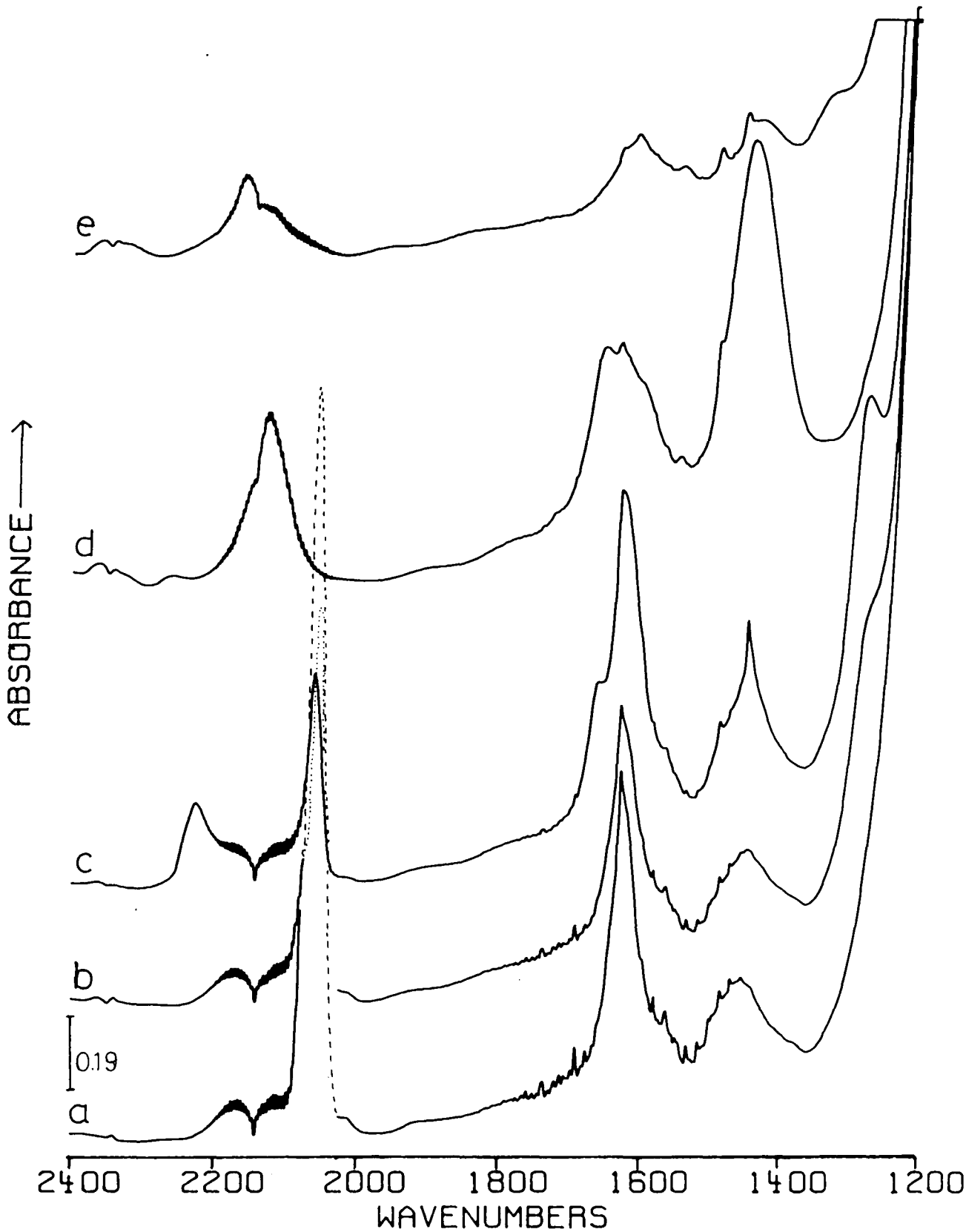

Figure 6.10 The reduction of Cu(II)Na-Y by CO in the presence of NH_3 (sample 1)

(a) sample + 10.7 torr of NH_3 + 146 torr of CO; sample (a) heated at:

(b) 358K, (c) 358K for 13 hours, (d) 473K and (e) 673K

(Y axis offset)

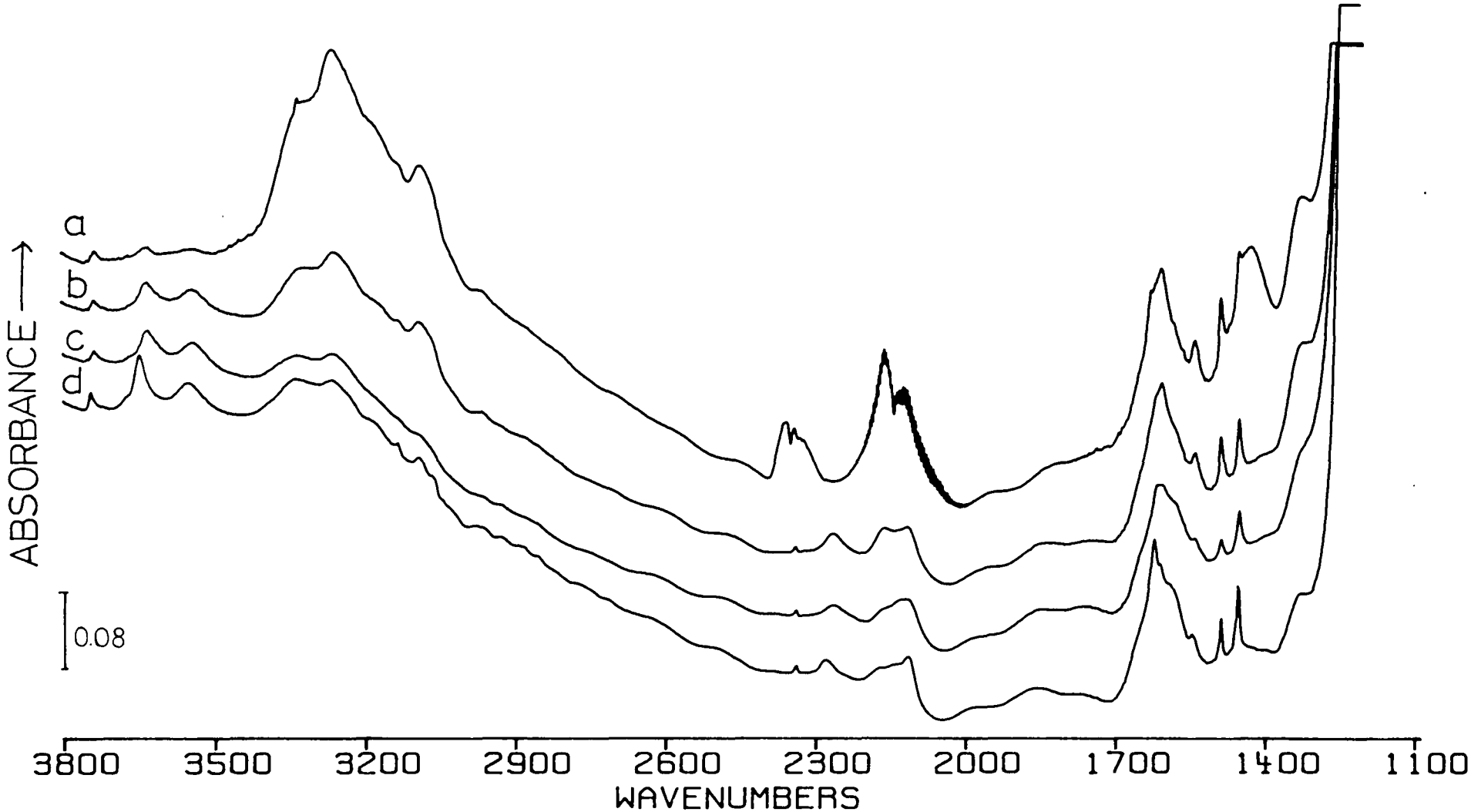

Figure 6.11 The reduction of Cu(II)Na-Y at 673K (sample 1)

(a) sample heated at 673K for 1 hour; (b) evacuation of gas phase at 673K;
(c) sample (b) evacuated for 3 hours; (d) sample (c) cooled to room temperature.
(Y axis offset).

The position of the intense ν(CO) of the carbonyl complex at 2060 cm^{-1} is shifted slightly compared with that reported in Section 6.5.3, due presumably to increased π-bonding in the $Cu(I)CO(NH_3)_n$ complexes. The bands displaying fine structure at *ca.* 2220-2100 cm^{-1} are due to gaseous CO.

Spectra of the Cu(II)Na-Y disc at various stages during the reduction are shown in Figures 6.10 and 6.11. After heating at 673K for 1 hour a noticeable drop in the transmission of the sample was observed, although the relative intensities of the bands remained unchanged. On removal of the zeolite disc from the cell its pinky-brown colour indicated that some Cu(O) clusters had been formed, explaining the drop in transmission. The adsorption of CO in Section 6.5.5 did not show any abnormalities due to the Cu(O) clusters, which are most probably formed on the external surfaces of the crystallites. We presume the large number of Cu(II) ions introduced by autoreduction were responsible for the ease of formation of the Cu(O) clusters.

The spectra in Figures 6.10 and 6.11 show a number of features which are summarized below:

(1) The bands at *ca.* 1444 cm^{-1} and 1484 cm^{-1} are due to NH_4^+ species formed during the reduction process. These bands reach their maximum intensity at 473K (Figure 6.10d). Above this temperature NH_4^+ is desorbed as NH_3 leaving OH groups in the zeolite framework.

(2) The bands observed in the 2160-2060 cm^{-1} region (2060, 2120 and 2160 cm^{-1}) which overlap with the bands of gaseous CO are due to Cu(I)-CO complexes. The shift to higher wavenumber with increasing temperature would indicate that the

Cu(I) ions are withdrawing into the sodalite cavity sites where π-bonding is less effective (Section 6.5.3). It is also observed that the intensity of the bands is much reduced at higher temperatures. This may presumably be attributed to the decreased stability of the complexes at high temperatures.

(3) On heating to 358K the cuprous ammine band reappears at 1273 cm^{-1} and increases in intensity overnight at this temperature. This observation is possibly linked with the decrease in intensity of the ν(CO) band. As the Cu(I)-carbonyls are reduced in number, more space is available in the supercages for the $[Cu(NH_3)_4]^{2+}$ complex to form. Above 358K, the 1273 cm^{-1} bond disappears as the $[Cu(NH_3)_4]^{2+}$ complexes dissociate to Cu(II) ions and NH_3 molecules.

(4) A band appears at *ca.* 2230 cm^{-1} after heating the zeolite at 358K for 13 hrs. (Figure 6.10c). The band, which disappears on heating above this temperature, we are unable to correlate with any of the NH_3 or CO complexes previously observed.

(5) Bands which appear in the 2400-2300 cm^{-1} are due to gaseous CO_2, a product of the reduction of the Cu(II) ions.

(6) On heating and at above 573K a shoulder develops at 1320 cm^{-1} which is not lost on subsequent evacuation and cooling of the sample. This band may possibly be due to the symmetric deformation of the $Cu(I)-(NH_3)_n$ complexes.

(7) After evacuation and cooling the residual structure in the spectrum is due to amine and carbonyl complex.

These seven points show that a variety of species are formed during the reduction of Cu(II) ⟶ Cu(I) by CO in

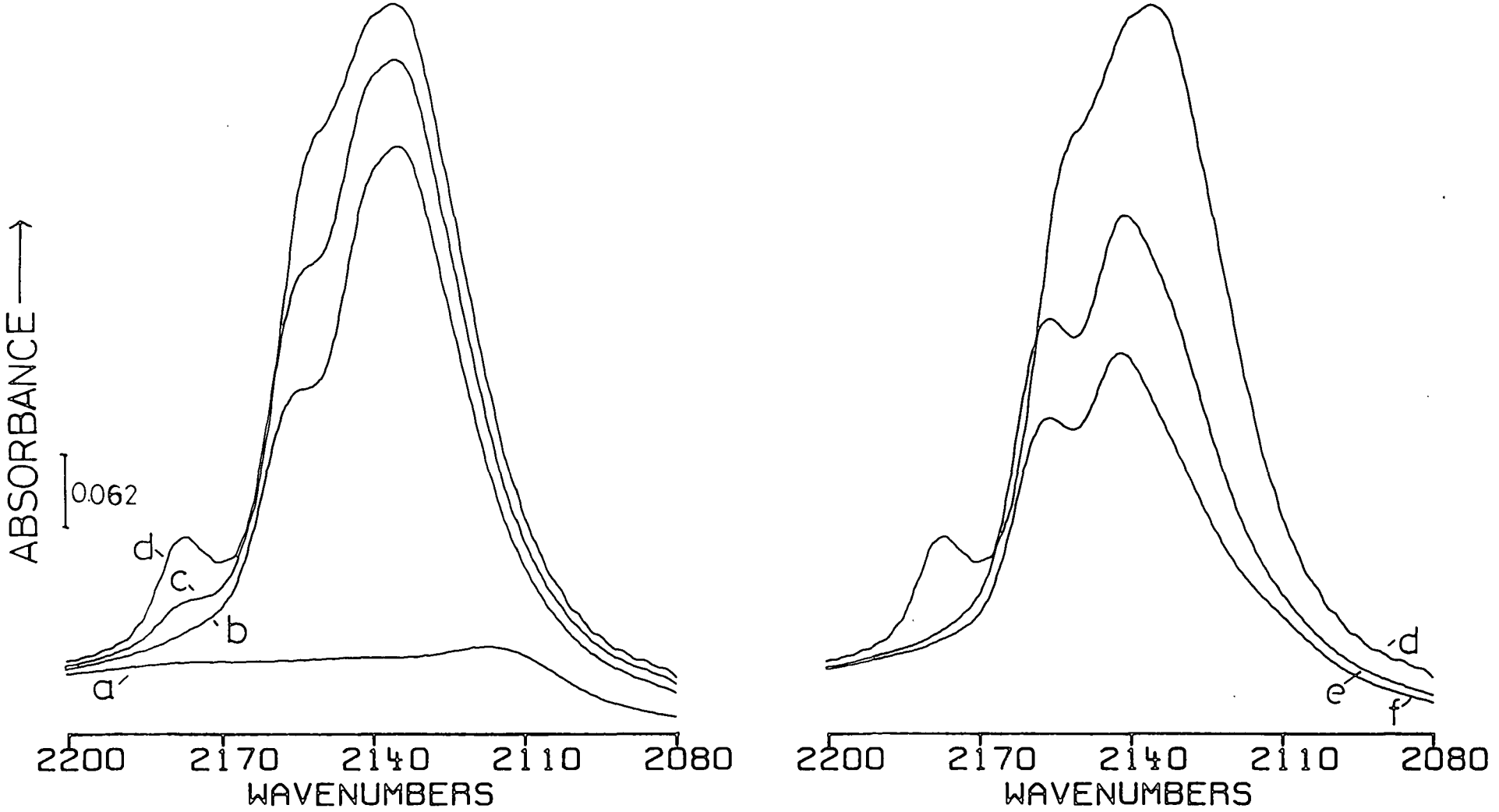

Figure 6.12 The adsorption and desorption of CO on Cu(I)Na-Y (sample 1)

(a) zeolite background after reduction, sample (a) with CO; (b) 0.2 torr, (c) 2.1 torr and (d) 9.4 torr, sample (d) after; (e) evacuation of gas phase, (f) evaucation for 10 minutes.

the presence of NH_3. The reduction is complicated by the fact that NH_3 on its own may reduce Cu(II) ions. At low temperatures the appearance of NH_4^+ species may indicate that this was the preferred mechanism. At higher temperatures the loss of the NH_4^+ species and the appearance of CO_2 in the spectrum would indicate that reduction by CO is preferred.

6.5.5 The adsorption of CO on to reduced Cu(II)Na-Y

In Figure 6.12 the spectra obtained when CO was adsorbed on to the Cu(I)Na-Y zeolite are shown. A comparison of this figure with the data for CO adsorbed on autoreduced Cu(II)Na-Y (Figure 5.4) shows the pattern of band intensities and positions to be the same. Following from the discussion in Section 5.7.1 we can conclude that reduction both with reducing agents and autoreduction led to similar distributions of Cu(I) ions in the zeolite lattice. Bonding considerations are therefore the same (Section 5.7).

In the background spectrum Figure 6.12a, the residual intensity at *ca.* 2120 cm^{-1} is associated with Cu(I) cations located in the supercages. These species may be associated with residual NH_3 in the zeolite framework.

6.6 Conclusions

Infrared spectra of Cu(II)Na-Y during dehydration revealed the presence of copper hydroxyl species formed during ion exchange of the zeolite. These species were found to dissociate on heating the sample above 530K, possibly to $(Cu\text{-}O\text{-}Cu)^{2+}$ and H_2O.

In the presence of ammonia the formation of copper ammine complexes has been observed and the interaction of ammonia with the structural hydroxyl groups. The latter interactions were only revealed in subtraction spectra. The formation of NH_4^+ species was shown by the bands at *ca.* 1450 cm^{-1}.

In addition a band at 1273 cm^{-1}, characteristic of the $\delta_s(NH_3)$ vibration of the $[Cu(NH_3)_4]^{2+}$ complex was shown to increase in intensity on the evacuation of NH_3 from the cell, and to decrease in intensity in the presence of CO. This behaviour was not reported by other authors who have studied the same systems. We have associated the behaviour of the 1273 cm^{-1} band:

(a) on evacuation, to the removal of NH_3 from hydrogen bonding sites to Cu(II) sites, so forming more $[Cu(NH_3)_4]^{2+}$ complexes, and (b) to the presence of CO to Cu(I)-$CO(NH_3)_n$ complexes which either block the formation of Cu(II)-ammine complexes or to the perturbation of the $\delta_s(NH_3)$ mode to low wavenumber.

Spectra of the reduction of Cu(II)Na-Y with CO and NH_3 indicated that at low temperatures reduction by NH_3 was preferred, whereas at higher temperatures reduction by CO occurred.

The adsorption of CO on to Cu(I)Na-Y showed the cations to be located in the same sites as those observed in auto-reduced Cu(II)Na-Y.

REFERENCES (Chap. 6)

1. Kruerke, U.K., US.Patent No. 3476 462 Feb.24, 1970.
2. Huang, Y.Y., J.Catal., 30, 187 (1973).
3. Herman, R.G., Lunsford, J.H., Bayer, H., Jacobs, P.A. and Uytterhoeven, J.B., J.Phys.Chem., 79, 2388, (1975).
4. Williamson, W.B., Flentge, D.R. and Lunsford, J.H., J.Catal., 37, 258 (1975).
5. Vansant, E.F. and Lunsford, J.H., J.Phys.Chem., 76, 2860 (1972).
6. Maxwell, I.E. and Drent, E., J.Catal., 41, 412, (1976).
7. Maxwell, I.E., Dowing, R.S. and Van Langen, S.A.J., Acta Physica et Chemica, 24, 215 (1978).
8. Huang, Y.Y., J.Am. Chem.Soc., 95, 6036 (1973).
9. Jacobs, P.A., de Wilde, W., Schoonheydt, R.A. and Uytterhoeven, J.B., J.Chem.Soc., Faraday Trans.I., 72, 1221 (1976).
10. Huang, Y.U. and Vansant, E.F., J.Phys.Chem., 77, 663 (1973).
11. Gallezot, Ben Taarit, Y. and Imelik, B., J.Catal., 26, 295 (1972).
12. Flentge, D.R., Lunsford, J.H., Jacobs, P.A. and Uytterhoeven, J.B., J.Phys.Chem., 79, 354 (1975).
13. Naccache, C. and Ben Taarit, Y., Chem.Phys.Lett., 11, 11 (1971).
14. Nakagawa, I. and Shimanouch,T.,Spectrochim.Acta., 22, 759 (1966).
15. Gatehouse, S.E., Livingstone, R.S. and Nyholm, R.S., J.Chem.Soc., 3137 (1958).
16. Ward, J., A.C.S. Monograph 171, p.118 (1976).
17. Ward, J., Trans.Faraday Soc., 67, 1489 (1971).
18. Ben Taarit, Y., Primet, M. and Naccache, C., Compt.Rend. 67, 1434 (1970).
19. Tarte, P., Spectrochim.Acta., 13, 107 (1958).
20. McWhinnie, W.R., J.Inorg.Nucl.Chem., 27, 1063 (1965).
21. Ferraro, J.R. and Walker, W.R., Inorg.Chem., 4, 1382 (1965).
22. Chao, C. and Lunsford, J.H., J.Chem.Phys., 57, 2890 (1972).

23. Turkevich, J., Ono, Y. and Soria, J., J.Catal., 25, 44 (1972).

24. Flanigen, E.M., ACS Monograph 171, p.80, (1976).

25. Herman, R.A. and Flentge, D.R., J.Phys.Chem., 82, 720 (1978).

26. Shimanouchi, T., "Tables of Molecular Vibrational Frequencies, Consolidated Volume I," NSRDS-NBS 39 (1972).

27. Nagagawa, I., Shimanouchi, T., Spectrochim.Acta, 22, 759 (1966).

28. Schmidt, K.H., Müller, A., J.Molecular Structure, 22, 343 (1974).

29. Nakamoto, K., "Infrared Spectra of Inorganic and Coordination compounds", J. Wiley & Sons (1970), 2nd. Ed., p.150.

30. Kadir, Z.A., Ph.D. Thesis, Durham, 1983.

31. Tomlinson, A.A.G. and Hathaway, B.J, J.Chem.Soc.A., 1905 (1968).

32. Clark, R.J.H. and Williams, C.S., J.Chem.Soc.A, 1425, (1966).

CHAPTER SEVEN

THE ADSORPTION AND REACTION OF ETHYNE ON ZINC EXCHANGED A ZEOLITE: AN INFRARED STUDY

7.1 Introduction

The work presented in this chapter has, in part, been published in the proceedings of the International Conference on Fourier Transform and Computerized Infrared Spectroscopy, Ottawa, 1985.[1] This published work relates to an abstract of a poster and Sections 7.4.1 and 7.4.2 contain some content from this work.

In this chapter the adsorption of ethyne on zinc exchanged type-A zeolite is discussed in detail. This work has revealed a system whose behaviour is very different to that reported for apparently related system.[2-6]

In view of the observations for ZnNa-A, we have also re-investigated the adsorption of ethyne on Na-A and Ag-A zeolites. This has shown that the behaviour of Ag-A is similar to ZnNa-A, with the formation of both reactive and stable species. On Na-A stable species have identified at three locations in the zeolite framework.

7.2 Previous Spectroscopic Studies of the Adsorption of Ethyne by Zeolites

Previous IR and Raman studies of the adsorption of C_2H_2 by zeolites have shown that four types of coordination may be envisaged between the C_2H_2 and the zeolite framework, *viz:*

(i) "End-on" interaction *via* hydrogen bonding between the acidic protons of C_2H_2 and framework oxygen atoms. In this case $\nu(C\equiv C)$ occurs at a wavenumber value[7] which is higher than the gas phase (1974 cm^{-1}).

(ii) "Side-on" interaction *via* overlap of the π orbitals of C_2H_2 with orbitals of the cation to form a π complex. $\nu(C\equiv C)$ has been reported to fall in the range 1912-1960 cm^{-1}[4-6] for π-bonded C_2H_2 on various ion exchanged forms of A and 13X zeolites.

(iii) C_2H_2 may lose one or both of its hydrogens to form acetylides (H-C≡C-M) or carbides (MC≡CM). $\nu(C\equiv C)$ for acetylides in zeolites have been reported in the range 1850-1961 cm^{-1}.[6,8]

(iv) Alternatively a reaction may occur in which C_2H_2 loses its identity, as for example, in the cyclotrimerization to form benzene on Ni(II) containing Y zeolite,[9] or the formation of polyethyne on K-X zeolite.[10]

As will be shown later, the ZnNa-A-C_2H_2 system involves the formation of more than one type of adsorbed species, one of which reacts to form ethanal. This contrasts markedly with published data on alkaline earth and alkali metal exchanged A zeolite, where only stable species have been observed.[5]

Tam *et al*,[5] have published IR and Raman data for C_2H_2 adsorbed on Li^+, Na^+, K^+, Mg^{2+} and Ca^{2+} exchange type A zeolites. On the Na^+ and Ca^{2+} exchanged forms all five fundamentals of adsorbed C_2H_2 were observed between the IR and Raman spectra (Table 7.1). For the other cationic forms only ν_2 was readily observed (C≡C stretching vibration) in both the

IR and Raman spectra. In all cases there was a lowering in the frequency of ν_2, showing a "side-on" interaction. This observation was in agreement with the X-ray structural data of Seff *et al*[11-14] for Na_{12}-A, $Mn_{4.5}Na_3$-A and Co_4Na_4-A but in contradiction with the earlier findings of Tsitsishvili *et al*.[13] The latter authors, in an IR study of C_2H_2 adsorbed on various ion-exchanged type A and X zeolites (Ni^{2+}, Co^{2+}, Mn^{2+}, Na^+ and Ca^{2+}) were unable to locate bands due to ν_2, but as bands due to ν_3 (antisymmetric C-H stretch) were observed, they proposed an "end-on" interaction.

TABLE 7.1 The assignment of Bands (cm^{-1}) due to ethyne adsorbed on Na-A and CaNa-A zeolites after ref.5.

Vibration	Gas phase activity	Na_{12}-A	$Ca_{4.14}Na_{3.72}$-A
ν_1(C-H)	R	3321	3327
ν_2(C≡C)	R	1953	1957
ν_3(C-H)	IR	3205	3214
ν_4 δ(H-C≡C)	R	642	640
ν_5 δ(H-C≡C)	IR	760	750

X-ray diffraction data for C_2H_2 adsorbed on $Mn_{4.5}Na_3$-A[13,14] and Co_4Na_4-A[14] has since shown C_2H_2 to only interact with the transition metal ions in the S_2^* sites. The Na^+ ions were observed to retreat into the S_2' sites on adsorption of C_2H_2, where they were unable to bond to the C_2H_2 molecules. From the crystallographic data it was proposed that the C_2H_2 was π-bonding to the cations.

In the case of Na_{12}-A, the diffraction results of Amaro and Seff[11,12] showed three C_2H_2 molecules to be associated with the Na^+ ions in the 6-oxygen rings (S_2^*). The remaining three C_2H_2 molecules were found to be associated with the cations in sites S_1 and S_3.

Consistent with the findings of Amaro and Seff above, Tam *et al*[5] found that in the Raman spectrum of Na_{12}-A and C_2H_2 the ν_2 band (1953 cm^{-1}) was distinctly asymmetric, and was subsequently resolved into bands centred at 1954 and 1949 cm^{-1}. It was suggested that the 1949 cm^{-1} band resulted from the interaction of C_2H_2 with the energetically more favourable S_1 cations, while the higher frequency band represented the interaction of C_2H_2 with the S_2^* cations.

A more recent study by neutron diffraction,[16] in which one molecule of C_2H_2 was adsorbed per cavity in Na_{12}-A, has confirmed that C_2H_2 energetically favours Na^+ in the S_1 or S_3 sites. In its equilibrium position the axis of the C_2H_2 molecule was found not to be parallel with the axis of the 8-oxygen ring window at these sites.

Howard *et al* have recently studied the adsorption of C_2H_2 on Ag_{12}-A by inelastic neutron scattering[3] (INS) and IR[4] spectroscopy. The INS data showed only one adsorption site for C_2H_2 within the zeolite framework, in contrast to the IR spectra where two different π bonded C_2H_2 species were identified, characterized by ν_2 at 1955 and 1912 cm^{-1}. These species were easily removed on evacuation. In addition part of the adsorbed C_2H_2 lost hydrogen and formed silver acetylide (ν_2 observed at 1820 cm^{-1}). Part of the liberated hydrogen formed hydroxyl groups within the framework, while the remainder was

proposed to form hydronium ions, characterised by a band at 1686 cm^{-1}. It will be shown later in this study that the 1686 cm^{-1} band is, in fact, due to ethanal formed from the adsorbed C_2H_2. A band at 1380 cm^{-1}, which was unassigned, has been found in the present study to be associated with the formation of ethanal.

No previous studies of C_2H_2 adsorbed zinc exchanged zeolites has been published. The crystal structure of Zn_5Na_2-A is available and has been described in Chapter Two.

7.3 Experimental

Two samples of zinc exchanged A zeolite were used for the C_2H_2 adsorption experiments. These were prepared as described in Chapter Three and analysed as $Zn_{4.3}Na_{3.4}$-A and $Zn_{1.1}Na_{10.9}$-A. Hereafter they will be referred to as ZnNa-A and low exchanged ZnNa-A, respectively. Linde Na_{12}-A, referred to hereafter as Na-A, was obtained from BDH and used without further purification.

The Ag_{12}-A zeolite used in the present work was supplied by J. Howard (Durham) and had been prepared as described in the literature.[17] This sample will be referred hereafter as Ag-A.

Ethyne (99.9%, British Industrial Gases Ltd.) was purified by passing the gas slowly through concentrated H_2SO_4. Ethyne (99 atom % D, Merck, Sharp and Dohme Ltd.) was used without further purification.

TABLE 7.2 A summary of the dehydration conditions used for the zeolite samples

Sample	Reference number	Maximum Temperature (K)	Time at maximum temperature (hours)
ZnNa-A	1	750	15
ZnNa-A	2	733	14
ZnNa-A	3	743	15
ZnNa-A	4	673	12
Low exchange ZnNa-A	5	716	15.5
Na-A	6	739	15
Ag-A	7	723	2

The dehydration, adsorption, *etc*. were carried out *in situ* as described in Chapter Three. A summary of the dehydration conditions each sample was subjected to is given in Table 7.2. Quantities of adsorbates are given in the results section.

The spectra for all samples, except sample 4, were measured on the Nicolet 605X spectrometer. The scan times, where relevant, are quoted in brackets in figure captions. If no scan time is given then a scan time of 238 seconds was used. The data for sample 4 was collected on the PE580 spectrometer using the conditions described in Section 3.4.1.

7.4 Results and Discussion

The results of the adsorption of C_2H_2 on ZnNa-A, Na-A and Ag-A will be discussed in different sections as follows:

(1) the adsorption of C_2H_2 on ZnNa-A;

(2) the effect of prolonged contact time of C_2H_2 adsorbed on ZnNa-A;

(3) the hydration of ethyne: comments on mechanism;

(4) the adsorption of C_2H_2 on Na-A;

(5) the adsorption of C_2H_2 on low exchanged ZnNa-A;

(6) prolonged C_2H_2 contact on Ag_{12}-A;

(7) the effect of heat on the hydration of C_2H_2over ZnNa-A.

7.4.1 The adsorption of C_2H_2 on ZnNa-A zeolite

On adsorption of C_2H_2 onto ZnNa-A zeolite several bands due to adsorbed species are observed (Figure 7.1), in the $\nu(C\equiv C)$ and $\nu(C-H)$ stretching regions of gaseous C_2H_2 (Table 7.3).

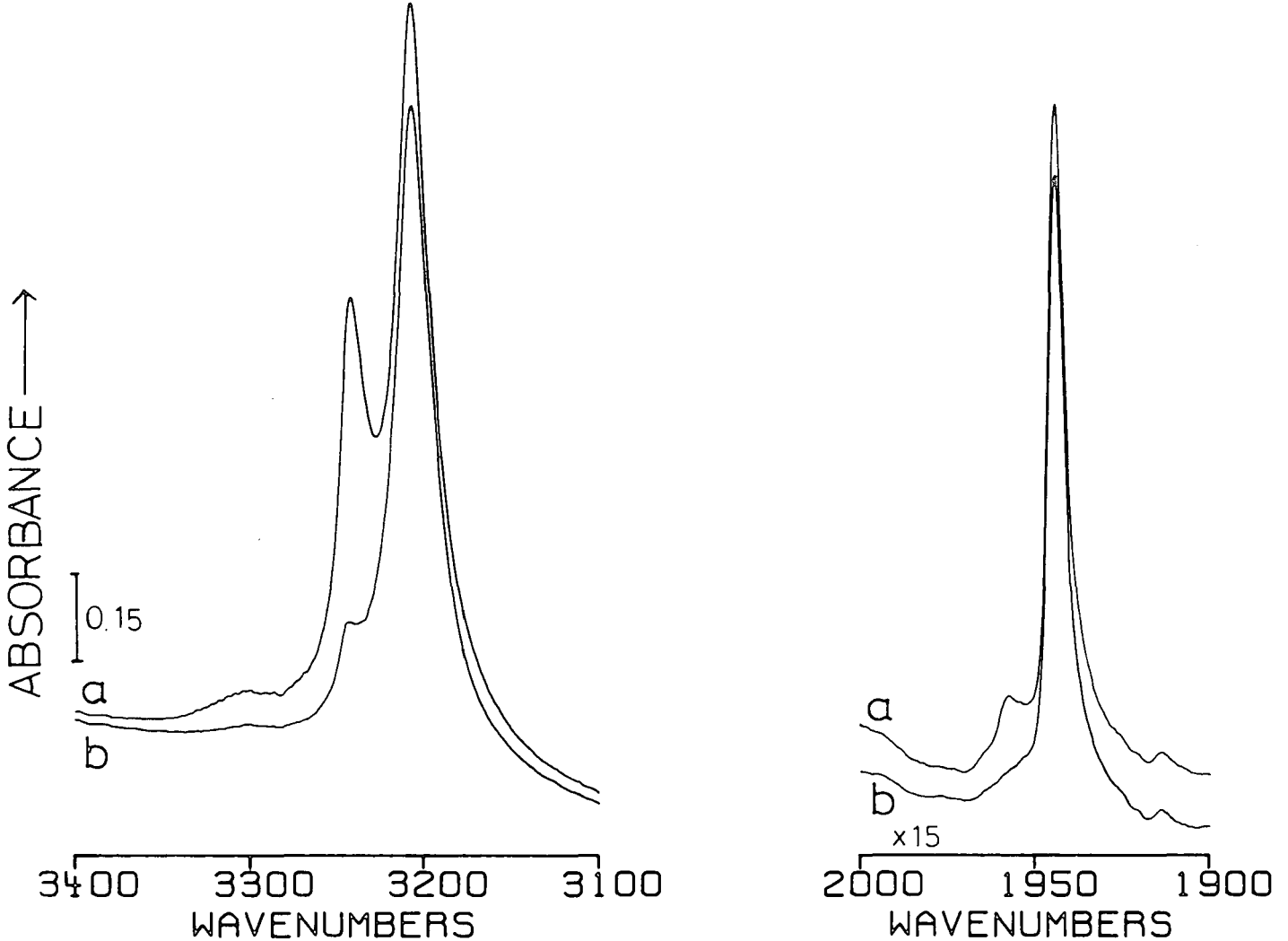

Figure 7.1 The effect of pressure on the spectrum of ethyne adsorbed on ZnNa-A zeolite (sample 1)

(a) Zeolite + 10.7 torr C_2H_2 (b) Zeolite + 1.0 torr C_2H_2

TABLE 7.3 Summary of the vibration bands (cm^{-1}) and their assignment for gaseous ethyne 18 and ethyne adsorbed on ZnNa-A zeolite

Assignment of gaseous ethyne	C_2H_2 [a]	C_2D_2 [a]	ZnNa-A + C_2H_2	ZnNa-A + C_2D_2	Assignment of adsorbed species
ν_1 C-H or C-D stretch	3374 [b]	2701			
ν_2 C-H or C-D stretch	3209 [c]	2439	3238	2403	νC-H) or ν(C-D) of π-bonded ethyne, species A.
			3203	2378	ν(C-H) or ν(C-D) or zinc-acetylide, species B.
ν_3 C≡C stretch	1974 [b]	1762	1955	1744	ν(C≡C) of π-bonded ethyne, species A.
			1943	1731	ν(C≡C) of zinc- acetylide, species B.
			1366	-	Unassigned, but due to zinc-acetylide
ν_5 C-H or C-D bend	730 [c]	537	763		δ(C≡C-H) of π-bonded ethyne, species A
ν_4 C-H or C-D bend	612 [b]	505	750		δ(C≡C-H) of zinc acetylide, species B

a. Selected value

b. Raman active only

c. Infrared active only.

In the region between 2000 and 1900 cm^{-1} two bands of very differing intensities were observed at 1955 and 1943 cm^{-1} (Figure 7.1(ii)). These may be assigned to the C≡C stretching vibration of adsorbed C_2H_2 at <u>two</u> sites, A and B, within the zeolite framework. This mode is formally IR inactive in gaseous C_2H_2. The observation and shift in the bands, with respect to the gas phase Raman value of 1974 cm^{-1},[18] indicates a lowering of symmetry and a weakening of the C≡C bond on adsorption.

In the ν(C-H) region two bands were observed at 3238 and 3203 cm^{-1}. By comparing the relative intensity changes of these bands, with those in the ν(C≡C) region, on increasing the pressure (Figure 7.1) and evacuation (Figure 7.2), the higher frequency band in each region can be assigned to species A and the lower frequency band to species B (Table 7.3). A band at *ca.* 1915 cm^{-1} in Figure 7.1 is due to a background feature.

When C_2D_2 is adsorbed onto ZnNa-A (Figure 7.3), the results obtained are similar to C_2H_2, but as expected, the bands are shifted to lower wavenumber. The two ν(C≡C) vibration are observed at 1744 and 1731 cm^{-1} and the ν(C-H) vibrations at 2403 and 2378 cm^{-1}. From the behaviour of these bands on increasing the pressure in the system and on evacuation compared with the C_2H_2 case, we assign higher wavenumber transition in each region to species A and the lower wavenumber one to species B (Table 7.3).

The ν(C≡C) vibration of gaseous C_2D_2 occurs at 1762 cm^{-1}, which is an isotopic shift of 0.892 compared to

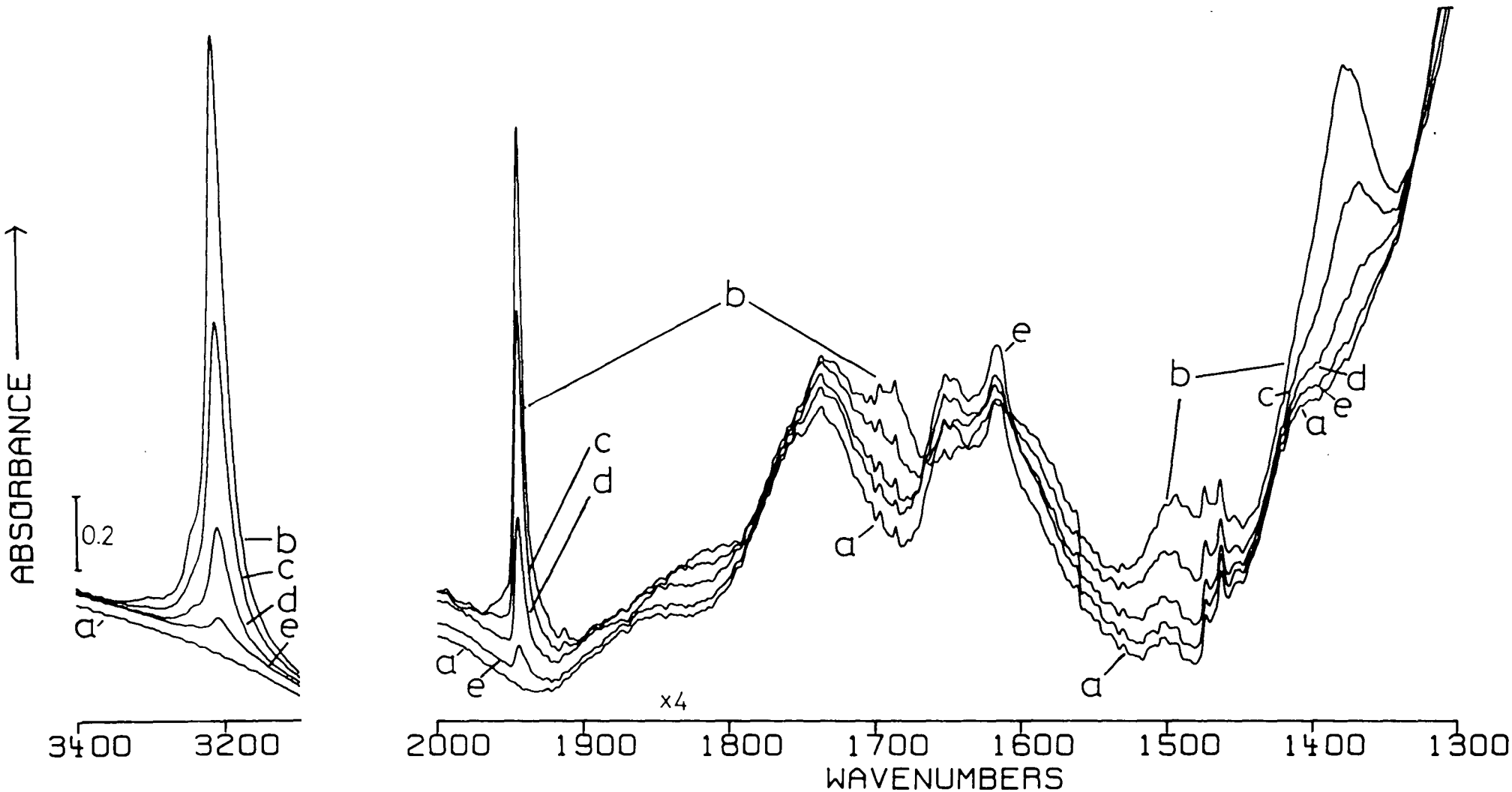

Figure 7.2 The immediate evacuation of C_2H_2 (14.2 torr) from ZnNa-A zeolite (sample 1)

(a) dehydrated zeolite background (238 sec.); (b) immediate evacuation of C_2H_2 after adsorption (16sec.)
(c) evacuation for 1.3 minutes (16 sec.); (d) evacuation for 10 minutes (31 sec.);
(d) evacuation for 1 hour (64 sec.).

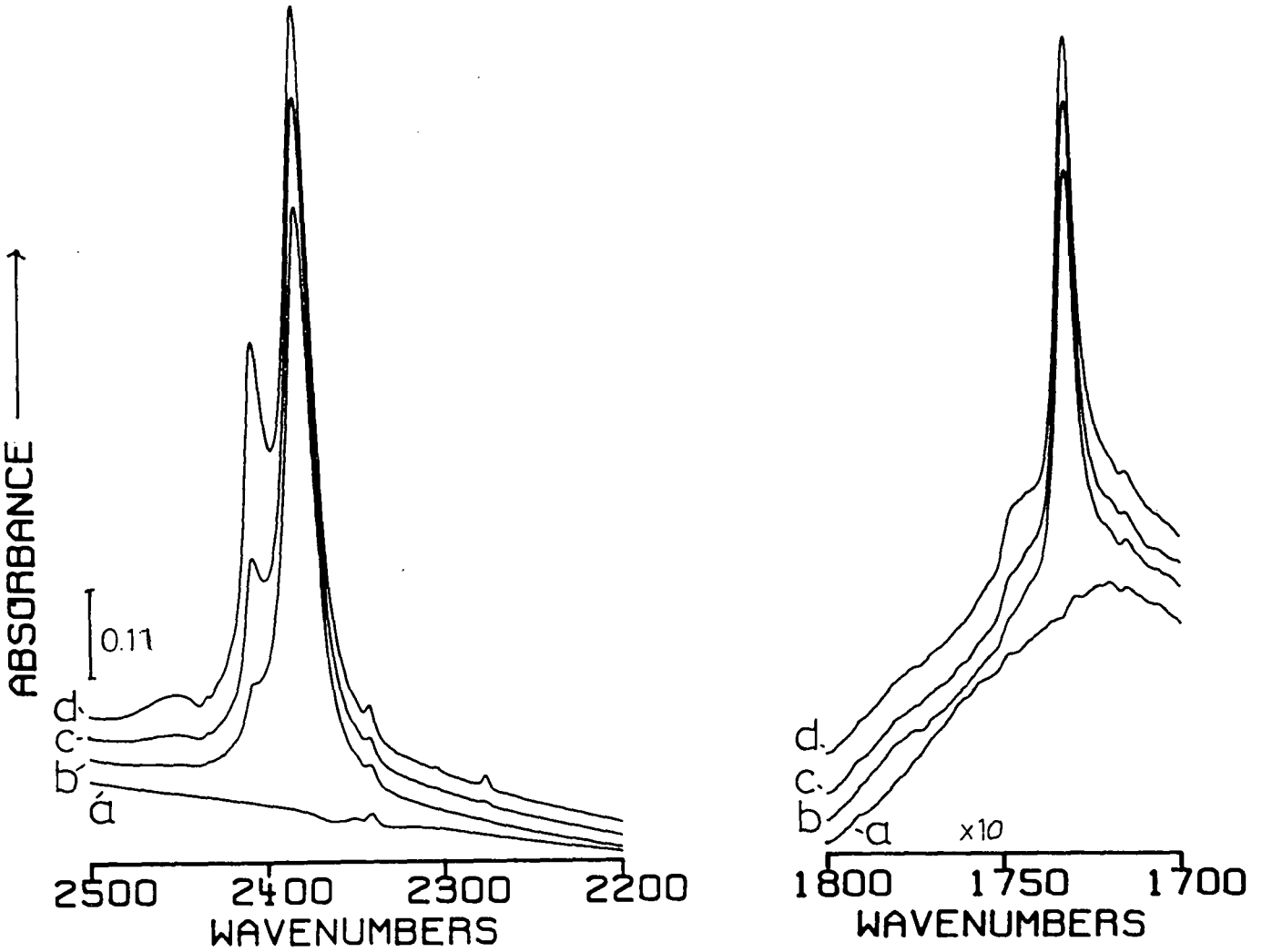

Figure 7.3 The effect of pressure on the spectrum of ethyne-d_2 adsorbed on ZnNa-A zeolite (sample 3)

(a) dehydrated zeolite background; (b) sample (a) + 1.5 torr C_2D_2; (c) sample (a) + 4.7 torr C_2D_2; (d) sample (a) + 13.6 torr C_2D_2 (scan time 64 seconds).

the C_2H_2 molecule. The isotopic shift of infrared active ν_3 mode calculated from the gas phase values (Table 7.3) is 0.741. Thus calculating the shifts of the bands assigned to species A and B, the following results are obtained:

	Gaseous ethyne	Species A	Species B
$\frac{\nu_3(C\text{-}D)}{\nu_3(C\text{-}H)}$	.741	.742	.742
$\frac{\nu(C\equiv C)_D}{\nu(C\equiv C)_H}$	.892	.892	.891

A comparison of the above shifts shows that the assignment of the bands to species A and B (Table 7.3) are realistic.

The assignment of the remaining band at 1366 cm^{-1} observed only in the spectrum of adsorbed C_2H_2 (Figure 7.2) is not so clear. No equivalent band was observed in the spectrum of C_2D_2 on ZnNa-A.

As later, in Section 7.4.2, adsorbed ethyne is shown to react with zeolitic water, to investigate the strength of the adsorption complexes. C_2H_2 (14.2 torr) was adsorbed and immediately evacuated from ZnNa-A. From the data shown in Figure 7.2 the bands at 3228 and 1955 cm^{-1} due to species A were observed to be immediately lost, while the remaining bands (3203, 1943, and 1366 cm^{-1}) decrease steadily in intensity over a period of 60 minutes. Clearly species A is due to weakly (physi)adsorbed C_2H_2, while species B is associated with strongly coordinating C_2H_2. From the behaviour of the 1366 cm^{-1} band on evacuation (Figure 7.2) it is reasonable to attribute this band to species B.

From previously published studies of C_2H_2 adsorbed on zeolites (Section 7.1) species A may be assigned to a side-on, π-bonded C_2H_2 complex formed with the charge compensating cations in the zeolite framework. In view of our observations (Chapter Four) that adsorbate molecules may interact with both the Zn^{2+} and Na^+ cation in ZnNa-A, further evidence is required to identify with which cation (Zn^{2+} or Na^+) Species A is formed.

In fact, in Section 7.4.2 it will be shown that species A, unlike species B, does not react with zeolitic water. Data, also presented later, shows that C_2H_2 adsorbed on Na-A gives bands in positions similar to species A and also has no reaction with zeolitic water. In view of these results, we assign species A to C_2H_2 adsorbed on the Na^+ cation.

The value of $\nu(C\equiv C)$ for species B (1943 cm^{-1}) falls within the range (1912-1960 cm^{-1}) normally associated with π-bonded C_2H_2. This does not, however, explain the existence of the band at 1366 cm^{-1}. An alternative explanation is to identify species B with zinc acetylide. Justification for this is obtained from published IR data on zinc-acetylides[19,20] (Table 7.4).

The bands due to species B were observed at 3202, 1943, 1366 and 750 cm^{-1}. Although these bands do not completely agree with either of the complexes given in Table 7.3, the overall similarity in band positions and number is clearly seen. Some differences in the band positions for an inorganic complex and one formed in a zeolite framework would clearly be expected, considering the unique nature of the zeolite framework environment.

TABLE 7.4 The infrared bands (cm^{-1}) and their assignments for some zinc-acetylide complexes.[19,20]

Assignment	$Zn(C\equiv CH)_2.2NH_3$[19]	$k_2[Zn(C\equiv CH)_4]$[20]
ν(C-H)	3236 (s)	3290 (s)
$\nu(C\equiv C)$	1961 (w)	1940 (w)
Unassigned	-	1370 (b,s)
$\nu(C\equiv C-H)$	-	660-670 (w)

s = strong, w = weak, b = broad.

The formation of zinc-acetylide will be accompanied by the release of H^+ into the zeolite framework. In subtraction data, of the spectrum before adsorption of C_2H_2, from that after adsorption, the loss of hydroxyl bands, present in the dehydrated zeolite, is observed. This indicates the interaction of the hydroxyl groups with the adsorbate species. We would expect H^+, released on acetylide formation, to interact with the structural hydroxyl groups, causing the ν(OH) stretching mode to disappear from the spectrum, as observed, as H_2O or H_3O^+ species were formed.

In the region below 1200 cm^{-1}, on adsorption of C_2H_2 a number of features are observed (Figure 7.4(a)→(d)). New bands occur at *ca.* 763, 750 and 730 cm^{-1} which may be assigned to the $\delta(C\equiv C-H)$, mode of species A, species B and gaseous C_2H_2 respectively (Table 7.2). The behaviour of a new band observed at 818 cm^{-1} (Figure 7.4(d)) resembles that of species B. This transition is on the side of the very

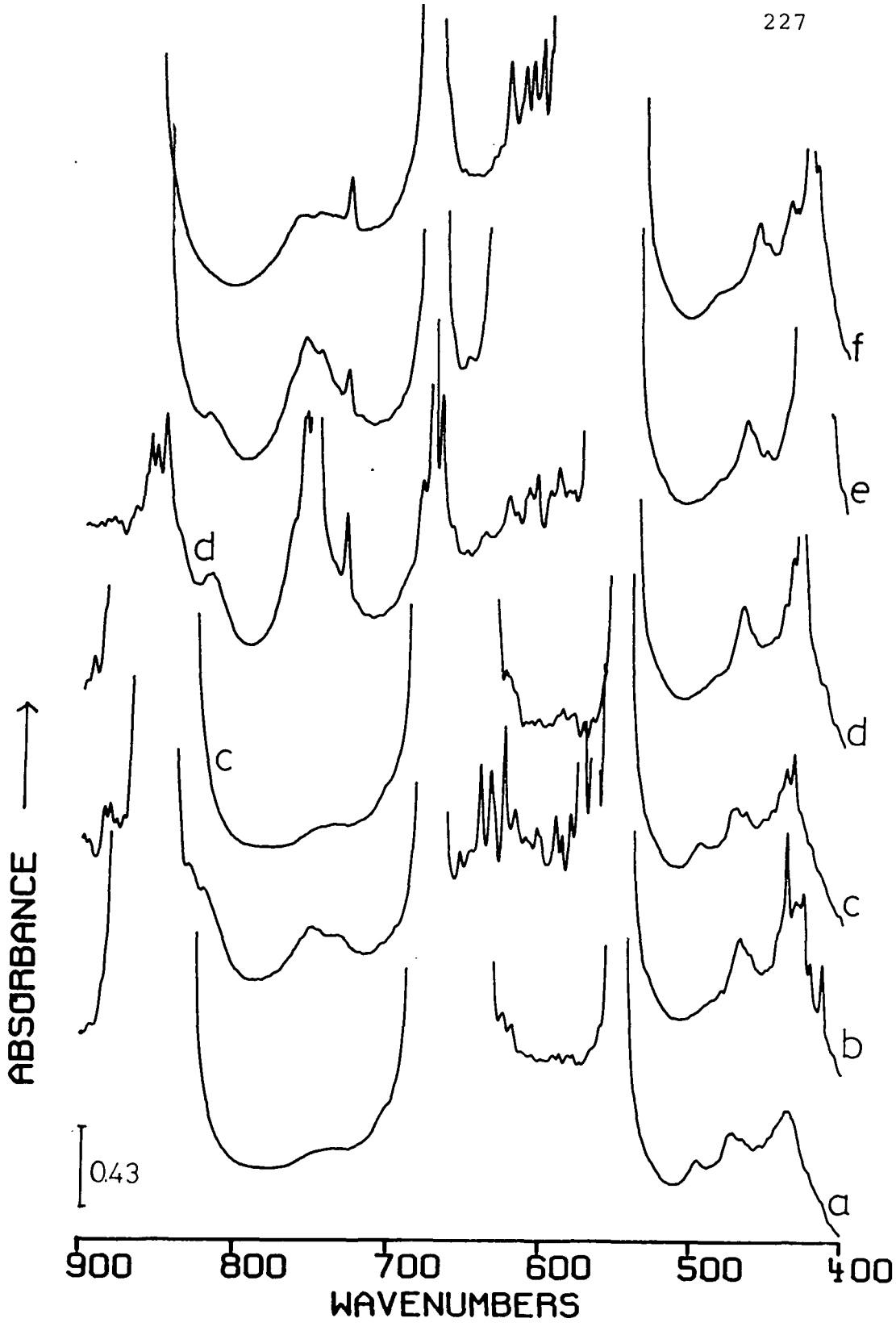

Figure 7.4 The spectra region below 900 cm^{-1} for C_2H_2 adsorbed on ZnNa-A zeolite (sample 1)

(a) dehydrated zeolite background; (b) immediate evacuation of 14.7 torr of C_2H_2; (c) evacuation of sample (b) for 1 hour; (d) readsorption of 8.5 torr of C_2H_2; (e) sample (d) after 8 hours; (f) sample (d) after 24 hours.

(y axis offset)

intense framework vibration at 950 cm^{-1} and therefore changes in the framework modes may be responsible. Thus the assignment of the 818 cm^{-1} band to species B must be regarded as tentative.

Below 500 cm^{-1} a band at 490 cm^{-1} is observed to disappear on adsorption of C_2H_2 and a band at 471 cm^{-1} to shift to 467 cm^{-1}. The movement of the latter band and changes which occur in the 450-400 cm^{-1} regions are all probably linked to small changes in cation location, as the T-O bending and pore opening modes are reported in these regions (Chapter Two). The band which disappears on adsorption at 491 cm^{-1} and reappears on evacuation (Figure 7.4(c)) may be due to the displacement of water and the formation of H_3O^+ on C_2H_2 adsorption.

7.4.2 Effect of prolonged contact time on ethyne adsorbed on ZnNa-A

(A) ZnNa-A and C_2H_2

When 8.5 torr of C_2H_2 was left in contact with ZnNa-A the bands at 3203, 1943, 818 and 750 cm^{-1} due to species B slowly decrease in intensity over a period of 24 hours (Figures 7.4 and 7.5). Simultaneously the band at 1366 cm^{-1} developed shoulders and a new band appeared at 1685 cm^{-1} (Figure 7.5(b)). After 24 hours the five species B bands had disappeared, while those due to species A remained (Figure 7.5(e)). The bands observed after 24 hours are summarized with their assignments in Table 7.5).

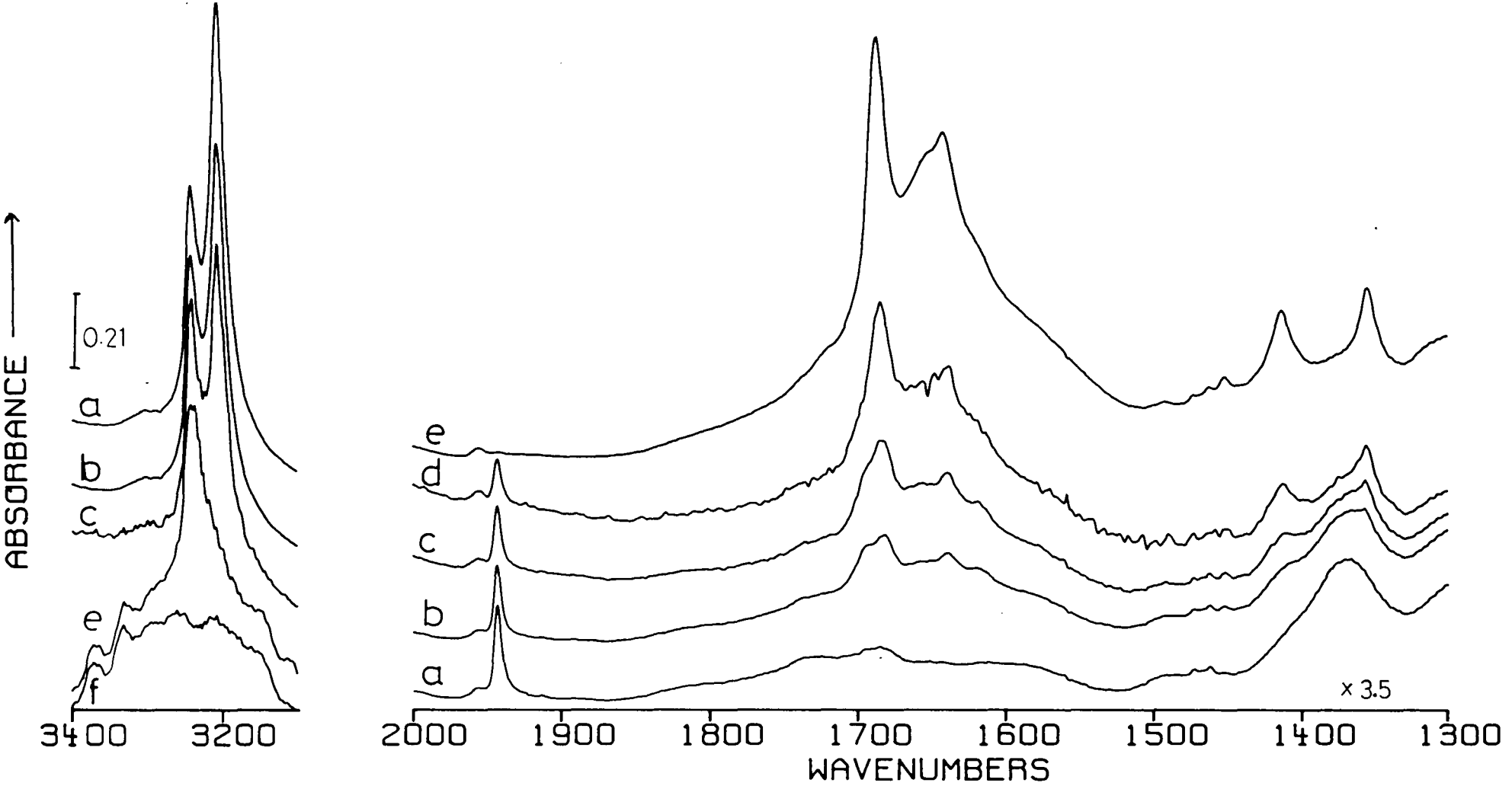

Figure 7.5 The adsorption of C_2H_2 (8.5 torr) on ZnNa-A zeolite: effect of prolonged contact (sample 1)

(a) spectrum 7.3e after the adsorption of 8.5 torr of C_2H_2, spectrum (a) after (b) 5 hours, (c) 8 hours, (d) 13 hours and (e) 24 hours C_2H_2 contact; (f) sample (e) after evacuation of gas phase (3400-3100 cm^{-1} region only). (Y axis offset).

TABLE 7.5 A summary of the bands (cm^{-1}) and their assignments in the 4000-1200 cm^{-1} region for ethyne adsorbed on ZnNa-A zeolite after prolonged contact

Band		Assignment
C_2H_2	C_2D_2	
3238		ν(C-H))
	2403	ν(C-D)) of species A.
1955		)
	1744	) ν(C≡C) of species A.
	1715	ν(C=O) of H-bonding ethanal
1685		)
	1666	) ν(C=O) of adsorbed ethanal
1652		ν(C=O) of ethanal
1640		δ(HOH) of zeolitic water
	1606	ν(C=C) of enol form of ethanal/ zeolitic water?
	1450	)
	1410	) δ(HOD) of zeolitic water
1414		)
		) δ(CH) and $\delta(CH_3)$ of adsorbed
1355		) ethanal
	1312	δ(C-H) / $\delta(CH_3/CH_2D/CHD_2)$ of H-bonding ethanal.

On evacuation species A was removed and new bands were observed at 1685, 1414 and 1355 cm^{-1} (Figures 7.5(f) and 7.6(b)). As the new band at 1685 cm^{-1} occurs in the region of ν(C=O) stretching vibrations, the new species was therefore assigned to ethanal, adsorbed on the zinc cations. Confirmation of this was obtained by the adsorption of ethanal onto a freshly prepared ZnNa-A zeolite (Figure 7.6(c)). The adsorption of

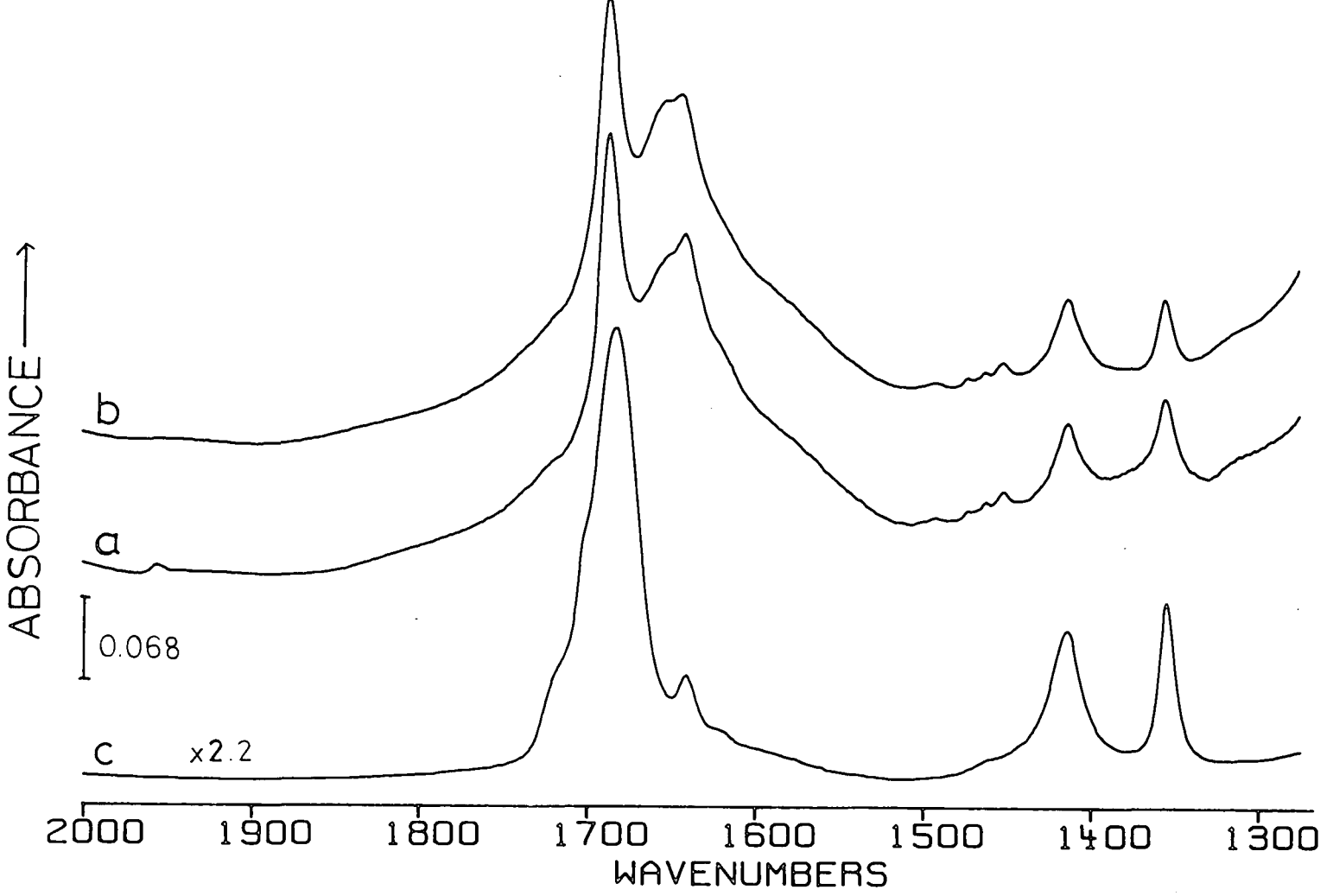

Figure 7.6 The identification of the product of C_2H_2 hydration on ZnNa-A zeolite

(a) ZnNa-A + C_2H_2 (8.5 torr) after 24 hours contact.

(b) sample (a) after evacuation of gas phase.

(c) ZnNa-A + ethanol (gas phase evacuated after adsorption of 4.8 torr. (Y axis offset)

ethanal by ZnNa-A will be discussed in Chapter Eight.

The two remaining bands in Figure 7.7(b) at *ca.* 1642 and 1652 cm^{-1} are tentatively assigned as follows: the 1652 cm^{-1} band to ethanal adsorbed on a second site (Chapter Eight) and the band at 1642 cm^{-1} to zeolitic water.

In Section 7.4.1 we assigned the band observed at 1366 cm^{-1} to a vibration of species B, which we proposed to be zinc-acetylide. The complete disappearance of the 1366 cm^{-1} band on ethanal formation and the observation still of bands due to the π-bonded species A, gives further weight to our assertion that species B is zinc-acetylide.

(B) ZnNa-A + C_2D_2

For C_2D_2 adsorbed on ZnNa-A we similarly observe the disappearance of species B with time. The data is illustrated in Figure 7.7 and summarized in Table 7.5, from which differences in the behaviour of the adsorbate bands of this system to those of the C_2H_2 system are observed.

Bands which appear in spectrum 7.7(e) at *ca.* 1410 and 1450 cm^{-1} are due to the deformation mode of HDO in the zeolite framework. Bands in the same positions have been observed for D_2O adsorbed on ZnNa-A.[21] The different desorption rate of the two bands on evacuating the sample after 24 hours is the same as observed previously for D_2O on ZnNa-A[21] (Figure 7.8).

With time new bands are observed at 1715, 1666 and 1312cm^{-1} which can be associated with ethanal formed by the hydration of

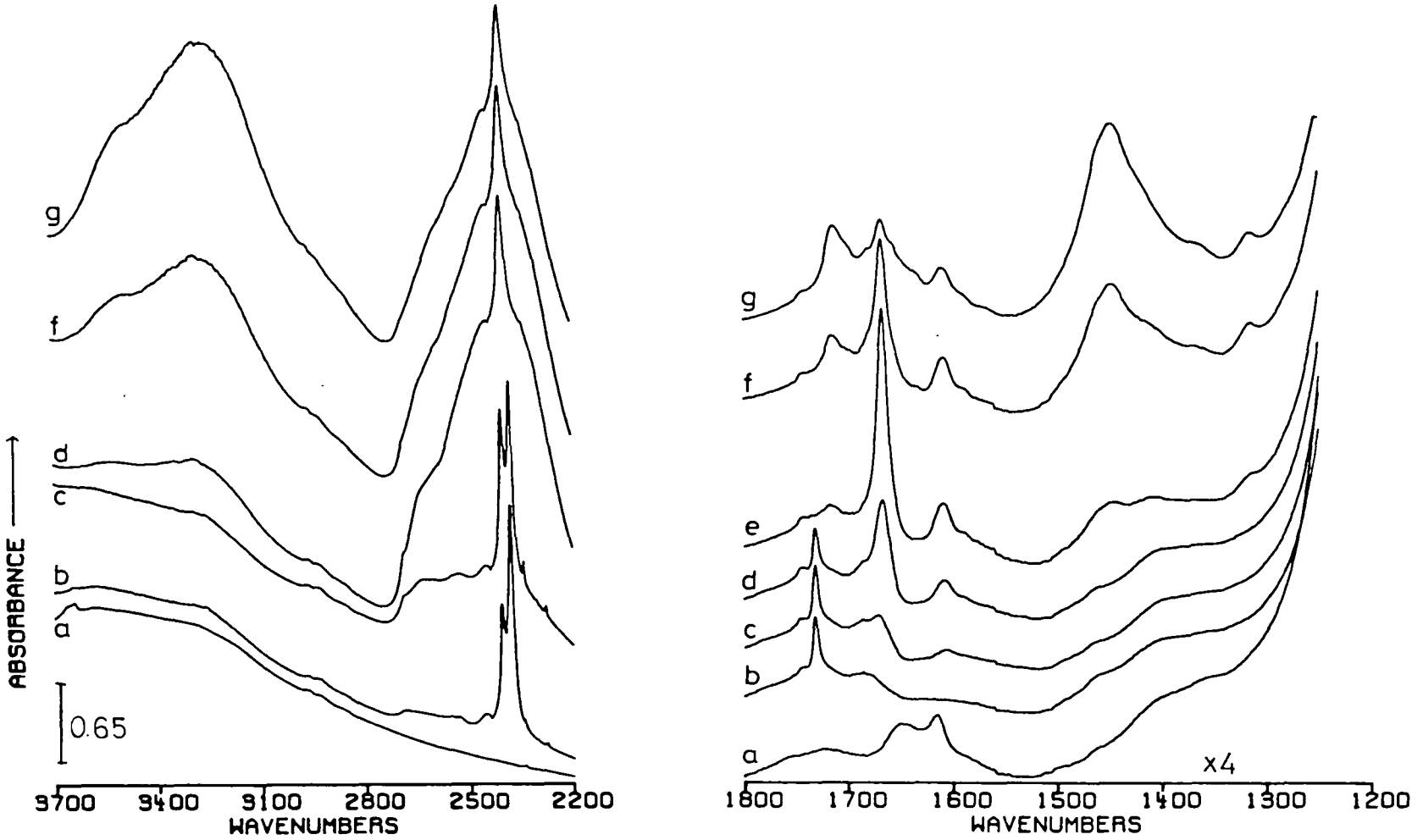

Figure 7.7 The adsorption of C_2D_2 on ZnNa-A: effect of prolonged contact (sample 3)

(a) dehydrated zeolite background, (b) sample (a) + 16.8 torr of C_2D_2 , sample (b) after (c) 30 minutes, (d) 3 hours, (e) 8 hours, (f) 13 hours, (g) 18 hours. (y axis offset)

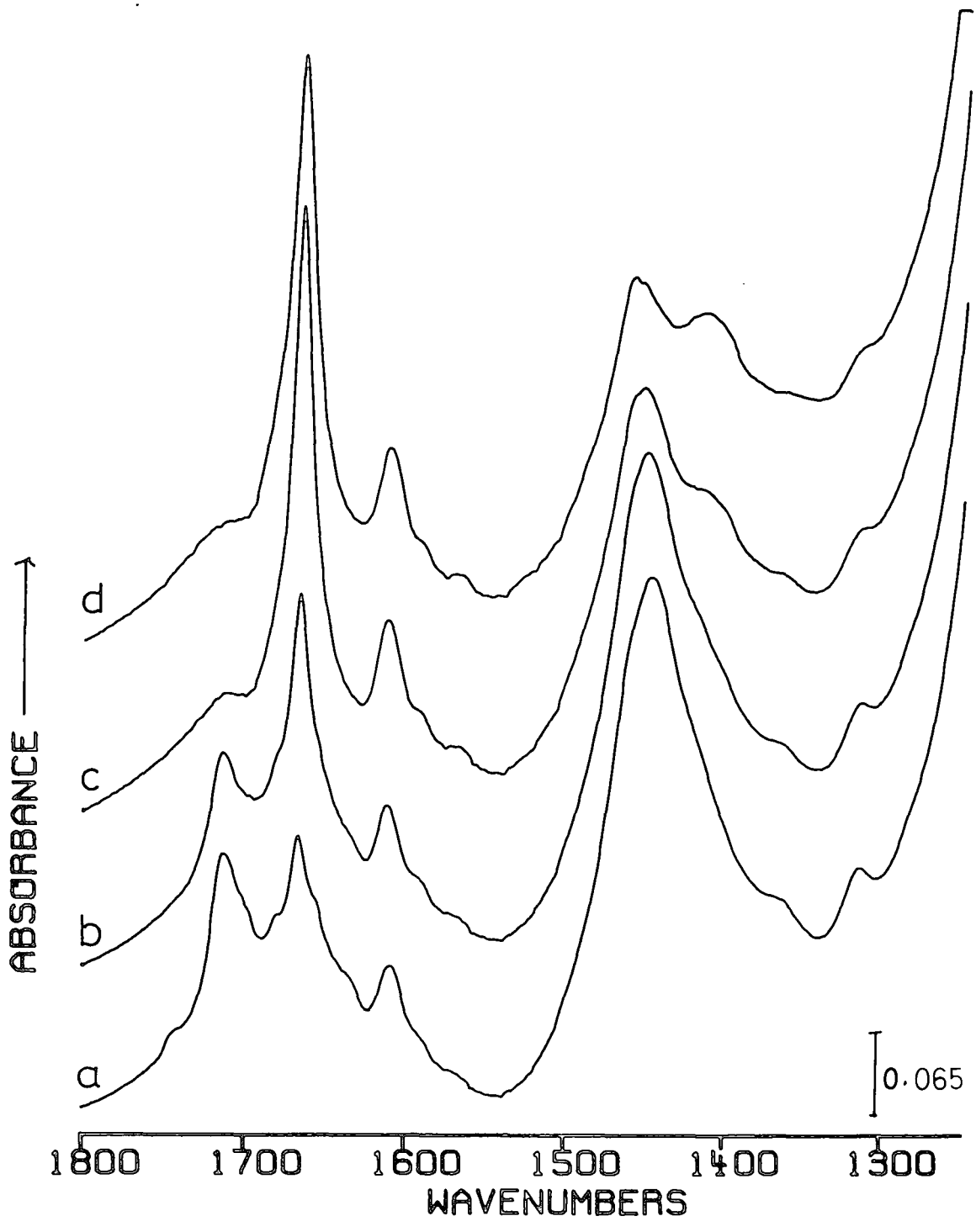

Figure 7.8 The evacuation of ZnNa-A + C_2D_2 after 18 hours contact (sample 3)

(a) ZnNa-A + C_2D_2 after 18 hours; (b) the immediate evacuation of sample (a), and evacuation of sample (a) for (c) 10 minutes, (d) 2 hours.

(y axis offset, scan time 64 sec.)

species B (Table 7.5). The ν(C=O) band of ethanal is first observed at 1666 cm^{-1}. As the contact time is increased we observe other bands to appear together at 1715 and 1312 cm^{-1}. These latter bands are observed as a large intensity increase in the ν(OH) and ν(OD) stretching vibrations becomes apparent. We therefore associate the new ν(C=O) band at 1715 cm^{-1} with ethanal hydrogenbonding in the zeolite cavities (Table 7.5). In agreement with this proposal the ν(C=O) band at 1666 cm^{-1} is seen to decrease in intensity as the hydrogen bonding complex is formed. On evacuation of the zeolite after 18 hours contact (Figure 7.8) water is removed from the zeolite cavities and the intensity of the 1666 cm^{-1} band is restored at the expense of that at 1715 cm^{-1}.

The final new band at 1312 cm^{-1} is in the region of the deformation region of C-H groups. This band is thus clearly associated with the deformation modes of partially deuterated ethanal formed from the hydration of C_2D_2. As the rapid deuteration of the OH group in the zeolite is observed on C_2D_2 adsorption, the ethanal species formed will be randomly deuterated. Hence the deformation mode at 1312 cm^{-1} cannot be assigned to particular deuterated ethanal molecule, without further investigations.

Finally in the C_2D_2 data a band appears after 30 minutes contact at 1606 cm^{-1}. Although the appearance of this band coincides with that of the 1666 cm^{-1} their behaviour on prolonged contact time differs. The intensity of the 1606 cm^{-1} band is observed to stay constant, while that of the 1666 cm^{-1} band decreases (Figure 7.7 (e→g)). Two assignments are

possible for the 1606 cm^{-1} band: (a) to the δ(HOH) mode of zeolitic water, (b) to the ν(C=C) mode of the enol form of ethanal. Without further investigation we are unable to specify which assignment is correct.

7.4.3 The hydration of ethyne: comments on mechanism

On adsorption of C_2D_2 onto ZnNa-A we observe the rapid disappearance of the ν(OH) and $\delta(H_2O)$ bands of zeolitic water (Figure 7.9) and the appearance of ν(OD) and δ(HOD) absorption bands. This indicates that on adsorption of C_2D_2 the very rapid exchange of the D atoms of C_2D_2 occurs.

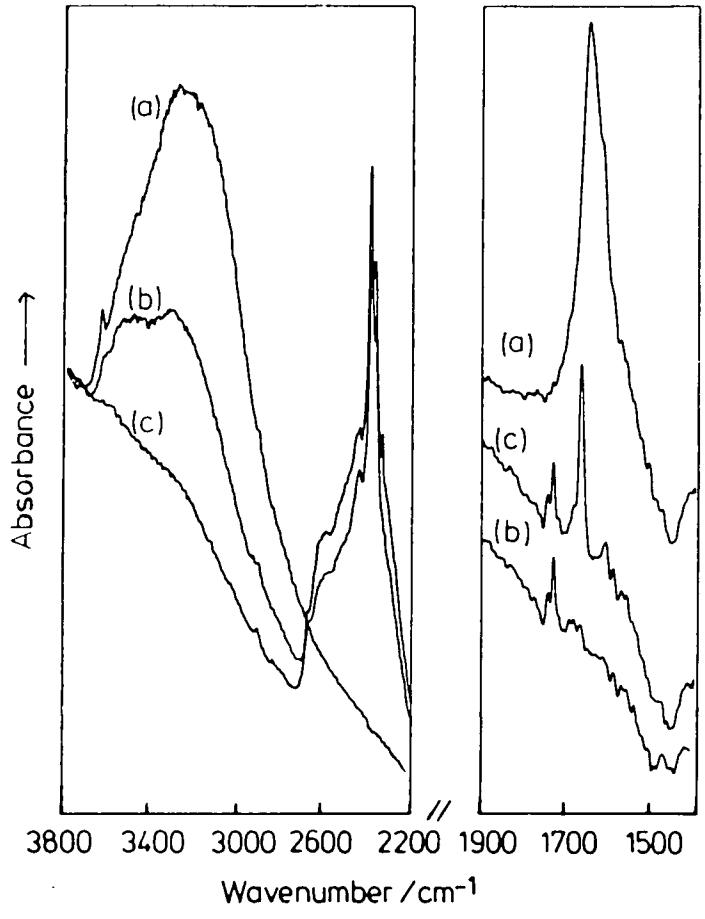

Figure 7.9 The adsorption of C_2H_2 on partially dehydrated ZnNa-A (sample 4)

(a) partially dehydrated zeolite background
(b) sample (a) + 17.2 torr of C_2D_2
(c) sample (b) after 1.5 hours. (y axis offset in (ii)).

Although the Ds of ethyne are acidic, the rapid exchange of D/H with zeolitic H_2O would not be expected. This observation is clearly consistent with our proposal of the formation of zinc-acetylide in the zeolite framework and the probable formation of H_3O^+ species (with adsorbed C_2H_2). It should also be noted that for other molecules we have never observed the disappearance of the ν(OH) and δ(HOH) modes of zeolitic water on adsorbtion.

It is obvious from the above observation that we are observing the hydration of ethyne *via* a zinc-acetylide intermediate. Clearly, therefore, the presence of zeolitic water is essential to the formation of the product.

The hydration of C_2H_2 in the presence of mercury salts and sulphuric acid has been known for a long time.[22] The mechanism of the hydration was suggested to occur by the formation of a π-bonded Hg^{2+}-C_2H_2 intermediate,[23] *viz*:

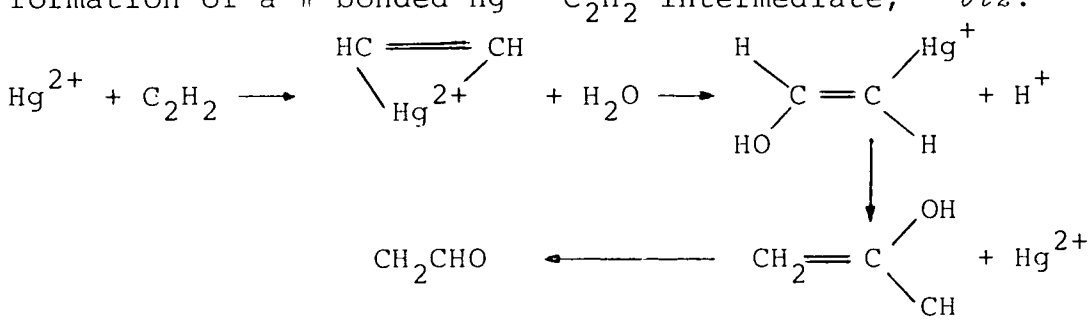

"enol" (unstable)

Copper sulphate-sulphuric acid solutions have also been shown to catalyse the hydration of ethyne.[24] In this instance, the mechanism has been proposed to include the formation of $Cu(HSO_4)C_2H^-$ species, *i.e.* copper acetylide complexes,[24] in acid media (H_2SO_4), *viz:*

$$Cu(HSO_4) + C_2H_2 \rightleftharpoons Cu(HSO_4)\ C_2H_2$$

$$Cu(HSO_4)\ C_2H_2 + H_2O \rightleftharpoons Cu(HSO_4)\ C_2H^- + H_3O^+$$

$$Cu(HSO_4)\ C_2H^- + H_3O^+ \rightleftharpoons Cu(HSO_4)\ CH{=}CHOH_2$$

$$Cu(H_2SO_4)CH = CHOH + H_3O^+ \rightleftharpoons Cu(HSO_4) + H_2O + CH_2 = CHOH_2^+$$

$$CH_2 = CHOH_2^+ + H_2O \longrightarrow CH_3CHO + H_3O^+$$

As in the ZnNa-A+C_2H_2 system, we have shown the reaction to occur *via* the zinc-acetylide intermediate, a similar series of mechanistic steps may be envisaged. Further work, involving the adsorption of partially deuterated ethanal will be needed to confirm the reaction mechanism.

The hydration of C_2H_2 on 13X zeolites containing Cd^{2+}, Zn^{2+}, Cu^{2+} and Ag^+ ions has been previously reported.[25] Kinetic studies using a differential reactor showed the main product to be ethanal, but small quantities of crotonaldehyde ($CH_3CH = CHCHO$) and ethanoic acid were also formed. The deactivation of the zeolites was observed, due to the formation of polymerized ethyne and ethanal.

Further investigations of the hydration of C_2H_2 on cadium exchanged 13X zeolites, using IR spectroscopy, have shown preadsorbed NH_3 to moderate the deactivation.[25] The NH_3 was shown to react with C_2H_2 to form pyridine, which blocks the Brönsted acid sites, responsible for the formation of higher products from C_2H_2 and CH_3CHO.

In the literature there have been no other previous reports of the hydration of ethyne by type A zeolites. No

discussion of the hydration mechanism on zeolites has appeared.

7.4.4 The adsorption of C_2H_2 on Na-A

Tam *et al*[5] have previously published IR and Raman data on C_2H_2 adsorbed on Na-A. As their data, summarized in Table 7.1, only included the publication of Raman spectrum, it was thought worthwhile to look closely at the bands observed in the FTIR spectrum and, in particular, the $\nu(C\equiv C)$ mode. We also wanted to investigate whether ethanal was produced after periods of prolonged contact to confirm the assignment of species A (Section 7.4.1) to C_2H_2 adsorbed on the Na^+ ions. The IR data obtained is presented in Figures 7.10 and 7.11 and summarized in Table 7.6.

On adsorption of C_2H_2 onto Na-A the slow uptake of C_2H_2 was observed by the increase in the intensity of the adsorption bands. It has previously been shown that adsorption of C_2H_2 is complete in about 15 hours.[12] The spectra obtained in this study over a period of 16 hours under various conditions show a number of changes in the $\nu(C-H)$ and $\nu(C\equiv C)$ regions (Figures 7.10 and 7.11) which will be interpreted in terms of the adsorption of C_2H_2 on Na^+ ions at different sites.

Tam *et al*[5] in their study allowed an equilibriation time of 20 hours before obtaining the Raman spectrum of C_2H_2 adsorbed on Na-A. From an analysis of the profile of the asymmetric $\nu(C\equiv C)$ band centred at 1953 cm^{-1}, they were

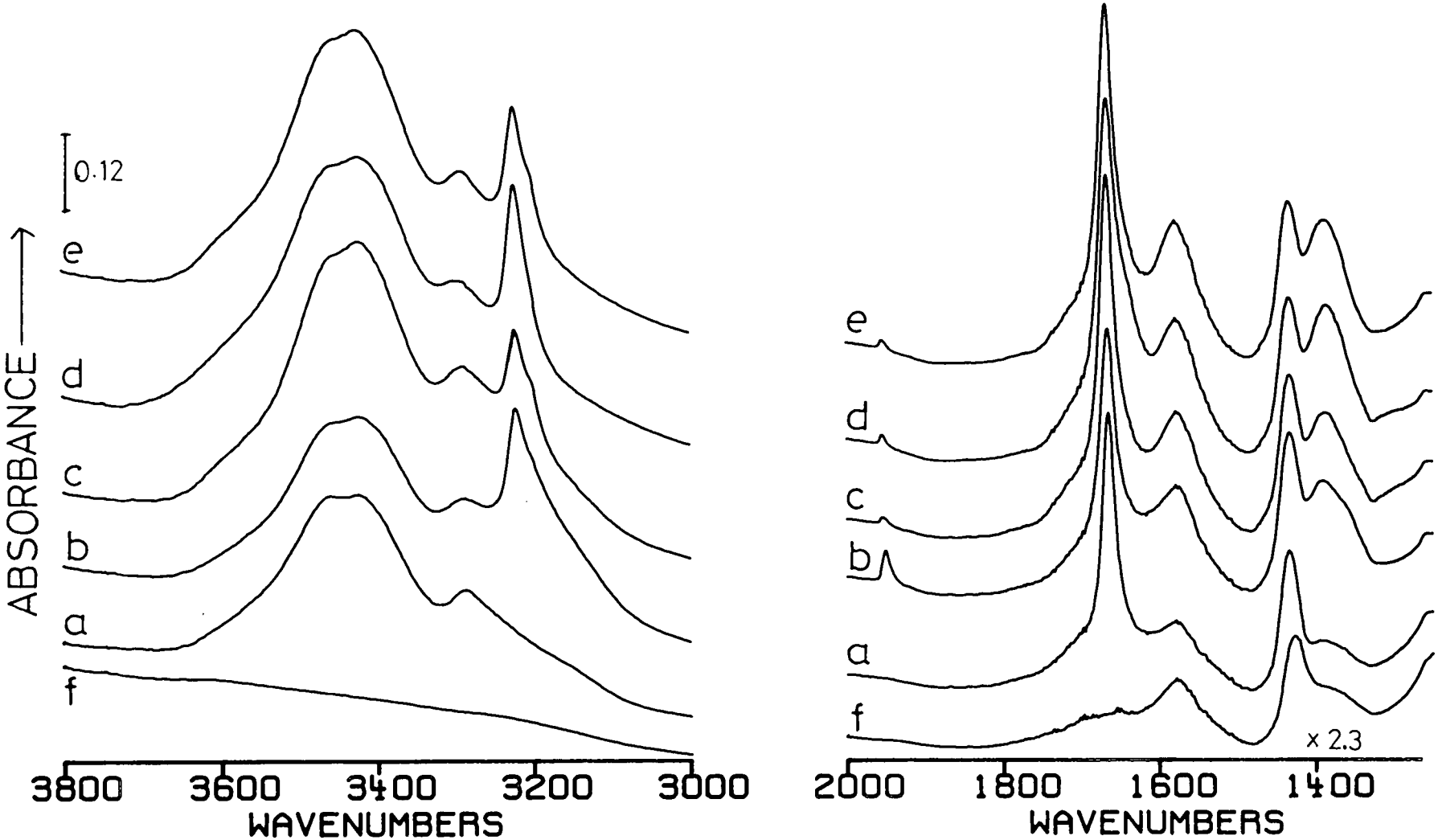

Figure 7.10 The adsorption of C_2H_2 on Na-A (sample 6)

(a) dehydrated zeolite background, (b) sample (a) + C_2H_2 5.4 torr after 20 minutes contact; (c) the adsorption of 14.7 torr of C_2H_2 after evacuation of (b) for 3.5 hours, (d) sample (c) after 16 hours, (e) immediate evacuation of sample (d), (f) evacuation of sample (d) at 660K. (Y axis offset)

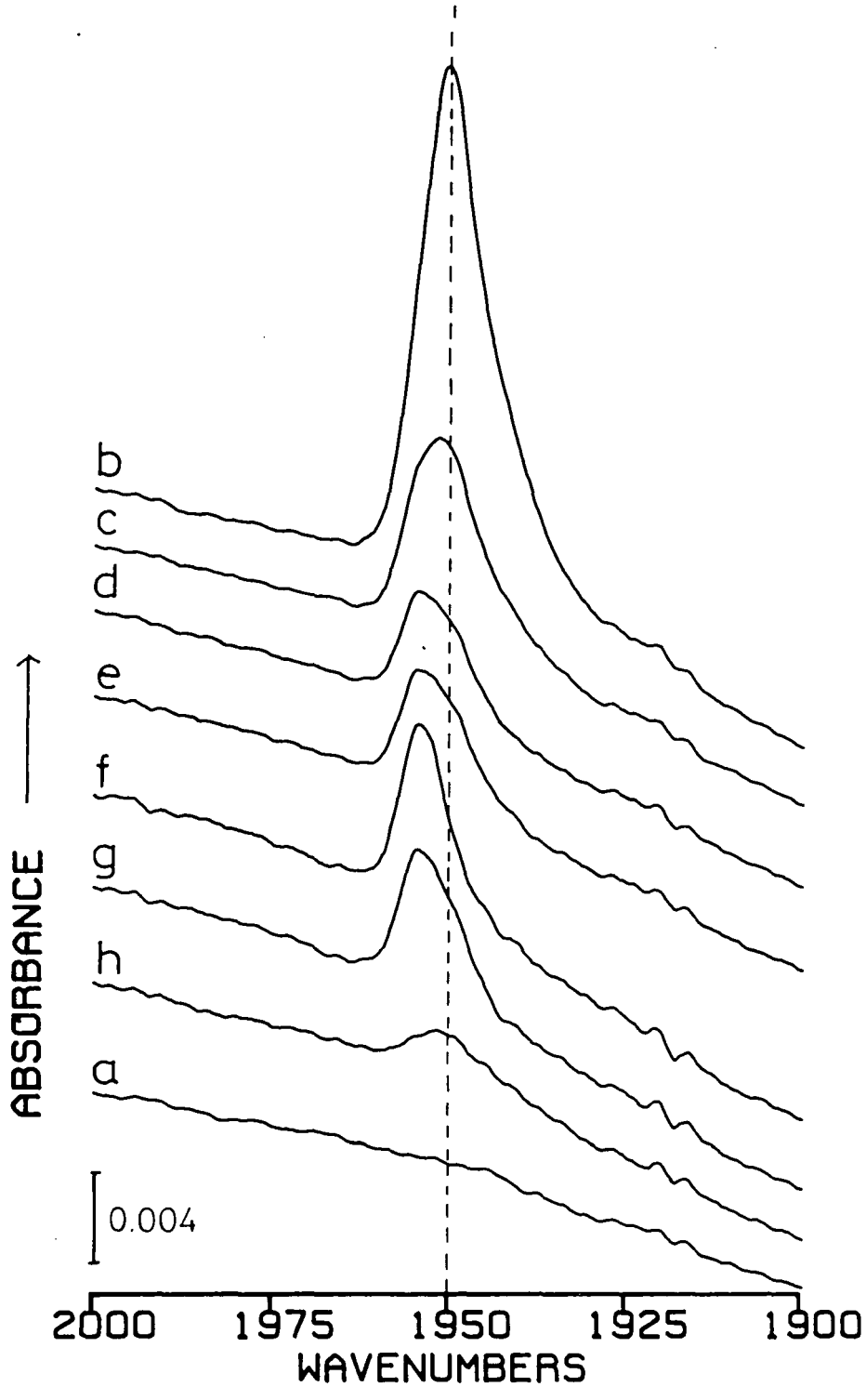

Figure 7.11 The $\nu(C\equiv C)$ band of C_2H_2 adsorbed on Na-A under different treatments (sample 6)

(a) dehydrated zeolite background; (b) sample (a) + C_2H_2 (5.4 torr) after 20 minutes contact; evacuation of (b) for (c) 6 minutes and (d) 3.5 hours; (e) readsorption of C_2H_2 (14.7 torr); (f) sample (e) after 16 hours; evacuation of sample (f) at (g) room temperature and (h) 423K.

(y axis offset)

TABLE 7.6 A summary of the infrared bands (cm^{-1}) observed in the present work and their assignment for ethyne adsorbed on Na-A

Band	Mode	Assignment	
3222	ν_3	ν(C-H) of different sites	A
3193			B
1954	ν_2	ν(C≡C) of different sites	A
1950			B
1942			C
1665		$\delta(H_2O)$ of zeolitic water	
1580		overtone and combination bands of framework or adsorbate	
1386			
760	ν_5	δ(C≡C-H)	

able to identify C_2H_2 adsorbed on two sites in the zeolite framework. The bands centred at 1954 and 1949 cm^{-1} were assigned to C_2H_2 adsorbed on cation in the S_2^* or S_3 and S_1 sites respectively. This work was in agreement with diffraction studies.[12,16] In Figure 7.11 the ν(C≡C) bands at various stages in our adsorption study are shown. Three ν(C≡C) bands are identified at 1954, 1950 and 1942 cm^{-1}, which are assigned to sites A, B and C respectively.

Initially (Figure 7.11(b)) the band is centred at 1950 cm^{-1} (Site B) and the band at 1940 cm^{-1} (Site C) is seen to give the whole band an asymmetric profile. On evacuation of C_2H_2 (Figure 7.11(c)), Site C disappears leaving the band due to Site B reduced in intensity at 1950 cm^{-1}. After 3.5 hours evacuation (Figure 7.11(d)) the band centre shifts and is observed at 1954 cm^{-1} (Site A) with Site B

present as a shoulder (1950 cm^{-1}). On readsorption of C_2H_2 (14.7 torr) the band profile is not observed to change (Figure 7.11(d)) and Site C is not now observed.

After leaving 14.7 torr C_2H_2 in contact with the sample for 16 hours the $\nu(C\equiv C)$ band centre is observed at 1954 cm^{-1} (Site A) with a shoulder at 1949 cm^{-1} (Site B). On evacuation the shoulder at 1949 cm^{-1} due to Site B increases in intensity, while the band at 1954 cm^{-1}, due to Site A is decreased in intensity. After desorption at 423K (Figure 7.11(h)) only a broad band due to Site B is observed at 1950 cm^{-1}.

In the $\nu(C-H)$ region the behaviour of the band at 3222 cm^{-1} may be correlated with that of the 1954 cm^{-1} band (Site A), while the 3193 cm^{-1} band can be attributed to Site B.

Despite the changes in the $\nu(C\equiv C)$ band listed above the spectrum after 16 hours is in reasonable agreement with the results reported by Tam *et al.*[5] The shift observed in ν_3 to 3222 cm^{-1} in our work compared to 3205 cm^{-1} reported by Tam *et al* may be due to different populations of cations in sites A and B. For ν_5, only one band was observed at 760 cm^{-1} which must be assigned to this mode on all three adsorption sites.

In accordance with the previous work of Tam *et al*[5] we will correlate Site A with C_2H_2 adsorbed at S_2^* and Site B with C_2H_2 coordinated to S_1 sites. This then means that Site C can be assigned to C_2H_2 adsorbed at S_3. Structural data (see Chapter Two) for Na-A has shown only one cation

per unit cell to be located in site S_3. As we observe Site C to disappear with prolonged contact, it is reasonable to propose that the cation at S_3 migrates to the S_2 sites. In agreement with this the intensity of the band at 1954 cm^{-1} due to Site A is observed to increase with prolonged C_2H_2 contact.

In addition to the above changes the intensity of the bands at 1580 and 1380 cm^{-1} present in the background spectrum (Figure 7.10(a)) are observed to increase on C_2H_2 adsorption. On desorption, by evacuation and heating, the bands return to their original intensity (Figure 7.10(f)). There are two possible reasons for the changes observed in these bands both associated with their assignment to overtone and combination modes: (1) overtone and combination modes of the framework, which are modified by cation movement and (2) overtone and combination bands of the adsorbed molecule (ν_5 and ν_9).

Tam *et al*[5] reported the desorption of adsorbed C_2H_2 from Na-A by evacuation for 1 hour at room temperature. In the present study using the very much more sensitive technique of FTIR spectroscopy, adsorbed C_2H_2 is still seen to be present after evacuation for 3.5 hours.

After prolonged contact of C_2H_2 with Na-A no bands due to ethanal were observed (Figure 7.10). It is therefore concluded that Na^+ ions do not promote the hydration of C_2H_2. In view of this fact, the assignment of species A in Section 7.4.1 to C_2H_2 coordinating to the Na^+ cations appears correct. It is noticed that the stability of the

C_2H_2-Na^+ complex on ZnNa-A is very much reduced compared to the Na-A zeolite. A similar observation has been made for propene adsorbed on ZnNa-A and Na-A (Chapter Four).

7.4.5 The adsorption of C_2H_2 on low exchanged ZnNa-A zeolite

Experiments on the adsorption of C_2H_2 on low exchanged ZnNa-A zeolite show that the adsorption behaviour was very similar to that of pure Na-A zeolite. For example, three bands for the C≡C stretch were observed at 1956, 1950 and 1942 cm^{-1} in good agreement with the band positions identified with Sites A, B and C in the Na-A zeolite (Section 7.4.4). In addition, unlike high exchanged ZnNa-A (Section 7.4.2), no ethanal was detected in the spectrum, after C_2H_2 had been in contact with the sample for 21 hours.

From the above evidence, it must be concluded that the Zn^{2+} ions are located in the sodalite cage sites, where they were unable to coordinate to C_2H_2.

Hence only bands due to C_2H_2 coordinating to the Na^+ ions in the supercage sites were observed and no ethanal formation occurred.

7.4.6 Prolonged ethyne contact on Ag_{12}-A

In a previous study of C_2H_2 adsorbed on Ag_{12}-A Howard and Kadir[4] observed a band at *ca.* 1690 cm^{-1} which they assigned to ν_4 of H_3O^+. The band, on comparison with the ZnNa-A + C_2H_2 system, resembles the transition we have assigned to adsorbed ethanal. It was therefore decided to examine

the Ag_{12}-A + C_2H_2 system over periods of prolonged C_2H_2 contact. The sample of Ag_{12}-A used in this new study was obtained from the previous authors and dehydrated for 2 hrs. at 673K in accordance with the previous study.[4]

The background spectrum of Ag_{12}-A after dehydration is shown in Figure 7.12(a). Bands observed at 3590-3300 and 1648 cm^{-1} are due to water readsorbed on cooling the sample. A weak band at 3610 cm^{-1} can be assigned to structural hydroxyl groups. This is in contrast to the previous study where very little water was readsorbed on cooling.

On adsorption of C_2H_2 onto the sample (Figure 7.12(b)) the $\delta(H_2O)$ band at 1648 cm^{-1} disappeared and the ν(OH) region was perturbed. New bands were clearly seen in the 3800-3000 cm^{-1} region, while only very weak features were observed below this. On subtracting the background spectrum (Figure 7.13) the bands due to adsorbed C_2H_2 are more easily seen, the positions of which agreed well with the published results of Howard and Kadir (Table 7.7).

It should be noted at this point with reference to subtraction spectra, that the work of Howard and Kadir was carried out on a dispersive instrument. This instrument did not have the computing power of the FTIR spectrometer used in the present study. Hence the generation of subtraction spectra, to aid the interpretation of the results, would not have been easily obtained by Howard and Kadir.

Above 2200 cm^{-1} the spectra obtained showed greater resolution than those of Howard *et al.* We observed two bands due to ν(C-H) of the adsorbed C_2H_2 at 3206 and

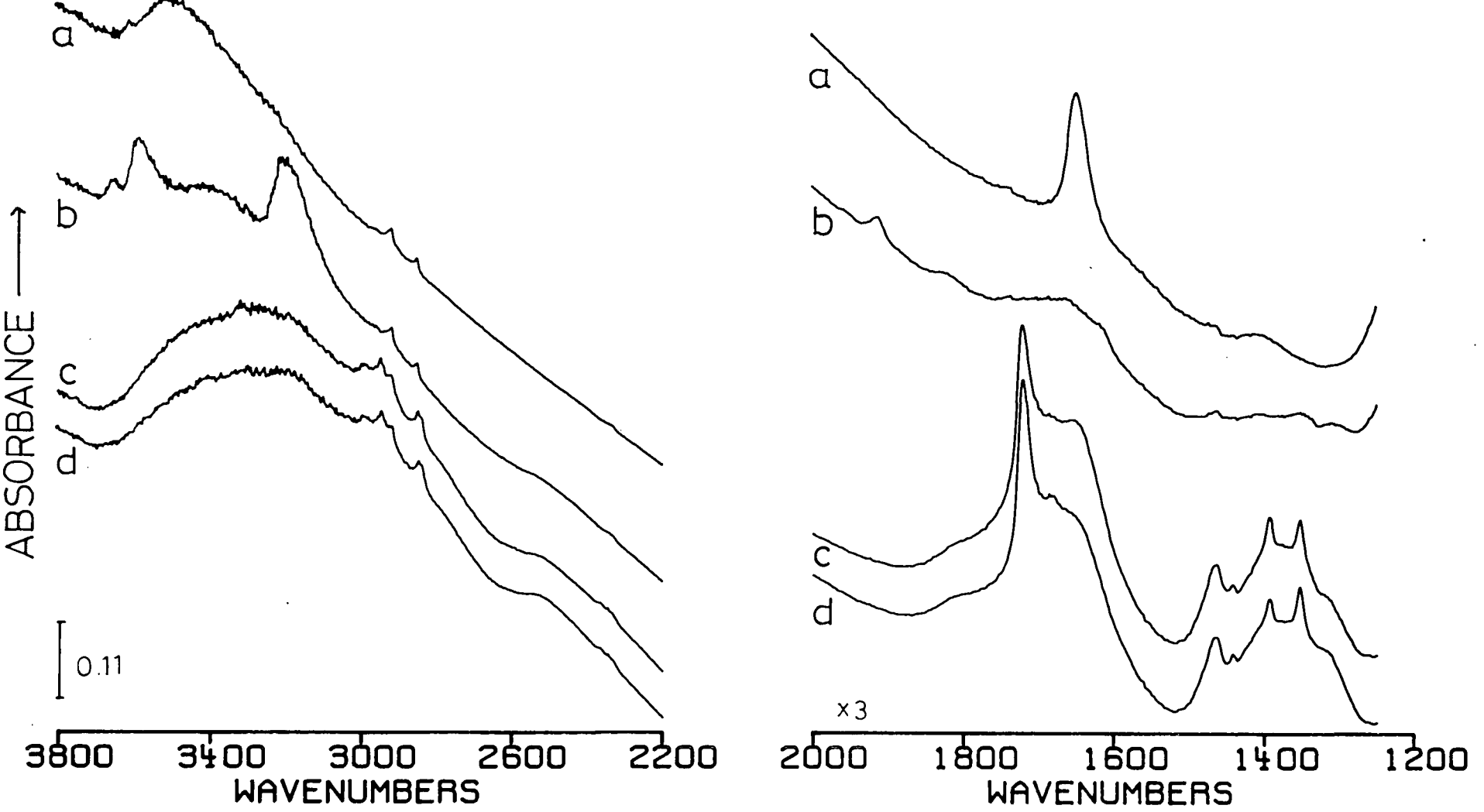

Figure 7.12 The adsorption of C_2H_2 on Ag_{12}-A: the effect of prolonged contact (sample 7)

(a) dehydrated zeolite background, (b) sample (a) + 20.7 torr of C_2H_2, (c) sample (b) after 16 hours contact, (d) sample (c) after evacuation of the gas phase. (y axis offset)

TABLE 7.7 A summary of the vibrational bands (cm^{-1}) and their assignment for ethyne adsorbed on Ag_{12}-A observed by Howard and Kadir[4] and in the present work

Howard and Kadir[4]	Present work			Assignment	
	Zeolite background	Initial adsorption positions from subtraction spectrum figure 2	After 16 hours contact	Howard and Kadir[4]	Present work
3592	3610	3655 3584		ν(OH)	ν(OH)
	3590 - 3300	negative feature 3490 (broad)			ν(OH) of hydroxyl groups and zeolitic water
3400-3100		3206 3171 (shoulder)		ν(C-H) of π-bonded	) ν(C-H) of adsorbed C_2H_2)
2500			3000 2950	Unassigned	hydrogen band bridging the $H_3O^+.H_2O$ ion.
1955		1950		) ν(C≡C) of π-bonded C_2H_2 on) different sites	
1820		1816		(C≡C) of acetylide	
			1719 1684 (broad)		) ν(C=O) of ethanal)
1686				ν_4 of H_3O^+	
	1648		1652		δ(H_2O) of zeolitic H_2O
			1465 1441 1415 (sh) 1393 1352 1314 (sh)		)))))) δ(C-H) modes of adsorbed ethanal
1460				framework vibration	
1380				unassigned	assignment unknown but probably due to the acetylide

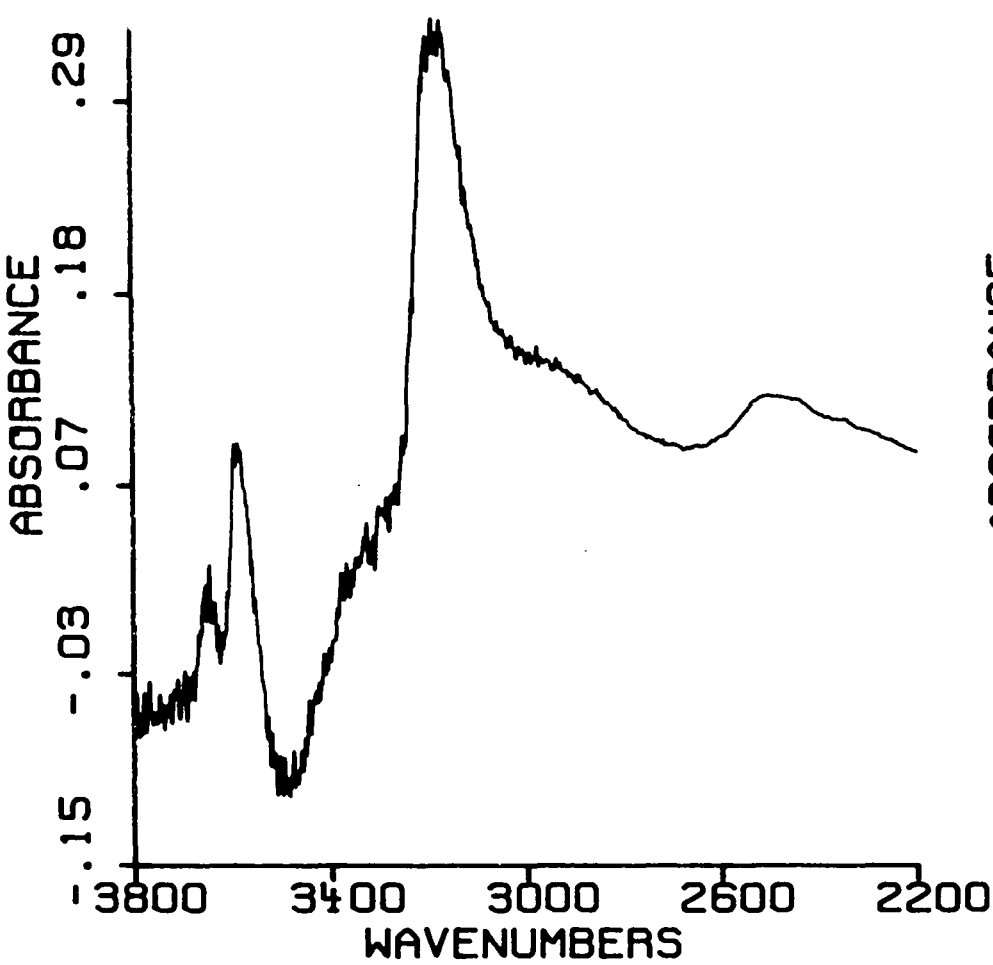

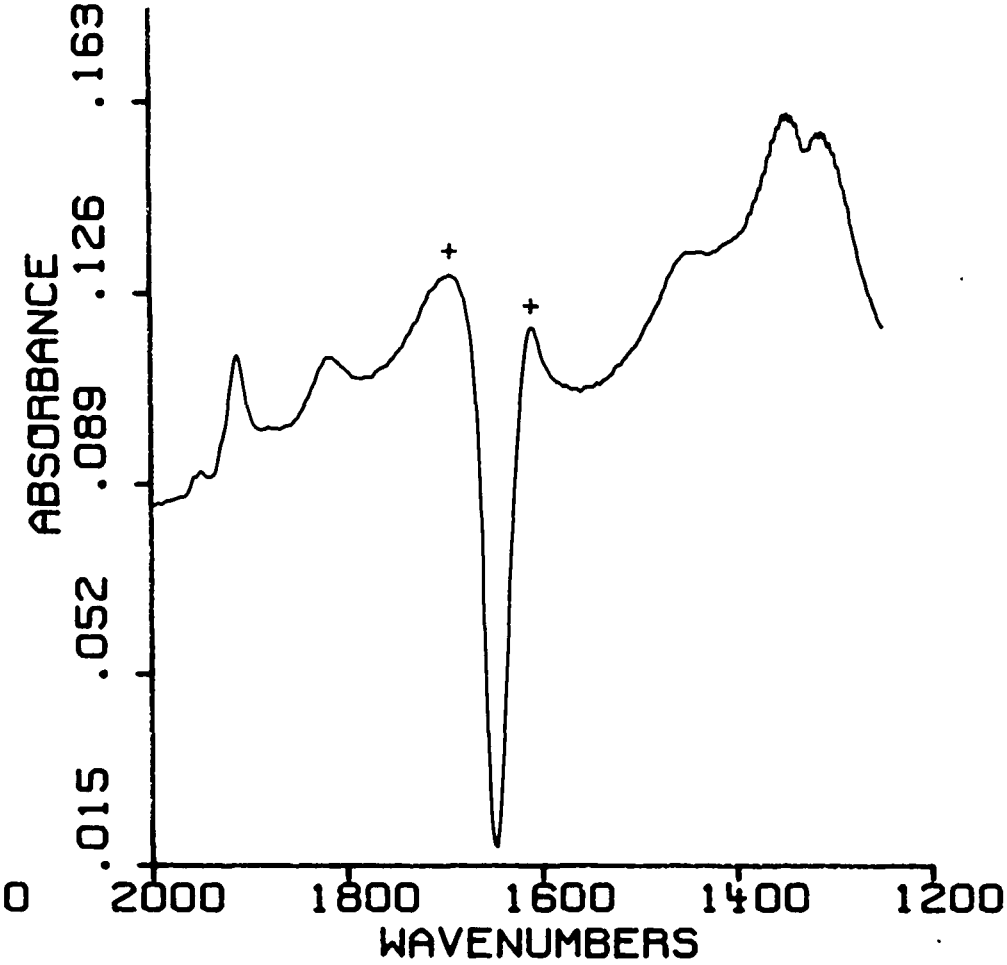

Figure 7.13 The subtraction spectrum of Ag-A + 20.7 torr of C_2H_2 - dehydrated zeolite background

N.B., features marked with a + are artefacts of the subtraction, and are not bands.

3171 cm^{-1}. ν(OH) bands were observed at 3655 and 3584 cm^{-1} as a result of the formation of Ag-acetylide. A negative feature is observed at *ca.* 3490 cm^{-1} in the subtraction spectrum shown in Figure 7.13. This shows us that, on adsorption of C_2H_2, the ν(OH) vibration at *ca.* 3500 cm^{-1} in the background spectrum are perturbed greatly or lost. We can associate this feature with the formation of H_3O^+ species resulting from acetylide formation. Although we now do not assign the band at *ca.* 1690 cm^{-1} to the H_3O^+ species, a band observed at *ca.* 2500 cm^{-1} which was also reported by Howard and Kadir, can probably be assigned to the hydrogen bond bridging the oxonium ion (H_3O^+. H_2O). A band at 2510 cm^{-1} has previously been reported by Corma *et al*[27] for this ion in Y zeolites.

After C_2H_2 has been in contact with the sample new bands are observed in the region between 1750-1200 cm^{-1} (Table 7.7 and Figure 7.12(c)). These new bands can be assigned to ethanal adsorbed in the framework. This was confirmed by the subsequent adsorption of ethanal on the sample after the evacuation of the gas phase for 90 minutes (Chapter Eight). The band thus assigned to the H_2O^+ at 1686 cm^{-1} by Howard and Kadir has now, clearly, been shown to be due to ethanal, formed by the slow hydration of ethyne. It should be remembered that in the present work the large quantities of water readsorbed on cooling the sample after dehydration will have increased the amount of ethanal formed. Thus the chances of observing the bands due to ethanal were greatly increased in the present study. Whereas, with the samples

Howard and Kadir, which readsorbed very little water on cooling, the chances of observing a number of bands due to ethanal over the time scale of their experiments, was very slim.

After 16 hours, subtraction spectra show clearly that the three $\nu(C\equiv C)$ bands are no longer present. From the present observations we are unable to state if both the Ag-acetylide and the π-bonded Ag-C_2H_2 species are active to C_2H_2 hydration.

Other features to note are the disappearance of the $\nu(OH)$ groups at 3650 and 3584 cm^{-1} on ethyne hydration. This shows the hydroxyl groups are part of the hydration process. A band observed at 1380 cm^{-1} by Howard and Kadir but not assigned, was not seen in the present work. The non-observation of this feature in the present work is perhaps due to the high water content of the sample. In view of the band observed in the same region in ZnNa-A + C_2H_2 system, which was assigned to Zn-acetylide, the band reported by Howard and Kadir is likely to be due to the Ag-Acetylide complex.

7.4.7 The effect of heat on the hydration of ethyne on ZnNa-A

In previous sections we have shown that C_2H_2 adsorbed on ZnNa-A, in the presence of zeolitic water, reacts to form ethanal. In order to probe the system further, a preliminary study has been made of the effect of heat on the hydration reaction. The spectra obtained are shown in Figure 7.14.

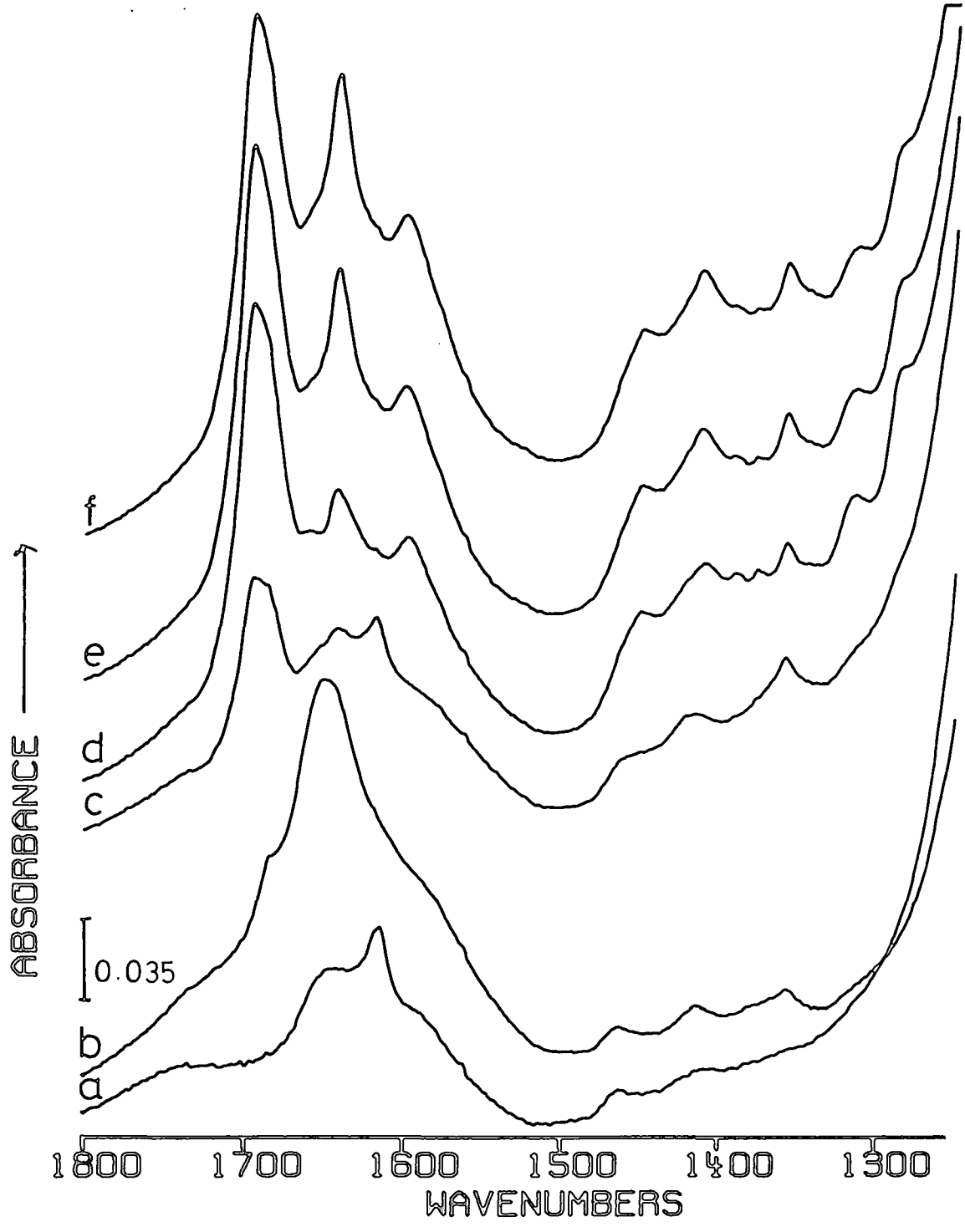

Figure 7.14 The effect of heat on the hydration of ethyne on ZnNa-A zeolite (sample 2)

(a) dehydrated zeolite background; (b) sample (a) + 6.7 torr after *ca.* 30 minutes, sample (b) heating at (c) 423K, (d) 473K, (e) 473K for 20 minutes and (f) 473K for 50 minutes.

(y axis offset)

At room temperature (Figure 7.14(b)) bands due to ethanal are visible at 1685, 1415 and 1355 cm^{-1}. A band at 1642 cm^{-1} is due to zeolitic water. As the temperature was raised new bands were observed at 1642, 1598, 1445, 1309 and 1284 cm^{-1} and the previously observed ethanal bands shift to 1692, 1411 and 1355 cm^{-1}. The new bands are obviously due to new products formed in the zeolite framework from ethyne and/or ethanal. The band observed at 1645 cm^{-1} is probably due to ethanal, as a band in this region has been observed when ethanal is adsorbed on ZnNa-A (Chapter Eight).

Although the assignment of the remaining bands cannot be definite without further investigation, the features at 1600 and 1450 cm^{-1} resemble the asymmetric and symmetric stretches of the OCO group. This species has been reported for ethanal adsorbed on alumina.[28] The remaining bands are probably due to CH_3 and CH_2 deformation modes. On ion exchanged 13X zeolites[25] (Section 7.2) quantities of ethanoic acid and crotonaldehyde were observed in the hydration products and these products may be responsible for the new bands observed on ZnNa-A.

This preliminary study has illustrated that the reaction of ethyne and ethanal on ZnNa-A is more complex at higher temperatures.

7.5 Conclusions

On adsorption of ethyne on ZnNa-A zeolite (high exchange), the formation of stable and reacting species has been observed. The stable species has been identified as ethyne π-bonded to the Na^+ ions in the framework, through a side-on interaction. The second species, which with time has been observed to react with zeolitic water to form ethanal, has been identified as zinc-acetylide. At higher temperatures, a preliminary study has shown that additional products are formed, which are probably carboxylate species.

The adsorption of ethyne on low exchanged ZnNa-A show that ethyne complexes were only formed with the Na^+ cations. The Zn^{2+} ions were, therefore, concluded to be located in the sodalite cages, where they are unable to form complexes with adsorbed ethyne. No hydration of ethyne was thus observed.

Ethyne adsorbed on Ag-A zeolite has also been shown to react with zeolitic water, forming ethanal, but no ethanal formation was observed when ethyne was adsorbed on Na-A. It is therefore concluded that the transition metal cations are responsible for promoting the hydration of ethyne to ethanal in the presence of zeolitic water.

The IR spectra of ethyne adsorbed on Na-A, has shown ethyne to form complexes with the Na^+ ions located in sites S_1, S_2^* and S_3 in the framework. The three $\nu(C\equiv C)$ bands were clearly resolved in the IR spectrum, in contrast to a previous Raman study.[5]

REFERENCES (Chap.7)

1. Howard, J. and Nicol, J.M., Proceedings of the 1985 International Conference on Fourier and Computerized IR Spectroscopy", The Proceedings of the Society of Photo-Optical Instrumentation Engineers (in press).

2. Howard, J. and Waddington, T.C., Surface Science, 68, 86 (1977).

3. Howard, J., Robson, K. and Waddington, T.C., Zeolites, 1, 175 (1981).

4. Howard, J. and Kadir, Z.A., Zeolites, 4, 45 (1984).

5. Tam, N.T., Cooney, R.P. and Curthoys, G., J.Chem.Soc., Faraday Trans.1, 72, 2577 (1976).

6. Tam, N.T., Cooney, R.P. and Curtheys, G., J.Chem.Soc., Faraday Trans. 1, 72, 5592 (1976).

7. Yates, D.J.C. and Lucchesi, P.J., J.Phys.Chem., 35, 243 (1961).

8. Rodinov, A.N., Timofeyuk, G.V., Talakeva, T.V., Shigorin, D.N. and Kocheshkov, K.A., Isz.Acad.Nauk.SSSR, Ser.Khim., 42 (1965).

9. Pitchat, P., Vedrine, J.C., Gallezot, P. and Imelik, B., J.Catal., 32, 190 (1974).

10. Heaviside, J., Hendra, P.J., Tsai, P. and Cooney, R.P., J.Chem.Soc., Faraday Trans., 1, 74, 2542 (1978).

11. Amaro, A.A. and Seff, K., J.Chem.Soc., Chem.Comm., 1201 (1972).

12. Amaro, A.A. and Seff, K., J.Phys.Chem., 77, 906 (1973).

13. Riley, P.E. and Seff, K., J.Am.Chem.Soc., 95, 8180 (1973).

14. Riley, P.E. and Seff, K., Inorg.Chem., 14, 714 (1975).

15. Tsitsishvili, G.V., Bagratishvili, G.D. and Oniashvili, N.I., Zh.Fiz.Khim., 43, 950 (1969).

16. Kahn, R., Cohen de Lara, E., Thorel, P. and Ginoux, J.L., Zeolites, 2, 260 (1982).

17. Howard, J., Robson, K., Waddington, T.C. and Kadir, A., Zeolites, 2, 2 (1982).

18. Shimanouchi, T., "Tables of Molecular Vibrational Frequencies, consolidated volumui", NSRDS-NBS 39 (1972).

19. Nast, R. Künzel, O. and Müller, R., Chem.Ber., 95, 2155 (1962).

20. Nast, R. and Müller, R., Chem.Ber., 91, 2861 (1958).

21. Howard, J. and Nicol. J.M., Unpublished work.

22. Kutzscherof, M.,Ber.7, 13 (1889).

23. Rochow, E.G., "The Chemistry of Organometallic Compounds", 112 (1957).

24. Dorfman, Ya.A. and Karazhanova, Russ.J.Phys.Chem., 49, 751 (1975).

26. Detreköy, E., Onyestyá,K.and Kalló, D., React.Kinet.Catal. Lett., 15, 443 (1980).

27. Corma, A., Agudo, A.L. and Fornes, V., J.Chem.Soc., Chem.Commun., 942 (1983).

28. Evans, H.E. and Weinberg, W.H., J.Chem.Phys., 71, 4789 (1979).

CHAPTER EIGHT

AN INFRARED STUDY OF ETHANAL ADSORBED ON SOME TYPE A ZEOLITES

8.1 Introduction

This study of adsorbed ethanal was motivated primarily by the identification of this molecule as the product of ethyne hydration on zinc and silver exchanged type A zeolites (Chapter Seven). In addition to work on Zn and Ag exchanged zeolites, we also report work on Na-A zeolite.

Considering the amount of published infrared data on adsorbate-adsorbent systems, surprisingly very little work has been carried out on ethanal adsorbed on catalytic surfaces.[1-5] The published work has shown that ethanal may either:

(a) form stable species by hydrogen bonding to surface hydroxyl groups[1] or coordinating to metal cation, or

(b) may react with the surface to form, for example, carboxylate species.[3,4]

Young and Sheppard[1] studied the adsorption of ethanal on silica. They observed the ν(C=O) vibration of ethanal, hydrogen bonding to the surface hydroxyl groups, at 1724 cm^{-1} compared with 1743 cm^{-1} in the vapour phase. On heating the sample at 393K crotonaldehyde was formed, characterized by bands at 1688 (ν(C=O)) and 1643 (ν(C=C)) cm^{-1}. It was proposed that the acidity of the surface hydroxyl groups promoted an aldol condensation between two ethanal molecules to form an aldol, which following dehydration yielded the unsaturated aldehyde, *viz:*

$$CH_3CHO \ldots HOSi \rightleftharpoons \underset{[I]}{CH_3CHOH^+} \ldots \bar{O}Si \rightleftharpoons \underset{[II]}{CH_2{=}CHOH} \ldots \overset{H}{\underset{|}{O}}Si$$

$$[I] + [II] \longrightarrow \overset{H}{\underset{|}{SiO}} \ldots \underset{[III]}{HO\text{-}CH(CH_3)\text{-}CH_2CHO} \ldots . HOSi$$

acetaldol

$$[III] \longrightarrow \overset{H}{\underset{|}{SiO}} \ldots H_2O + CH_2CH = CHCHO \ldots HOSi$$

crotonaldehyde

In contrast to the relatively simple spectrum of ethanal adsorbed on silica, the IR spectrum of ethanal adsorbed on $ZnCl_2$ [5] was somewhat more complex. The number of bands observed in the $\nu(C{=}O)$ region was found to depend on pressure and contact time. Bands observed at 1715, 1705, 1685 and 1675 cm^{-1} were assigned to the $\nu(C{=}O)$ vibrations of ethanal coordinating to the $ZnCl_2$ surface, while a fifth band at 1630 cm^{-1} was attributed to the $\nu(C{=}C)$ vibration of the enol form.

Studies of ethanal adsorbed on MgO [3] and Alumina [4] have both shown the presence of carboxylate groups. On alumina, however, only a carboxylate species was identified by inelastic electron tunneling spectroscopy. The band assignments are summarized in Table 8.1. On MgO_3, in addition to bands due to carboxylates, at 1565 and 1415 cm^{-1}, bands at 1712, 1688, 1674, 1485, 1368, 1330 and 1268 cm^{-1}, in the IR spectrum, were assigned to physisorbed ethanal, hydrogen bonding to the surface hydroxyl groups.

Studies of ethanal adsorbed on zeolites has been limited to work by Kiselev *et al* [2] on Li and Cs exchanged type X zeolites

TABLE 8.1 A summary of the inelastic tunneling spectrum of 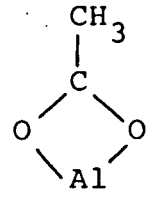 formed by the adsorption of ethanal on alumina[4]

Band (cm^{-1})	Assignment
1605	OCO asymmetric stretch
1472	OCO symmetric stretch
1423	CH_3 asymmetric deformation
1395, 1343	CH_3 symmetric deformation

---

and decationated zeolite Y. The position of ν(C=O) of adsorbed ethanal was found to be dependent upon the cation size, for ion exchanged X zeolites, *i.e.* Li-X = 1720 cm^{-1} and CS-X = 1703 cm^{-1}. The C-H deformation modes of adsorbed ethanal were identified for both zeolites at 1453 and 1355 cm^{-1}.

In decationized zeolite-Y[2] ethanal was found to interact with the structural hydroxyl groups. Bands due to a physisorbed species, which was removed on evacuation, were identified at 1698, 1428 and 1358 cm^{-1}. A number of other features were also noted at 1660, 1645, 1600 and 1460 cm^{-1}. The CO group of ethanal interacting with the aprotic centers on the surface of the decationized zeolite was assigned to the band at 1660 cm^{-1}. the remaining features at 1645, 1600 and 1460 cm^{-1} were observed to increase in intensity on evacuation and heating. These were attributed either to the formation of surface

carboxylate compounds or to the presence of two types of aprotic centers of different acidity.

In the case of ethanal adsorbed on type A zeolites, we have observed the formation of a number of surface species. The interpretation of the spectra has been based both on experience of the behaviour of adsorbate-zeolite systems and on the previously published work discussed above.

8.2 Experimental

$Zn_{4.3}Na_{3.4}$-A, (ZnNa-A) was prepared and analysed as described in Chapter Three. This sample was dehydrated at 739K for 16 hours before ethanal adsorption, according to the procedures described in Chapter Three.

The Na_{12}-A (Na-A) sample used for the ethanal adsorption work was the sample used in the previous chapter after ethyne had been desorbed by evacuation and heating at 660K for 30 minutes.

Similarly the disc used for the Ag_{12}-A (Ag-A) + ethanal experiment was the same one used in the previous chapter for the ethyne adsorption, after it had been evacuated for 90 minutes at room temperature. This treatment does not remove all of the ethanal produced from the hydration of ethyne. However, heating the sample would have reduced the transmission of the disc, which was not desirable.

Ethanal (99%, Aldrich Chemical Company Ltd.) was purified by the freeze-pump-thaw technique before use.

All data was obtained on the Nicolet 60SX spectrophotometer using a scan time of 4 minutes for the Na-A and ZnNa-A data and 2 minutes for the Ag-A data.

8.3 Results and Discussion

The results obtained for the adsorption of ethanal will be discussed in two parts:

(i) the initial adsorption and identification of stable ethanal species;

(ii) the behaviour of Na-A and ZnNa-A on desorption of ethanal by evacuation and heating.

8.3.1 The adsorption of ethanal

For comparison with the spectra of adsorbed ethanal, the vapour phase IR spectrum of ethanal in the sample cell, at various pressures, is shown in Figure 8.1. In Table 8.2 the normal modes and their selected frequencies of gaseous ethanal, taken from the literature,[6] are given. A comparison of this table and the spectrum in Figure 8.1, shows the figure to be very much more complicated. This is due to the presence of P, Q and R branches, and overtone and combination bands of the normal modes.[7]

In the IR spectra of ethanal adsorbed on Na-A, ZnNa-A and Ag-A zeolites a number of intense features are observed (Figures 8.2-8.7). These spectra show common features, indicating the formation of similar species within the zeolite framework.

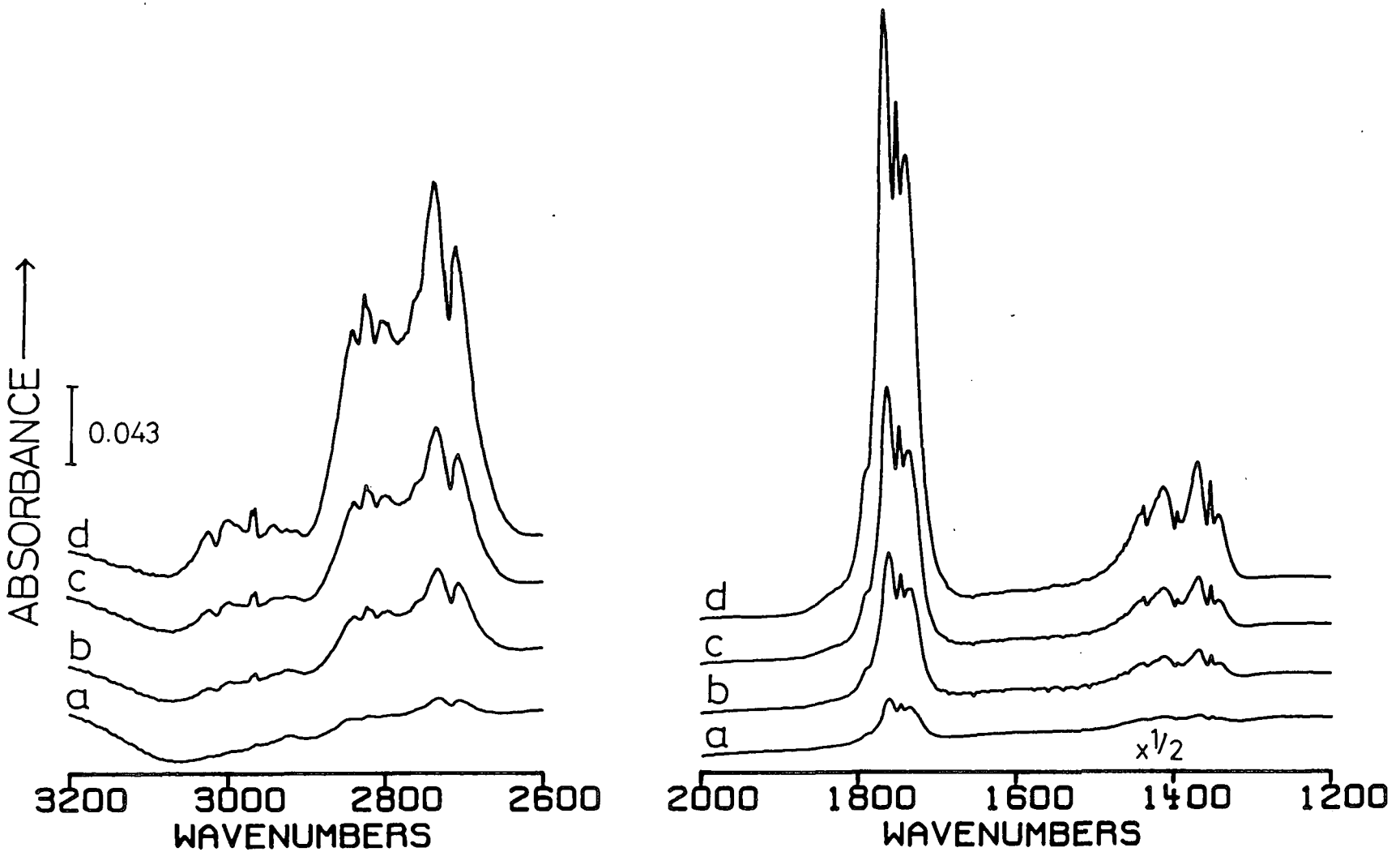

Figure 8.1 The IR spectra of vapour phase ethanal in the sample cell (path length 48mm)

(a) 1.8 torr, (b) 5.9 torr, (c) 10.7 torr, (d) 23.0 torr.

(y axis offset).

TABLE 8.2 Assignments and positions (cm^{-1}) of the normal modes of gaseous ethanal in the region above 1200 cm^{-1}, after ref. 6

Assignment[a]	Position (cm^{-1})
ν_1 (CH_3 d-stretch)	3005
ν_{11} (CH_3 d-stretch)	2967
ν_2 (CH_3 sym. stretch)	2917
ν_3 (C-H stretch)	2822
ν_4 (C=O stretch)	1743
ν_5 (CH_3 d-deform.)	1441
ν_{12} (CH_3 d-deform.	1421
ν_6 (C-H bend)	1400
ν_7 (CH_3 sym.-deform.)	1352

a. d = degenerate, deform = deformation of
sym = symmetric.

The 3800-2700 cm^{-1} region

On adsorption of ethanal, the spectra in the 3800-2700 cm^{-1} (Figures 8.2-8.4), show a number of new features which can be assigned in the perturbation of the structural hydroxyl groups and the C-H stretching vibrations of adsorbed ethanal. These data are summarized in Table 8.3.

In the background spectra of Na-A and ZnNa-A (Figures 8.2(i)a and 8.3(i)a) the features between 2800-300cm^{-1} are due to the instrument, as described in Section 3.4.2. In the case of Na-A the intense bands at 3460, 3424 and 3288 cm^{-1} are due to the ν(OH) vibrations of water, readsorbed on cooling the sample (Section 4.4.1). A very weak band at 3712 cm^{-1}

TABLE 8.3 The band positions (cm^{-1}) and their assignments for ethanal adsorbed on some type A zeolites

Na-A[a]	ZnNa-A	Ag-A[a]	Assignment[b]
3478	3384		Hydrogen bonding interactions at two sites
3276	3184		
2995	3005	2996	ν_1 CH_3 stretch
2967	2956	2944	ν_{11} CH_3 stretch
2910	2912	2917	ν_2
2873	2881	2848	ν_3 CH stretch
2840 (sh)	2861	2828	ν_3 CH stretch
2773	2763		overtone and combination bands of adsorbed ethanal
2741	2743	2736	overtone and combination bands of adsorbed ethanal
1713	1717		ν(C=O) of ethanal adsorbed at Na ions
		1718	ν(C=O) of hydrogen bonding ethanal
	1704		ν(C=O) of hydrogen bonding ethanal
	1682	1681	ν(C=O) of ethanal adsorbed on Ag or Zn ions
1410	1415	1410(br)	CH_3 antisymmetric deformation
1351	1352	1351	CH_3 symmetric deformation
		1311	C-H bend.

a. sh = shoulder, br = broad.

b. see Table 8.2.

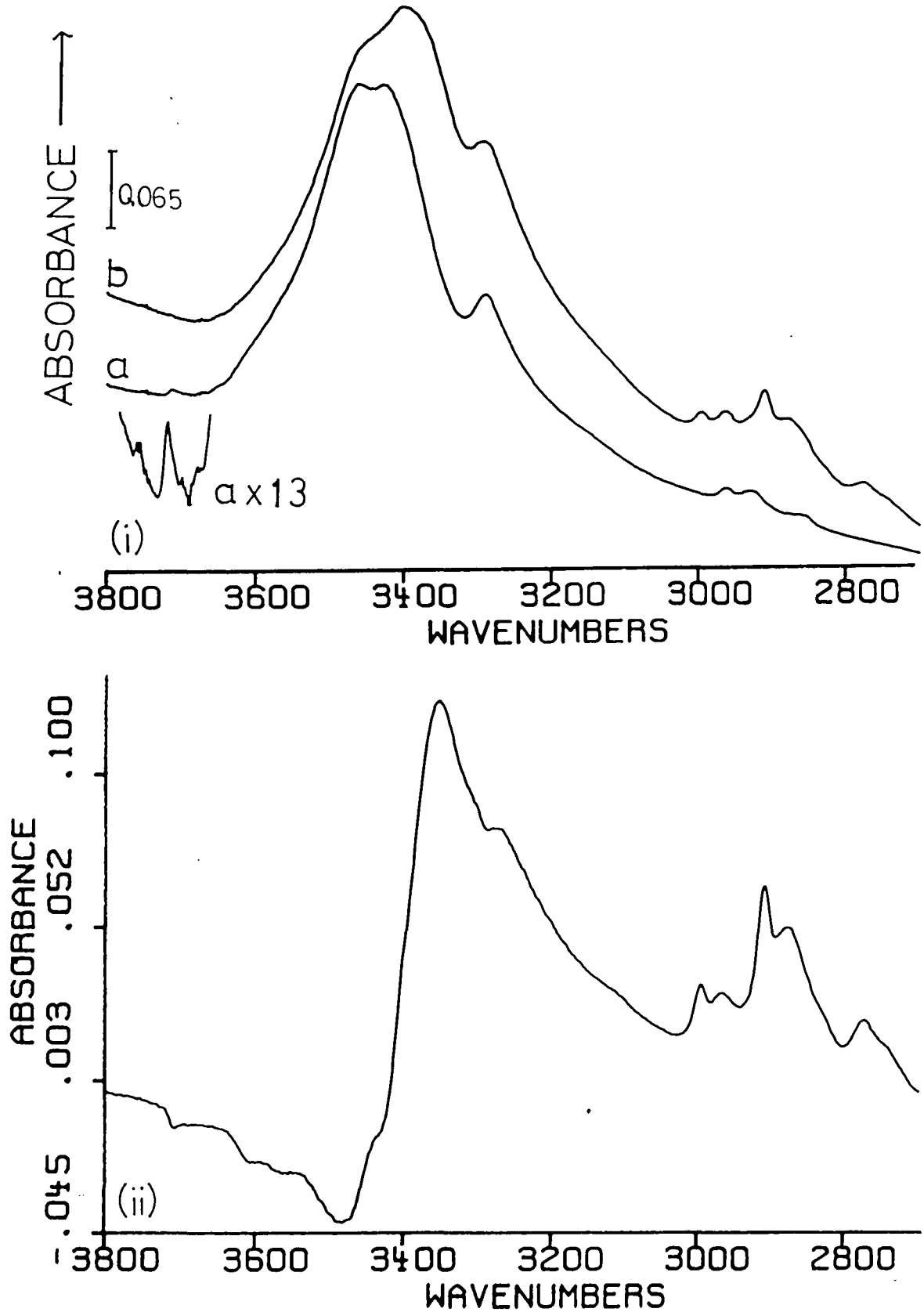

Figure 8.2 The C-H stretching region of ethanal adsorbed on Na-A

(i) (a) dehydrated zeolite background, (b) sample (a) on evacuation of ethanal vapour (14.4 torr);

(ii) subtraction spectrum of spectrum (b) - spectrum (a) in (i) above.

(y axis offset in (i)).

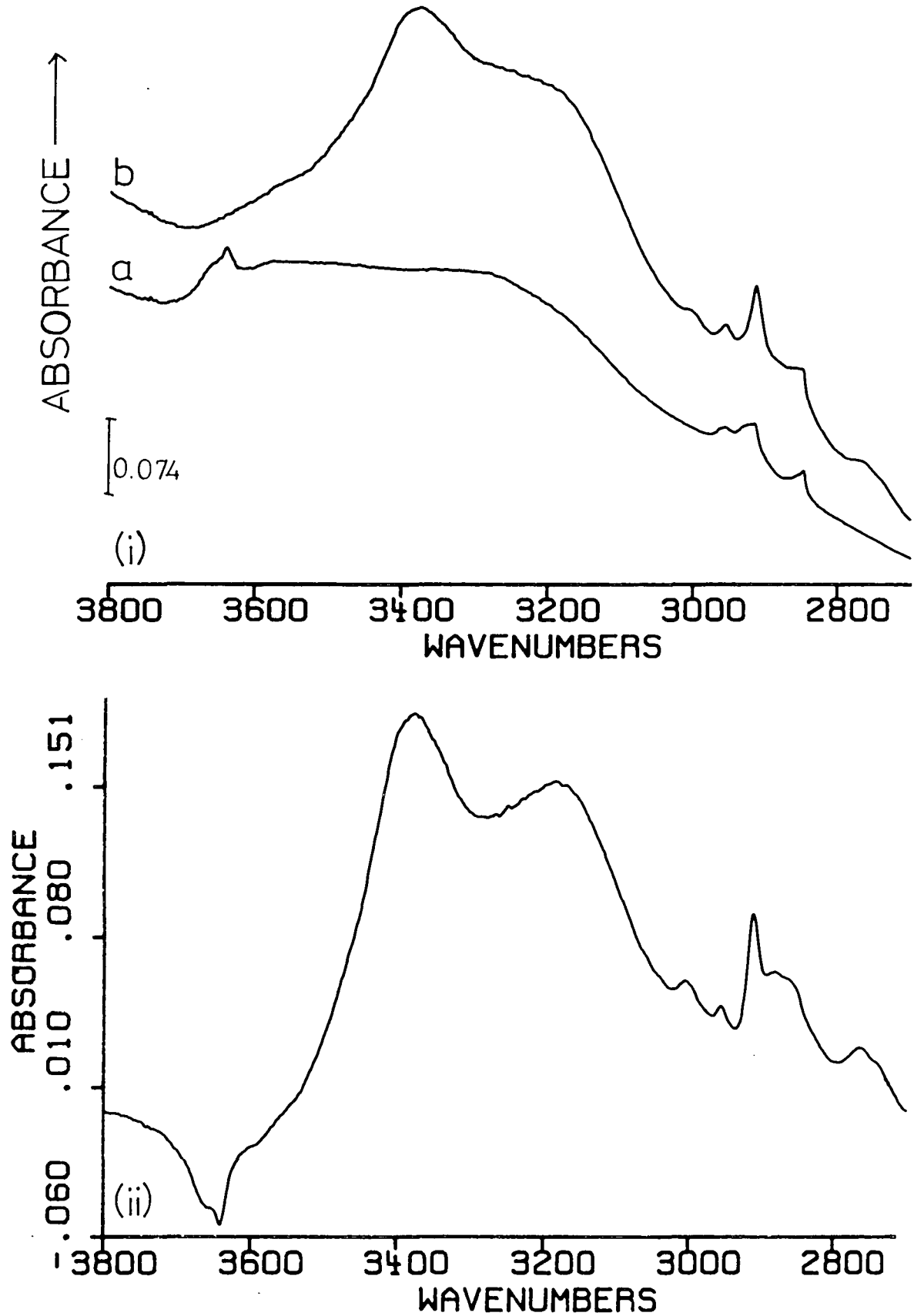

Figure 8.3 The C-H stretching region of ethanal adsorbed on ZnNa-A zeolite

(i) dehydrated zeolite background, (b) sample (a) on evacuation of ethanal vapour (4.7 torr).

(ii) subtraction spectrum of spectrum (b) - spectrum (a) in (i) above.

(y axis offset in (i) above.)

in the background spectrum can be assigned to framework hydroxyl groups, (Figure 8.2(i)(a)).

The background spectrum of ZnNa-A shows a sharp feature at 3650 cm^{-1} due to hydroxyl groups, probably associated with the cations (Section 2.4.2): while the broad feature observed at *ca.* 3350-3100 cm^{-1} can be assigned to hydrogen bonding interactions of water readsorbed on cooling. The ν(OH) bands observed in the background spectrum of this particular sample of ZnNa-A were stronger than those observed in previous samples (Chapters Four, Seven and Nine).

On adsorption of ethanal new broad bands were observed at *ca.* 3400 cm^{-1} for Na-A and 3384 and 3184 cm^{-1} for ZnNa-A in the region above 3100 cm^{-1} (Figure 8.2(i) and 8.3(i). The disappearance of the higher wavenumber ν(OH) vibrations, observed more clearly in subtraction spectra (Figures 8.2(ii) and 8.3(ii)), show these former bands to be due to hydrogen bonding interactions. These interactions will be between the surface hydroxyl groups and the carbonyl group of ethanal. The broadness, shift to lower wavenumber and significant increase in intensity, with respect to the free ν(OH) modes, is typical of hydrogen bonding interactions.[8,9] The presence of two hydrogen bonding bands in the case of ZnNa-A, clearly shows that of two hydrogen bonding species are formed within the zeolite framework. Previous studies of hydrogen bonding surface species,[8] would indicate that complexes of the type:

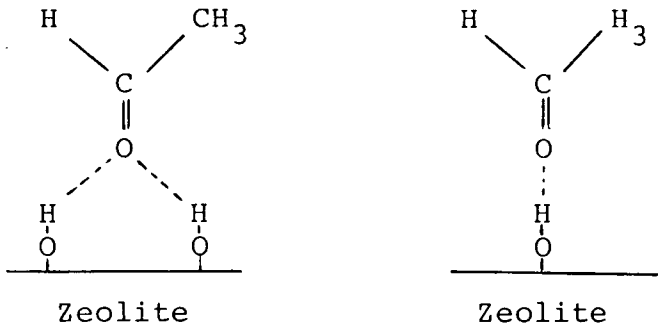

may be responsible for these two species. In Na-A zeolite the presence of one new ν(OH) band showed only one type of hydrogen bonding complex to be formed.

On evacuation of ethanal from Na-A and ZnNa-A zeolites the new ν(OH) bands are observed to slowly disappear.

The background spectrum of Ag-A zeolite is shown in Figure 8.4(a). The spectrum was obtained after the evacuation of the sample for 90 minutes to remove ethanal formed from the hydration of C_2H_2 (Chapter Seven). After this evacuation treatment, weak bands due to adsorbed ethanal were still observed in the 3000-2700 cm^{-1} region. A broad feature at *ca.* 3500-3100 cm^{-1} is possibly due to hydrogen bonding ν(OH) group interacting with the adsorbed ethanal. The sharp band at 3572 cm^{-1} can be assigned to structural OH groups, probably associated with the cations. On adsorption of ethanal the ν(OH) band at 3572 cm^{-1} immediately disappears (Figure 8.4(b)) as the OH groups interact with the adsorbate molecule. Evacuation, which removes the loosely coordinated ethanal, restores the intensity of the ν(OH) bands (Figure 8.4(e)).

In the region between 3500-3000 cm^{-1}, there appears, from the data shown in Figure 8.4 to be some perturbation of the hydrogen bonding ν(OH) bands on ethanal adsorption. If

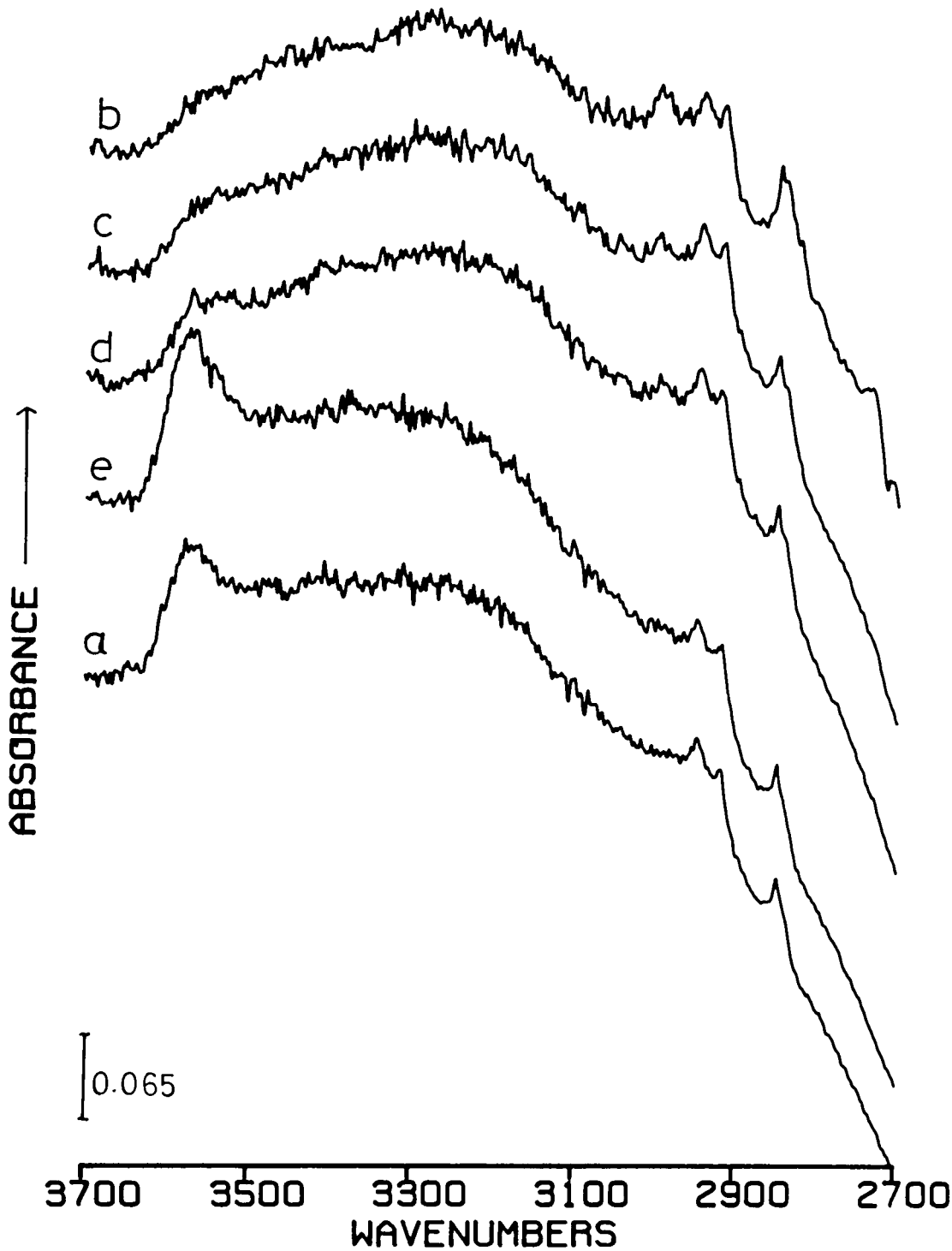

Figure 8.4 The C-H stretching region of ethanal adsorbed on Ag-A zeolite

(a) zeolite background after evacuation of C_2H_2/CH_3CHO for 90 minutes (Chapter 7); (b) sample (a) + 11.6 torr of ethanal; (c) evacuation of sample (b) to 0.9 torr; (d) on evacuation of sample (c); (e) evacuation of sample (c) for 120 minutes.

(y axis offset)

these spectra are overlaid, then, in actual fact, no new ν(OH) bands are observed, but the shape of the background level in this region does change. This causes the effects observed in Figure 8.4. From these observations it can probably be concluded that the change in background level is caused by an increase in the number of hydrogen bonding species. The absence of large changes for Ag-A, as observed for Na-A and ZnNa-A zeolites on ethanal adsorption, can be explained by the initial presence of these hydrogen bonding species: this being due to the incomplete removal of ethanal from the ethyne hydration experiment (see Section 8.2).

In the C-H stretching region between 2700-3100 cm^{-1} new bands due to adsorbed ethanal are observed for all three zeolites. These data are summarized and assigned in Table 8.3, by reference to the gas phase data.[6,7] The observation of two ν_3 vibrations for adsorbed ethanal indicates the formation of more than one adsorption complex in the framework. This is confirmed by the observation of multiple ν(C=O) bands.

The bands observed below 2800 cm^{-1} are assigned to overtone and combination bands of the adsorbed ethanal. Overtone and combination bands are clearly seen in the data for gaseous ethanal in Figure 8.1, and were assigned by the authors in reference[7].

On evacuation and heating the ν(C-H) bands are gradually reduced in intensity as the ethanal is desorbed. No new bands are observed.

The 1800-1250 cm^{-1} region

In this region bands due to the ν(C=O) stretching vibrations and the $\delta(CH_3)$ deformation modes are observed (Figures 8.5-8.7). The data for the three zeolites are summarized in Table 8.3. In spectra 8.5(b) and (c), 8.6(b), (c) and (d) and 8.7(b) and (c) bands observed at 1761, 1746 and 1733 cm^{-1} are due to the P, Q and R branches of gaseous ethanal. These bands are clearly observed in the spectra of gaseous ethanal shown in Figure 8.1. On evacuation of ethanal from the sample cell (Figures 8.5(d), 8.6(e) and 8.7(d)), these bands are immediately removed.

For all three zeolites two general observations are made from the spectra obtained on the adsorption of ethanal:

(i) A shift of between 23-63 cm^{-1} to lower wavenumbers is observed in the frequency of the C=O stretching vibration, from the gas phase value of 1743 cm^{-1} (Table 8.3).[6] These shifts are typical of those observed for ethanal adsorbed on a variety of surfaces, *e.g.* MgO, Li-X, H-Y, as discussed in Section 8.1.

(ii) The deformation modes observed below 1500 cm^{-1}, unlike the ν(C=O) vibrations, show very little change on increasing the pressure or on evacuation of the ethanal (Figures 8.5-8.7). This indicates that the interaction of the ethanal is *via* the carbonyl end, and that the CH_3 group is only slightly perturbed by adsorption. In agreement with this, the deformation modes are observed to have values very like those observed in the gas phase (Tables 8.2 and 8.3).

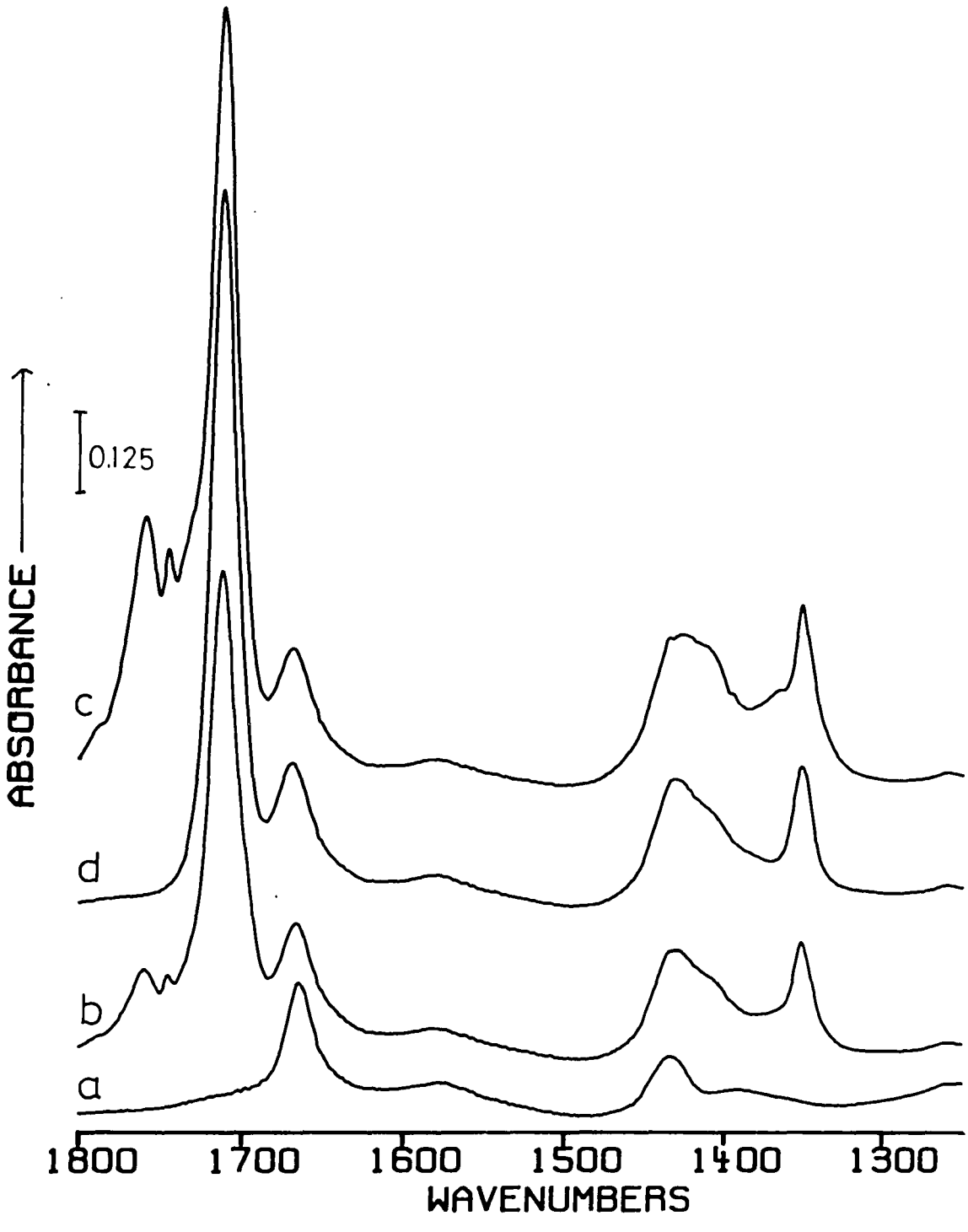

Figure 8.5 The 1800-1250 cm^{-1} region of ethanal adsorbed on Na-A zeolite

(a) dehydrated zeolite background, (b) zeolite + 4.7 torr of ethanal, (c) zeolite + 14.4 torr of ethanal, (d) on evacuation of ethanal from sample (c).

(y axis offset)

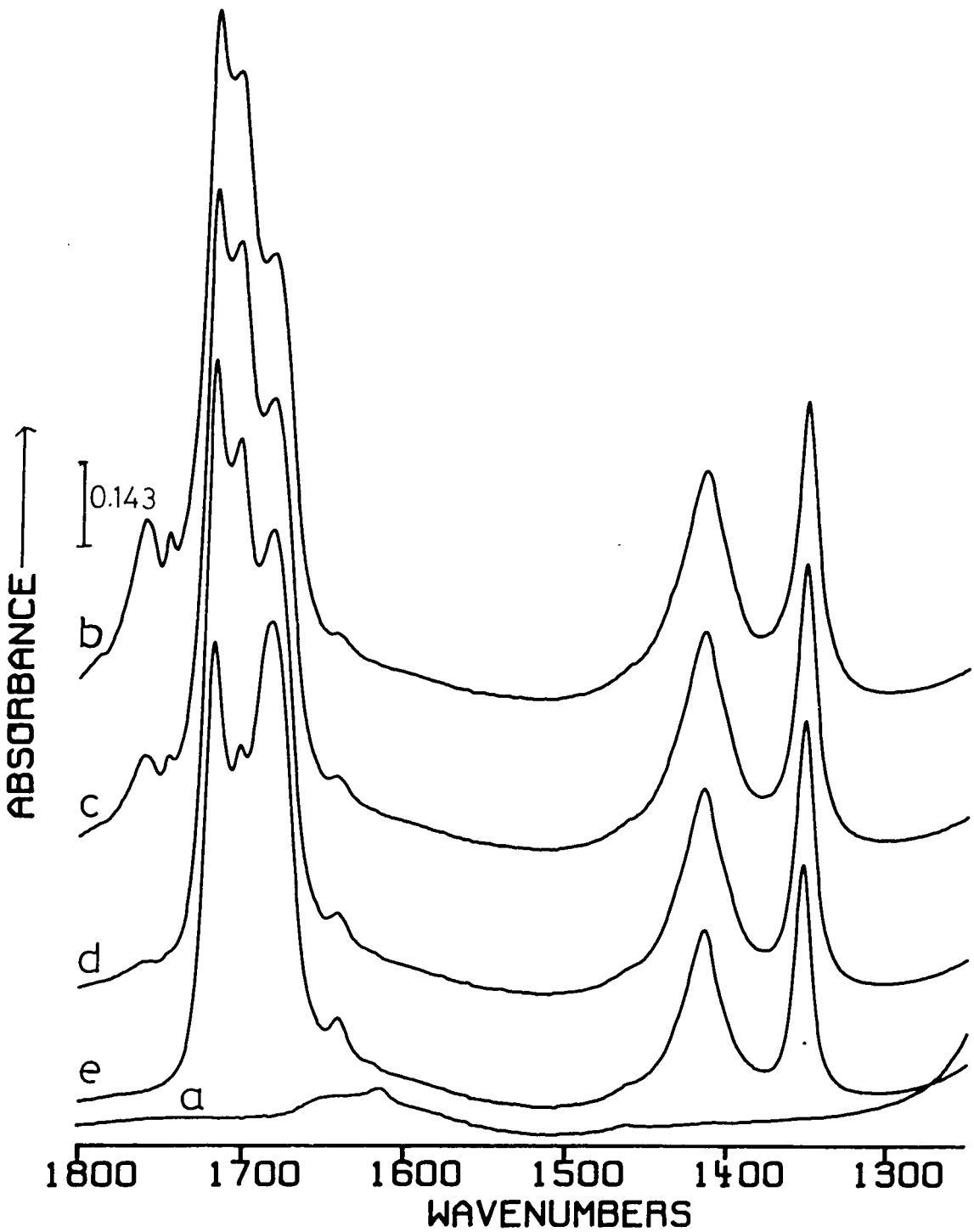

Figure 8.6 The 1800-1250 cm^{-1} region of ethanal adsorbed on ZnNa-A zeolite

(a) dehydrated zeolite background, (b) zeolite + 10.1 torr of ethanal, (c) evacuation of sample (b) to 4.8 torr, (d) evacuation of sample (c) to 0.8 torr, (e) on evacuation of ethanal from sample (d).

(y axis offset)

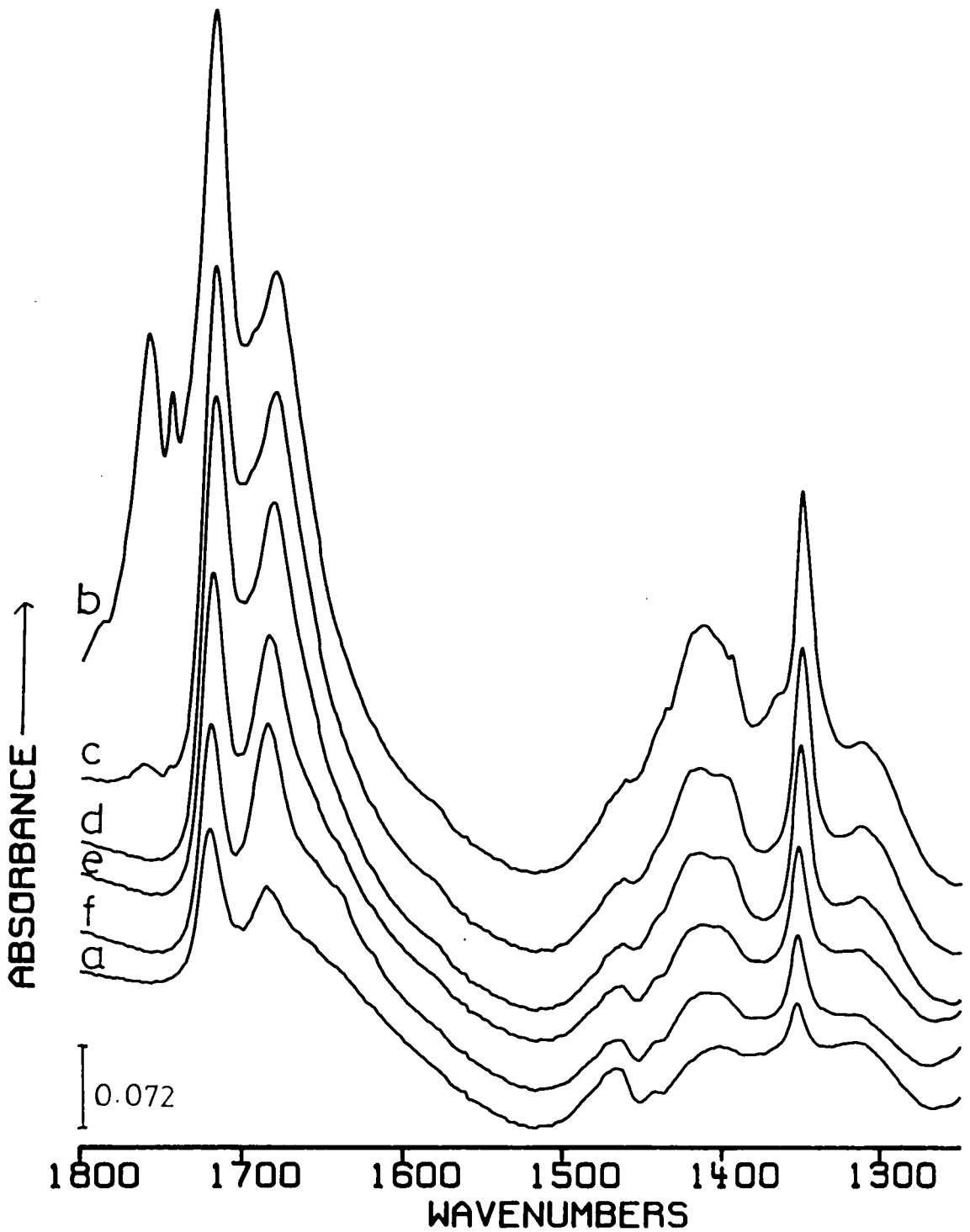

Figure 8.7 The 1800-1250 cm^{-1} region of ethanal adsorbed on Ag-A

(a) zeolite background after evacuation of C_2H_2/CH_3CHO for 90 minutes (Chapter 7); (b) zeolite + 11.6 torr of ethanal, (c) evacuation of sample (b) to 0.9 torr, (d) on evacuation of sample (c), (e) evacuation of sample (c) for 30 minutes, (f) evacuation of sample (c) for 120 minutes.

(y axis offset)

The spectra of ethanal adsorbed on Na-A are shown in Figure 8.5. After the removal of the gas phase by evacuation (Figure 8.4(d)), a very strong band which can be assigned to ν(C=O) is observed at 1713 cm^{-1}. Below 1500 cm^{-1} the bands which are assigned to the CH_3 deformation modes are observed at 1410 and 1351 cm^{-1}. The feature in the background spectrum at *ca.* 1670 cm^{-1} is due to the deformation mode of adsorbed water (Section 4.4.1), while the band at *ca.* 1435 cm^{-1} is attributable to carbonates or overtone and combination bands of the framework vibrations (Chapter Seven). The presence of one ν(C=O) vibration indicates the formation of a single type of adsorbed species. We assign this species to ethanal co-ordinating to the Na(I) ions, due to the cation dependent bands observed in similar positions on Li and Cs exchanged X zeolites[2] (Section 8.1). This assignment does not, however, explain the weak hydrogen bonding interaction observed above 3000 cm^{-1}, described previously. The only explanation for this is that the ν(C=O) of the hydrogen bonding species is of weak intensity and is present beneath the very strong ν(C=O) vibration of ethanal coordinating to the Na(I) cations.

The spectra of ethanal adsorbed on ZnNa-A (Figure 8.6) is much more complicated than that observed for ethanal adsorbed on Na-A (Figure 8.5). On adsorption of ethanal three new ν(C=O) vibrations are observed at 1717, 1704 and 1682 cm^{-1} in Figure 8.6(b). (The bands above 1730 cm^{-1} are due to gaseous ethanal). On reducing the overpressure of ethanal in the cell, the relative intensity of the three bands is observed to change. Clearly, Figures 8.6(b)→8.6(e) show that

the species characterized by the band at 1704 cm^{-1} is desorbed most readily. In view of this observation, this band is assigned to ethanal hydrogen bonding to the framework hydroxyl groups. The remaining two bands are assigned to ethanal coordinating to the cations. The similarity between the position of the ν(C=O) vibration at 1717 cm^{-1} and that observed for ethanal adsorbed on Na-A leads us to assign the 1717 cm^{-1} band to ethanal adsorbed on the Na(I) ions. The third band at 1682 cm^{-1} is then assigned to an ethanal complex formed with the Zn(II) ions. The $\delta(CH_3)$ modes of all three complexes are observed at 1415 and 1352 cm^{-1}. These bands show no variation on evacuation or changing the pressure of ethanal in contact with the sample.

Finally, on ZnNa-A a weak band is seen at *ca.* 1642 cm^{-1}. This band will be discussed and assigned in Section 8.3.2.

The Ag-A disc onto which ethanal was absorbed (Figure 8.7(a)) showed weak bands due to adsorbed ethanal formed from the hydration of ethyne in Chapter Seven. The desorption treatment used after ethyne adsorption (evacuation for 90 minutes) was not able to completely remove these bands. On adsorption of ethanal (11.6 torr), these weak features are very much increased in intensity, as the concentration of adsorbed ethanal is increased. Two ν(C=O) vibrations are observed at 1718 and 1681 cm^{-1}. As the higher wavenumber band was observed to be more readily removed by evacuation (Figure 8.7(d) and (e)), we assign this band to ethanal interacting with the framework hydroxyl groups. The 1681 cm^{-1} band is then assigned to the adsorption of ethanal on the Ag(I) cations. In contrast to

Figure 8.4, where very little change was observed in the 3800-2700 cm^{-1} on desorption of ethanal, major changes are observed in the ν(C=O) region. This shows the ν(C=O) band to be very much involved in coordination and a sensitive indicator to the formation of ethanal complexes at different sites.

In addition to the observation on Ag-A of two CH_3 deformation modes, at 1410 and 1351 cm^{-1}, a third band is observed at 1311 cm^{-1}. This band is assigned to the C-H bending mode which is observed at 1400 cm^{-1} in the gas phase. On Na-A and ZnNa-A no C-H bending mode was observed. The large shift seen on Ag-A and the non-observation on the other two zeolites studied, show this mode to be strongly perturbed on adsorption. As the interaction of ethanal to the zeolite surface is occurring *via* the carbonyl of the $-C\overset{H}{\underset{O}{=}}$ group, a large perturbation of the C-H bending modes is to be expected.

8.3.2 Desorption of ethanal

No data on the desorption of ethanal from Ag-A was obtained in the present study. For Na-A and ZnNa-A the spectra obtained are shown in Figures 8.8 and 8.9 respectively. These figures show that a number of new bands appear in the 1700-1550 region on the desorption of ethanal. We will assign these modes to new species formed from the reaction of ethanal on the zeolite surface at elevated temperatures.

For Na-A the desorption data is shown in Figure 8.8. As the sample is evacuated for 60 minutes the intense ν(C=O) band at 1713 cm^{-1} is reduced in intensity as ethanal

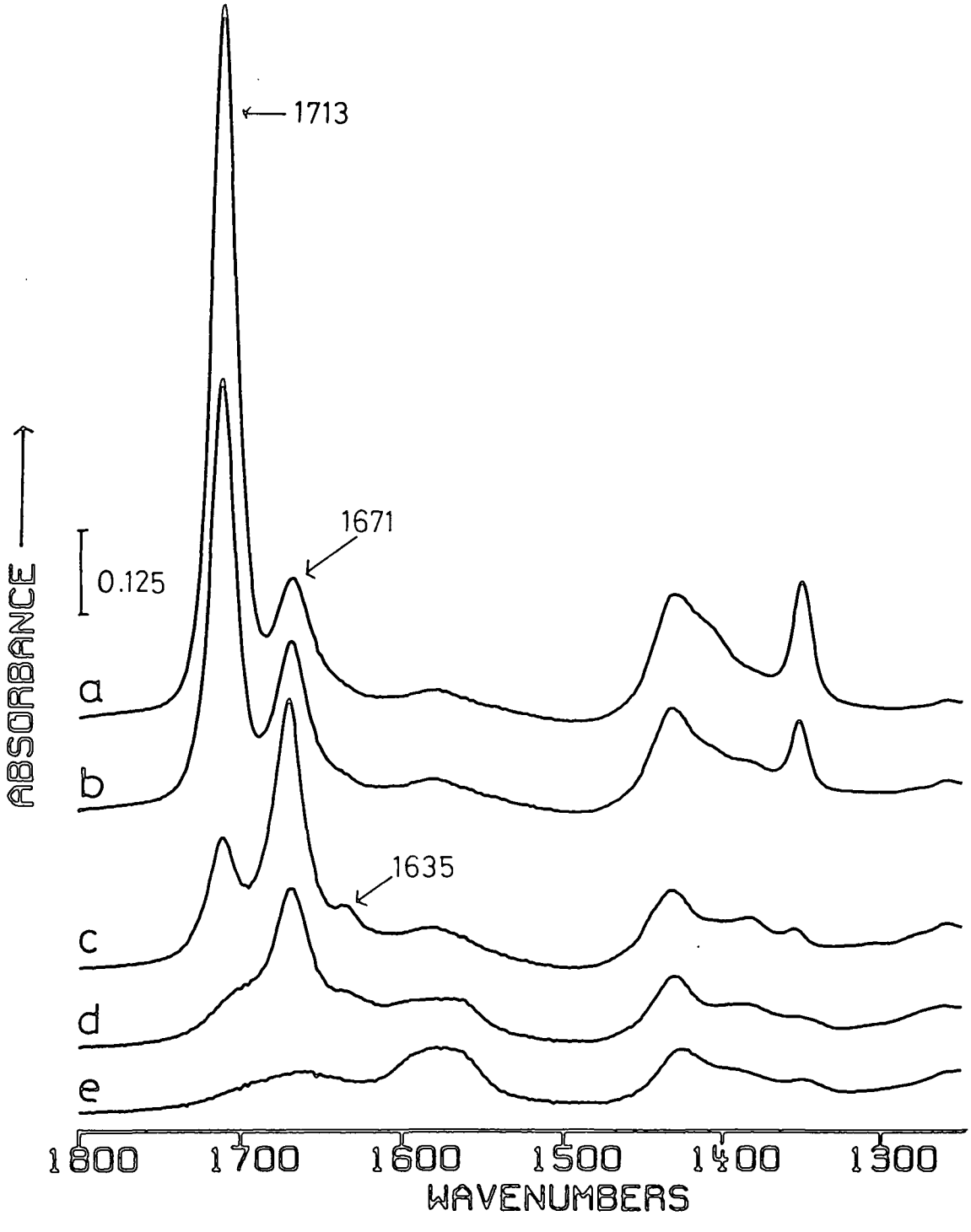

Figure 8.8 The desorption of ethanal from Na-A zeolite

(a) spectrum on evacuation of ethanal (see Figure 8.4), (b) evacuation of sample for 60 minutes, evacuation and heating of sample (b) at: (c) 423K, (d) 493K, and (e) 693K.

(y axis offset)

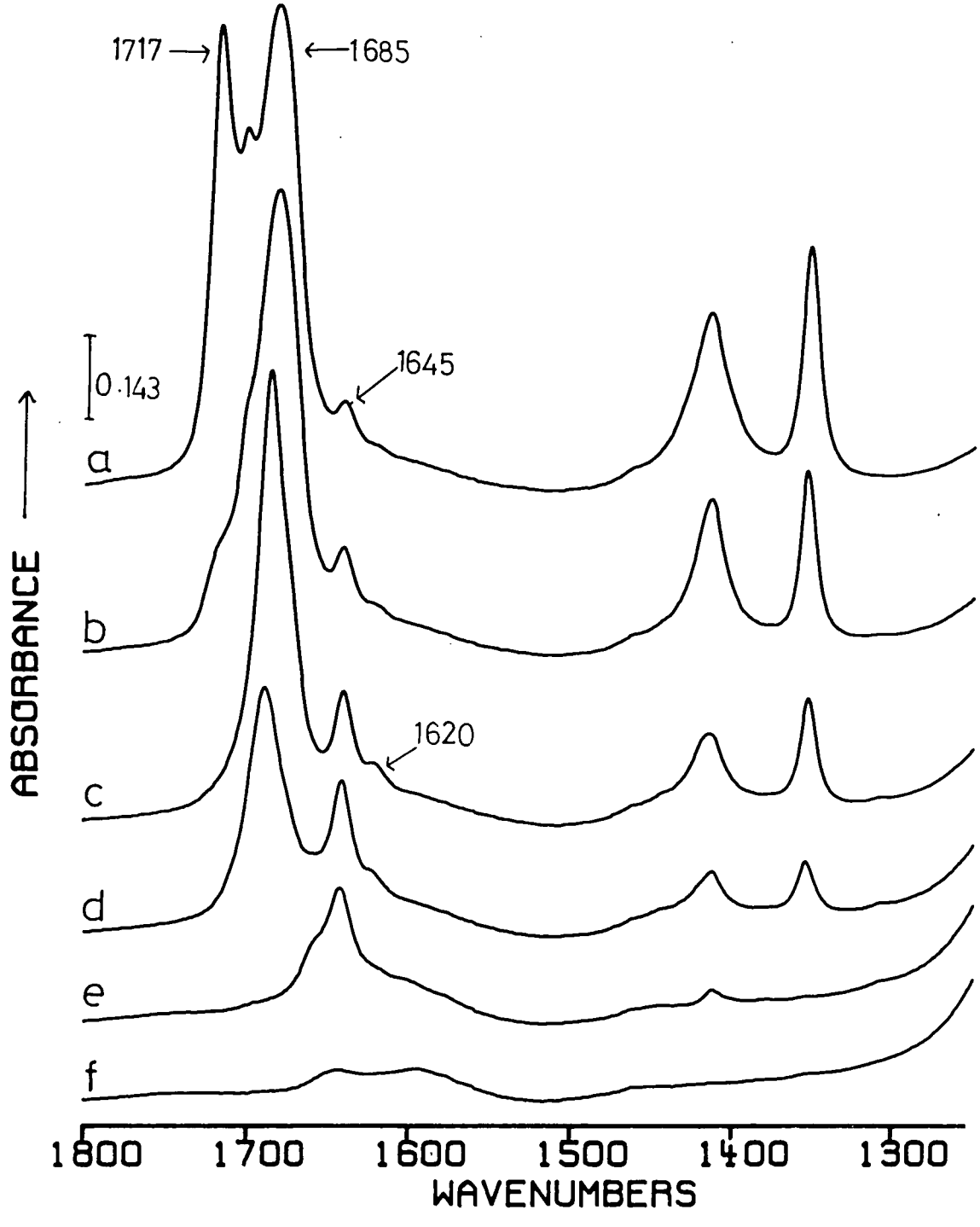

Figure 8.9 The desorption of ethanal from ZnNa-A zeolite

(a) spectrum on evaucation of ethanal (see Figure 8.5), (b) evacuation of sample for 45 minutes; evacuation and heating of sample (b) at: (c) 423K, (d) 488K, (e) 593K and (f) 733K.

(y axis offset)

is removed from the framework (Figures 8.8(a) and (b)). When the sample is subsequently heated to 423K while being evacuated, two new bands are observed at 1671 and 1635 cm^{-1} (Figure 8.8(c)).

For other systems described in this thesis, bands which appeared on desorption were due to the removal of an intense feature which revealed a weak component. In the present case the new bands at 1671 and 1635 cm^{-1} are clearly due to new species formed by the reaction of adsorbed ethanal and probably water or hydroxyl groups in the zeolite cavities.

Above 423K the bands at 1671 and 1635 cm^{-1} are considerably reduced in intensity, and a third new, but broad, band is observed at *ca.* 1575 cm^{-1}. This latter band is still observed when the sample is heated to 693K.

During the desorption the CH_3 deformation modes in the 1420-1300 cm^{-1} region are reduced in intensity and no new bands are observed which can be correlated with the other new features. After heating to 693K, some residual intensity was observed at between 1420 and 1350 cm^{-1}, which must be associated with the 1575 cm^{-1} band.

Data obtained on desorbing ethanal from ZnNa-A by evacuation and heating is shown in Figure 8.9. At room temperature, on the immediate evacuation of ethanal from the cell (Figure 8.9(a)), three strong ν(C=O) bands are observed at 1717, 1704 and 1682 cm^{-1}, which were assigned to three different sites in Table 8.3. A foruth weak band is observed at 1645 cm^{-1}. On evacuating the sample these bands are observed to change.

Firstly, by evacuating and heating to 423K the two higher frequency ν(C=O) bands at 1717 and 1704 cm^{-1} are completely removed (Figure 8.9(c)). They are both still present as weak features after evacuation for 45 minutes (Figure 8.9(b)). The band at 1704 cm^{-1} was assigned to ethanal hydrogen bonding through the carbonyl group to structural hydroxyl groups. This particular species was observed to be relatively weakly adsorbed by the intensity decrease of the 1704 cm^{-1} band on reducing the pressure in the cell (Section 8.3.1). Therefore the disappearance of the band by spectrum 8.9(d) is not surprising. The second band to disappear rapidly was observed at 1717 cm^{-1} and assigned to an ethanal complex formed with the Na(I) cations. The complex in ZnNa-A is seen to be more weakly adsorbed than the same species observed in Na-A zeolite. A similar difference in desorption behaviour was observed for the Na(I)-propene complex in the Na-A and ZnNa-A (Chapter Four).

As the sample was heated (Figures 8.9(c) - 8.9(d)), the 1685 cm^{-1} band decreased in intensity as the Zn(II)-ethanal complex was desorbed. Simultaneously bands due to new species were observed at 1645 and 1620 cm^{-1}. Heating to 593K completely removed the 1685 cm^{-1} species, while the 1645 and 1620 cm^{-1} bands were still observed. These latter two bands are, as in the Na-A case, due to new species formed by the reaction of ethanal with the zeolite surface. It would appear that these species arise from the Zn(II)-ethanal complex, as only this complex is present in the framework at 423K.

In the CH_3 deformation region very little change is seen in the band at 1415 and 1352 cm^{-1} on evacuation, even though major changes occur in the ν(C=O) region (Figures 8.9(a) and (b)). Obviously, from this observation, the major contribution to the former bands must be from the Zn(I)-ethanal complex. Heating causes the disappearance of both bands. But at 593K a weak band is observed at 1415 cm^{-1}, which we must associate with the band at 1642 cm^{-1}.

Interpretation of the changes which occur on desorption

The changes described above on the desorption of ethanal on evacuation and heating from Na-A and ZnNa-A are clearly associated with the reaction of adsorbed ethanal at elevated temperatures. It is strongly expected that heating a sample in the presence of gaseous ethanal would increase greatly the intensity of the bands due to the new species.

A comparison of the new bands with those observed for ethanal adsorbed on silica,[1] MgO,[3] alumina[4] and decationized zeolite Y[2] would lead us to assign these new bands, except the 1642 cm^{-1} band on ZnNa-A and the 1671 cm^{-1} on Na-A, to carboxylate species (Section 8.1). These will be formed by the reaction of the adsorbed ethanal with water or hydroxyl groups in the zeolite framework.

In decationized zeolite Y[2] bands observed at 1645, 1600 and 1460 cm^{-1} were found to increase intensity on evacuation and heating. These bands were assigned to either carboxylate species or to new aprotic centers. The bands observed at 1671 cm^{-1} on Na-A and 1642 cm^{-1} ZnNa-A we prefer to assign to

ethanal adsorbed on new, probably aprotic centers formed by the action of evacuation and heat on the samples.

8.4 Conclusions

The IR spectra of ethanal adsorbed on some type A zeolites (Na(I), Zn(II) and Ag(I)) have been reported for the first time.

It has been observed that on adsorption of ethanal framework hydroxyl groups are perturbed. Hydrogen bonding complexes between the carbonyl group of ethanal and the framework hydroxyl groups have been envisaged.

In addition to hydrogen bonding complexes, the coordination of ethanal to the charge compensating cations has been observed characterized by their ν(C=O) frequencies, *viz.* Na(I) = 1713 cm^{-1}, Zn(II) = 1682 cm^{-1} and Ag(II) = 1681 cm^{-1}. In ZnNa-A interaction of ethanal with both the Na(I) and Zn(II) cations was observed.

When ethanal was desorbed from ZnNa-A and Na-A, the action of heat has been observed to cause the reaction of the adsorbed ethanal with the framework. Carboxylate species were identified.

The behaviour of ethanal adsorbed on type A zeolites has been observed to be very similar to that reported for X and Y type zeolites.[2] In both cases the action of heat was shown to cause the formation of new species.

REFERENCES (Chap.8)

1. Young, R.P. and Sheppard, N., J.Catal,1,223 (1967).

2. Geodakyan, K.T., Kiselev, A.V. and Lygin, V.I., Russ.J.Phys.Chem., 41, 476 (1967).

3. Low, M.J.P., Jacobs, H. and Takezawa, N., Water air soil pollut. 2, 61 (1973).

4. Evans, H.E. and Weinberg, W.H., J.Chem.Phys., 71, 4789 (1979).

5. Nanni, P. and Gesmundo, F., Ann.Chim.(Rome), 58, 429 (1968).

6. Shimanouchi, T., "Tables of Molecular Vibrational Frequencies, Consolidated Volume I", NSRDS-NBS 39 (1972).

7. Hollenstein, H. and Günthard, Hs.H., Spectrochim.Acta.A., 27, 2027 (1971).

8. Schuster, P., Zundel, G. and Sandorfy, C., "The hydrogen Bond. Recent developments in theory and experiments", North Holland Publishing Company, Amsterdam, 1976.

9. Kiselev, A.V. and Lygin, V.I., "Infrared Spectra of Surface Compounds", Wiley, New York, 1972.

CHAPTER NINE

AN IR AND INS STUDY OF ETHENE ADSORBED ON ZnNa-A ZEOLITE

9.1 Introduction

The work presented in this chapter has been published in part, in the proceedings of the First International Conference on the Structure of Surfaces.[1]

The only full investigation by IR spectroscopy of ethene (C_2H_4) adsorbed ion-exchanged type A zeolites, has been a study by Howard *et al*[2] of the fully silver exchanged form (Ag_{12}-A) under various dehydration treatments.[2] In common with an earlier IR investigation of C_2H_4 adsorbed on ion-exchanaged type 13-X zeolites,[3] the formally infrared inactive (in the isolated molecule) vibrations ν_2 (C=C stretch) and ν_3 (CH_2 deformation) were observed showing that olefin interaction with the surface had taken place [4] and that dissociation had not occurred. Under all pretreatment conditions, the authors observed the adsorption of C_2H_4 at two sites within the Ag_{12}-A framework. However, whilst zeolite samples pretreated at a higher dehydration temperature held C_2H_4 equally strongly on both sites, those samples pretreated at a lower temperature held C_2H_4 less strongly on one site than the other. This work was in agreement with an inelastic neutron scattering study by the same authors,[5] which located two distinct adsorption sites but there was discrepancy with the X-ray study of Kim and Seff[6] in which only one adsorption site was located.

In the earlier IR study by Carter *et al*[3] of C_2H_4 adsorbed on Li^+, Na^+, K^+, Ag^+, Ba^+, Ca^{2+} and Cd^{2+} exchanged (greater than 90%) type 13-X zeolites, spectra were reported

in the region 3300-1300 cm^{-1}. Bonding was shown to be weak by the complete removal of the adsorbed gas upon evacuation at room temperature, from all but the silver and cadmium exchanged forms. In the latter zeolites evacuation at temperatures in excess of 473K were necessary to displace the C_2H_4.

A scheme[3,7] was proposed for cation-C_2H_4 interaction in which a σ-bond is formed by overlap of the olefin π orbitals with either a 5s or 5sp orbital of the cation. Additionally, in the case of silver, back donation was suggested to occur from filled silver 4d orbitals into the vacant π^* orbitals of C_2H_4 according to the Chatt-Dewar-Duncanson Model.[8,9]

Of direct relevance to the present study Tomaselli *et al*[10] have recently reported the FT-IR spectrum of C_2H_4 adsorbed on Na-A zeolite. In the presence of 100 torr of C_2H_4 four bands were observed in the 2200-1200 cm^{-1} region at 1946 ($\nu_7 + \nu_8$), 1664 (ν_2), 1450 (ν_{12} CH_2 deformation) and 1339 (ν_3) cm^{-1}. An <u>increase</u> in ν_2, relative to the gas phase value of 1623 cm^{-1} had not previously been reported for C_2H_4 either adsorbed or in organometallic complexes. The spectrum was interpreted in terms of a non-rotating adsorbed species formed between one C_2H_4 molecule and 2 Na(I) ions in the supercage. The two Na(I) ions (in sites S_1 and S_2) were proposed to lie in the plane of the ethylene molecule, such that they caused a compression of the H-C-H angle, justifying the increase in ν_2. We consider that without further detailed quantitative analysis this interpretation must be regarded as tentative.

No details were given either of the region above 2200 cm^{-1} so that the effect of the proposed change of geometry on the

ν(C-H) modes can be observed, or of the desorption behaviour of the adsorbed species.

The motivation for the present study came mainly from paucity of IR spectroscopic data on C_2H_4 adsorbed on type A zeolites. We have, in addition, studied the C_2H_4 + ZnNa-A system by inelastic neutron scattering (INS) spectroscopy, as this technique has been shown to give valuable information on zeolite-adsorbate interactions.[5,11]

As INS studies were not the main objective of this thesis, only a brief outline of INS spectroscopy with respect to adsorbate-adsorbent systems will be given.

9.2 Inelastic Neutron Scattering Spectroscopy of Adsorbed species.

In vibrational studies of species adsorbed within zeolite frameworks most attention has centred on the changes in the internal mode frequencies of the adsorbate with respect to the free molecule.[2,3,10] On adsorption the three rotations and translational degress of freedom of the free molecule usually become hindered (Figure 9.1). These modes directly reflect the surface-adsorbate bonding and their frequencies can therefore be used to calculate force constants and barriers to rotation. While this type of analysis provides a sensitive test for any model of adsorbate-adsorbent interaction these modes have generally not been studied because of the difficulties in observing them using optical spectroscopy, *viz:*

(A) the modes occur below 1200 cm^{-1} and in this region zeolite frameworks are usually extremely absorbing in the infrared;

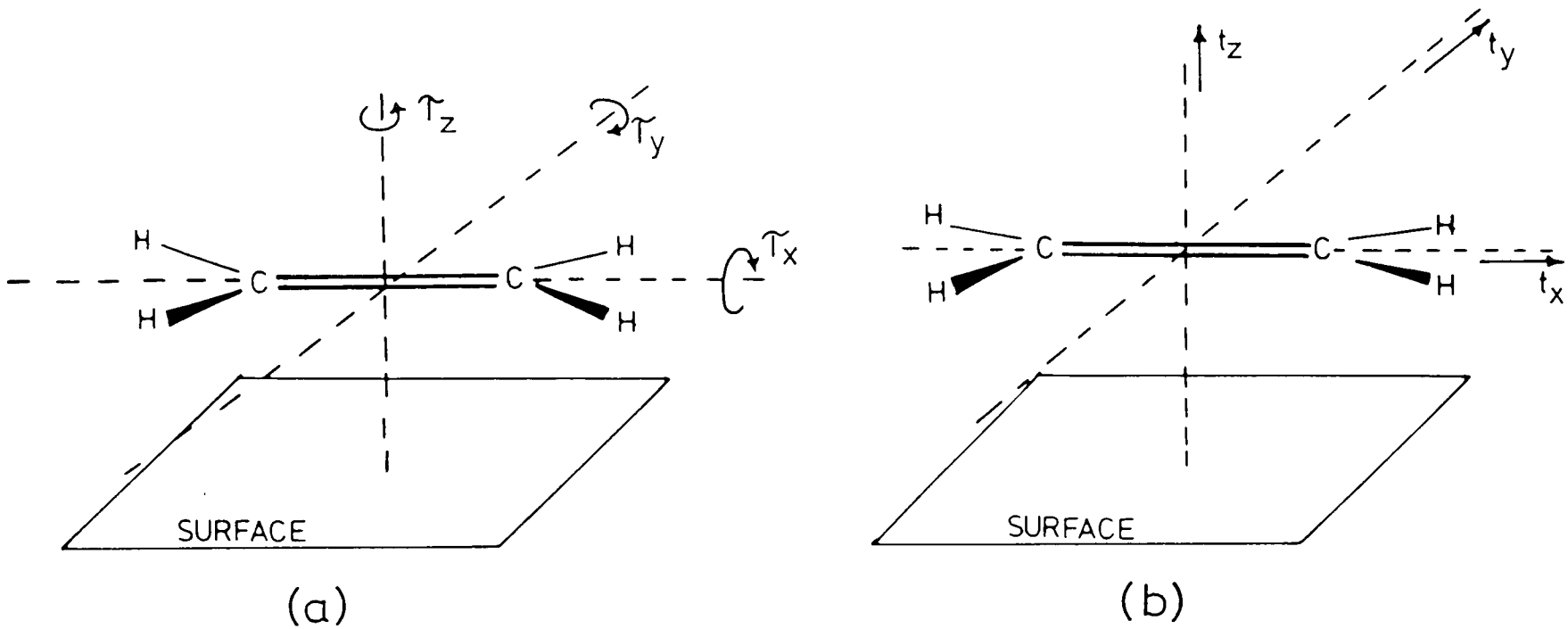

Figure 9.1 Ethene - surface modes

(a) Hindered rotations: T_2 torsion one; τ_y torsion "y" or antisymmetric stretch; τ_x torsion "x" or barrelling mode.

(b) Hindered translations: t_3 symmetric stretch; t_y wagging mode; t_x rocking mode.

(B) many zeolites fluoresce making Raman experiments difficult or impossible;

(C) it is known from work on organometallic complexes that at least some of these modes are very weak in optical spectra.

None of these difficulties applies to INS spectroscopy for which there are also no electromagnetic selection rules.[12] In an INS experiment the scattering mechanism involves direct interaction between the incident neutron and the scattering nucleus. Each nucleus has a characteristic incoherent cross section (σ). The value for the hydrogen atom (80×10^{-24} cm^2) is some 20 times larger than the value for any other element. The intensities of INS bands are dependent upon a number of factors,[12] two of which are the σ value and the mean square amplitude of vibration of the atoms in the normal mode. Since the mean square amplitude of vibration is greatest for atoms of the lightest mass and the value of σ of the hydrogen atom is large, those modes which involve hydrogen will dominate the INS spectrum. Thus in zeolite-adsorbate studies in which the σ value of the atoms of the dehydrated zeolite are small, compared with the hydrogen atoms of the adsorbate the INS spectrum will be dominated by the vibration of the adsorbate.

In INS spectroscopy deuteration of an adsorbate molecule, does not only result in the shifts of bands due to the mass effect. The σ value for D (2×10^{-24} cm^2) is 40 times less than that of H, therefore the intensity of vibrations is also severely affected. By the selective deuteration of a molecule, the assignment modes can be made easily.

The aim of the INS studies of the ZnNa-A + C_2H_4 system was two-fold, *viz:*

(A) to investigate the low wavenumber region; and

(B) to use a prototype spectrometer to investigate the high wavenumber (>2000 cm^{-1}) region with the aim of locating the C-H stretching vibrations of the adsorbated, which are not observed in the IR spectrum.

9.3 Experimental

The samples of ZnNa-A were prepared and analysed as described in Chapter Three. The IR spectra of adsorbed C_2H_4 were obtained by the method outlined in Chapter Three using the PE580B Spectrophotometer. Two samples of ZnNa-A were used, $Zn_{4.3}Na_{3.4}$-A and $Zn_{3.2}Na_{5.6}$-A. As the spectra obtained were identical for both samples, results will only be presented for the higher ion-exchange form. C_2H_4 gas (British Industrial Gases) was purified by the freeze-pump-thaw technique before use.

Neutron scattering measurements were made using the beryllium filter spectrometer at AERE Harwell (100-800 cm^{-1})[12] and the filter difference spectrometer (300-4000 cm^{-1}) at Los Alamos National Laboratory.[13] For the Harwell data the transition frequencies have been calculated from the peak maxima using standard corrections factors.[14] The Los Alamos data was analyzed as previously described.[13] For the INS experiments the samples (approx. 50g) were pretreated as for the IR measurements (713k for 15.5 hr. at 10^{-5} - 10^{16} torr) and the samples held in thin-walled aluminium cells. The spectrum of the degassed zeolite was obtained to serve as a background, C_2H_4 was then adsorbed and the spectrum re-run. At Harwell,

coverages of 0.95 and 1.75 C_2H_4 molecules per supercage on $Zn_{3.2}Na_{5.6}$-A and of 1.75 C_2D_4 molecules per supercage on $Zn_{3.8}Na_{4.5}$-A were studied. The Los Alamos experiment on $Zn_{3.8}Na_{4.5}$-Ainvolved an adsorption capacity of 1.03 C_2H_4 molecules per supercage. Adsorption was carried out at ambient temperature, where all the C_2H_4 (C_2D_4) was observed to be chemisorbed (no residual overpressure). The Harwell measurements were made at 80K, while a temperature of 12K was used at Los Alamos. The effect of the lower temperature employed at Los Alamos will, at most, be band narrowing in the spectrum.

Though samples with different degrees of ion-exchange were used for the INS and IR measurements the effect on the spectra is negligible, as IR measurements at both ends of the ion-exchange range gave identical results. All samples, regardless of ion-exchange will hereafter be referred to as ZnNa-A.

9.4 Results and Discussion

9.4.1 Infrared data in the region 1700-1200 cm^{-1}

The IR spectrum of dehydrated ZnNa-A and of C_2H_4 adsorbed on it (overpressure of 5 torr) are shown in Figure 9.2, (a) and (b). Bands due to internal modes of the adsorbed species are clearly seen at 1326, 1451 and 1602 cm^{-1}. These transitions are readily assigned by comparison with the optical data[15] for gaseous C_2H_4 (Table 9.1). The change in activity of ν_2 and ν_3 on adsorption reflects a symmetry lowering from D_{2h} of gaseous C_2H_4. On evacuation for five minutes the

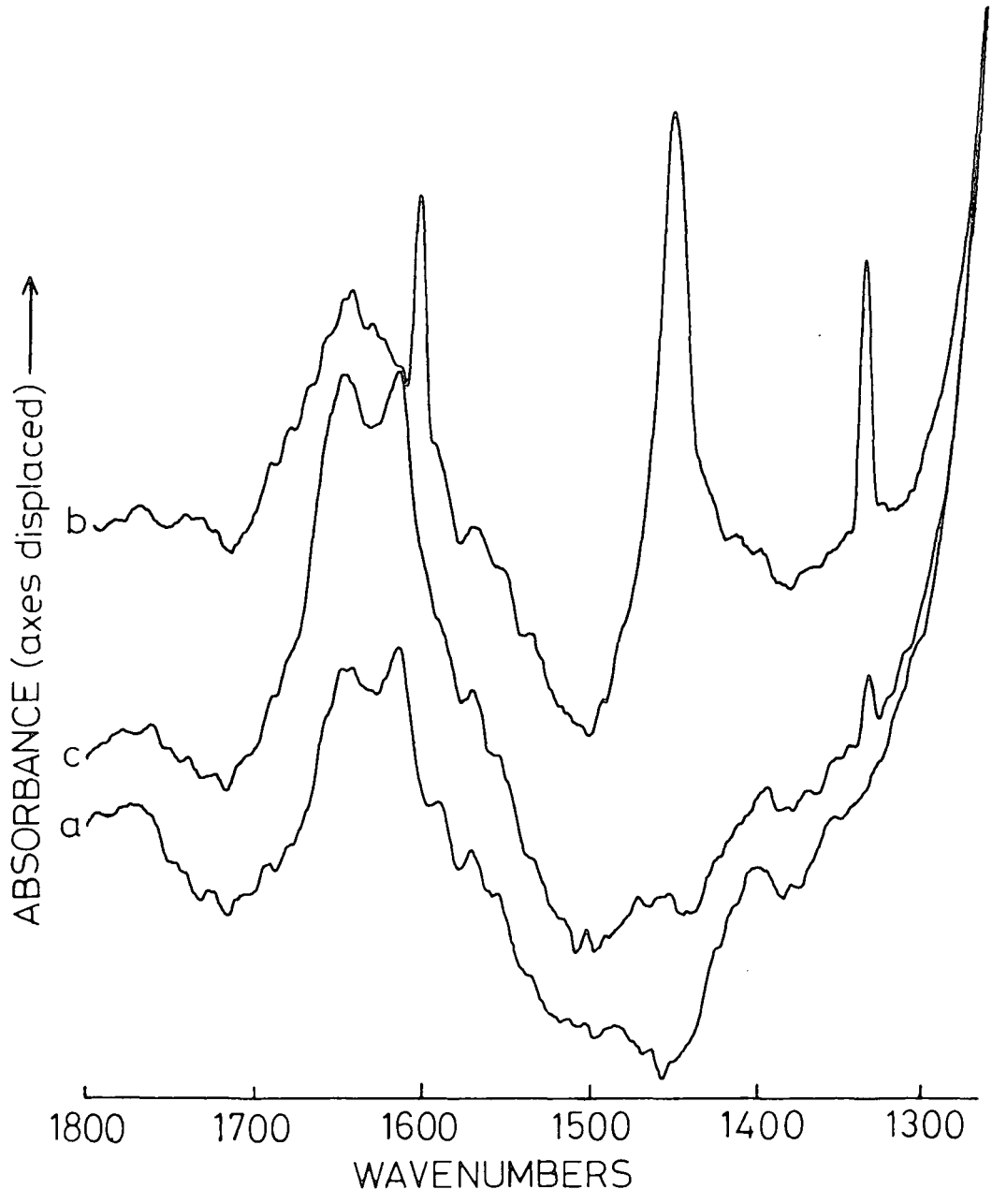

Figure 9.2 Ethene adsorbed on dehydrated ZnNa-A

(a) Background (degassed zeolite)

(b) Sample (a) + 5 torr of C_2H_4

(c) Sample (b) evacuation for 5 minutes.

TABLE 9.1 IR bands (cm^{-1}) and their assignments for C_2H_4 adsorbed on ZnNa-A zeolite

Assignment	Activity (gas phase)	Gas phase[15]	Adsorbed
ν_2(C=C stretch)	Raman	1623	1602
ν_{12}(CH_2 deformation)	IR	1443	1451
ν_3(CH_2 deformation)	Raman	1342	1326

---

intensities of the bands fall by at least a factor of 10 (Figure 9.2(c)). These observations are indicative of relatively weak non-dissociative adsorption at a single site. This is in contrast to C_2H_4 adsorbed on Ag_{12}-A,[2] where two distinct adsorption sites were observed. The adsorption of propene has been observed to occur in ZnNa-A on both the Zn(II) and Na(I) ions (Chapter Four). In the present study the observations from the IR spectrum of only one site and our experience that preference will be the formation of transitional metal complexes, we propose that the C_2H_4 is adsorbed on the Zn(II) ions located at site S_2^* in the α-cage, as C_2H_4 is too large to enter the β-cages. Though a stable Na(I)-C_2H_4 complex has been proposed,[10] it must be remembered that after partial ion-exchange of Na-A, it is very unlikely that two Na(I) will be located close enough to form a complex of the proposed structure. The narrowing of the IR bands which takes place on adsorption indicates that the adsorbed molecule is not freely rotating, in agreement with similar complexes in other A[2,10] and in some 13-X type[3] zeolites.

In view of the intense bands observed in the 1700-1200 cm^{-1} region, it is remarkable that we do not observe any bands due

to the C-H stretching modes of adsorbed C_2H_4 (expected at *ca.* 3000 cm^{-1}). A similar observation has been reported by Carter *et al*[3] for Cd-X zeolite, and also observed for Cd exchange A zeolite by us,[16] though these modes have readily been observed in a wide range of other ion exchange zeolites.[2,3]

The absence of the ν(C-H) modes must be a consequence of subtle electronic changes which occur on adsorption of C_2H_4. These are possibly due to the nature of the cations, as zinc and cadmium are found in the same group in the periodic table. The essential first step to a further understanding of these electronic changes is a good normal coordinate analysis, but this obviously requires the frequencies of the modes to be known. We have therefore studied the ZnNa-A + $C_2H_4(C_2D_4)$ system using INS spectroscopy, with the aim of locating the C-H stretching vibrations and identifying the zeolite surface interactions. The spectra obtained are shown in Figures 9.3 and 9.4 and summarized in Table 9.2.

TABLE 9.2 INS data (cm^{-1}) and assignments for C_2H_4 adsorbed on ZnNa-A zeolite

C_2H_4	C_2D_2	Observed deuteration shift	Predicted deuteration shift	Assignment
183	156	0.84	0.86	τ_y
130	237	0.76	0.73	τ_x
490 566				Amplified zeolite modes
636				Overtone of τ_x
825				CH_2 rock
1024				CH_2 twist
1460				ν(C=C) CH_2 scissoring CH_2 rock, *etc.*
3050				C-H stretching modes

9.4.2 INS data below 400 cm^{-1}

Two distinct bands are seen in the INS spectra of both C_2H_4 and C_2D_4 in this region and little change is observed on increasing the coverage. Since these bands are not amplified surface modes (as thefrequency shifts on deuteration) and there are no intramolecular modes below 586 cm^{-1}, these transitions must be hindered rotations and/or translations of the adsorbed molecule relative to the zeolite surface (Figure 9.1). The higher wavenumber transition occurs at 310 (C_2H_4) and 237 (C_2D_4) cm^{-1} and assuming these to be the same mode, this yields an isotropic ratio of 0.76. Using a Zeise's Salt geometry[17] for the adsorbed C_2H_4 an isotropic shift of 0.73 is predicted for the hindered rotation (τ_x) about the C=C axis (Figure 9.1). No other mode has such a large isotropic shift, since no other mode involves little or no carbon atom motion (Table 9.3). Therefore the only reasonable assignment to the 310 (C_2H_4) and 273 (C_2D_4) cm^{-1} bands is to the hindered rotation (τ_x). The corresponding mode was observed at 417 (C_2H_4) and 298 (C_2D_4 cm^{-1} in silver exchange A zeolite.[5] Since the adsorbed ethene is not easily removed on evacuation from Ag_{12}-A[2], it is reasonable to expect a higher frequency in this case. The corresponding mode in Zeise's salt ($[KPtCl_2(C_2H_4)H_2O]$) occurs at 1180 cm^{-1}, [18] in the solid state: since the metal-ethene bond in this very stable complex is much stronger than in the complex formed in zeolites.

The lower wavenumber bands at 183 (C_2H_4) and 156 (C_2D_4) yield an isotropic ratio of 0.84. This is in good agreement with that expected (0.86) for the hindered rotation about an

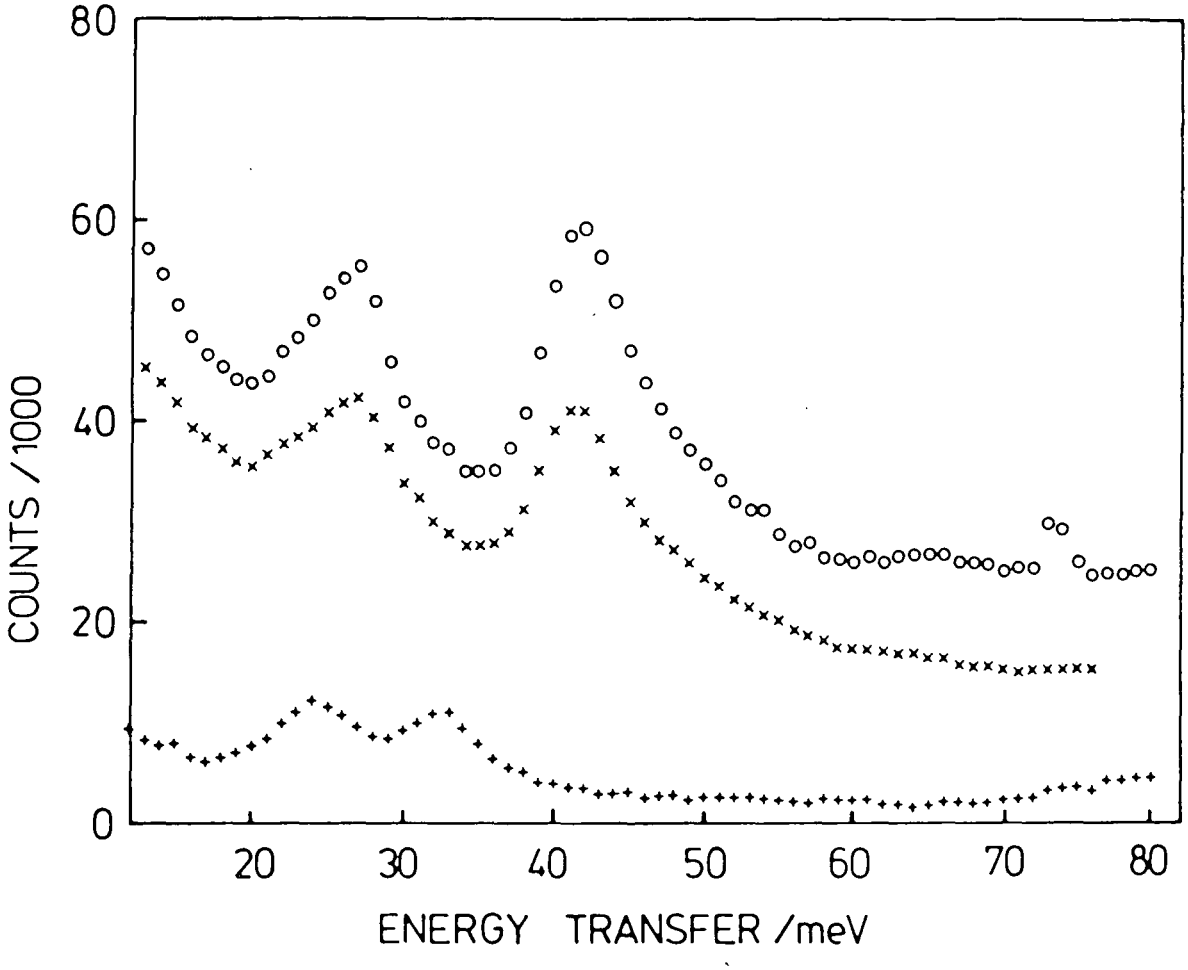

Figure 9.3 INS data (80K) obtained at AERE Harwell for ethene adsorbed on ZnNa-A

O ZnNa-A + C_2H_4 (0.95 molecules per supercage)

X ZnNa-A + C_2H_4 (1.75 molecules per supercage)

\+ ZnNa-A + C_2D_4 (1.75 molecules per supercage)

(data have had the spectrum of degassed zeolite subtracted and the "O" data points have been multiplied by a factor of 2. 1 me V $\sim$ 8.067 cm^{-1}).

TABLE 9.3 Deuteration shifts predicted for Zeolite-ethene vibrations assuming a 'Zeise's Salt' geometry for the adsorbed ethene molecule.[17]

Mode*	Deuteration shift
τ_x	0.73
τ_y	0.86
τ_z	0.84
t_x	0.94
t_y	0.94
t_z	0.94

* The three hindered rotations and three hindered translations of ethene relative to the zeolite surface are defined in Figure 9.1.

---

axis parallel to the surface, τ_y in Figure 9.1. This corresponds to the antisymmetric metal-ethene stretching mode of organometallic complexes, and in Zeise's Salt, τ_y, occurs at 490 cm^{-1}, once again reflecting its stronger bonding.[18]

9.4.3 INS data above 400 cm^{-1}

The INS data on ZnNa-A + C_2H_4 in this region, shown in Figure 9.4, was obtained using the filter difference spectrometer at Los Alamos. Clearly the intense band at 318 cm^{-1} corresponds to τ_x observed at 310 cm^{-1} using the Harwell spectrometer. The overtone of this band is seen at 636 cm^{-1}. Above this value relatively narrow bands occur at 825 and 1023 cm^{-1} with broader features centered at *ca.* 1460 and 3050 cm^{-1}. The broad features clearly contain

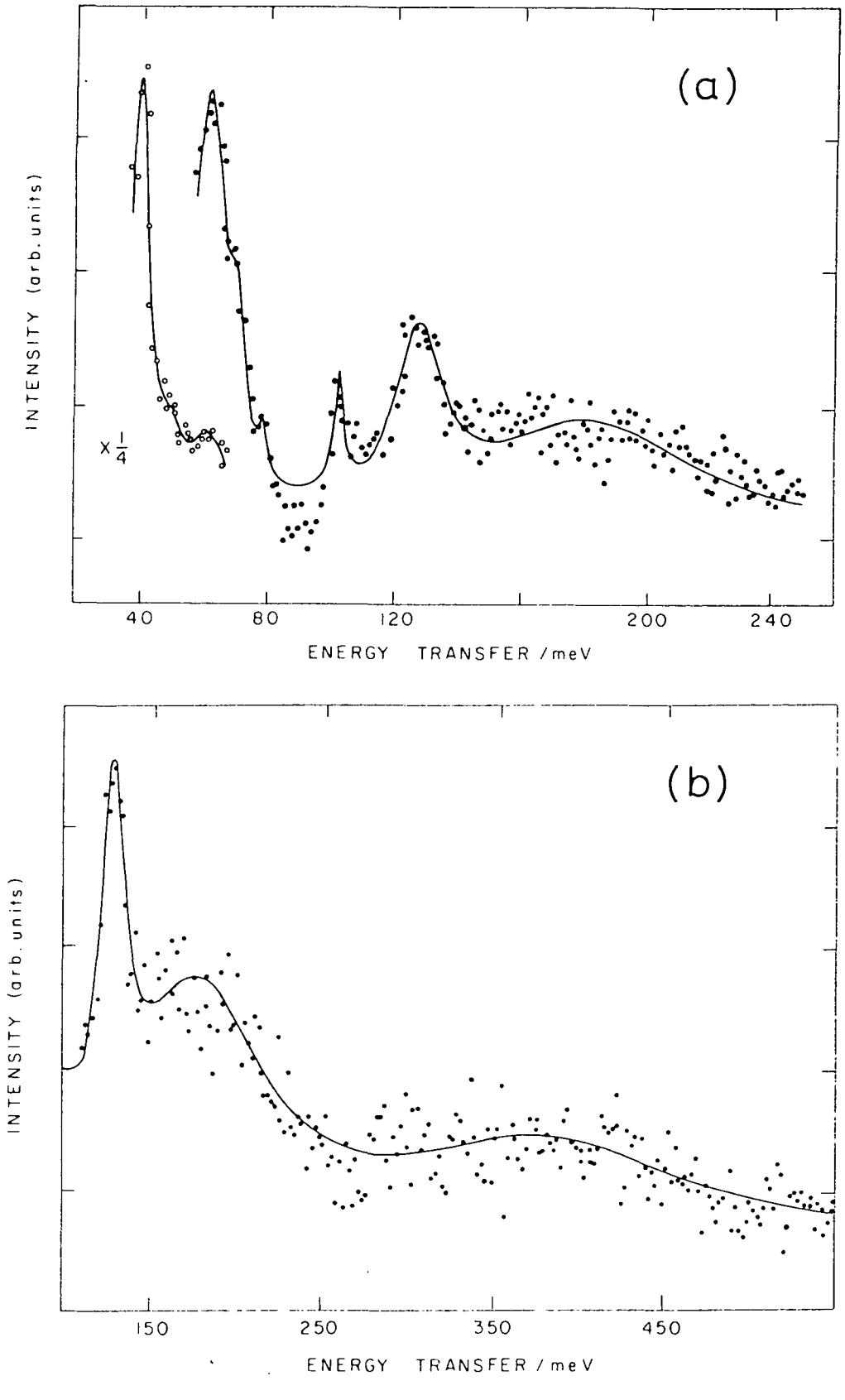

Figure 9.4 INS Spectrum (12K) of ethene adsorbed on ZnNa-A obtained at Los Alamos.

(spectrum of degassed zeolite has been subtracted. 1 meV $\sim$ 8.067 cm^{-1}).

a number of unresolved features. The 1460 cm^{-1} band must contain a number of modes including the ν_2, ν_3 and ν_{12} modes observed in the infrared spectrum in the 1700-1200 cm^{-1} region.

The 3050 cm^{-1} band we must assign to the four C-H stretching modes. These modes were not observed in the IR data, we presume due at most to a small dipole moment, but because INS data has no such rules these vibrations are observed, though the quality of the data is poor. Clearly, further work would be valuable in this region using a low Q (momentum transfer) spectrometer,[12] which would give better energy resolution (*ca.* 10 times) and lead to narrower bands, providing the information necessary to attempt a normal co-ordinate analysis on the system. The observation of these C-H modes indicates that the nature of the complex is indeed similar to those previously reported for 13-X[3] and Ag_{12}-A[2] zeolites, and that their non-observation in the IR spectrum is due to the nature of the cation which must perturb the electronic structure of the ethene molecule.

The assignment of the 825 (sharp) and 1024 cm^{-1} bands is more difficult. Although bands are observed in the INS spectrum of Zeise's Salt,[18] at 840 and 1030 cm^{-1}, in good agreement with the C_2H_4 + ZnNa-A data, the data for the complex also contains an intense band at 720 cm^{-1}. No similar band is found for the zeolite complex. Examination of the previously published INS data for C_2H_4 + Ag13-X shows bands at *ca.* 820 and 1000 cm^{-1} with a minimum close to 700 cm^{-1}. No INS data has been published in this region for the C_2H_4 + Ag_{12}-A system. Thus the ZnNa-Aand Ag13-X data are comparable in this respect and the adsorbed molecule is spectroscopically more similar to gaseous

C_2H_4 than it is to the strongly bonded form in Zeise's Salt.

The INS bands at 720 and 840 cm^{-1} in Zeise's Salt were assigned[11] to CH_2 rocking modes (ν_{17} and ν_{23}). In the gas phase these modes (ν_{10} and ν_6 respectively) occur at 826 and 1236 cm^{-1}.[15] It is likely, therefore, that the 825 and 1024 cm^{-1} bands we observe correspond to the CH_2 rock and CH_2 twisting modes which occur at 826 (ν_6) and 1023 (ν_4) cm^{-1} respectively in uncoordinated C_2H_4.[15]

The remaining weak bands in the region 480-650 cm^{-1} are tentatively assigned to framework vibrations of the zeolite enhanced in intensity by the "riding" motion of the adsorbed species. This tentative assignment is made because none of the hindered rotations or translations of adsorbed C_2H_4 can occur in this region nor are there any intramolecular C_2H_4 modes.

9.5 Conclusions

In contrast to studies of C_2H_4 adsorbed on Ag_{12}-A, the present study has revealed only one adsorption site, the Zn(II) ions, for C_2H_4 adsorbed on ZnNa-A. Using INS spectroscopy the C-H stretching vibrations which are surprisingly absent in the IR spectrum, have been observed. This has shown that subtle changes in the electronic structure of the adsorbed C_2H_4 molecule caused by the nature of the cations must be responsible for the IR inactivity of these bands. A complex similar to those previously reported on Ag_{12}-A and 13-X type zeolites may be envisaged for C_2H_4 adsorbed on ZnNa-A.

REFERENCES (Ch.9)

1. Howard, J. Nicol, J.M. and Eckert, J. "The structure of surfaces", Springer series in Surface Science 2, 219, (1985), Van Hove, M.A. and Tong, S.Y, (Eds.), Springer-Verlag, Berlin-Heidelberg.

2. Howard, J., Kadir, Z.A. and Robson, K., Zeolites, 3, 113 (1983).

3. Carter, J.L., Yates, D.J.C., Lucchesi, P.J., Elliott, J.J., and Kevorkian, V., J.Phys.Chem., 70, 1126 (1966).

4. Sheppard, N. and Yates, D.J.C., Proc.Roy.Soc.A., 238, 69 (1956).

5. Howard, J., Robson, K., Waddington, T.C. and Kadir, Z.A., Zeolites 2, 2 (1982).

6. Kim, Y. and Seff, K., J.Am.Chem.Soc., 100, 175 (1978).

7. Yates, D.J.C., Chem.Eng.Progr.Symp.Ser.63, 73, 56 (1967).

8. Dewar, M.J.S., Bull.Soc.Chim. France 18, C71 (1951).

9. Chatt, J. and Duncanson, L.A., J.Chem.Soc., 2939 (1953).

10. Tomaselli, V.P., Caracciolo, A. and Busca, G., Mater. Chem.Phys., 10, 499 (1984).

11. Howard, J., Waddington, T.C. and Wright, C.J., J.Chem.Soc., Faraday Trans.II, 73, 1768 (1977).

12. Howard, J. and Waddington, T.C., "Advances in Infrared and Raman Spectroscopy", Vol.7, Chapter 3, Clark, R.J.H. and Hester, R.E. (eds.), Heyden, 1980.

13. Taylor, A.D., Wood, E.J., Goldstone, J.A. and Eckert, J., Nucl.Instr. and Meth. 221, 408 (1984).

14. Taylor, A.D. and Howard, J., J.Phys.E.Sci.Instr., 15, 1359 (1982).

15. Shimanouchi, T., "Tables of Molecular Vibrational Frequencies", Volume I, NSRDS, 1972.

16. Howard, J., Kadir, Z.A. and Nicol, J.M., unpublished results.

17. Love, R.A., Koetzle, T.F., Williams, A.J.B., Andrews, L.C. and Bau, R., Inorg.Chem., 14, 2653 (1975).

18. Hiraishi, J., Spectrochim.Acta., 25A, 749 (1969).

APPENDIX A

RESEARCH COLLOQUIA AND CONFERENCES

The Board of Studies in Chemistry requires that each postgraduate research thesis contains an appendix listing:

(A) All research colloquia, research seminars and lectures arranged by the Department of Chemistry during the period of the author's residence as a postgraduate student. (* indicates attendance and + indicates absence from Durham due to research at a central neutron facility).

(B) All research conferences attended and papers presented by the author during the period when the research for the thesis was carried out. (* indicates paper presented).

(A) Research Colloquia, Seminars and Lectures held in the Department of Chemistry during the academic years 1982-1985

27. 9.82* Dr. W.K. Ford (Xerox, Webster, N.Y.) "The dependence of the electron structure polymers on their molecular architecture".

13.10.82* Dr. W.J. Feast (Durham), "Approaches to the synthesis of conjugated polymers".

14.10.82* Prof. H. Suhr (Tübingen, FRG), "Preparative chemistry in non equilibrium plasmas".

27.10.82* Dr. C.E. Housecroft (Oxford High School/Notre Dame), "Bonding capabilities of butterfly-shaped Fe_4 units. Implications for C-H bond activation in hydrocarbon complexes".

28.10.82* Prof. M.F. Lappert, FRS (Sussex), "Approaches to asymmetric synthesis and catalysis using electron-rich olefins and some of their metal complexes".

15.11.82 Dr. G. Bertrand (Toulouse, France), "Curtius rearrangement in organometallic series: A route for new hybridised species".

24.11.82* Prof. F.R. Hartley (R.M.C.S., Shrivenham), "Supported metal-complex hydroformylation catalysts".

24.11.82* Prof. G.G. Roberts (Applied Physics, Durham), "Langmuir-Blodgett films: Solid state polymerisation of diacetylenes".

8.12.82* Dr. G. Wooley (Trent), "Bonds in transition metal-cluster compounds".

12. 1.83+ Dr. D.C. Sherrington (Strathclyde), "Polymer-supported phase transfer catalysts".

9. 2.83 Dr. P. Moore (Warwick), "Mechanistic studies in solution by stopped flow F.T.-NMR and high pressure NMR line broadening".

21. 2.83* Dr. R. Lynden-Bell (Cambridge), "Molecular motion in the cubic phase of NaCN".

2. 3.83+ Dr. D. Bloor (Queen Mary College, London), "The solid-state chemistry of diacetylene monomers and polymers".

8. 3.83+ Prof. D.C. Bradley, FRS (Queen Mary College, London), "Recent developments in organo-imido-transition metal chemistry".

9. 3.83* Dr. D.M.J. Lilley (Dundee), "DNA, sequence, symmetry, structure and supercoiling".

11. 3.83 Prof. H.G. Viehe (Louvrain, Belgium), "Oxidation on sulphur".

16. 3.83 Dr. I. Gosney (Edinburgh), "New extrustion reactions: organic synthesis in a hot-tube".

25. 3.83* Prof. F.G. Baglin (Nevada, USA), "Interaction induced Raman spectroscopy in supracritical ethane".

4. 5.83* Prof. P.H. Plesch (Keele), "Binary ionisation equilibria between two ions and two molecules. What Ostwald never thought of".

10. 5.83 Prof. K. Burger (Munich, FRG), "New reaction pathways from trifluoromethyl-substituted heterodienes to partially fluorinated heterocyclic compounds".

11. 5.83 Dr. N. Isaacs (Reading), "The application of high pressures to the theory and practice of organic chemistry".

13. 5.83* Dr. R. De Koch (Michigan/Amsterdam), "Electronic structural calculations in organometallic cobalt cluster molecules. Implications for metal surfaces".

13. 5.83* Dr. T.B. Marder (UCLA/Bristol), "The chemistry of metal-carbon and metal-metal multiple bonds".

16. 5.83 Prof. R.J. Lagow (Texas, USA), "The chemistry of polylithium organic compounds. An unusual class of matter".

18. 5.83* Dr. D.M. Adams (Leicester), "Spectroscopy at very high pressures".

25. 5.83 Dr. J.M. Vernon (York), "New heterocyclic chemistry involving lead tetra-acetate".

15. 6.83 Dr. A. Pietrzykowski (Warsaw/Strathclyde), "Synthesis, structure and properties of aluminoxanes".

22. 6.83* Dr. D.W.H. Rankin (Edinburgh), "Floppy molecules - the influence of phase on structure".

5. 7.83 Prof. J. Miller (Camfinas, Brazil), "Reactivity in nucleophilic substitution reactions".

5.10.83* Prof. J.P. Maier (Basel, Switzerland), "Recent approaches to spectroscopic characterization of cations".

12.10.83 Dr. C.W. McLeland (Port Elizabeth, Australia), "Cyclization of aryl alcohols through the intermediacy of alkoxy radical and aryl radical cations".

19.10.83 Dr. N.W. Alcock (Warwick), "Aryl tellurium (IV) compounds, patterns of primary and secondary bonding".

26.10.83* Dr. R.H. Friend (Cavendish, Cambridge), "Electronic properties of conjugate polymers".

30.11.83* Prof. J.M.G. Cowie (Stirling), "Molecular interpretation of non-relaxation processes in polymer glasses".

14.12.83 Prof. R.J. Donovan (Edinburgh), "Chemical and physical processes involving the ion-pair states of the halogen molecules".

10. 1.84* Prof. R. Hester (York), "Nanosecond laser spectroscopy of reaction intermediates".

18. 1.84* Prof. R.K. Harris (UEA), "Multi-nuclear solid state magnetic resonance".

8. 2.84* Dr. B.T. Heaton (Kent), "Multi-nuclear NMR studies".

15. 2.84+ Dr. R.M. Paton (Edinburgh), "heterocyclic syntheses using nitrile sulphides".

7. 3.84* Dr. R.T. Walker (Birmingham), "Synthesis and biological properties of some 5-substituted uracil derivatives; yet another example of serendipity in antiviral chemotherapy".

21. 3.84* Dr. P. Sherwood (Newcastle), "X-ray photoelectron spectroscopic studies of electrode and other surfaces".

23. 3.84 Dr. A. Ceulemans (Leuven), "The development of field-type models of the bonding in molecular clusters".

2. 4.84 Prof. K. O'Driscoll (Waterloo), "Chain ending reactions in free radical polymerisation".

3. 4.84* Prof. C.H. Rochester (Dundee), "Infrared studies of adsorption at the solid liquid interface".

25. 4.84 Dr. R.M. Acheson (Biochemistry, Oxford), Some heterocyclic detective stories".

27. 4.84 Dr. T. Albright (Houston, USA), "Sigmatropic rearrangement in organometallic chemistry".

14. 5.84* Prof. W.R. Dolbier (Florida, USA), "Cycloaddition reactions of fluorinated allenes".

16. 5.84 Dr. P.J. Garratt (UCL), "Syntheses with dilithiated vicinal diesters and carboximides".

31. 5.84* Dr. A. Haaland (Oslo), "Electron diffraction studies of some organometallic compounds".

11. 6.84* Dr. J.B. Street (IBM, California), "Conducting polymers derived from pyrroles".

19. 9.84+ Dr. C. Brown (IBM, California), "New superbase reactions with organic compounds".

21. 9.84+ Dr. H.W. Gibson (Signal UOP, Illinois), "Isomerization of polyacetylene".

7.11.84* Professor W.W. Porterfield (Hampden-Sydney College, Virginia), "There is no Borane chemistry - only Geometry".

28.11.84 Dr. T.A. Stephenson (Edinburgh), "Some recent studies in platinum metals chemistry".

11. 1.85 Emeritus Prof. H. Suschitzky (Salford), "Fruitful Fissions of Benzofuroxanes and Isobenzimidazoles (umpslung of o-phenylendiamine)".

13. 2.85 Dr. G.W.J. Fleet (Oxford), "Synthesis of some alkaloids from carbohydrates".

20. 2.85* Dr. J. Dwyer (UMIST), "Zeolites".

12. 3.85 Professor K.J. Packer (B.P. Ltd., Sunbury), "NMR Investigations of the Structure of Solid Polymers".

21. 3.85* Dr. M. Poliakoff (Nottingham), "New methods for detecting organometallic intermediates in solution".

28. 3.85* Professor H. Ringsdorf/Mainz, FRG), "Polymeric hiposomers as Models for Biomembranes and Cells".

24. 4.85 Dr. M.C. Grossel (Bedford College, London), "Hydroxypyridane dyes - bleachable one-dimensional metals?".

1. 5.85* Dr. D. Parker (I.C.I. plc, Wilton), "Application of radioisotopes in industrial research".

7. 5.85* Professor G.E. Coates (Wyoming, USA), "Chemical education in Britain and America: successes and deficiencies".

8. 5.85 Professor D. Tuck (Windsor, Ontario), "Lower Oxidation state chemistry of Indium".

8. 5.85* Professor A. Williams (Aberystwyth), "Liquid crystalline polymers".

14. 4.85 Professor J. Passmore (New Brunswick, Canada), "The synthesis and characterization of some novel selenium-iodine cations, aided by ^{77}Se NMR spectroscopy".

15. 5.85 Dr. J.E. Packer (Auckland, New Zealand), "Studies of Free Radical Reactions in aqueous solutions using ionising radiation".

17. 5.85* Professor I.D. Brown (McMaster, Canada), "Bond Valence as a model for Inorganic Chemistry".

22. 5.85 Dr. M. Hudlicky (Virginia State University, USA), "Preferential Elimination of Hydrogen fluoride from vicinal Bromofluoro-compounds".

22. 5.85 Dr. R. Grimmett (Otago, New Zealand), "Some aspects of Nucleophilic substitution in Imidazoles".

4. 6.85* Dr. P.S. Belton (Food Research Institute, Norwich), "Analytical Photoacoustic Spectroscopy".

13. 6.85 Dr. D. Woollins (Imperial College, London), "Metal-Sulphur-Nitrogen Complexes".

14. 6.85 Professor Z. Rappoport (Jerusalem), "The rich mechanistic world of nucleophilic vinylic substitution".

19. 6.85 Dr. T.N. Mitchell (University of Dortmund), "Some synthetic and NMR spectroscopic studies of organotin compounds".

(B) Attendance of Research Conferences and Summer Schools

15. 4.83 Graduate Symposium, Durham.

5-9.9.83 International Conference on Fourier Transform Spectroscopy, Durham.

18-24.9.83 Summer School: Experimental techniques in neutron scattering, Reading.

11. 4.84* Graduate Symposium, Durham.

12-13.6.84* Nicolet 1984 FTIR Users Meeting, Warwick.

13-16.8.84* International Conference on the Structure of Surfaces, Berkely, CA, USA.

20. 3.85* Spectroscopic Investigation of Chemisorbed Layers, Daresbury Laboratory.

29. 3.85 Postgraduate Symposium, Durham.

15-19.4.85 Partial attendance at:

Polymer Surfaces and Interfaces, Durham.

24-28.6.85* International Conference on Fourier and Computerized infrared spectroscopy, Ottawa, Canada.

17-19.7.85* British Zeolite Association's eighth annual Meeting, Chester.